UNIVERSITAT POLITÈCNICA DE CATALUNYA
Programa de Doctorat en Enginyeria Ambiental

Ph.D. thesis

Desert dust characterization in Northern Africa, Middle East and Europe through regional dust modelling, and satellite-borne and ground-based observations

Sara Basart Alpuente

Directors: Dr. Carlos Pérez García-Pando (Department of Applied Physics and Applied Maths, Columbia University and NASA Goddard Institute for Space Studies)

Dr. Emilio Cuevas Agulló (Centro de Investigación Amosférica de Izaña-Agencia Estatal de Meteorología; CIAI-AEMET)

Tutor: Dr. José María Baldasano Recio (Universitat Politècnica de Catalunya, UPC; Barcelona Supercomputing Center-Centro Nacional de Supercomputación, BSC-CNS)

Barcelona, December 2011

A la meva petita-gran família.

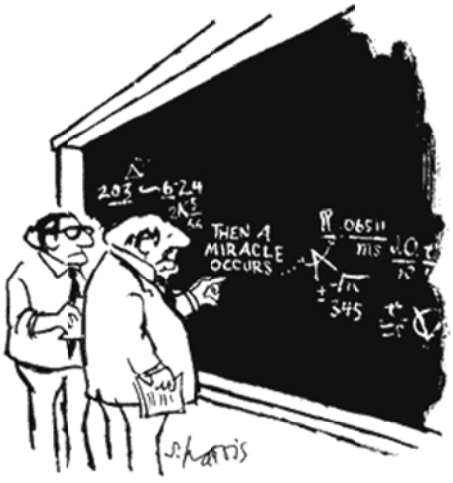

"I THINK YOU SHOULD BE MORE EXPLICIT HERE IN STEP TWO."

Acknowledgements

En primer lugar quiero dar las gracias a mis 3 directores de tesis por su apoyo y por no haber dudado que habría un día en que esta tesis llegaría a su fin y de los que espero no se hayan arrepentido. A Emilio Cuevas por darme la oportunidad de vivir una tormenta extratropical además de unas cuantas calimas, y de enseñarme los entresijos de la parte instrumental de esta tesis. A José María Baldasano por sus consejos, su apoyo, su ayuda con la elaboración del documento y la rigurosidad de sus correcciones. Y especialmente, enviar un gran abrazo a Carlos Pérez. Darle mil gracias por dedicarme parte de su tiempo, sus terapias de choque, consejos, críticas, por ayudarme con mi inglés nivel medio y por dejar parte de su salud mental en estos años.

Als meus pares, la Jose i en Joaquim, que sempre ens han animat a la lectura, inspirat per l'estudi i a aprendre coses noves, i sobretot a tindre bones discussions a les sobretaules que mai han estat avorrides. A la meva germana Yolanda que té una capacitat de treball i concentració que sempre he intentat imitar. Una gran abraçada i moltes gràcies per la vostra paciència i recolçament incondicional.

Este ha sido un largo camino en el que he compartido pequeños momentos con muy variopintas personas en distintos puntos del mundo a los que no quiero dejar de agradecer esos instantes: las de Badalona, Marián y Rafa, mis compis de física (Manu e Isabel), los chicos del Departament Medi Ambient (las Maris y el Antonio), mis meteocompañeros, mis niñas de Tenerife que consiguieron que cambiará mi *aSento* y no me *trabará* por nada (Jenny, Gladys, Elisabeth, Aday, Sergio y el Blues Bar), los creativos muchachos de Barcelona que me enseñan la otra cara de la ciudad, los de Zaragoza que me mostraron la ruta de la buena comida y bebida además de los espectaculares cielos que trae el Cierzo, los de París que me mostraron que un piso de 20m^2 puede ser una gran mansión, la que ha compartido conmigo mucho más que un piso (la vasca Naiara), la fantástica Agurtxane, las terapias de los viernes en la Rosa con Luca, aquellos que habéis sobrevivido a la insoportable levedad del ser, mi gato, los que nos dejaron pero que siempre tienen un lugar en mis recuerdos; mis tíos, primos y sobrinos postizos, y Marta que se merece un agradecimiento destacado y un besazo porque es más que una prima (¡prima, ai lof yu!).

También quiero enviar un saludo a los chicos del Observatorio de Izaña o ahora llamado Centro de Investigación Atmosférica de Izaña (CIAI) que tanto saben de cacharrear y que fueron los que vieron el inicio de la presente tesis. Y como no, a mis compañeros del BSC, los que todavía seguís por aquí, a los recién llegados, a los que estáis de paso, a la sección Mordor, a los de support (que espero quiten mi foto de su pared de los más buscados) y helpdesk, a las chicas de la tercera planta, y a los que cambiaron de aires. En especial, quiero enviar un saludo a Oriol por su capacidad de transmitir paz y serenidad así como su

paciencia infinita y su capacidad de sintetizar complejos conceptos en pequeñas frases de tres palabras; a Karsten por ser mi guía laberíntico en los entresijos del código del modelo y como no, a María Teresa que siempre está a mí lado (no solo físicamente) y la que se merece un agradecimiento destacado y un enorme besazo.

La presente tesis se desarrolló en el marco de dos proyectos del Ministerio de Educación y Ciencia: el proyecto CICYT (CICYT CGL2006-11879) y el proyecto CALIOPE (CALIOPE 441/2006/3-12.1, A357/2007/2-12.1, A357/2007/2-12.1, 157/PC08/3-12.0). Dichos proyectos incluyen el desarrollo, mejora, evaluación e implementación del modelo regional de polvo DREAM (Dust Regional Atmospheric Model) para el pronóstico de intrusiones de polvo saharianas en la Península Ibérica, el Mediterráneo y las Islas Canarias. Asímismo, agradecer a la Agencia Estatal de Meteorología (AEMET) y al Barcelona Supercomputing Center-Centro Nacional de Supercomputación (BSC-CNS) por el apoyo técnico y económico para la realización de la presente tesis.

Furthermore, this investigation was also possible thanks to the collaboration of many scientists. I would like to acknowledge all the co-authors of the publications done in the context of this thesis.

I greatfully acknowledge the collaboration of Gian Paolo Gobbi to help a student to write her first paper. Moreover, I am especially indebted to Slobodan Nickovic (the DREAM's dad) and Michael Schulz for the support to develop the dissertation related to air quality and dust modelling. A short visit to the Laboratoire des Sciences du Climat et de l'Environnement (LSCE/IPSL) of the Centre National de la Recherche Scientifique (CNRS) and the Commissariat à l'Energie Atomique (CEA) derived in a very fruitful collaboration in the framework of the Sand and Dust Storm Warning Advisory and Assessment System (SDS-WAS) and AEROCOM projects. Michael, many thanks for your time, I really appreciate your generosity and patience.

All the model simulations have been made possible by their implementation on the MareNostrum supercomputer hosted by BSC-CNS. I am especially indebted to the EMEP, AERONET and PHOTONS networks, and the research groups that contribute to them who kindly provided their data. I also acknowledge the MISR, MODIS and TOMS mission scientists and associated NASA personnel for the production of the data used in this research effort.

A tots, moltes gràcies! ¡Muchas gracias! Thank you very much! Merci beaucoup!

Summary

A large amount of mineral dust is mobilized over arid regions and injected into the atmosphere under favourable weather conditions. Estimates of global dust input based on ground based and satellite observations, and modelling studies range from several hundred to thousands megatons per year. The impact of mineral dust upon climate, ecosystems and air quality (and consequently on economic activities and human health) represents a major scientific and societal issue. The most prominent example of this transport is the export of desert mineral dust from the Saharan region.

The aim goals of the present Ph.D. thesis are to ***evaluate the behaviour and to improve the forecasting skills of a regional dust model*** and to ***characterize the mineral dust content in Northern Africa, Europe and Middle East***. Within this framework, the BSC-DREAM8b regional model and the AERONET sun photometers are the main tools in the context of the present research.

Comparison between modelled and observed values can not be adequately understood if the measurements are not segmented into their more fundamental aerosol components. An accurate aerosol characterization was performed by means of long-term series of aerosol optical depth (AOD) from AERONET sun photometers over for Northern Africa, Northeastern Atlantic Ocean, Mediterranean and Middle East. The analysis of this data was conducted applying the graphical method of Gobbi and co-authors which allows to discriminate and to monitor different aerosol. The method permits to infer other physical aerosol properties as fine mode radius and fractional contribution to AOD and separate AOD growth due to fine-mode aerosol humidification and/or coagulation from AOD growth due to the increase in coarse particles or cloud contamination. The results showed that mineral dust was the most important constituent in Northern Africa and Arabian Peninsula. Small pollution particles were abundant in sites close to urban and industrial areas of Continental and Eastern Europe and Middle East, as well as, important contributions of biomass burning were observed in the sub-Sahel region in winter. Under specific meteorological conditions, desert dust transport to Southern Europe was observed from spring to autumn and decreasing with latitude with contributions above 40% to the aerosol column content. In this region, dust usually appeared mixed with fine pollution aerosols.

Desert dust models are essential to complement dust-related observations, understand the dust processes and predict the impact of dust on surface level particulate matter concentrations. Regional models, in particular, are well suited for simulations of individual dust outbreaks. Currently, the BSC-DREAM8b model is operated and further developed in Barcelona Supercomputing Center-Centro Nacional de Supercomputación (BSC-CNS) and

has been delivering operational desert dust over Northern Africa, Middle East, Europe and Asia in the last years. Despite that BSC-DREAM8b has reached a level of delivering reliable operational dust forecasts capable to predict all the major dust events in areas affected by Saharan dust long-range transport, it is necessary to evaluate its behaviour also in desert dust sources areas.

In this context, BSC-DREAM8b and the original DREAM model as well as different research model versions were annually evaluated over Northern Africa, the Mediterranean Basin and Middle East using AERONET measurements and seasonal averages from satellite aerosol products. The model evaluation highlighted that BSC-DREAM8b and DREAM strongly underestimated the dust fields in the Sahel during the winter Harmattan season and overestimated dust concentrations during spring rainy events in the Mediterranean. The introduction of new dry deposition scheme and an updated wash-out ratio in the wet deposition scheme improved the long-range transport, in particular over the Mediterranean, although significant underestimation remained in the Sahel in winter. The inclusion of a topographic preferential source mask improved the localization of the main North African sources and consequently the long-range dust transport to Europe and Atlantic regions. The inclusion of a more physically-based dust emission scheme with a new soil texture database led to reasonably good results at source areas and in regions affected by dust after long-range transport. However, in the latter case, the use of a preferential source mask did not introduce significant improvements in the comparison with the observed values.

Since the European atmosphere is composed by a variety of different aerosol components, it is necessary to take into account different aerosol sources at the same time (i.e. natural and anthropogenic). The long-range dust transport over Europe was evaluated and analysed with an annual simulation of the CALIOPE high-resolution air quality modelling system. The CALIOPE modelling system integrates a set of models including CMAQ which calculates biogenic, anthropogenic and sea salt aerosol; and BSC-DREAM8b which provides desert dust. For the evaluation, we used daily PM_{10}, $PM_{2.5}$ and aerosol components from the EMEP/CREATE network; total, coarse and fine AOD from AERONET sun photometers and seasonal averages from satellite aerosol products.

Overall the CALIOPE system could reproduce reasonably well the daily variability of the main components and the seasonal aerosol patterns in Europe. However, the PM and AOD levels were underestimated. The evaluation of the aerosol components highlights that the modelling system underestimates measured fine fractions for carbonaceous matter and secondary inorganic aerosols (SIA; i.e. nitrates, sulphates and ammonium). As a result, a simple model bias correction based on the chemical composition observations was

applied to the model simulation in order to provide an estimation of the spatial and seasonal distribution of the different aerosol components over Europe. The scores of the bulk parameters were significantly improved after applying this model correction. The simulated aerosol concentrations presented maximum values over the industrialized and populated areas of the Po Valley and the Benelux regions. SIA were dominant in the fine fractions representing up to 80% of the aerosol budget in latitudes beyond 40ºN. A second maximum was detected over Eastern and Southern Europe. High values in Southern Europe were linked to the transport of coarse particles from the Sahara desert which contributed up to 40% of the total aerosol mass. Close to the surface, maxima dust seasonal concentrations (> 30 $\mu g/m^3$) were found between spring and early autumn. These results showed that desert dust is the main responsible of the exceedances of the PM_{10} EU air quality threshold (50 $\mu g/m^3$) in large areas south of 45ºN.

Resum

Una gran quantitat de pols que és mobilitzada en les regions àrides del planeta, és injectada a l'atmosfera sota condicions meteorològiques favorables. A partir de mesures terrestres i de satèl·lit, a més a més d'estimacions obtingudes a partir de models, es calcula que en tot el planeta s'emeten entre centenars i milers de megatones de pols per any. L'impacte que té la pols mineral en el clima, els ecosistemes i la qualitat de l'aire, i per tant, en la salut humana i les activitats econòmiques, representa una qüestió social i científica de gran rellevància. La font més important d'emissió de pols mineral a nivell global és la regió del Sàhara.

Els principals objectius de la present tesi doctoral són el d'***avaluar el comportament i el de millorar les capacitats de predicció d'un model regional de pols*** així com el de ***caracteritzar el contingut de pols desèrtica en el nord d'Àfrica, Orient Mitjà i Europa***. En aquest marc de treball, el model regional de pols BSC-DREAM8b i els fotòmetres de la xarxa internacional AERONET són les principals eines que seràn utilitzades en el transcurs de la present investigació.

La comparació entre valors observats i simulats no pot ser adequadament entesa si les mesures no estan separades en els seus components fonamentals. Així, es va dur a terme una caracterització d'aerosols per al nord d'Àfrica, Europa i Orient Mitjà. Aquesta caracterització està basada en sèries d'espessor òptic d'aerosols (AOD; *Aerosol Optical Depth* en anglès) dels fotòmetres de la xarxa AERONET. L'anàlisi d'aquesta base de dades es va realitzar aplicant el mètode de Gobbi i co-autors. Aquest mètode gràfic permet deduir diferents propietats òptiques i físiques dels aerosols (com són el radi efectiu del mode fi i la contribució de les fraccions fines i gruixudes a l'AOD), a més a més, de diferenciar entre diferents processos que fan augmentar el valor de l'AOD com són la humidificació i/o coagulació de les fraccions fines o l'increment de partícules més gruixudes a causa de la presència de núvols. Els resultats van mostrar que la pols mineral és l'aerosol més important al nord d'Àfrica i Aràbia. En estacions properes a zones urbanes i industrials de regions continentals i de l'est d'Europa i Orient Mitjà es van observar partícules fines associades a fonts antropogèniques. També es van detectar importants contribucions en les fraccions fines degudes a la crema de biomassa a la zona del sub-Sahel durant l'hivern. El transport de pols desèrtica cap al sud d'Europa està associat a determinats patrons meteorològics estacionals. Com a resultat, en zones del sud d'Europa, la pols desèrtica es va observar entre primavera i tardor, i la seva contribució (que va arribar superar el 40%) decreixia cap a latituds més al nord. En aquest darrer cas, la pols desèrtica acostumava a trobar-se barrejada amb altres tipus d'aerosols d'origen antropogènic.

Els models de pols són essencials per complementar les observacions, entendre els processos associats al cicle de la pols i predir el seu impacte en les concentracions en superfície del material particulat (PM; *Particulate Matter* en anglès). En particular, els models regionals són adequats per a la simulació d'episodis individuals d'instrusió de pols desèrtica. Actualment, el model de pols BSC-DREAM8b és mantingut i desenvolupat en el Barcelona Supercomputing Center–Centre Nacional de Supercomputació (BSC-CNS). En els darrers anys, aquest model ha proporcionat prediccions diàries de concentracions de pols desèrtica en dos dominis: Nord d'Àfrica–Europa–Europa–Orient Mitjà i Àsia. Malgrat que el BSC-DREAM8b ha arribat a aconseguir una qualitat de pronòstic operacional capaç de reproduir els episodis d'intrusió saharians més importants que afecten al Mediterrani i Europa, és necessari avaluar el seu comportament en regions font de pols.

En aquest context, el model BSC-DREAM8b i la seva versió original, el model DREAM, així com diferents versions experimentals, van ser avaluats per a un cicle estacional complet utilitzant les dades de la xarxa AERONET i promitjos estacionals de productes d'aerosols de diferents satèl·lits pel Nord d'Àfrica, Orient Mitjà i Europa. Els resultats de l'avaluació del model van mostrar que tant el BSC-DREAM8b com el DREAM subestimaven les concentracions de pols a la regió del Sahel durant l'estació hivernal del Harmattan. Per contra, importants sobreestimacions en l'oest del Mediterrani es van detectar coincidint amb episodis plujosos a la primavera. L'inclusió d'un nou esquema de deposició seca a més de l'actualització de la relació de rentat en l'esquema de deposició humida del model, van aconseguir millores en el transport a llarga distància, en particular sobre el Mediterrani malgrat que les subestimacions a la zona del Sahel van continuar sent persistents a l'hivern. La introducció d'una màscara de fonts preferents en l'esquema d'emissió basada en la topografia del terreny va millorar la localització de les principals regions font en el Nord d'Àfrica. Com a conseqüència, es van observar millores en el transport de llarga distància cap a Europa i les regions atlàntiques. La inclusió d'un nou esquema d'emissió (que inclou parametritzacions físiques més complexes) a més d'una nova base de dades de textura de sòls va aconseguir bons resultats en regions font així com en regions afectades pel transport de pols a llarga distància. En aquest cas, l'introducció d'una màscara de fonts preferents en l'esquema d'emissió no va mostrar significants millores en comparació dels valors observats.

A Europa, es poden trobar diferents tipus d'aerosols associats a diferents fonts d'emissió (tant naturals com antropogèniques) que s'han de tenir en compte quan s'analitzen les contribucions dels aerosols sobre el continent europeu. El transport de pols sahariana cap a sud d'Europa va ser avaluat i analitzat mitjançant una simulació del sistema de modelització de qualitat de l'aire CALIOPE. El sistema de modelització CALIOPE integra un conjunt de models dels quals el BSC-DREAM8b i el model fotoquímic CMAQ proporcionen les

estimacions d'aerosols. Per a l'avaluació de CALIOPE es van utilitzar diverses fonts de dades de xarxes en superfície (com la xarxa europea de qualitat de l'aire EMEP/CREATE i la xarxa AERONET) i mitjanes estacionals de productes d'aerosols de satèl.lits. L'avaluació va mostrar que malgrat subestimar les concentracions d'aerosols, CALIOPE és capaç de capturar les variabilitats diàries observades en les estacions en superfície així com reproduir els patrons estacionals observats en els productes de satèl·lit. L'avaluació dels aerosols per components va mostrar que les espècies químiques amb major subestimació pel que fa a les observacions estaven associades a les fraccions fines de carbó elemental i orgànic així com als aerosols secundaris inorgànics (nitrats, sulfats i amoni). Com a resultat, es va aplicar un senzill mètode de correcció de l'error als resultats de la simulació basat en les observacions de la composició química per tal de mostrar una estimació espaial i temporal de la distribució dels diferents aerosols presents a Europa. L'anàlisi d'aquesta simulació va mostrar que les màximes concentracions d'aerosols es van localitzar a zones poblades i industrialitzades del Benelux i de la Vall del Po. Aquests màxims estaven associats a les fraccions fines compostes d'aerosols secundaris inorgànics (observant-se contribucions de més del 80%). Màxims secundaris es van detectar a l'est i sud d'Europa. Les altes concentracions en el sud d'Europa estaven associats al transport de pols sahariana que contribuïa en més d'un 40% al total de la massa en columna. Prop de la superfície, les màximes concentracions estacionals associades al transport de pols (> 30 $\mu g/m^3$) van ser observades entre primavera i estiu. A més a més, els resultats de la simulació anual d'aerosols per Europa va mostrar que el transport de pols sahariana és el principal responsable de la superació del límit diari de PM_{10} establert per la Unió Europea (50 $\mu g/m^3$) en extenses àrees al sud dels 45ºN.

Resumen

Una gran cantidad de polvo se moviliza en regiones áridas del planeta y se emite a la atmósfera bajo condiciones meteorológicas favorables. A partir de medidas realizadas en superficie y desde satélite, además de estimaciones obtenidas a partir de modelos, se calcula que en todo el planeta se emiten entre centenares y miles de megatoneladas de polvo cada año. El impacto que tiene el polvo mineral en el clima, los ecosistemas y la calidad del aire, y por lo tanto, en la salud humana y en las actividades económicas, representa una cuestión social y científica de gran relevancia. La fuente más importante de emisión de polvo mineral a nivel global es la región del Sáhara.

Los principales objetivos de la presente tesis doctoral son el de ***evaluar el comportamiento y el de mejorar las capacidades de predicción de un model de regional de polvo*** así como el de ***caracterizar el contenido de polvo desértico en el norte de África, Europa y Oriente Medio***. En este marco de trabajo, el modelo regional de polvo BSC-DREAM8b y los fotómetros de la red internacional AERONET son las principales herramientas que serán utilizadas en el transcurso de la presente investigación.

La comparación entre valores observados y simulados no puede ser adecuadamente comprendida si las medidas no están separadas en sus componentes fundamentales. Así, se llevó a cabo una caracterización de aerosoles para el norte de África, Europa y Oriente Medio. Dicha caracterización está basada en series de espesor óptico de aerosoles (AOD; *Aerosol Optical Depth* en inglés) de la red AERONET. El análisis de esta base de datos se realizó aplicando el método de Gobbi y co-autores. Este método gráfico permite deducir diferentes propiedades ópticas y físicas de los aerosoles (como son el radio efectivo del modo fino y la contribución de las fracciones finas y gruesas del AOD), además, de diferenciar entre diferentes processos que hacen augmentar el AOD como son la humidificación y/o coagulación de las fracciones finas o el incremento de partículas más gruesas a causa de la presencia de nubes. Los resultados muestran que el polvo mineral es el aerosol más importante en regiones desérticas del norte de África y Arabia. En estaciones cercanas a zonas urbanas e industriales de regiones continentales y del este de Europa y Oriente Medio se observaron partículas finas asociadas a fuentes antropogénicas. También se detectaron importantes contribuciones en el modo fino debidas a la quema de biomasa en la zona del sub-Sahel durante el invierno. El transporte de polvo desértico hacia el sur de Europa está asociado a determinados patrones meteorológicos estacionales. Como resultado, en zonas del sur de Europa, el polvo desértico se observó entre primavera y otoño, y su contribución (que llegó superar el 40%) decrecía hacia latitudes más al norte. En este caso, el polvo desértico acostumbraba a encontrarse mezclado con otros tipos de aerosoles de origen antropogénico.

Los modelos de polvo son esenciales para complementar las observaciones, entender los procesos asociados al ciclo del polvo y predecir su impacto en las concentraciones en superficie del material particulado (PM; *Particulate Matter* en inglés). En particular, los modelos regionales son adecuados para la simulación de episodios individuales de instrusión de polvo desértico. Actualmente, el modelo de polvo BSC-DREAM8b es mantenido y desarrollado en el Barcelona Supercomputing Center–Centro Nacional de Supercomputación (BSC-CNS). En últimos años, dicho modelo ha proporcionado predicciones diarias de concentraciones de polvo desértico en dos dominios: Norte de África–Europa–Europa–Oriente Medio y Asia. A pesar que el BSC-DREAM8b ha llegado a alcanzar una calidad de pronóstico operacional capaz de reproducir los episodios de intrusión saharianos más importantes que afectan al Mediterráneo y Europa, es necesario evaluar su comportamiento en regiones fuente de polvo.

En este contexto, el modelo BSC-DREAM8b y su versión original, DREAM, así como diferentes versiones experimentales, fueron evaluados para un ciclo estacional completo utilizando los datos de los fotómetros de la red AERONET y promedios estacionales de productos de aerosoles de diferentes satélites para el Norte de África, Europa y Oriente Medio. Los resultados de la evaluación del modelo mostraron que tanto el BSC-DREAM8b como el DREAM subestimaban las concentraciones de polvo en la región del Sahel durante la estación invernal del Harmattan. Por el contrario, importantes sobrestimaciones en el oeste del Mediterráneo se detectaron coincidiendo con episodios lluviosos en primavera. La inclusión de un nuevo esquema de deposición seca además de la actualización de la relación de lavado en el esquema de deposición húmeda del modelo, lograron mejoras en el transporte a larga distancia, en particular sobre el Mediterráneo a pesar de que las subestimaciones en la zona del Sahel fueron persistentes en invierno. La introducción de una máscara de fuentes preferentes en el esquema de emisión basada en la topografía del terreno mejoró la localización de las principales regiones fuente en el Norte de África. Como consecuencia, se observaron mejoras en el transporte de larga distancia hacia Europa y las regiones atlánticas. La inclusión de un nuevo esquema de emisión (que incluye parametrizaciones físicas más complejas) además de una nueva base de datos de textura de suelos logró alcanzar buenos resultados en regiones fuente así como en regiones afectadas por el transporte de polvo a larga distancia. En este caso, la introducción de una máscara de fuentes preferentes en el esquema de emisión no mostró significantes mejoras en comparación con los valores observados.

En Europa, se pueden encontrar diferentes tipos de aerosoles asociados a diferentes fuentes de emisión (tanto naturales como antropogénicas) que hay tener en cuenta cuando se analizan las contribuciones de los aerosoles sobre el continente europeo. El transporte de polvo sahariano hacia sur de Europa fue evaluado y analizado mediante una simulación

del sistema de modelización de calidad del aire CALIOPE. El sistema de modelización CALIOPE integra un conjunto de modelos de los que el BSC-DREAM8b y el modelo fotoquímico CMAQ proporcionan las estimaciones de aerosoles. Para la evaluación de CALIOPE se utilizaron varias fuentes de datos de redes en superficie (como la red europea de calidad del aire EMEP/CREATE y la red AERONET) y promedios estacionales de productos satelitales de aerosoles. La evaluación mostró que a pesar de subestimar las concentraciones de aerosoles, CALIOPE es capaz de capturar las variabilidades diarias observadas en las estaciones en superficie así como reproducir los patrones estacionales observados en los productos de satélite. La evaluación de los aerosoles por componentes mostró que las especies químicas con mayor subestimación con respecto a las observaciones estaban asociadas a las fracciones finas de carbon elemental y orgánico así como a los aerosoles secundarios inorgánicos (nitratos, sulfatos y amonio). Como resultado, se aplicó un sencillo método de corrección del error a los resultados de la simulación basado en las observaciones de la composición química para dar una estimación espacial y temporal de la distribución de los diferentes aerosoles presentes en Europa. El análisis de la simulación anual mostró que las máximas concentraciones de aerosoles se localizaron en zonas pobladas e industrializadas del Benelux y del Valle de Po. Estos máximos estaban asociados a las fracciones finas compuestas de aerosoles secundarios inorgánicos (alcanzando contribuciones de más del 80%). Máximos secundarios se detectaron al este y sur de Europa. Las altas concentraciones en el sur de Europa se asociaban al transporte de polvo sahariano que contribuía en más de un 40% al total de la masa en columna. Cerca de la superficie, las máximas concentraciones estacionales asociadas al tranporte de polvo (> 30 $\mu g/m^3$) fueron observadas entre primavera y verano. Además, los resultados de la simulación anual de aerosoles para Europa mostraron que el transporte de polvo sahariano es el principal responsable de la superación del límite diario de PM_{10} establecido por la Unión Europea (50 $\mu g/m^3$) en extensas áreas al sur de los 45ºN.

Publications related to this Thesis

International Jounals Included in the Science Citation Index (SCI)

1. Amiridis, V., Kafatos, M., Pérez, C., Kazadzis, S., Gerasopoulos, E., Mamouri, R. E., Papayannis, A., Kokkalis, P., Giannakaki, E., **Basart, S.**, Daglis, I., and Zerefos, C.: The potential of the synergistic use of passive and active remote sensing measurements for the validation of a regional dust model, Ann. Geophys., 27, 3155-3164, doi:10.5194/angeo-27-3155-2009, 2009.

2. **Basart, S.**, Pérez, C., Cuevas, E., Baldasano, J. M., Gobbi, G. P.: Mineral dust characterization for North of Africa, Northeastern Atlantic, Mediterranean Basin and Middle East from direct-sun AERONET observations. Atmos. Chem. Phys., 9, 8265–8282, doi:10.5194/acp-9-8265-2009, 2009.

3. Pay, M. T., Piot, M., Jorba, O., Gassó, S., Gonçalves, M., **Basart, S.**, Dabdub, D., Jiménez-Guerrero, P., and Baldasano, J. M.: A Full Year Evaluation of the CALIOPE-EU Air Quality Modeling System over Europe for 2004, Atmos. Environ., 44, 3322-3342, doi:10.1016/j.atmosenv.2010.05.040, 2010.

4. Papanastasiou, D. K., Poupkou, A., Katragkou, E., Amiridis, V., Melas, D., Mihalopoulos, N., **Basart, S.**, Pérez, C. and Baldasano, J. M.: S. An Assessment of the Efficiency of Dust Regional Modelling to Predict Saharan Dust Transport Episodes, Advances in Meteorology, 2010(154368), doi:10.1155/2010/154368, 2010.

5. **Basart, S.**, Pay, M.T., Jorba, O., Pérez, C., Jiménez-Guerrero, P., Schulz, M. and Baldasano, J. M.: Aerosols in the CALIOPE air quality modelling system: validation and analysis of PM levels, optical depths and chemical composition over Europe, Atmos. Chem. Phys. Discuss., 11, 20575–20629, doi:10.5194/acpd-11-20575-2011, 2011.

6. Borrego, C., Monteiro, A., Pay, M. T., Ribeiro, I., Miranda, A.I., **Basart, S.**, and Baldasano, J. M.: How bias-correction can improve air quality forecast over Portugal, Atmos. Environ., 45, 6629-664, doi: 10.1016/j.atmosenv.2011.09.006, 2011.

7. Folch, A., Costa; A., and **Basart, S.**: Validation of the FALL3D ash dispersion model using observations of the 2010 Eyjafjallajökull volcanic ash clouds, Atmos. Environ., In Press, Accepted Manuscript, doi:10.1016/j.atmosenv.2011.06.072, 2011.

8. Guirado, C., Cuevas, E., Cachorro, V., Mimouni, M., Zeudmi, L., Toledano, C., Alonso-Pérez, **S., Basart**, S., Blarel, L., Goloub, P., and Baldasano, J.M.: Preliminary characterization of columnar aerosol properties (AOD-AE) at the Saharan Tamanrasset (Algeria) station, Opt. Pura Apl., 44(4), 635-639, 2011.

9. Haustein, K., Pérez, C., Baldasano, J.M., Jorba, O., **Basart, S.**, Miller, R.L., Janjic, Z., Black, T., Nickovic, S., Todd, M. and Washington, R.: Atmospheric dust modeling from meso to global scales with the online NMMB/BSC-Dust model: 2. Regional experiments in North Africa, Atmos. Chem. Phys. Discuss., 11, 30273–30331, doi:10.5194/acpd-11-30273-2011, 2011.

10. Pay, M.T., Jiménez-Guerrero, P., Jorba, O., **Basart, S.**, Querol, X., Pandolfi, M., and Baldasano, J.M.: Spatio-temporal variability of concentrations and speciation of particulate matter across Spain in the CALIOPE modeling system. Atmos. Environ., In Press, Accepted Manuscript, doi:10.1016/j.atmosenv.2011.09.049, 2011.

11. Pérez, C., Haustein, K., Janjic, Z., Jorba, O., Huneeus, N., Baldasano, J.M., Black, T., **Basart, S.**, Nickovic, S., Miller, R.L., Perlwitz, J., Schulz, M. and Thomson, M.: Atmospheric dust modeling from meso to global scales with the online NMMB/BSC-Dust model – Part 1: Model description, annual simulations and evaluation, Atmos. Chem. Phys., 11, 13001-13027, doi:10.5194/acpd-11-13001-2011, 2011.

12. Kokkalis, P., Mamouri, R.E., Todua, M., Didebulidze, G.G., Papayannis, A., Amiridis, V., **Basart, S.**, Pérez, C., and Baldasano, J.M.: Ground, satellite and simulation-based analysis of a strong dust event over Abastumani, Georgia during May 2009, International Journal of Remote Sensing, Accepted Manuscript, 2012.

13. **Basart, S.**, Pérez, C., Nickovic, S., Cuevas, E., Schulz, M. and Baldasano, J. M.: Development and evaluation of BSC-DREAM8b dust regional model over Northern Africa, the Mediterranean and the Middle East regions, Tellus B, Sumitted Manuscript.

Chapter in Books

1. Pérez, C., Baldasano J.M., P. Jiménez-Guerrero, O. Jorba, K. Haustein, E. Cuevas, **S. Basart**, S. Nickovic, "Dust modeling and forecasting at the Barcelona Supercomputing Center: activities and developments. WMO/GEO Expert Meeting on an International Sand and Dust Storm Warning System". Barcelona, Spain, 7-9 Nov. IOP Conf. Ser.: Earth Environ. Sci. 7 012013 doi: 10.1088/1755-1307/7/1/012013, 2009.

International Congresses and Workshops

1. Baldasano, J.M., C. Pérez, O. Jorba, P. Jiménez-Guerrero, E. Cuevas, **S. Basart**, J.J. Bustos, S. Alonso-Pérez, S. Rodríguez, C. Marrero, M. Manso, M.A. Martínez, M. Velázquez, M. Palomares, X. Querol, J. Pey, L. Barrie, S. Nickovic, "WMO Sand and Dust Storm Warning System (SDS-WS) for Europe, Africa and Middle East: a GEO-oriented System". In the International Conference on "Secure and Sustainable Living: Social and Economic Benefits of Weather, Climate and Water Services", Madrid, Spain, 19-22 March, 2007.

2. Rodríguez, S., E. Cuevas, I. Toledo, **S. Basart**, P. Goloub, "An assessment of the AERONET aerosols size distribution by comparison with in-situ measurements at Izaña Global Atmospheric Watch Observatory: An analysis from clean-air to high Saharan dust concentration conditions". IUGG XXIV General Assembly, Perugia, Italy, 2-3 July, 2007.

3. Baldasano J.M., E. Cuevas, C. Pérez, O. Jorba, P. Jiménez-Guerrero, **S. Basart**, S. Alonso-Pérez, M.A. Martínez, X. Querol, J. Pey, L. Barrie, S. Nickovic, "WMO Sand and Dust Storm Warning System (SDS-WS) for Europe, Africa and Middle East: a

GEO-oriented System". 7th EMS Annual Meeting / 8th ECAM, Madrid, Spain, 1-5 October, 2007.

4. Cuevas, E., J.M. Baldasano, C. Pérez, X. Querol, **S. Basart**, M.Á. Martínez, O. Jorba, P. Jiménez, L. Barrie, S. Nickovic, "WMO Sand and Dust Storm Warning System (SDS-WS) for Europe, Africa and Middle East: a GEO-oriented System". In WMO/GEO Expert Meeting on an International Sand and Dust Storm Warning System, Barcelona, Spain, 7-9 November, 2007.

5. Pérez, C., J.M. Baldasano, P. Jiménez-Guerrero, O. Jorba, K. Haustein, E. Cuevas, **S. Basart**, S. Nickovic, "Dust modeling and forecasting at the Barcelona Supercomputing Center: activities and developments". In WMO/GEO Expert Meeting on an International Sand and Dust Storm Warning System, Barcelona, Spain, 7-9 November, 2007.

6. **Basart**, **S.**, C. Pérez, E. Cuevas, J.M. Baldasano, "Aerosol retrospective analysis over North of Africa, North-eastern Atlantic Ocean, Mediterranean and Middle East from AERONET sites". 10th IGAC conference 2008, Annecy, France, 7-12 November, 2008.

7. **Basart**, **S.**, C. Pérez, E. Cuevas, J.M. Baldasano, "Aerosol retrospective analysis for North of Africa, Northeastern Atlantic, Mediterranean and Middle East from AERONET sites". Third International Dust Workshop, Leipzig, Germany, 15-17 Setember, 2008.

8. **Basart**, **S.**, C. Pérez, E. Cuevas, J.M. Baldasano, "Evaluation of a regional mineral dust model over Northern Africa, Southern Europe and Middle East with AERONET data". European Geosciences Union EGU 2009 Conference, Vienna, Austria, 20-24 April, 2009.

9. **Basart**, **S.**, C. Pérez, E., J.M. Baldasano, "Verification of a Sand and Dust Storm (SDS) forecast model for North Africa, Europe and Middle East with AERONET data". Atmospheric Science Conference, Barcelona, Spain, 7-11 September, 2009.

10. Balis, D., Giannakaki, E., Amiridis, V., Pérez, C., **Basart, S.**, "Saharan dust observations over Thessaloniki using backscatter/Raman lidar and BSC/DREAM model". International Symposium on Tropospheric Profiling: Needs and Techonologies, Delft, the Netherlands, 18-23 October, 2009.

11. C. Pérez, K. Haustein, O. Jorba, Z. Janjic, **S. Basart**, J.M. Baldasano, "Atmospheric mineral dust modeling from meso to global scales with the NMMB/BSC-DUST". AAAR, 28th Annual Conference, Minneapolis, USA, 26-30 October, 2009.

12. Cuevas E., J.M. Baldasano, M. Schulz, S. Nickovic, C. Pérez, **S. Basart**, K. Serradell, D. Carrio, E. Terradellas, L. Barrie."The Regional Sand and Dust Storm Warning Advisory and Assessment System Regional Center for Northern Africa, Europe and Middle East". WMO-CAS XV, Incheon, Republic of Korea, 16-17 November, 2009.

13. Baldasano J.M., M. Piot; O. Jorba; M. Goncalves; M.T. Pay; **S. Basart**; P. Jiménez and S. Gassó. "CALIOPE: an Operational Air Quality Forecasting System for Europe and

Spain". Mesoscale Modelling For Air Pollution Applications: Achievements And Challenges (COST 728 Final Workshop), Organisers: COST 728, WMO/GURME and MEGAPOLI, Geneva, Switzerland, 25-26 February, 2010.

14. Pay, M.T., M. Piot, O. Jorba, **S. Basart**, S. Gassó, D. Dabdub, P. Jiménez-Guerrero, J.M. Baldasano. "Chemical Composition of Particulate Matter in Spain: Modeling Evaluation of the CALIOPE System for 2004". European Geosciences Union EGU 2010 Conference, Vienna, Austria, 2-7 May, 2010.

15. **Basart S.**, M.T. Pay, M. Piot, C. Pérez, E. Cuevas, O. Jorba, J.M. Baldasano. "Aerosol Optical Depth over Europe: Evaluation of the CALIOPE air quality modelling system with direct-sun AERONET observations". European Geosciences Union EGU 2010 Conference, Vienna, Austria, 2-7 May, 2010.

16. Piot M., M.T. Pay, O. Jorba, **S. Basart**, S. Gassó, X. Querol, M. Pandolfi, J.M. Baldasano and the DAURE team. "Preliminary Modelling Results of the Chemical Composition of Particulate Matter in NE Spain for the DAURE Campaign". European Geosciences Union EGU 2010 Conference, Vienna, Austria, 2-7 May, 2010.

17. Guirado C., E. Cuevas, V. Cachorro, M. Mimouni, L. Zeudmi, C. Toledano, S. Alonso, **S. Basart**, L. Blarel, P. Goloub, J.M. Baldasano. "Preliminar characterization of columnar aerosols properties (AOD-AE) at the Saharan Tamanrasset (Algeria) station". 37th Annual European Meeting Atmospheric Studies Optical Methods, Valladolid, Spain, 23-27 August, 2010.

18. Cuevas E., J.M. Baldasano, C. Pérez, C. Camino, E. Terradellas, **S. Basart**, K. Serradell. "Service chain analysis in support to health community O-INT_3.1 Core requirements to support forecast of meningitis". Second MACC Assembly, Toulouse, France, 18-22 October, 2010.

19. Baldasano, J. M., M. T. Pay, O. Jorba, J. Ortiz, M. Gonçalves, **S. Basart**, S. Gassó, P. Jiménez-Guerrero. "Evaluation of the Spanish operational air quality forecasting system: diagnostic and near real time". International Workshop on Air Quality Forecasting Research, Québec, Canada, 16-18 November, 2010.

20. Terradellas, E., J.M. Baldasano, **S. Basart**, F. Benincasa. "WMO SDS-WAS. Regional Center for Northern Africa, Middle East and Europe". 9th EARLINET-ASOS Workshop, Evora, Portugal, 7-9 February, 2011.

21. Folch, A., **S. Basart**, A. Costa. "Modeling and forecasting the Eyjafjallajökull volcanic ash cloud using the FALL3D ash dispersion model", European Geosciences Union EGU 2011 Conference, Vienna, Austria, 3-8 April, 2011.

22. **Basart, S.**, M.T. Pay, C. Pérez, O. Jorba, J.M. Baldasano. "Aerosol surface levels, chemical composition and optical depth over Europe in the CALIOPE air quality modelling system". European Geosciences Union EGU 2011 Conference, Vienna, Austria, 3-8 April, 2011.

23. Haustein K., C. Pérez, J.M. Baldasano, **S. Basart**, R.L. Miller, Z. Janjic, T. Black, S. Nickovic, M. Todd, R. Washington, Y. Govaerts. "A model for prediction of mineral

dust from meso to global scales: Regional experiments for North Africa", European Geosciences Union EGU 2011 Conference, Vienna, Austria, 3-8 April, 2011.

24. Borrego, C., A. Monteiro, I. Ribeiro, A.I. Miranda, M. T. Pay, **S. Basart**, J. M. Baldasano. "How different air quality forecasting system (should) operate over Portugal?", 14th Conference on Harmonisation within Atmospheric Dispersion Modelling for Regulatory Purposes, Kos, Greece, 2-6 October, 2011.

National conferences

1. Piot M., M. T. Pay, O. Jorba, **S. Basart**, S. Gassó, X. Querol, M. Pandolfi, A. Alastuey, D. Dabdub, J. M. Baldasano. "Evaluating the CALIOPE air quality modelling system: gas-phase chemistry and chemical composition of particulate matter over Iberian Peninsula for 2004 at high horizontal". Segones Jornades de Meteorologia i Climatologia de la Mediterrània Occidental, Valencia, Spain, 11-12, March 2010.

Projects and collaborations

1. The Spanish Ministry of the Environment and Rural and Marine Affairs (Ministerio de Medio Ambiente y Medio Rural y Marino) project called: "MEJORA DEL MODELO REGIONAL ATMOSFERICO DE POLVO MINERAL (DREAM) PARA LA PREDICCION DE EVENTOS DE POLVO SAHARIANO EN EL MEDITERRANEO Y LAS ISLAS CANARIAS" with reference CGL2006-11879.

2. The Spanish Ministry of Education and Science (Ministerio de Educación y Ciencia) project called: CALIOPE with reference 157/PC08/3-12.0.

3. The World Meteorological Organization (WMO; www.wmo.int) initiative called Dust Storm Warning Advisory and Assessment System (SDS-WAS; http://sds-was.aemet.es/) Programme.

4. The Institute of Marine Science of the Spanish National Research council (CSIC) project called: "Aerosol deposition and ocean plankton dynamics (ADEPT)".

5. The Monitoring Atmospheric Composition & Climate (MACC) Project (MACC O-INT Work-Package 3.1): "Meningitis linked to mineral dust transport in the Sahel".

Contents

Chapter 1

1 Introduction

Mineral dust is recognized as one of the most abundant aerosols globally. Dust storms have a number of impacts upon the environment including radiative forcing, and biogeochemical cycling. They transport material over many thousands of kilometres. They also have a range of impacts on humans, not least on human health. Dust storms and associated mineral aerosol transport are mainly driven by meso and synoptic scale atmospheric processes. It is therefore essential that the dust aerosol process and background atmospheric conditions that drive the dust emission and atmospheric transport be represented by means of aerosol models with sufficiently well resolved spatial and temporal resolution.

The present chapter provides an overview of aerosols (focusing on desert dust) and its effects as well as a revision of the state-of-art of the dust regional numerical models. The present Ph.D. thesis is developed in the framework of the experience at the Earth Sciences department of the Barcelona Supercomputing Center–Centro Nacional de Supercomputación (BSC-CNS). Therefore, the latest developments and current activities in the field of sand and dust storm modelling and forecasting in the research group are also revised.

1.1 A general description of aerosols

Aerosol is a term derived from the fact that matter "floating" in air is a suspension (a mixture in which solid or liquid or combined solid-liquid particles are suspended on a fluid, i.e. liquid or gas). Aerosol particles range in size from molecular clusters on the order of 1 nm to 100 μm (Figure 1.1). The stable clusters formed by homogeneous nucleation and the smallest solid particles that compose agglomerates have a significant fraction of their molecules in the surface layer. The size of aerosol particles is usually given as the radius of the particle (assuming a spherical shape). Aerosols are usually assigned into one of the following four size categories:

- *Nucleation* mode: 0.001 - 0.01 μm radius
- *Aitken* mode: 0.01 - 0.1 μm radius
- Large particles, or *accumulation* mode: 0.1 - 1 μm radius
- Giant particles, or *coarse* particle mode: > 1 μm radius

Aerosols are formed by the conversion of gases to particles, the disintegration of liquids or solids, or the resuspension of powdered material. Aerosol formation from a gas results in much finer particles than disintegration processes (except when condensation takes place directly on existing large particles). Dust, smoke, fume, haze, and mist are common terms for aerosols. Mists are composed of liquid droplets. Dust usually refers to solid particles produced by disintegration, while smoke and fume particles are generally smaller and formed from the gas phase.

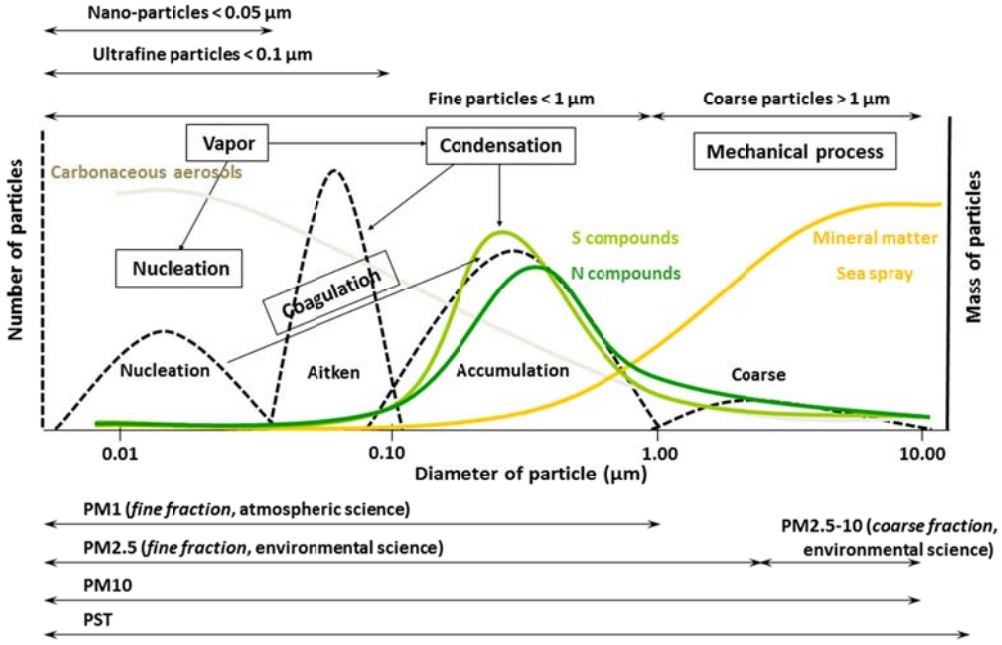

Figure 1.1 *Relationship between particulate matter (PM), size, number of particles (discontinuous line), and chemical mass composition (solid line). Aerosol physical processes are represented in boxes. Adapted from Warneck (1988) and Harrison and van Grieken (1998).*

Atmospheric aerosol consists of material emitted directly from sources (primary component, for instance, sea-salt, mineral aerosols -or dust-, volcanic dust, smoke and soot, some organics), and material formed by gas-to-particle conversion in the atmosphere (secondary component, for instance, sulfates, nitrates, and some organics). The secondary component is usually the result of chemical reactions which take place in either the gas or aerosol phases. These atmospheric aerosols can be emitted by a great variety of natural and anthropogenic sources resulting in a large variability of their chemical characteristics. The removal of particulate material from the atmosphere takes place by dry or wet deposition.

The different types of aerosols display different microphysical and optical properties. Examples of the global distribution of anthropogenic and natural aerosols have been derived from a variety of sensors such as Multi-angle Imaging SpectroRadiometer (MISR) instrument (Figure 1.2). These maps were generated from data acquired during the December 2001 through November 2002 time period. The southern tropical Atlantic is dominated by clean maritime air. The central African coast is a relatively well-defined region covered by smoke from biomass burning in Africa during wintertime. The Northern tropical Atlantic is under heavy mineral dust influx from Africa and the Northern Atlantic is impacted by anthropogenic aerosols from North America and Europe.

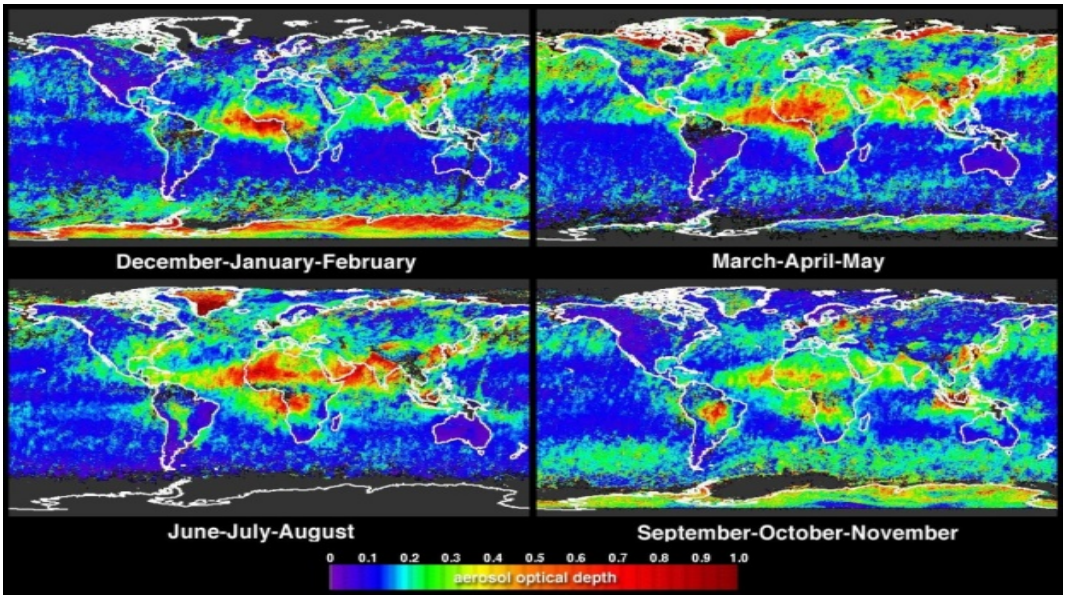

Figure 1.2 *Seasonal global aerosol amount, expressed as AOD in MISR's green spectral band (558 nm) Extracted from NASA Langley Atmospheric Sciences Data Center (http://eosweb.larc.nasa.gov/).*

So, atmospheric particles vary greatly in sources, production mechanisms, sizes, shapes, chemical composition, amount, distribution in space and time, but also in how long they survive in the atmosphere (i.e., lifetime). The lifetime of an atmospheric particle ranges from less than 1 h for nuclei mode aerosols to some days for aerosols in accumulation mode. Coarse particles can be suspended in the atmosphere from some few days (for the smallest particles, < 2 μm) to some few minutes for very large particles (> 40 μm).

For many applications aerosols can be characterized sufficiently by measuring aerosol optical depth (AOD), composition, particle size distribution and shape (consequently single

scattering albedo, phase function and asymmetry factor). Concerning the chemical composition, the aerosols can be found as individual chemical species such us sea salt (NaCl), sulfate (SO_4^{2-}), nitrate (NO_3^-), soot (elemental carbon) and minerals (e.g., quartz, SiO_4) or as multi-component aerosols, which are complex compounds make-up of many chemical species. The chemical composition of the atmospheric aerosol can be used to resolve its sources, natural or anthropogenic, by a method based on chemical signatures. On the other hand, aerosol properties that are used to assess climate and visibility impacts can be divided in two groups: "Extensive properties", which depend on the aerosol concentration, and "intensive properties" independent of the amount of the aerosol present (Ogren, 1995).

Also, particulate matter (PM) is usually classified into three categories depending on their size: PM_{10}, $PM_{2.5}$ and PM_1 comprise particles with an aerodynamic diameter less than or equal to 10, 2.5 and 1 μm, respectively. Measurements of PM_{10} are considered to represent the "thoracic" fraction of the ambient particles. $PM_{2.5}$ is the finer "alveolar" fraction. PM_1 fraction provides, better than $PM_{2.5}$, information on the particle sources, as PM_1 represents in reasonable approximation combustion particles and secondary aerosol, while PM_{10}-PM_1 can be attributed to mechanically-produced and geogenic particles (Rodríguez et al., 2011).

The optical properties of aerosols are responsible for many spectacular atmospheric effects, such as richly coloured sunsets, corona, halos and rainbows. It also plays an important role in visibility and affects the Earth's radiation balance. These optical effects caused by aerosols are a direct result of the scattering and the absorption of light by aerosol particles. Aerosol particles that are illuminated by a beam of light scatter and absorb some of that light and thereby diminish the intensity of the beam. This process is called extinction and deals only with the attenuation of light along an axis. While all aerosol particles will scatter light, only those made of absorbing material will absorb light. The scattering of light by very small particles (less than 0.05 μm in diameter) is described in relatively simple terms by Rayleigh's theory, the theory of molecular scattering. The scattering by large particles, those greater than 100 μm, can be analysed readily by geometric optics, the tracking of refracted rays of light through the particle. In between these sizes, we find the Mie scattering region. In this size range, where particle size and the wavelength of light have the same order of magnitude, the scattering of light by aerosol particles is a complicated phenomenon.

The interaction of aerosol particles and light forms the basis for an important class of instruments used for measuring aerosol particle size and concentration. AOD or aerosol optical thickness (AOT; as it is normally named by the space remote sensing community) is the basic parameter in the study of optical properties of aerosols. This parameter provides an estimation of the amount of aerosols in the atmospheric column. Namely, it is the

degree to which aerosols prevent the transmission of light and is defined as the integrated extinction coefficient over a vertical column of unit cross section. Extinction coefficient is the fractional depletion of radiance per unit path length. The spectral dependence of the AOD is related to the particle size and it is possible to be fit from the Ångström's law ($AOD_\lambda \sim \lambda^{-\alpha}$) (Ångström, 1929). The lowest values of Ångström parameter (α) are associated to large particles, in which the extinction doesn't have spectral dependency, whereas the highest values are associated to the fine particle presence, whose scattering has a strong spectral dependency.

Atmospheric aerosols are a fundamental component of the Earth's atmospheric chemistry and radiative balance. They influence climate directly and indirectly. They directly affect radiation transfer on global regional scales directly through scattering and absorbing various radiation components and indirectly, by modifiying the optical properties and lifetime of clouds. Indirect effects result from their role as cloud condensation nuclei (CNN) in changing droplet size distributions that affect the optical properties of clouds and precipitation. Aerosol distribution is also essential information in the study of the Earth's climate and biochemical cycles, for climate change assessment, and for the atmospheric correction of satellite remote sensing data.

Effects of the atmospheric aerosol on human health have led to the establishment of ambient air-quality standards. Adverse health effects have stimulated many controlled studies of aerosol inhalation by humans and animals. Recently, Domínguez-Rodríguez et al. (2011) have concluded that the exposure to ultrafine particles is risk factor that precipitates admission by heart failure.

There is much uncertainty concerning the chemical components of the atmospheric aerosol that produce adverse health effects detected in epidemiological studies (WHO, 2005; Pope et al., 2009). Increasing amounts of potentially harmful air pollutants are being emitted into the atmosphere exerting stress on the natural environment, with impacts at local, regional and global scales (Baldasano et al., 2003). Information on the concentrations of particulates, the emissions sources, transport and sinks are required by public agencies responsible for monitoring environmental hazards to human health, and in the formulation of policy on local and transboundary pollution. Although much of the anthropogenic or natural components arise in urban or arid regions such as deserts, it is often advected across national boundaries and affects remote environments.

Table 1.1 *Comparison between air quality standards of PM_{10} and $PM_{2.5}$ (in $\mu g/m^3$).*

	Average Time	WHO	EU	NAAQS	CAAQS
PM_{10}	1 year	20	40	-	20[a]
	24 h	50	50	150	50
$PM_{2.5}$	1 year	10	25[b]	15	12
	24 h	25	-	35	-

a: geometric average
b: with effect from 1 January 2015.

Numerous instances recommend or impose levels for air pollutants such as PM_{10} and $PM_{2.5}$. In addition, ultrafine particles (particles smaller than 0.1 μm) have recently attracted significant scientific and medical attention although there aren't sufficient evidences to establish a limit value. The World Health Organization (WHO) establishes Guideline Values (GV), European Union (EU) establishes Limit Values for Air Quality (LVAQ) for its States Members and in the United States, the Environmental Protection Agency (EPA) establishes National Ambient Air Quality Standards (NAAQS) and the Air Resources Board of California establishes California Ambient Air Quality Standards (CAAQS) more restrictive than EPA standards. Table 1.1 shows a comparison between several air quality standards for PM_{10} and $PM_{2.5}$.

1.2 The scientific context

1.2.1 Desert dust in the global system

With the possible exception of sea-salt aerosol, the mineral dust loading in the atmosphere is the most abundant of all aerosol species (IPCC, 2001). On the global scale, dust mobilization appears to be dominated by natural sources (Tegen et al., 2004). Due to the prevalence of arid surfaces with reduced vegetation cover and high winds, much of the observed atmospheric dust is derived from susceptible surfaces within dryland regions (e.g., Prospero et al., 2002). Prospero et al. (2002) argue that topographic lows are the predominant sources of atmospheric desert dust because they are regions into which water transports soil, thus providing a source of soil particles which are easily wind eroded.

Conventionally dust refers to soil particles < 0.6 mm, but in practice only those particles below 0.1 mm (100 μm) can be transported by suspension and be present in a dust cloud. In aerosol science, dust alludes to airborne mineral particles and not to household dust, which contains a high percentage of synthetic particles, such as lint. As it is summarized by Squires (2001), dust particles move in one of three modes of transport depending on

particle size, shape and density of the particle, designated as suspension, saltation and creep (Figure 1.3). The suspension mode includes dust particles < 0.1 mm in diameter and also clay particles (2 μm). The fine particles may be transported at high altitudes (6 - 8 km) and over distances of thousand kilometers. Saltating particles (i.e. 0.01 < diameter < 0.5 mm) leave the surface, but are too large to be suspended. The remaining particles (> 0.5 mm) are transported in the creep mode. These roll along by the wind impacting particles upon the land surface, favoring the movement of other particles.

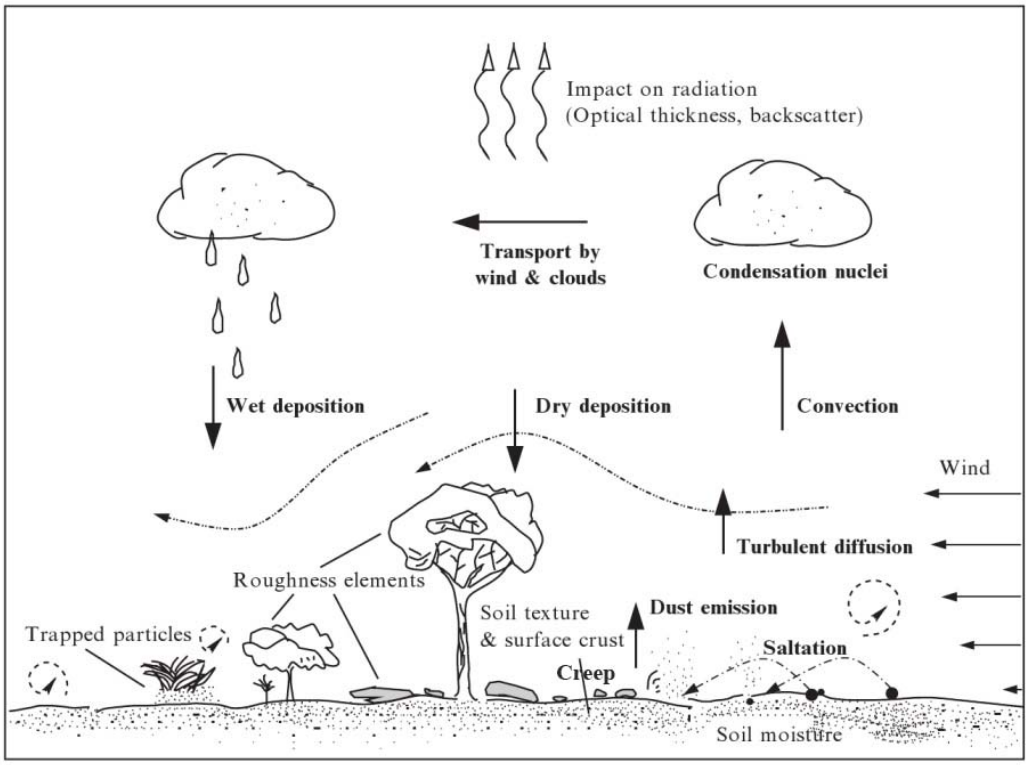

Figure 1.3 *Physics and modelling of wind erosion: entraiment, transport, deposition and impact on radiation and clouds of the desert dust. Atmospheric conditions, soil properties, land-surface characteristics and land-use practice control the erosion process. Adapted from Shao (2008).*

In the atmosphere, dust is moved by the prevailing winds and transported vertically by convective processes, as well as adiabatic vertical motion associated with frontal systems. Atmospheric dust settles to the Earth's surface both through molecular and gravitational settling (dry deposition) and wet deposition with precipitation (Figure 1.3). In dry deposition process, large particles sediment out more quickly than smaller particles, which leads to a shift towards smaller particle sizes during transport. Wet deposition can occur either below a cloud, when raindrops, snowflakes or hailstones scavenge dust as they fall or

within a cloud when dust particles are captured by water droplets and descend to surface by rain. Wet deposition can sometimes be manifested in the phenomenon of "blood rains". Dust atmospheric lifetime depends on the particle size, ranging from a few hours for particles larger than 10 μm, to up to several weeks for sub-μm sized dust particles.

A tool that has become increasingly important in recent years for identifying, tracking and analysing large-scale dust events and for the validation and improvement of dust models are remote sensing techniques. The increased spectral, spatial and temporal resolution of the new generation of satellite sensors as Polarization and Directionality of the Earth's Reflectances (POLDER), Spinning Enhanced Visible and InfraRed Imager (SEVIRI), Moderate-resolution Imaging Spectroradiometer (MODIS), Cloud-Aerosol Lidar and Infrared Pathfinder Satellite Observation (CALIPSO) and MISR (see Figure 1.2) have provided greater insights into dust distributions.

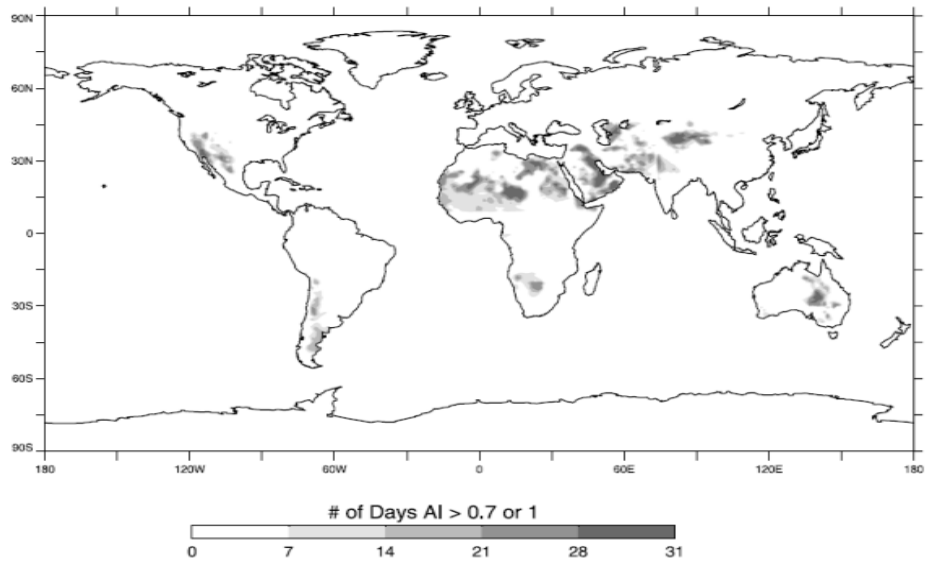

Figure 1.4 *The global distribution of TOMS dust sources. This Figure is a composite of selected monthly mean TOMS Aerosol Index (AI) frequency of occurrence distributions for specific regions using those months which best illustrate the configuration of specific dust sources. Extracted from Prospero et al. (2002).*

Satellite images give a global picture of dust storm activity, provide information on areas for which there are no meteorological station data, allow the tracking of individual dust plumes, enable sources of dust to be located and give information on parameters such as AOD. Figure 1.4 shows the global distribution of dust sources as derived from the Total Ozone Mapping Spectrometer (TOMS) sensor which suggests that the major source regions of contemporary mineral dust production are found on the desert regions of the

Northern Hemisphere, in the broad "*dust belt*" that extends from the eastern subtropical Atlantic eastwards through the Sahara Desert to Arabia and southwest Asia. There is remarkably little large-scale dust activity outside this region. In particular, the Southern Hemisphere is devoid of major dust activity (Prospero et al., 2002; Washington et al., 2003; Engelstaedter and Washington, 2007a). There is a large zone with high dust production in central Asia, centred over the Taklamakan Desert in the Tarim Basin. Central Australia has a relatively small zone, located in the Lake Eyre Basin. Southern Africa has two zones, one centered on the Mkgadikgadi basin in Botswana and the other on the Etosha Pan in Namibia. In Latin America, there is only one easily identifiable zone, this is in Atacama located in the vicinity of one of the great closed basins of the Altiplano – the Salar de Uyuni. North America has only one relatively small zone with high values, located in the Great Basin.

Estimates of the total soil dust emissions to the atmosphere on a global scale show a wide range of values (Zender et al., 2004). These uncertainties arise from the fact that the dust cycle is currently estimated using models that are constrained by available measurements and retrievals. The Saharan sources are considered by far the most active ones in the world (Brooks, 1999; Washington et al., 2003; Ginoux et al., 2004; Kaufman et al., 2005). Estimates of the amount of dust exported annually are still not reliable, but some studies suggest that an annual production of 1000 - 3000 $Tg \cdot yr^{-1}$ (Zender et al., 2004; Cakmur et al., 2006) with the largest contributions emitted from the North African (50 - 70%) and Asian deserts (10 - 25%) and probably accounts for almost half of all the aeolian material supplied to the world's oceans (e.g. Hand et al., 2004; Fan et al., 2006).

There is a large temporal and spatial variability in dust emissions in the dust belt. As shown in Figure 1.5, in North Africa the maximum dust transport occurs in summer (Prospero and Nees, 1986; Perry et al., 1997; Moulin et al., 1998; Prospero, 1999; Rodríguez et al., 2001a; Prospero et al., 2002; Barnaba and Gobbi, 2004). Dust is transported from the Sahara over the Atlantic, often reaching the Caribbean (Prospero and Nees, 1986), southern Florida (Prospero, 1999); and the eastern United States as far north as New England (Perry et al., 1997). There is also considerable transport in winter months when large quantities of dust are carried into the Caribean and South America (Prospero et al., 1981; Swap et al., 1992). In Middle East, activity peaks in late spring and summer and is at a minimum in winter. Over the Indian subcontinent, dust activity increases in spring and decreases in summer with the onset of the southeast monsoon. In Asia, dust activity peaks in spring (Prospero et al., 2002; Goudie and Middleton, 2006). Asian dust often crosses the Pacific to North America, resulting in significant concentrations over large areas (VanCuren, 2003). One dust event from China is documented to have continued across the Atlantic and deposited measurable dust amounts in the Alps (Grousset et al., 2003).

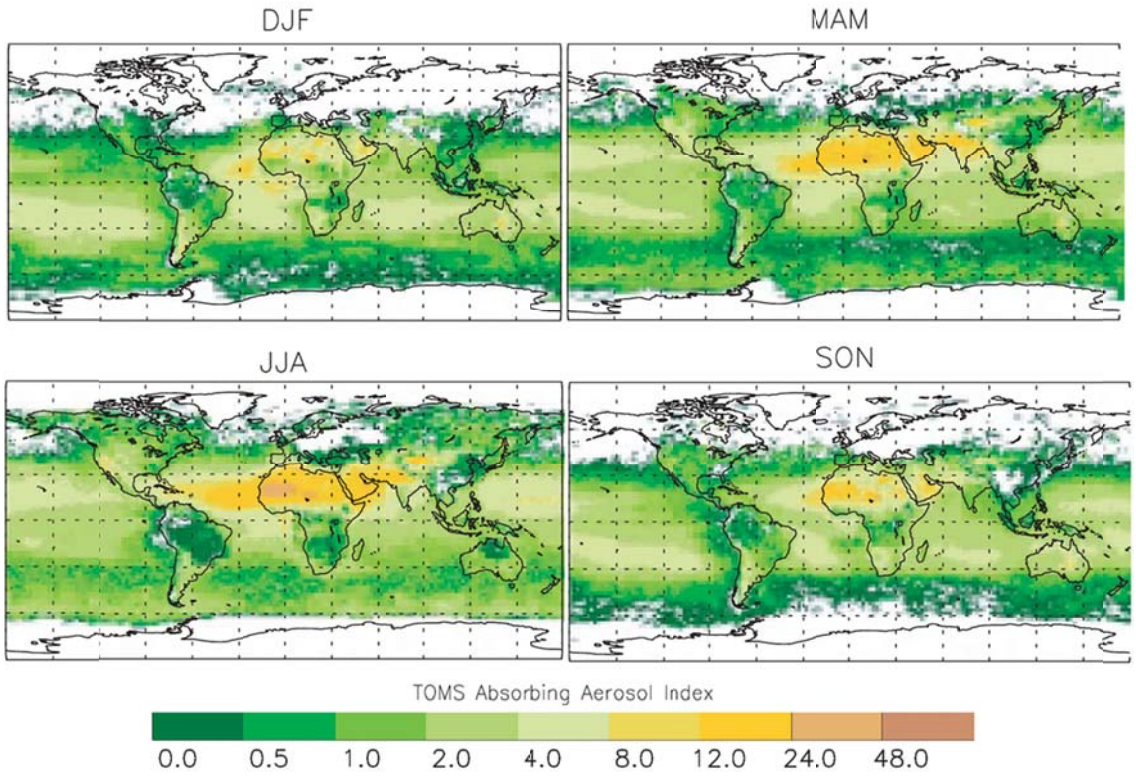

Figure 1.5 *Seasonal distribution with the remotely sensed absorbing Aerosol Index (AI) from TOMS, averaged for 5 years (1986 – 1990). Areas of high contributions of absorbing black carbon aerosol and cloud cover were excluded from the TOMS AI result. Adapted from Tegen et al. (2003).*

The domination of large particles ($r > 0.6$ μm) in desert dust aerosol is the principal feature differentiating the optical properties of dust from fine-mode dominated biomass burning and urban–industrial aerosols (Dubovik et al., 2002, see Figure 1.6). The dust size distribution shows a dominant coarse mode at 1 - 5 μm and a secondary mode around 0.5 μm of effective radius (Pinker et al., 2001; Tanré et al., 2001; Rodríguez et al., 2007; Rodríguez et al., 2011). Due to the domination of large particles, desert dust scattering increases or is neutral with λ, while absorption of solar radiation is very weak for wavelengths greater than 550 nm. However, dust exhibits a pronounced absorption in the blue spectral range (Dubovik et al., 2002). Measurements during the Puerto Rico Dust Experiment (PRIDE) show large mode sizes (typically 3.5 μm) for dust that has travelled from North Africa to Puerto Rico (Reid et al., 2003; Grini and Zender, 2004). Comparisons of the size distribution of African dust measured in the Canary Islands off the coast of West Africa with those in Puerto Rico show only a relatively minor shift to smaller sizes after a transport of about 4000 km (Maring et al., 2003). While typically the

dust mass median diameter is relatively small, large dust particles (> 75 μm) have been transported to great distances over remote ocean regions (Betzer et al., 1988).

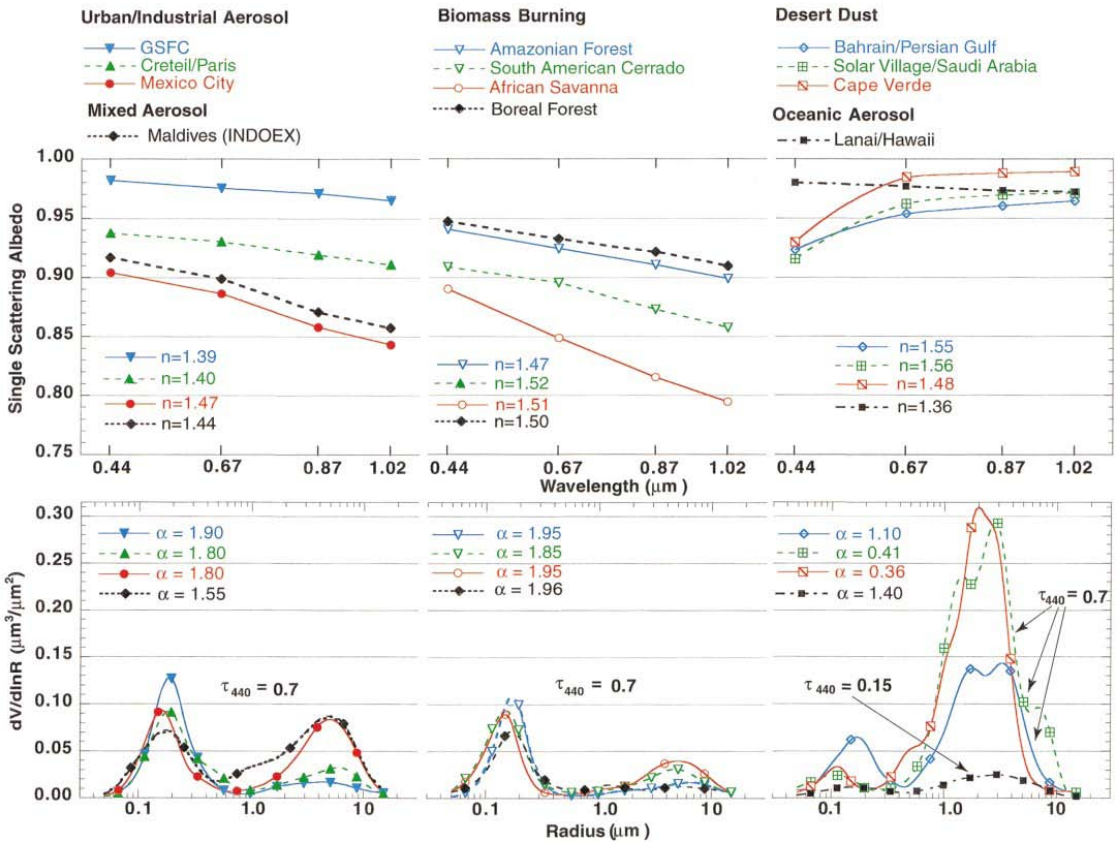

Figure 1.6 *The averaged optical properties of different types of tropospheric aerosol retrieved from the worldwide AERONET network of ground-based sunphotometers. Urban–industrial, biomass burning, and desert dust aerosols are shown for* $\tau_{ext}(440) = 0.7$. *Oceanic aerosol is shown for* $\tau_{ext}(440) = 0.15$ *since oceanic background aerosol loading does not often exceed 0.15. Also,* $\omega_0(\lambda)$ *and the refractive index n shown for Bahrain was obtained only for the cases when* $\alpha \leq 0.6$ *(for higher* α, $\omega_0(\lambda)$ *and refractive index n were very variable due to a significant presence of urban–industrial aerosol). However, we show the particle size distribution representing all observations in Bahrain (complete range of* α*). Ångström parameter* α *is estimated using optical thickness at two wavelengths: 440 and 870 nm. Extracted from Dubovik et al. (2002a).*

As for any type of atmospheric aerosol particles, the environmental and climatic impacts of mineral dust depend on its physico-chemical properties, that is, composition, shape, size and mixing state of the particles (Raes et al., 2000). Mineral dust consists of irregular particles, often aggregates of different composition, of sizes varying from tenths of nanometers to hundreds of microns. The size distribution evolves rapidly according to time after emission (Pye, 1987).

Atmospheric aerosols are known to impact the climate evolution but they still represent one of the largest uncertainties in climate change studies (IPCC, 2007). Among the different aerosol types, mineral dust is one of the major contributors to Earth's radiative budget, since its radiation backscattering is very important. It can also impact the terrestrial irradiance especially over the sources due to relatively large size of the dust particles which interact efficiently with terrestrial radiation. Mineral dust modifies the transfer of solar radiation (spectral range: 0.3 – 3 μm wavelength) through the atmosphere by scattering and absorption processes. Depending on the size distribution, chemical composition and shape of the dust particles (which determine their optical properties: extinction coefficients, single scattering albedo and phase functions), and furthermore depending on the vertical position/extent of the dust layer and the local surface albedo, the mineral dust particles may have a positive (heating of climate system) or negative (cooling) radiative forcing (e.g. Claquin et al., 1999; Sokolik and Toon, 1999; Tanré et al., 2003). Many studies have explored the radiative forcing of mineral dust (e.g., Tegen et al., 1996; Perlwitz et al., 2001; Tanré et al., 2003; Meloni et al., 2004; Derimian et al., 2006; Balkanski et al., 2007; Tegen et al., 2010) with a wide range of results. In the global annual average dust net radiative forcing at the top of the atmosphere is most likely negative (i.e., inducing a cooling) for desert dust (Kaufman et al., 2001; Dubovik et al., 2002; Horvath et al., 2002; di Lorio et al., 2003; Balkanski et al., 2007; Yoshioka et al., 2007), but regionally positive values may occur over bright surfaces like snow-covered or desert areas (Tegen et al., 1996; Hansen et al., 1997).

Numerous studies show the changes in the top-of-atmosphere (TOA) radiative flux as consequence of the presence of dust using results of global simulations. There still is a considerable uncertainty in these dust radiative forcing estimates (Balkanski et al., 2007). The Fourth Assessment Report (IPCC, 2007) reported that the Dust Radiative Effect (DRE) due to mineral aerosols lies in the range of -0.56 to +0.1 W m^{-2}. Case studies of instantaneous dust net radiative forcing during individual dust events find negative TOA values higher than −6 W m^{-2} (Christopher and Jones, 2007; Zhu et al., 2007) or negative values larger than −400 W m^{-2} at the surface (Costa et al., 2006).

Modelling studies and satellite retrievals do not agree on the amplitude and/or sign of the direct radiative perturbation from dust. Modelling studies have systematically overpredicted mineral dust absorption compared to estimates based upon satellite retrievals. One cause of uncertainties in computations of the direct radiative forcing of dust aerosol is the lack of information on the wavelength−dependent complex refractive index of dust particles from different source regions of the world (Balkanski et al., 2007). Therefore, there is a clear need for better measuring the dust physical and optical properties within the solar and the

terrestrial spectrum. Furthermore, the knowledge of the aerosol vertical distribution of desert dust is critical for a correct estimate of the radiation profiles in the troposphere.

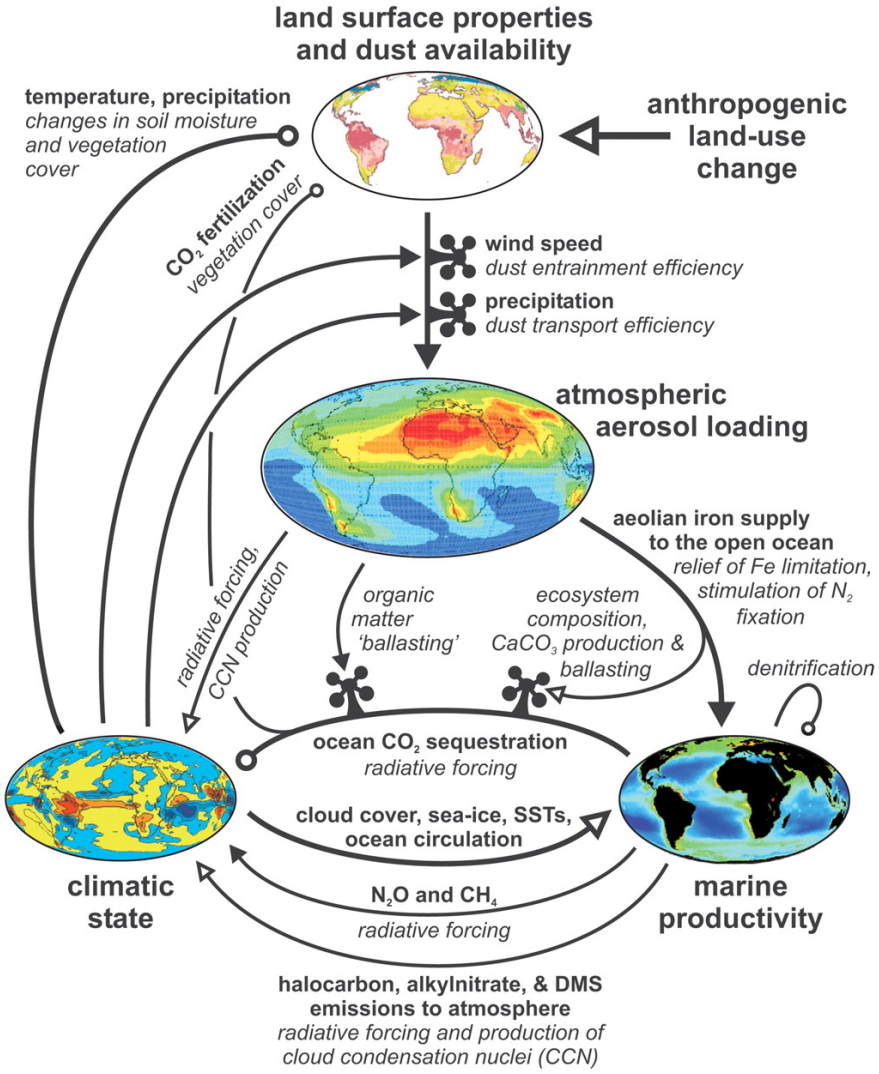

Figure 1.7 *Schematic view of global iron and dust connections. Highlighted are the four critical components (clockwise from top): the state of the land surface and dust availability, atmospheric aerosol loading, marine productivity, and some measure of climatic state (such as mean global surface temperature). The sign of the connections linking these varies; where the correlation is positive, the line is terminated with a solid arrowhead. Where the correlation is negative, the termination is an open circle. Connections with an uncertain sign are terminated with an open arrowhead. The mechanism by which the link acts is displayed in italics. Finally, the "water tap" symbols represent a secondary mechanism modulating the effect of a primary mechanism. Extracted from Jickells et al. (2005).*

In addition to direct effects, dust also has an indirect effect on the weather (Figure 1.7). The indirect effect of dust on cloud formation and precipitation still has uncertainties

(Mahowald et al., 2003). The interaction of dust with clouds is not well understood, partly because, in general, aerosol-cloud interactions are not well understood, and particularly because of a dearth of cloud microphysical measurements in dusty regions. Mineral dust modifies the size distribution and the phase of cloud particles by acting as CCN and as ice nuclei (IN). This may in turn affect indirectly the atmospheric radiative balance and thus weather and climate (IPCC, 2007; Zeng et al., 2009), as well as the development of precipitation (Levin and Cotton, 2008). One the one hand, mineral dust generates large concentrations of CCN (Rosenfeld et al., 2001) mostly in the small size range that can lead to cloud formation dominated by small droplets. As a result, this could lead to droplet coalescence reduction and suppressed precipitation (Teller and Levin, 2006). On the other hand, mineral dust coated with sulphate and other soluble materials as nitrates can generate large CCN (Levin et al., 1996; Li and Shao, 2009) and consequently large drops, which would accelerate precipitation development through a droplet growth by collection. Additionally, by the so-called semidirect effect dust affecting the thermal atmospheric structure can modify cloud formation (Hansen et al., 1997). Mineral dust may affect air temperatures through the absorption and scattering of radiation (Li et al., 1996; Moulin et al., 1997; Miller and Tegen, 1998, Pérez et al., 2006a). Additionally, dust affects photolysis rates and ozone chemistry by modifying the ultraviolet (UV) radiation (Dentener et al., 1996; Martin et al., 2003; Liao et al., 2004). Mineral dust particles are particularly known to act as efficient heterogeneous IN (e.g. DeMott et al., 2003; Klein et al., 2010).

Furthermore, the entrainment, transport and deposition of dust can present a variety of problems to inhabitants in and around desert areas such as deaths and damage caused in traffic accidents, road disruption, aviation operations and impacts in the human health, such us allergies, respiratory diseases and eyes infections (WHO, 2005). It is also thought to be linked to health risks, such as epidemics of lethal meningitis in the semi-arid sub-Saharan territory known as the Sahel belt (Thomson et al., 2006; Pérez, 2010; Pérez et al., 2011a) and increased incidences of paediatric asthma attacks in the Caribbean (Gyan et al., 2005). Since iron is an important micronutrient, deposition of iron in mineral aerosols (Fung et al., 2000) can impact the carbon cycle and atmospheric CO_2 (Jickells et al., 2005). Moreover, desert dust deposition also influences the biochemical cycles (Figure 1.7) of both oceanic and terrestrial ecosystems (Tegen and Fung, 1995; Okin et al., 2004; Mahowald et al., 2005; Aumont et al., 2008).

1.2.1.1 African Dust

African dust has an important impact on climatic processes, nutrient cycles, soil formation and sediment cycles. These influences spread far beyond Africa, thanks to the great distances over which African dust is transported as it has been observed from satellite

observations (e.g. Dulac et al., 1992; Moulin et al., 1998; Israelevich et al., 2002; Ginoux and Torres, 2003; Legrand et al., 2004; Thieuleux et al., 2005; Ben-Ami et al., 2010; Christopher and Jones, 2010). Studies based on the inspection of satellite images (Middleton and Goudie, 2001; Prospero et al., 2002; Washignton et al., 2003; Schepanski et al., 2007; Koven and Fung; 2008) suggest that there are two major source areas in Africa: the Bodélé Depression and an area covering eastern Mauritania, western Mali and southern Algeria (Figure 1.4).

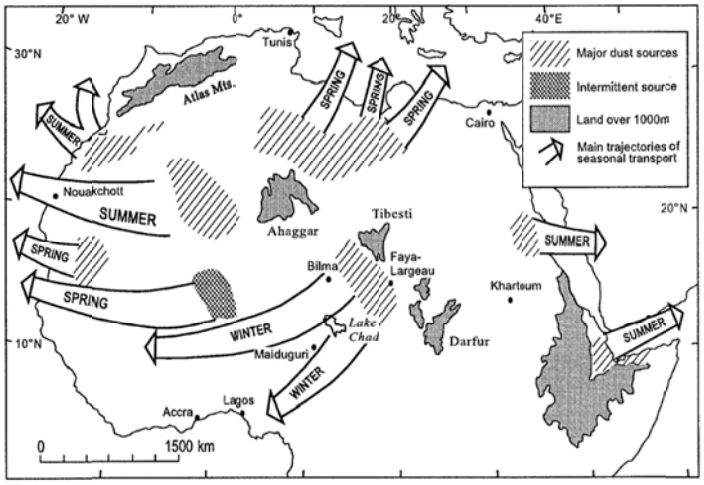

Figure 1.8 *Saharan dust source areas after Middleton (1986). Extracted from Middelton and Goudie (2001).*

The seasonal pattern of dust activity in North Africa evolves during the year as changing seasons (Figure 1.8) bring strong winds and low precipitation to different regions (d'Almeida, 1986; Marticorena and Bergametti, 1995; Tegen et al., 2002; Kaufman et al., 2005; Engelstaedter et al., 2006; Klose et al., 2010). The winter dust activity is greatest in low latitudes; as the year progresses, dust activity shifts to higher latitudes (Prospero et al., 2002; Klose et al., 2010). From October to December, dust activity appears to be very limited over the entire area and from April to June is observed the highest dust occurrence (Middelton and Goudie, 2001; Schepanski et al., 2007). The transport is driven by the latitudinal shift of the Intertropical Front which corresponds to the convergence zone between the northern winds, called the Harmattan, and the monsoon winds coming from the South. From late February to early May the Harmattan wind index is maximum (Sultan et al., 2005) inducing strong winds in the Sahel. During summertime, the dust activity is at maximum (Prospero et al., 2002; Engelstaedter et al., 2006) and the dust transport moves to northern latitudes.

African dust is regularly transported from its source areas along three main transport paths with a marked seasonal behaviour (Figure 1.5 and Figure 1.8): westward over the North Atlantic ocean (Carlson and Prospero, 1972; Moulin et al., 1997; Chiapello et al., 2005; Alonso-Pérez et al., 2007; Ben-Ami et al., 2010), to North America (Perry et al., 1997) and South America (Swap et al., 1992); northward across the Mediterranean to southern Europe (Rodríguez et al., 2001a; Querol et al., 2002; Ryall et al., 2002; Gerasopoulos et al., 2003; Corradini et al., 2004; Barkan et al., 2005; Meloni et al., 2007; Toledano et al., 2007a; Papayannis et al., 2008; Heintzenberg, 2009; Wagner et al., 2009) and sometimes as far north as Germany (Müller et al., 2003) and United Kingdom (Dall'Osto et al., 2010) and Scandinavia (Franzen et al., 1994); and along easterly trajectories across the eastern Mediterranean (Balis et al., 2000; Kubilay et al., 2000; Andreae et al., 2002; Balis et al., 2006; Fotiadi et al., 2006; Saliba et al., 2010), to Middle East (Ganor et al., 1991; de Meij and Levieveld, 2010).

During winter, the dust layers over the West African continent are situated at lower levels than during summer (Kalu, 1979; Cavalieri et al., 2010) and gradually descend throughout their travel over the Atlantic (Generoso et al., 2008). In winter months, transported Saharan dust is observed at near-surface layers, while in summer the dust layer is elevated (Ben-Ami et al., 2009). This is due to seasonally different meteorological regimes especially over the Sahel and the Western Sahara. In summer strong mixing occurs further north over the Sahel/South Sahara due to northward shift of the convergence zone associated to the Hadley cell. Over the ocean, the Saharan dust layer is transported above the trade winds inversion (up to 5 – 7 km above sea level) (Kalu, 1979, Chiapello et al., 1997; Generoso et al., 2008) in north hemispheric summer. In winter the dust is transported within the trade wind layer at altitudes below 1.5 – 3 km (Chiapello et al., 1997; Barkan et al., 2004; Pérez et al., 2004; Córdoba-Jabonero et al., 2011).

In the Mediterranean basin, transport of desert dust aerosol occur at different levels, mainly within and above the planetary boundary layer (e.g. Gobbi et al., 2000; Dulac and Chazette, 2003; Pappalardo et al., 2003; Pérez et al., 2004; Barkan et al., 2005; de Tomasi and Perrone, 2006; Mona et al., 2006; Colette et al., 2008; Papayannis et al., 2008, Sicard et al., 2011; Córdoba-Jabonero et al., 2011) with maximum altitudes registered during summertime. While in spring maximum dust impact is found over Eastern-Central Mediterranean (Formenti et al., 2001; Sciare et al., 2003; Vrekoussis et al., 2005; Balis et al., 2006; Pace et al., 2006), in summer-fall, there is a shift to the Central-Western Mediterranean (Deuze et al., 1988; Silva et al., 2003; Viana et al., 2005; Toledano et al., 2007a; Papayannis et al., 2008). In winter, minimum incidence of long range dust transport is observed (Dayan et al., 1991; Moulin et al., 1998; Rodríguez et al., 2001a; Israelevich et al., 2002; Querol et al., 2002; Papayannis et al., 2008) agreeing with a minimum emission

activity in the source regions and maximum of precipitation. In this season, a residual dust activity is found on the Western part of the Mediterranean basin, while the beginning of a "new dust cycle" is also detected in the South-Eastern Mediterranean.

There is no strong evidence to support changes in the frequency of African dust events. The results presented in Mahowald et al. (2010) suggest that desert dust roughly doubled over the 20th century over much, but not all the globe. However, the North African source shows the dominance for controlling much of the climate impact of desert dust. Dust coming from North Africa observed at Barbados has changed by a factor of 4 between the wet 1960s and the dry 1980s (Prospero and Nees, 1986; Prospero and Lamb, 2003). Analyses of land based data (Goudie and Middelton, 1992; N'Tchayi et al., 1994, 1997) demonstrate that the frequency of dust storms in the Sahel have increased since the 1950s. Fiol et al. (2005) concluded that dust rains in Palma de Mallorca are on the increase based on data from 1982 to 2003 and recently, Ganor et al. (2010) observed the increasing trend in dust storm occurrence during the period between 1958 and 2006 in the Eastern Mediterranean. Moreover, an increase of the frequency of rainfall loaded with such dust red rain in the last decades is documented for a site in northeastern Spain (Àvila and Peñuelas, 1999) and observations of 7 years (1998 - 2004) from the Sea-viewing Wide Field of view Sensor (SeaWiFS) show a strong interannual variability of dust transport over the Mediterranean Sea, as well as an increasing trend in dust transport during the study period (Antoine and Nobileau, 2006). These works indicate there is an increase of Saharan dust intrusions in the entire region around the Mediterranean Basin. In contrast, 20 years of dust measurements at Midway in the North Pacific do not show any long term trends (Prospero et al., 2002) although there have been some periods when dust activity did increase somewhat, especially in late 1990s for several years.

These fluctuations in dust observed far from the dust source regions can be due to a combination of source, transport and depositional changes. It is difficult to determine the relative importance of each factor. It has also been suggested that changes in dust event frequency may be caused by changes in meteorological patterns and climate (Moulin et al., 1997; Ginoux et al., 2004; Mahowald et al., 2010; Alonso-Perez et al., 2011), changes in the biochemistry cycle linked to iron that is transported with desert dust (Mahowald et al., 2010) and changes in the land surface conditions (Middleton and Goudie, 2001; Moulin and Chiapello, 2004).

1.2.1.2 Arabian Dust

Middle East, largely made up of the Arabian Plateau and the Tigris-Euphrates Basin, is an area where dust storms are important phenomena over large tracts of the arid and semi-arid regions (Prospero, 2002). One of the largest sand deserts in the world, the Rub' Al Khali

desert occupies much of the southern interior of the Arabian Peninsula. Rub' Al Khali is connected to the An-Nafud sand sea in the north by the Ad-Dahna.

Figure 1.9 shows the patterns of the dust-storm frequency and the blowing-dust frequency in Middle East. The sources in this region extend in a continuous band from the upper reaches of the Tigris-Euphrates basin to the coast of Oman (Prospero, 2002). The seasonal variation of dust activity in Middle East is complex and differs for different regions. Over much of the peninsula, dust is active all year long, but is relatively low in winter months. Dust activity grows strong in March and April, peaks in June and July and weakens in September.

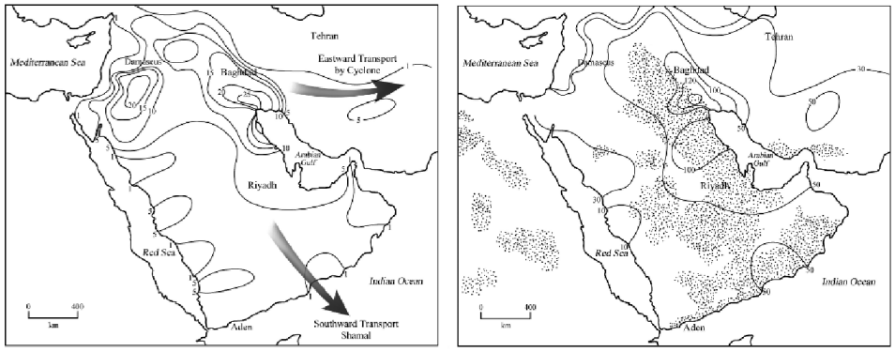

Figure 1.9 *Annual frequency of dust storms (visibility less than 1000 m, left) and annual frequency of dust events (visibility less than 11 km, right) in Middle East. Dotted are the areas of high annual TOMS Aerosol Index (AI). Adapted from Middleton (1986).*

The climate in the Middle East is mainly affected by three preassure systems (Prospero, 2002), the Siberian anticyclone in winter over central Asia, the moonson cyclone in summer over the Indian Subcontinent and the depressions travelling from northwest Africa across Middle East in the non-summer seasons. Severe dust storms are summertime phenomena associated with the Shamal. Much of the dust entrained by the Shamal is deposited in the Persian Gulf and the Arabian Sea. In some areas (e.g. Negev, Jordan, western and northern Iraq and the northern part of Saudi Arabia), the peak dust season occurs in spring and winter. In these seasons, dust storms are generated by the depressions moving easterward from the Mediterranean. In addition, localizad dust storms may be generated by the outflows associated with thunderstorm downdraft, know as the Haboob.

Athough much dust is raised locally over Middle East, substancial amounts of dust come from the Sahara. The type of synoptic situation responsible is the passage of an advancing

cold front and the associated strong surface winds ahead of it penetrating south-eastwards from the Mediterranean Sea deep into the northern Sahara and Libyan Desert (Goudie and Middleton, 2006). The Red Sea shore of Africa can be another major source over western Saudi Arabia, particularly the plain of the ephemeral Baraka River and the Tokar Delta (Goudie and Middleton, 2006).

1.2.2 Desert dust models

A variety of regional and global models of the dust aerosol cycle have been developed since early 1990s. Most of the modelling work focused on climatic studies was motivated by the need to represent aerosol concentrations and their impact upon radiation at the global scale. Dust generation is a very high complex process, highly variable on spatial and temporal scales that respond in a non-linear way to a variety of environmental factors, such as soil moisture content, the type of surface cover or surface atmospheric turbulence. Dust models are essential to complement dust-related observations, understand the dust processes and predict the impact of dust on surface level PM concentrations.

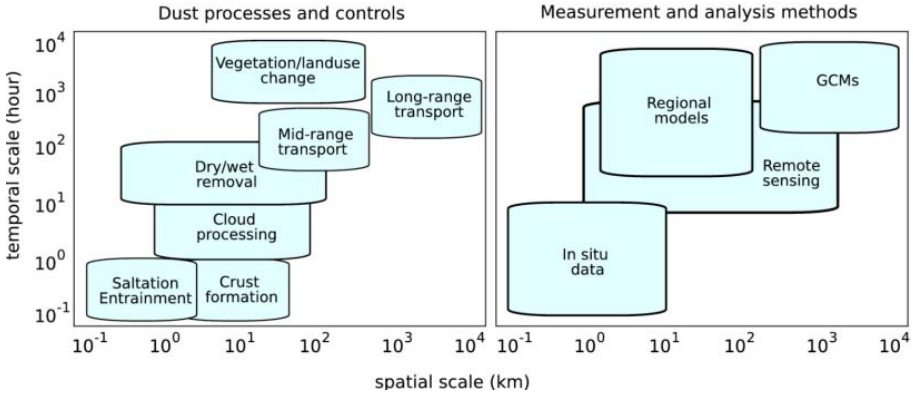

Figure 1.10 *Dust processes span over five orders of magnitude in space and time.*

Accurate representation of dust sources and sinks is critical for providing realistic magnitudes and patterns of atmospheric dust fields. As shown in Figure 1.10, dust processes span over five orders of magnitude in space and time. To correctly describe and quantify the dust cycle, one needs to understand equally well local-scale processes such as saltation and entrainment of individual dust particles as well as large-scale phenomena such as mid- and long-range transport.

Apart from global dust models, a number of regional models have been developed to describe the dust cycle for key regions like the Sahara (e.g., Marticorena et al., 1997; Nickovic et al., 2001) and Asia (e.g., Zhang and Carmichael, 1999; Gong and Zhang, 2008). In recent years, there have been significant advances in representing mineral dust in several types of regional models, ranging from the chemical transport models (Carmichael et al., 2003; Tanaka et al., 2003; Bessagnet et al., 2004), regional climate models (e.g., Zakey et al., 2006; Zhang et al., 2009), to numerical weather prediction models (e.g., Perez et al., 2006a). Such increasing interest is driven to a large extent by a number of advantages offered by the regional models compared to the global circulation models. Regional models, in particular, are well suited for simulations of individual dust outbreaks. Their finer spatiotemporal resolution and multiple physical parameterizations allow for more realistic representation of the topography, soil conditions, mesoscale circulations, and enable better validation against observations.

Model intercomparison in source regions (e.g. Uno et al., 2006; Todd et al., 2008) demonstrates that dust emission remains as a key source of significant errors. The dust emission that results in the production of mineral aerosols from soil grains, involves complex, nonlinear processes that are governed by the meteorology (e.g. Knippertz et al., 2009; Engelstaedter and Washington, 2007b) as well as by the state and properties of land surfaces (e.g. Callot et al., 2000; Ginoux et al., 2001; Zender et al., 2003a).

Dust emission schemes that have been developed and used in the regional models range from simple type schemes, in which the vertical dust flux depends on a prescribed erodible surface fraction and fixed threshold friction velocity (Gillette and Passi, 1988; Uno et al., 2001) to advanced schemes, in which the surface characteristics are taken into account explicitly in the parameterizations of the threshold friction velocity, and horizontal and vertical fluxes (Marticorena and Bergametti, 1995; Shao et al., 1996; Alfaro and Gomes, 2001; Shao et al., 2003; Shao, 2004). The advanced, physically-based dust production schemes provide more realistic representation of the emission process. However, they require additional information on land surface properties and input parameters, and are much more complicated to implement. Some data and variables are readily available within a regional model framework, since it is designed to simulate the meteorological fields as well as land surface characteristics involved in land-atmosphere interaction processes. Dust modelling systems, such as CFORS (Uno et al., 2003), COAMPS (Liu and Westphal, 2001), SKIRON (Spyrou et al., 2010) and DREAM (Nickovic et al., 2001) have utilized rather simple dust emission schemes to model vertical dust fluxes. Up to date, a number of regional dust modelling systems have incorporated physically-based dust emission schemes (with various modifications): for instance, COSMO-MUSCAT (Heinold et al., 2007), CHIMERE-DUST (Menut et al., 2007), RegCM3 (Santese et al., 2010), MesoNH (Grini et

al., 2006) and WRF-DuMo (Darmenova et al., 2009). The modelling systems vary greatly in their choice of emission parameterizations and the set of input parameters driving the schemes.

Dust emission fluxes are widely modelled through parameterizations of suspension (by which soil particles are suspended into the air), saltation (sandblasting) and creeping (slow progression of soil and rock) processes associated with wind erosion (Figure 1.3). The initial size distribution of emitted dust is either based on soil texture data that are not always available and have large uncertainty due to spatial heterogeneity, or on measurements of the background dust in the atmosphere, which may not be representative of the dust in its emission fluxes because the lifetime of dust particles is size dependent (e.g. Tegen et al., 1997; Ginoux et al., 2001; Shaw et al., 2008).

The size distributions of dust particles in the atmosphere are mainly represented using modal or sectional approaches in aerosol models. A modal approach represents the size distribution of aerosols by several overlapping intervals, called modes, normally assuming a log-normal distribution within each mode, while a sectional approach represents the size distribution of aerosols by several discrete size bins, which are defined by their lower and upper dry particle diameters. Generally speaking, a modal approach is less accurate because of its assumption of log-normal distribution and limited number of modes, but it is computationally cheaper than a sectional approach that uses more bins.

As shown in Figure 1.3, mineral dust particles are removed from the atmosphere through dry deposition processes (such as molecular and turbulent diffusion and gravitational settling) and wet deposition processes (such as rainout and washout). Close to the source areas dry deposition is the dominant deposition mechanism for dust particles. Dry deposition depends on the variety of factors such as meteorological conditions near the surface, physicochemical properties of mineral dust and the nature of the surface itself. In regional models dry deposition flux of dust particles is often quantified as the product of the dust concentration in the first model layer and the dust deposition velocity. Different parameterizations of the deposition velocity of particles have been developed in the literature. The most commonly used formulation is based on the resistance concept (e.g., Giorgi et al., 1986; Zhang et al., 2001). In this approach, dry deposition is represented as three resistances in series (aerodynamic resistance to transfer, resistance to transfer across the quasi-laminar surface layer and resistance to surface uptake) in parallel to a second pathway-gravitational settling velocity. The latter is computed from the slip-flow corrected Stokes law. A commonly used model for computing size-resolved particle deposition velocity is that proposed by Slinn (1982). The long-range transport of large particles cannot be simulated using conventional knowledge of dry-deposition processes (Slinn and Slinn,

1980; Colarco et al., 2002; Reid et al., 2003; Zender et al., 2003b; Grini and Zender, 2004). Additional processes need to be included in models to account for the transport of large particles.

Dust is also washed out of the atmosphere by precipitation. To simulate the poorly understood wet removal process, many researchers use simple scavenging ratios (e.g., Tegen and Fung, 1994; Luo et al., 2003) based on observational estimates (Duce and et al., 1991). However, other models use more explicit microphysics to incorporate aerosols into clouds and wash them out (Rasch et al., 2001). Jung and Shao (2006) performed an intercomparison of the wet deposition schemes used in regional and global dust models. They reported a great diversity in the type and level of complexity of employed parameterizations ranging from the use of fixed scavenging ratios below cloud to relatively sophisticate in- and below cloud parameterizations.

Efficiency of in-cloud scavenging depends mainly on dust solubility, which controls the dust particles scavenging efficiency. In turn, dust solubility depends on the mineralogical composition and the pH of the aqueous phase. None of the regional models treats explicitly the mineralogical composition and hence a simplified assumption on the soluble fraction of dust must be made. The modelling of the mixing state of dust poses a large challenge in the regional models, so the rain-out removal rates of dust particles remain poorly constrained. Several studies have also included the impact of mixing dust with soluble sulphate thereby increasing the hygroscopic properties of the dust (Fan et al., 2004). Despite the differences in simulating wet and dry deposition, current models yield a reasonable match with the few observations of total deposition (e.g. Ginoux et al., 2001; Huneeus et al., 2011).

Such dust models represent an important contribution to understanding the dust cycle and the role of dust in the climate system. Therefore, the evaluation of these models is an important issue in order to determine the degree of uncertainty in estimates of dust emission and transport from a range of model simulations, as well as highlight the sources of uncertainty in these estimates and help inform the interpretation of dust forecasts. An exhaustive comparison of different models between each other and against observations can reveal weaknesses of individual models and provide an assessment of uncertainties in simulating the dust cycle (e.g. Uno et al., 2006; Todd et al., 2008).

The evaluation of regional mineral dust models against observations is difficult. Measurements of aerosol properties from ground or space exist. However, all these remote sensing measurements are highly integrated: not only over the atmospheric column but also over all aerosol components. Thus, investigations for the treatment of a particular aerosol type may be limited to seasons and regions, when or where that aerosol type dominates the

aerosol composition such as Saharan dust outbreaks in the Mediterranean Basin (e.g. Pérez et al., 2006b; Sicard et al., 2011).

1.2.3 Research at the Barcelona Supercomputing Center

This thesis is a continuation and extending the lines of research that were initiated at the Earth Sciences Department at BSC–CNS (www.bsc.es) headed by of Dr. José Mª Baldasano. A brief summary of the main activities of the group is given bellow.

The initial research topics related with Earth Sciences Department at BSC-CNS inherits the experience of the Environmental Modelling Laboratory of the Technical University of Catalonia (LMA-UPC). The areas of research are focused mainly on projects that may provide further understanding of air quality modelling, mineral dust modelling, meteorological modelling and global and regional climate modelling. The high performance capabilities of MareNostrum supercomputer hosted by BSC-CNS enable the Earth sciences Department to increase the spatial and temporal resolution of Earth Systems, in order to improve knowledge of dynamic patterns of air pollutants in complex terrains and interactions and feedbacks of physico-chemical processes occurring in the atmosphere.

The Earth Sciences Department at BSC-CNS operates daily regional dust and air quality forecasts and conducts intensive modelling research for short-term operational prediction of mineral dust, as well as long-term dust reanalysis for climatological studies. Next, the latest developments and current activities in the field of sand and dust storm modelling and forecasting are summarized.

1.2.3.1 Dust modelling and forecasting at BSC

The Earth Sciences Department at BSC-CNS maintains dust forecast operations with the updated version of the former Dust Regional Atmospheric Model (DREAM; Nickovic et al., 2001) called BSC-DREAM8b (Pérez et al., 2006a,b) and conducts modelling research and developments for short-term prediction. BSC-DREAM8b has been delivering operational desert dust 72 h forecast over Northern Africa, Middle East, Europe and Asia since May 2009 (www.bsc.es/projects/earthscience/DREAM). The operational resolution is 1/3º x 1/3º and 24 vertical layers up to 15 km in the vertical.

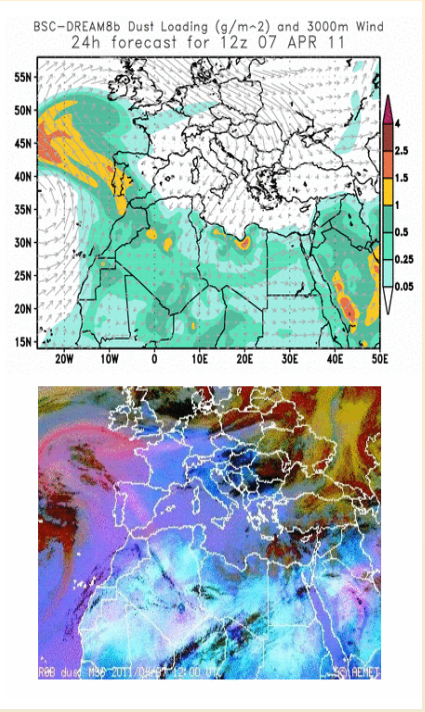

Figure 1.11 *24h BSC-DREAM8b forecast (top panel) and MSG dust RGB product (bottom panel) for 7th April 2011 at 12 UTC.*

MSG dust product is RGB composite based upon infrared channels of SEVIRI. It is designed to monitor the evolution of dust storms over deserts during both day and night. The combination does allow however the further (24 hour) tracking of dust clouds as they spread over the sea. The RGB combination exploits the difference in emissivity of dust and desert surfaces. In the MSG/RGB image (Figure 1.11; bottom) dust appears pink or magenta. Dry land looks from pale blue (daytime) to pale green (nighttime). Thick, high-level clouds have red-brown tones and thin high-level clouds appear very dark (nearly black). Emissions and subsequent transport of individual dust events can be very well observed and followed in the RGB composite pictures.

Observation networks such as the European Lidar Network (EARLINET; www.earlinet.org), the AErosol RObotic NETwork (AERONET; http://aeronet.gsfc.nasa.gov/), satellite and ground level PM levels, outline the good skills of BSC-DREAM8b concerning both the horizontal and vertical extent of the dust plume in particular dust events in the Mediterranean Basin (e.g. Pérez et al., 2006a; Amiridis et al., 2009; Papanastasiou et al., 2010). Additionally, the model has been validated and tested against measurements at source regions from the experimental data of Saharan Mineral Dust Experiment (SAMUM; Haustein et al., 2009) and Bodélé Dust Experiment (BoDEX; Todd et al., 2008) campaigns. In order to improve dust forecasts and implement model versions and operational products, daily evaluation with near-real time observations (Figure 1.11) is conducted in collaboration with the Spanish Weather Service (AEMET; www.aemet.es) and the Spanish National Research council (CSIC). Currently, the evaluation system includes satellites (MSG and MODIS) and sunphotometers (AERONET). Ongoing activities involve the inclusion of lidars, visibility reports and surface concentration measurements to the evaluation system.

1.2.3.2 Inclusion of Saharan dust in an air quality forecasting system for Europe

Daily operational high-resolution air quality forecasts are maintained for Europe (at 12 km x 12 km horizontal resolution) and Spain (at 4 km x 4 km horizontal resolution) under the umbrella of the CALIOPE system (Baldasano et al., 2008a; www.bsc.es/caliope) funded by the Spanish Ministry of the Environment. Its main objective is the development of an operational air quality modelling system for Spain providing routine air quality forecasts with very high resolution for the Iberian Peninsula, Balearic and Canary Islands with nesting in urban areas. In contrast to many other forecasting systems, CALIOPE includes a non-climatic representation of Saharan dust transport. The CALIOPE system is based on a set of models that integrates a meteorological model (WRF-ARW), an emission processing model (HERMES-EMEP), a chemical transport model (CMAQ) and a desert dust model (BSC-DREAM8b) which is offline coupled. The forecasts are evaluated on a daily basis against ground-based and satellite observations to establish confidence of the modelling system predictions among users, identify problems and routinely improve the system.

The performance of the CALIOPE has been quantitatively evaluated with discrete and categorical (skill scores) statistics by a comparison of the first-layer simulations results of CMAQ + BSC-DREAM8b and the values measured in the European air quality stations belonging to the ground-based measurements from the European Monitoring and Evaluation Programme (EMEP; www.emep.int) with available data for the year 2004 in Pay et al. (2010). The results presented in Jiménez-Guerrero et al. (2008a) indicated an improvement in the discrete statistics for PM_{10} and $PM_{2.5}$ concentrations when using CMAQ + BSC-DREAM8b compared to CMAQ-alone simulations (the normalised bias improves from -20% to -9% when considering all the stations in Europe for an seasonal cycle). This improvement in the quality of the predictions becomes more important in those southern stations undergoing larger impacts of Saharan dust outbreaks.

1.2.3.3 Long term model integrations from 1958 to 2006

The study of long-term trends of mineral dust transport and its relation with climatic variability is of great importance for the further improvement of mid-range and long-range dust events forecasting. A 48-year model simulation with the BSC-DREAM model was performed for the period 1958 - 2006 at 0.3º x 0.3º resolution (implemented in MareNostrum supercomputer) in order to analyse the monthly, seasonal and year-to-year variation of the atmospheric dust load, surface concentration, deposition and the frequency and duration of the events over the Mediterranean and the Eastern North Atlantic.

Satellite observations and in situ measurements of concentrations at the Izaña station (Canary Islands) for the period 1987 - 1999 and in southern Europe were used for model

validation (Pérez et al., 2007). Simulated winter dust concentration levels are well correlated with the available background observations for the 1998 – 2004 period. The analysis of the model results showed a two-fold increase in winter dust concentrations over the 1980 – 2006 period with respect to the 1958 – 1979 period, corresponding to the strengthening and eastward shift of the Azores High (Alonso-Pérez et al., 2011).

1.2.3.4 An online mineral dust model within the global/regional NMMb model

Other research activities involve the diagnosis of the behaviour of Earth System Modelling codes in a supercomputer framework and the improvement of parallel versions of atmospheric models to increase their horizontal and temporal resolution. Since 2008, one of the most important efforts are made in the development of a new generation atmospheric mineral dust model (NMMb/BSC-Dust; Pérez et al., 2011b; Haustein et al., 2011) as well aerosol global and gas-phase chemistry (NMMb/BSC-CHEM; Jorba et al., 2010) coupled on-line to the new generation unified meteorological core of the Non-hydrostatic Multiscale Model on the Arakawa B grid model (NMMb; Janjic, 2005; Janjic and Black, 2007) of the National Centers for Environmental Prediction (NCEP). The new NMMb/BSC-Dust modelling system (Pérez et al., 2011b) is intended to be a powerful tool for research and to provide efficient global and regional chemical weather forecasts at sub-synoptic and mesoscale resolutions on MareNostrum supercomputer including a physically-based dust emission scheme taking into account the effects of saltation and sandblasting, soil moisture and viscous diffusion close to the ground.

As shown in the recent monthly and annual evaluation of Pérez et al. (2011b), the NMMb/BSC-Dust provides a good description of the horizontal distribution and temporal variability of the dust. At a global scale the model lies within the top range of the dust global models participating in the AeroCom project (http://dataipsl.ipsl.jussieu.fr/AEROCOM/; Huneeus et al., 2011) in terms of performance statistics for surface concentration, deposition and AOD. At regional domain at high resolution (without dust data assimilation) covering Northern Africa, Middle East and Europe, the NMMb/BSC-Dust is capable to reproduce the main source regions in the Sahara as well as the column dust loading, its spatial distribution and the vertical extension of the dust plume as shown in the results recently presented in Haustein et al. (2011) and Pérez et al. (2011b).

1.2.3.5 The Sand and Dust Storm Warning Advisory and Assessment (SDS-WAS) Programme

Dust storms produce a variety of problems to inhabitants in and around desert areas such as deaths and damage caused in traffic accidents, road disruption, aviation operations and impacts on human health, such us allergies, respiratory diseases and eye infections (WHO,

2005). The seriousness of the problem inspired the development of the World Meteorological Organization (WMO) Programme Sand and Dust Storm Warning Advisory and Assessment System (SDS-WAS) (http://www.wmo.int/sdswas). The SDS-WAS Programme bridges the technological gap between research and operational services and its purpose is to achieve comprehensive, coordinated and sustained observations and modelling capabilities of the sand and dust storms, in order to improve its monitoring state, increase the understanding of its formation processes, and enhance prediction capabilities.

Regional activities related to modelling, observations and applications are coordinated through two Regional Centers: the Asia/Central Pacific Regional Center for SDS-WAS at the China Meteorological Agency in Beijing, China (www.sds.cma.gov.cn) and the Regional Center for Northern Africa, Middle East and Europe (NA-ME-E; http://sds-was.aemet.es/) is based at BSC-CNS (www.bsc.es) and AEMET (www.aemet.es) in partnership with other operational and research organisations (e.g. ECMWF, MeteoFrance, LISA, LSCE, IFT, EUMETSAT or AERONET/PHOTONS). BSC-DREAM8b is one of the dust forecast models participating in Regional Center for Northern Africa, Middle East and Europe.

1.3 Scope and structure of the Thesis

Chapter 1 has provided an overview of the scientific context of the thesis. The study of desert dust, its entrainment, transport and deposition is a topic of growing importance in investigations of global environmental change and air quality (and consequently on economic ativities and human health). At the global scale, the Sahara desert and its margin are the world's major source of aeolian soil dust.

Dust models offer a framework for studying the dust cycle and enable not only the simulation of the global dust cycle but the predictions of dust storms. In particular, regional dust models are well suited for simulations of individual dust outbreaks. However, the evaluation of regional mineral dust models is difficult. Satellite and ground-based remote sensing observations are now producing data suitable for evaluation activities. These measurements are highly integrated, not only over the atmospheric column but also over all aerosol components. Thus investigations for the treatment of a particular aerosol type (like desert dust) are limited to seasons and regions, when or where that aerosol type dominates the aerosol composition.

Within this framework and following the lines of research of the Earth Sciences Department at BSC-CNS, the main goals of this thesis are to ***evaluate the behaviour and***

improve the forecasting skills of a regional dust model and ***characterize the mineral dust content in Northern Africa, Middle East and Europe***. Satellite data and ground-based observations are used for the model evaluation and aerosol characterization. Thus, this investigation involves developments of dust atmospheric model and new methodologies to characterizate aerosols from the observational data including in-situ and remote sensing measurements which are used for the evaluation and interpretation of the model outputs. The **BSC-DREAM8b** model (Nickovic et al., 2001; Pérez et al., 2006a,b) and **AERONET** observations (Holben et al., 1998) are the main tools used in the present research.

The focus and structure of the Chapters are summarized below.

Chapter 2 provides an aerosol characterization over Northern Africa, Northeastern Atlantic, Mediterranean and Middle East based on the analysis of AERONET sun photometer measurements. Sun photometry, with variable measurement approaches has been developed in recent years to deduce the variability of critical atmospheric aerosol properties. AERONET (Holben et al., 1998) is a federated remote sensing network of well-calibrated sun photometers and radiometers located at over 200 sites covering all major tropospheric aerosol regimes around the world. AERONET stations provide columnar aerosol optical parameter information (e.g. AOD, size distribution or single scattering albedo) through direct measurements and inversion techniques. These data constitute a high-quality, ground-based aerosol climatology and, as such, have been widely used for aerosol process studies, as well as for evaluation and validation aerosol models of local, regional or global extent (e.g. Kinne et al., 2003; Hunneeus et al., 2010) as well as aerosol products from satellite retrievals (e.g. Remer et al., 2005; Martonchik et al., 2004). Comparisons between modelled (or satellite retrieved) values and measurements cannot be adequately understood if the optical measurements and model estimates of these measurements are not segmented into their more fundamental components. For the aerosol characterization using AERONET data, we extensively have tested and applied the graphical method of Gobbi et al. (2007) to track and discriminate different aerosol types. The method permits to infer other physical aerosol properties as fine mode radius and fractional contribution to AOD and separate AOD growth due to fine-mode aerosol humidification and/or coagulation from AOD growth due to the increase in coarse particles or cloud contamination. The results are used in the model quantitative evaluation and the analysis of results presented in **Chapters 3** and **4**.

In **Chapter 3**, the original DREAM model and the updated BSC-DREAM8b model version as well as 4 different research model versions have been evaluated for the year 2004 over desert dust source areas (Northern Africa and Middle East) and areas affected by dust

long-range transport (the Mediterranean and Europe) in order to evaluate the model performance. Modelling certain extreme dust events such as those driven by synoptic weather systems can be easier than modelling the day-to-day evolution of the background concentration. In a forecast context, it is mandatory to account for all dust events, light or strong. Near sources, semi-permanent background concentrations may lead to environment and health damages similar or even greater than those of sporadic intense dust events. The daily forecast of atmospheric dust concentration is thus the main challenge for the modellers. The results of the annual comparison in hourly basis of the modelled dust AOD against AERONET data and its ability to reproduce the observed seasonal cycle by means satellite aerosol products are presented. Within this aim, a new methodology to discriminate desert dust contributions from direct-sun AERONET stations based on the results presented in the **Chapter 2** is used. The intercomparison between different model versions aims to highlight the regional and seasonal differences in estimates dust transport from a range of model simulations. The objective is not to rank the model performance but rather highlight the weaknesses of the model in various aspects of the simulation. Therefore, these results can help to point to the key foci for future research to constrain and to test and implement new model approaches.

The European atmosphere is composed by a variety of different aerosol components and mineral dust has a high contribution in Southern Europe. It is necessary to take into account other different aerosol sources at the same time (i.e. natural and anthropogenic) when the aerosol contributions over Europe are analyzed. The long-range dust transport over Europe is evaluated and analysed with an annual simulation of the CALIOPE high-resolution air quality modelling system. This estimates the aerosol from two models, CMAQ and BSC-DREAM8b. CMAQ calculates biogenic, anthropogenic and sea salt aerosol and BSC-DREAM8b provides desert dust. **Chapter 4** discusses the results of the detailed evaluation of the CALIOPE modelling system to simulate the daily aerosol distribution over Europe for year 2004 in terms of using PM levels, AOD and chemical composition measurements. Following, the spatial and seasonal distribution of the different aerosol fractions over Europe based on the model results and observations are estimated and analysed. Finally, the number of exceedances of the EU limits due to natural desert dust is also estimated.

In contrast to many other forecasting systems, CALIOPE air quality modelling system (see Section 1.2.3) includes a non-climatic representation of African dust transport adding offline the BSC-DREAM8b outputs. In addition to anthropogenic, biomass burning and maritime aerosols, Mediterranean countries and also central Europe are often under the influence of long-range Saharan dust transport (e.g. Papayannis et al., 2008). It has been shown that desert dust from North Africa cannot be adequately represented by introducing

dust climatological boundary conditions due to the highly episodic nature of the events in the region (e.g. Vautard et al., 2005). For this reason, the results of the aerosol characterization for 2004 are focused on desert dust contributions to the European atmosphere and their impact on air quality. A first attempt to estimate the fraction of natural mineral dust to measured total PM_{10} levels, or their fraction on the exceedance of EU limits, respectively, is also included in the discussion showing that desert dust regional modelling can be regarded as a useful tool for air quality managers, since the current the regulations establish that an exceedance attributable to natural sources may be subtracted when assessing compliance with air quality limit values.

Chapters 2, **3** and **4** are presented in a similar form as they have been published or submitted to an international SCI journal and include their own introduction, specific methodology, results, discussion and conclusions. Because part of the methodological aspects and data are common in different chapters, some adjustments have been performed with respect to the journal version in order to avoid unnecessary repetitions. **Chapter 5** includes the main harmonized conclusions of the present work, and recommendations for future research, considering the specific conclusions exposed in **Chapters 2**, **3** and **4**. Finally, all references are compiled in **Chapter 6**.

Chapter 2

2 Aerosol characterization from direct-sun AERONET observations

2.1 Introduction

Aerosols frequently exhibit widely varying optical properties over time due to diffusion and aging processes such as coagulation, humidification, scavenging by precipitation and gas to particle phase conversion (Schuster et al., 2006). These processes combined with varying source strength and/or advection by local to synoptic meteorological processes create a dynamic atmospheric constituent affecting climate, environment and public health (IPCC, 2007).

Ground-based aerosol remote sensing does not provide global coverage; however, its numerous spectral measurements of solar radiation are well suited to reliably and continuously derive aerosol optical properties. In spite of high temporal and spatial aerosol variability, there are a rather limited number of general categories of aerosol types with distinctly different optical properties which are associated with different sources and emission mechanisms.

AOD at wavelength λ is the standard parameter measured by sunphotometers as those operating in AERONET (Holben et al., 1998). The AOD spectral dependence is mainly driven by the scattering efficiency and can be expressed by means of the classical Ångström's equation ($AOD(\lambda) \sim \lambda^{-\alpha}$) (Ångström, 1929). In the solar spectrum, the Ångström exponent (α) is a good indicator of the dominant size of the atmospheric particles. AOD generated mainly by submicron particles are characterized by $\alpha > 1$ whereas supermicron aerosols would lead to $\alpha < 1$. As shown in numerous studies (e.g. Eck et al., 1999; Reid et al., 1999; Holben et al., 2001; Dubovik et al., 2002; Smirnov et al., 2002a; Pace et al., 2006; Kaskaoutis et al., 2007), the combined use of the AOD and α allows to distinguish between different aerosol types. As opposite to clean atmospheres (AOD < 0.15) dominated by oceanic aerosols, high values of AOD are characteristic of turbid atmospheres affected by biomass burning, dust plumes or urban pollution (Dubovik et al., 2002). Fluctuations of α reflect aerosol size distribution variations. The maximum value of α (equal to 4) corresponds to molecular extinction. Values near zero (or even negative) correspond to coarse-mode aerosols (sea spray and desert dust) indicating a neutral AOD wavelength dependence, while values of α above 1.5 indicate significant

presence of fine-mode particles (mainly smoke or urban aerosols). However, different aerosol types may be present in the air column at the same time, influencing the observed optical parameters (Chandra et al., 2004) and resulting into intermediate α values. Remer and Kaufman (1998) showed as well that relative humidity is a determining parameter for the size of aerosol particles. Hygroscopic growth at high relative humidities increases AOD (and reduces α), due to the enlargement of soluble particles such as sulphates (Levin et al., 1996).

Therefore, α alone does not provide unambiguous information on the relative weight of coarse and fine modes because the optical effects of aerosols are essentially bimodal in nature. In some cases, large fine mode particles can present the same α as a mixture of coarse mode and small fine mode particles (Gobbi et al., 2007). Several studies have discussed how the spectral variation of α can provide additional information about the aerosol size distribution (e.g. Kaufman, 1993; Eck et al.,1999; Reid et al. 1999; O'neill et al, 2003; Schuster et al., 2006; Gobbi et al., 2007). In this sense, Kaufman (1993) pointed-out that negative values of the difference $\delta\alpha = \alpha(440,613) - \alpha(613,1003)$ indicate the dominance of fine mode aerosols, while positive differences reflects the effect of two separate particle modes. Eck et al. (1999) showed how, in the wavelength range of 340 – 870 nm, α can increase by a factor of 3 – 5 as wavelength increases for biomass burning and urban aerosols, while remaining constant or decreasing in the presence of mineral dust. O'Neill et al. (2003) demonstrated that an Ångström exponent-based separation of coarse from fine mode contribution to AOD is feasible in part because of the coarse mode AOD spectral variation being approximately neutral. Schuster et al. (2006) addressed the link between Ångström exponent curvature and the ratio between fine and total aerosol volume. Gobbi et al. (2007) introduced a straight-forward graphical framework that allows to discriminate different aerosol types based on aerosol spectral measurements by sunphotometers which can be characterized by three independent pieces of information: AOD, α and the spectral curvature of α ($\delta\alpha$). Plotting data in this space allow for inference of the aerosol fine mode size and fractional contribution to total AOD.

In this chapter, we extensively test the new graphical method introduced by Gobbi et al. (2007) in order to analyze and quantify the contribution of mineral dust to the total aerosol load in Northern Africa, Northeastern Atlantic, Mediterranean Basin and Middle East. Other aerosol types also dominate the atmospheric aerosol load in this region: maritime aerosol, continuously formed over the Mediterranean Sea, the Persian Gulf or the North Atlantic Ocean; fine pollution aerosol (in white and green in Figure 2.1) mainly originating from urban and industrial areas of Continental and Eastern Europe, Middle East and along

Nil River; as well as, important contributions of biomass burning (in red in Figure 2.1) generated in Africa mainly in winter.

This chapter provides a thorough overview of the aerosols present into our study region and how the aerosol properties are influenced by long-range transport and local sources. Data and methods are described in Section 2.2 and Section 2.3. Results are presented in Section 2.4 where we discuss about the main transport paths of desert dust from source areas and their seasonal behaviour, as well as, the variation of its optical properties through the year in each region of the study area.

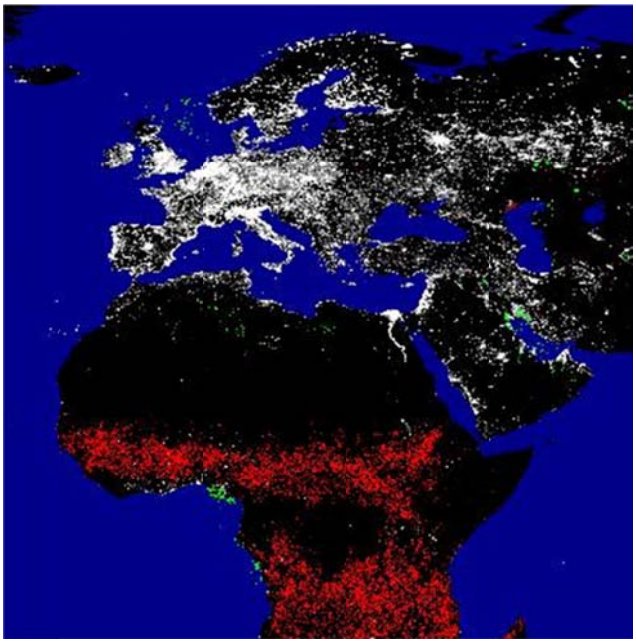

Figure 2.1 *DMSP Nighttime Lights. Four primary types of lights were identified: human settlements - cities, towns, and villages (white), fires (red), gas flares (green), and heavily lit fishing boats (blue). The four types of lights were distinguished from each other based on their appearance, persistence and location. Fires were identified as ephemeral lights on land. Lights from human settlements occur on land and are persistent over time. Gas flares are extremely bright, have a circular appearance, and have no major city present when cross referenced against an atlas. The heavily lit fishing boats are collections of lights found in certain ocean areas and are primarily the result of squid fishing. Produced using cloud-free portions of low-light imaging data acquired by the U.S. Air Force Defense Meteorological Satellite Program (DMSP) Operational Linescan System (OLS). Date range covers January 1 - December 31 2003. Data analysis and digital image creation by NOAA-NESDIS-National Geophysical Data Center-Earth Observations Group Boulder, Colorado USA (http://www.ngdc.noaa.gov/dmsp).*

Table 2.1 *Description of the selected AERONET stations. Class of location which are defined as stations: above 1000 m (H), over arid and desert areas (D), over the ocean (O), over remote and urban areas (R/U) and over littoral areas (C); first and last measurement date, the number of total measurements (Dataset), the number of days (N) and months (Mo.) in the observation periods as well as the percentage of cloud screened data (C) and the percentage of observations with AOD < 0.15 with respect to the total number of measurements (B) of the selected AERONET stations.*

AERONET site	CODE	Class	First data	Last data	Dataset	N	Mo.	C (%)	B (%)
North-Western Africa									
Agoufou	AGO	D	25/09/2003	31/05/2007	39530	1147	45	30.88	12.28
Banizoumbou	BAN	D	16/10/1995	05/07/2007	77529	2575	108	36.20	13.48
Capo Verde	CVR	O	21/10/1994	11/04/2007	46216	2496	125	39.29	26.21
Dahkla	DAH	R/UC	13/02/2002	05/11/2003	18789	563	22	25.70	52.60
Dakar	DAK	R/UC	04/12/1996	12/10/2006	38454	1387	69	33.91	10.48
Djougou	DJO	R/U	24/02/2004	07/05/2007	22012	819	36	34.99	2.43
IER Cinzana	CIN	D	01/06/2004	26/05/2007	33207	971	36	31.09	10.09
Ilorin	ILO	R/U	25/04/1998	27/05/2006	23556	1307	66	38.45	5.00
Izana	IZO	HO	17/06/1997	16/10/2006	26993	690	31	37.51	85.48
Ouagadougou	OUA	D	01/01/1995	15/03/2005	44820	1779	74	38.20	11.55
Saada	SAA	D	01/07/2004	02/06/2006	19512	509	21	25.64	45.15
Santa Cruz Tenerife	SCO	O	15/07/2005	07/05/2007	11487	449	23	36.40	63.99
Iberian Peninsula and Mediterranean Basin									
Avignon	AVI	R/U	08/12/1999	26/06/2006	41605	1548	77	33.84	75.11
Barcelona	BCN	R/UC	16/12/2004	24/05/2006	9457	357	18	37.60	68.35
Blida	BLI	R/UC	30/10/2003	16/11/2006	15573	701	37	33.94	54.70
Cabo da Roca	ROC	R/UC	10/12/2003	27/02/2007	11774	551	32	37.14	77.31
Cairo EMA	CAI	R/U	13/04/2005	23/03/2006	5012	269	12	54.79	21.85
Carpentras	CAR	R/U	18/02/2003	24/10/2007	35308	1177	54	33.93	74.42
El Arenosillo	ARE	R/UC	16/02/2000	12/06/2006	39380	1344	61	26.75	76.63
Evora	EVO	R/U	03/07/2003	09/07/2006	24470	749	34	28.33	81.27
Forth Crete	CRE	R/UC	04/01/2003	06/11/2006	33625	1072	47	23.65	66.48
Granada	GRA	R/U	29/12/2004	11/11/2007	20882	631	29	32.75	69.77
IMC Oristano	ORI	R/UC	30/05/2000	21/10/2003	24251	934	42	26.70	70.16
IMS-METU-Erdemli	ERD	R/UC	12/11/1999	03/05/2006	34910	1218	57	24.23	55.32
Lampedusa	LAM	R/UC	27/06/2000	12/06/2006	17361	813	39	22.46	65.65
Lecce University	LEC	R/UC	08/03/2003	28/11/2006	26361	988	42	32.04	62.78
Nes Ziona	ZIO	R/U	24/02/2000	21/11/2006	42077	1577	72	31.08	54.90
Palencia	PAL	R/U	23/01/2003	24/05/2006	22220	796	39	32.48	86.75
Rome Tor Vergata	ROM	R/U	15/02/2001	20/12/2006	33773	1310	62	35.24	71.40
Sede Boker	SED	D	25/01/1996	20/10/2007	80901	2549	110	27.96	66.18
Thessaloniki	THE	R/UC	03/09/2005	06/05/2007	12883	426	21	30.09	54.73
Toulon	TUL	R/UC	15/11/2004	16/05/2007	20054	703	31	32.97	80.34
Villefranche	VIL	R/UC	07/01/2004	19/01/2007	19431	643	31	32.45	69.45
Middle East									
Bahrain	BHR	R/UC	23/07/1998	02/10/2006	28936	1117	49	23.71	17.86
Dhabi	DHA	R/UC	05/10/2003	30/09/2007	27601	791	30	27.18	12.81
Dhadnah	DHD	R/UC	28/06/2004	21/09/2007	40494	1046	40	22.29	15.37
Hamim	HMM	D	22/06/2004	07/08/2007	27094	876	37	23.73	19.36
Mussafa	MUS	R/UC	04/10/2004	14/03/2006	17892	480	18	30.19	14.49
Solar Village	SVI	D	22/02/1999	12/11/2006	87802	2259	87	24.00	25.19

2.2 Measurement data

Aerosol optical properties in the entire atmospheric column are routinely observed within the AERONET (Holben et al., 1998) program. This is a federation of ground-based remote sensing aerosol networks established by NASA and LOA-PHOTONS (CNRS) and is greatly expanded by collaborators from national agencies, institutes, universities, individual scientists, and partners. The standardized network procedures of instrument maintenance, calibration, cloud screening, and data processing allow for quantitative comparison of the aerosol data obtained at different times and locations (Holben et al., 1998; Smirnov et al., 2000).

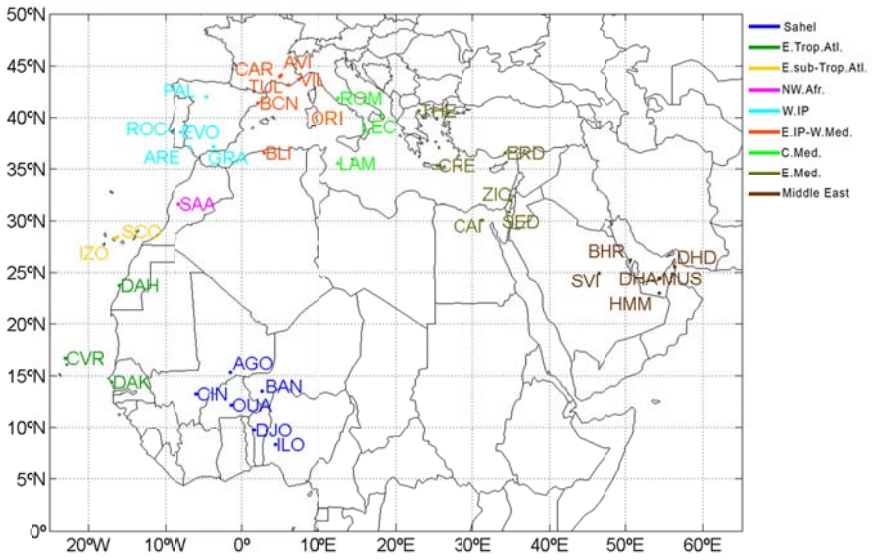

Figure 2.2 *Spatial distribution of the 39 AERONET stations selected into our study domain. The different colours indicate the different regions which are defined as: Sahel, Eastern Tropical Atlantic (E.Trop.Atl), Eastern sub-Tropical Atlantic (E.sub-Trop.Atl), North-Western Africa (NW.Afr), Western Iberian Peninsula (W.IP); Eastern Iberian Peninsula-Western Mediterranean (E.IP-W.Med), Central Mediterranean (C.Med), Eastern Mediterranean (E.Med) and Middle East. Acronyms are defined in* ***Table 2.1****.*

These instruments can only retrieve data during daytime, because they rely on extinction measurements of the direct and scattered solar radiation at several nominal wavelengths (340, 380, 440, 500, 675, 870 and 1020 nm plus a 936 nm water vapour band). The instrument is out of operation for some weeks while necessary yearly calibration is carried out. Consequently the data coverage in a given station is typically limited to 100 – 250 days per year. The typical uncertainty in the AOD measured by AERONET instruments ranges

from 0.01 to 0.02 and is spectrally dependent with higher errors in the UV spectral range (Holben et al., 1998; Dubovik et al., 2000). These data are provided in three categories: 1) raw (level 1.0), 2) cloud-screened (level 1.5) following the methodology described by Smirnov et al. (2000), and 3) cloud-screened and quality-assured (level 2.0). However, it is worth mentioning that some cases of variable aerosol plumes (like intense Saharan dust outbreaks in regions near the desert) could be screened by the cloud-screening algorithm. Conversely, stable uniform cloud might pass the algorithm thresholds and be identified as cloud free (Smirnov et al. 2000).

Since the goal of this study is to obtain an aerosol characterization over a large region with standardized measurements, quality-assured direct-sun data in the 440 – 870 nm wavelength range is used since these channels are highly accurate and they are available in all AERONET instruments. In order to achieve a good temporal coverage, only stations which provided data covering at least the 12 months of the yearly cycle within the 1994 - 2007 period were chosen. Table 2.1 and Figure 2.2 report the location of the 39 selected AERONET sites. Table 2.1 lists additional information including type of site, observation periods and percentage of cloud screened data.

2.3 Aerosol classification

In this study we discriminate the fraction of AOD due to large mineral particles from other aerosol types, based on the graphical framework introduced in Gobbi et al. (2007) (Figure 2.3) which allows to: 1) infer aerosol fine mode size and fractional contribution to the total AOD; and 2) separate AOD increases due to fine-mode aerosol humidification from AOD increases due to the increase in coarse particles.

The method relies on the combined analysis of α derived for the wavelength pairs of 440 - 675 nm and 675 - 870 nm and its spectral curvature, represented by $\delta\alpha = \alpha(440,675) - \alpha(675,870)$. For the definition of these coordinates ($\delta\alpha$ vs. α space or AdA coordinates), reference points corresponding to bimodal size distributions characterized by a fine mode modal radii (R_f; solid black lines in Figure 2.3) as well as the ratio of fine mode to total AOD (η; dashed blue lines in Figure 2.3) have been determined on the basis of typical refractive index of urban/industrial aerosol ($m = 1.4 - 0.001i$). Varying coarse mode modal radii have been considered and shown to have a minor impact on such reference points. The level of indetermination of this classification scheme is of the order of 25% for R_f and ~ 10% for η for refractive index varying between $m = 1.33 - 0.00i$ and $m = 1.53 - 0.003i$. Within this level of indetermination, the scheme is robust enough to provide an operational classification of the aerosol properties.

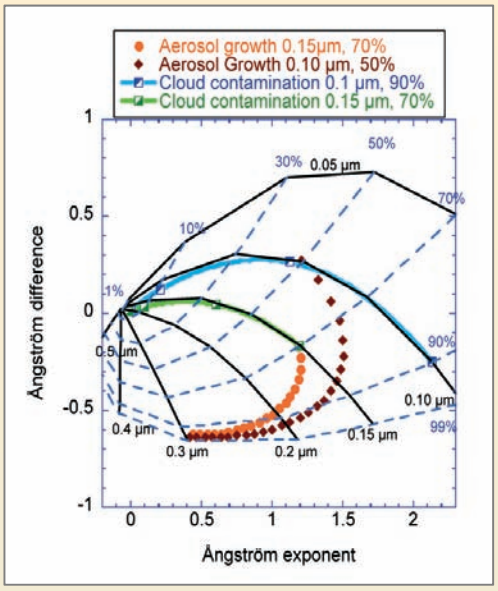

The black solid lines are each for a fixed size of the fine mode R_f and the dashed blue lines for a fixed fraction contribution η of the fine mode to the AOD at 675 nm. Split squares represent the effects of a cloud contamination of 0, 50, 90 and 99% in the AOD of two grid points initially (0% contamination) located at: 1) η = 70%, R_f = 0.15 µm (bright green line) and 2) η = 90%, R_f = 0.1 µm (turquoise line). This contamination results in a departure from the original grid points along the constant R_f lines and towards the origin. Conversely, hydration of the aerosol fine mode (two starting conditions simulated: 1) η = 50%, R_f = 0.1 µm (brown diamonds), and 2) η = 70%, R_f = 0.15µm (orange circles)) is accompanied by a movement towards the origin along the opposite direction, with concurrent increase in R_f and η.

Figure 2.3 *Simulations of the classification of the aerosol properties as a function of the Ångström exponent $\alpha(440, 870)$ and the difference $\delta\alpha = \alpha(440,675) - \alpha(675,870)$, for bimodal, lognormal size distributions with refractive index m = 1.4 – 0.001i extracted from Gobbi et al. (2007).*

In this space, we represent AOD (at 675 nm) by a colour scale. In order to avoid errors larger than ~ 30% in the calculation of $\delta\alpha$, only AOD > 0.15 are considered. Both aging and humidification of pollution aerosol, and cloud contamination could decrease α. However, these processes behave quite differently in the AdA coordinates, as shown in Figure 2.3. Cloud contamination is associated to concurrent increase in AOD and coarse mode fraction taking place along constant R_f curves (bright green and turquoise lines), while hydration leads to a growth in both R_f and η (brown diamonds and orange circles). In general, growth of AOD along R_f lines means an increase in coarse particle extinction. If cloud screening is efficient, only dust particles or maritime aerosols can cause AOD growth along R_f curves.

O'Neill (2009) showed that these families of contour lines in the AdA space are essentially discretized illustrations of analytical parabolic forms in the space formed by the continuously differentiable Ångström exponent (α) and its spectral derivative (α'). As shown in O'Neill et al. (2003), these variables permit the spectral discrimination of coarse and fine mode optical depth from the spectral shape of AOD by means of a Spectral Deconvolution Algorithm (SDA, O'Neill et al., 2001, 2003). The SDA retrievals (O'Neill et al., 2003) are also available in the AERONET website.

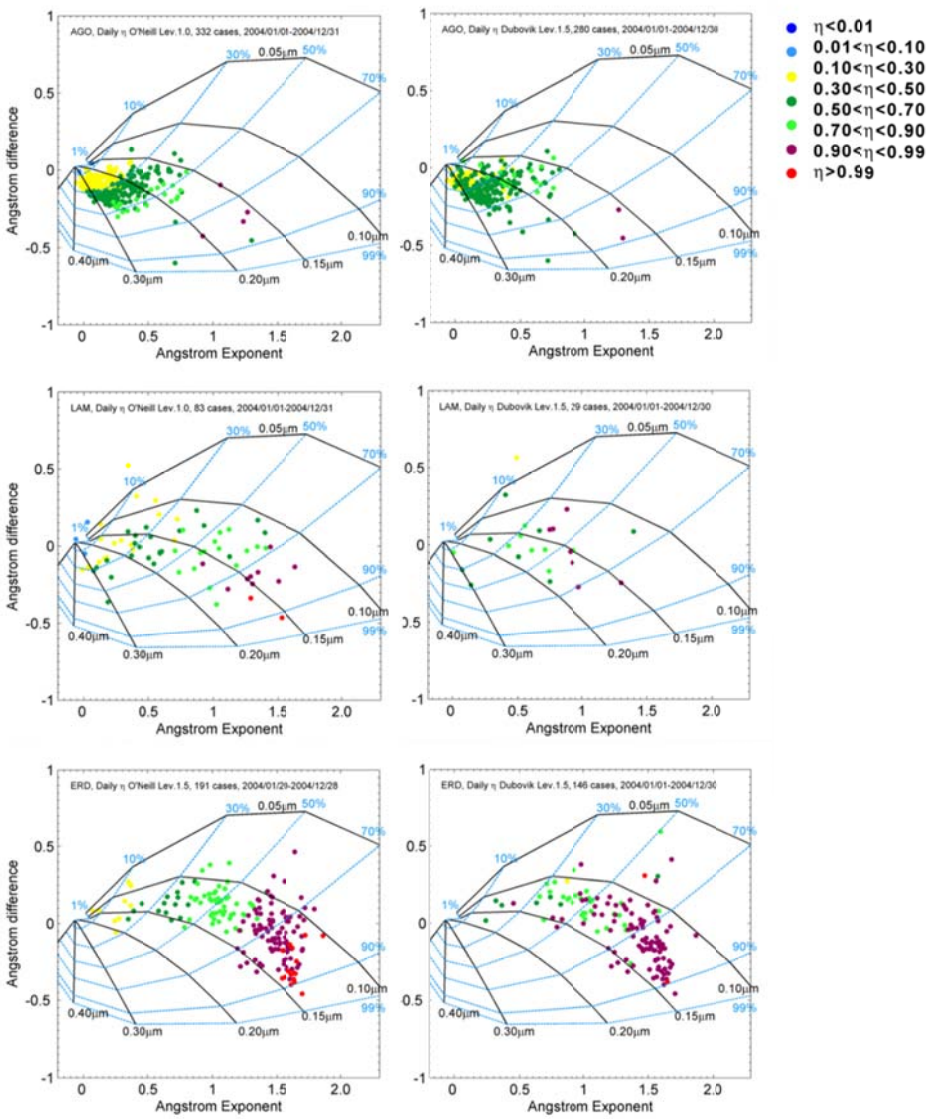

Figure 2.4 *Daily Fine Mode Fraction (η) averages for AGO, LAM and ERD stations. For each station, daily η averages (color code) obtained by O'Neill inversion algorithm (right panels) and daily η averages obtained by means of sky Dubovik inversion products (left panels) are plotted in the AdA space using the daily α and $\delta\alpha$ average calculated from direct-sun observations. In all the plots, only daily η averages associated to daily AOD > 0.15 are shown. Acronyms are defined in* ***Table 2.1****.*

The SDA algorithm yields fine (submicron) and coarse (super-micron) AOD at a standard wavelength of 500 nm. The algorithm fundamentally depends on the assumption that the coarse mode Ångström exponent and its derivative are close to zero. Its advantage lies in the fact that it produces useful indicators of aerosol size discrimination at the frequency of extinction measurements.The amplitude of the errors of these derived parameters varies as

the inverse of the total AOD. There are, in addition to measuremental errors in AOD errors due to the uncertainty in the assumed values of the spectral curvature in each mode (O'Neill et al., 2001) which are most critical in coarse mode dominated conditions.

In order to check the confidence of η retrieved with the graphical method used in the present work with respect to other inversion algorithms, we performed a comparison against the SDA retrievals products and sky-radiance Dubovik fine mode inversion products (Dubovik and King, 2000; Kinne, 2009) of AERONET. Daily η averages over for 2004 for several stations included into our study domain were plotted in the AdA space used in our analysis (Figure 2.4).

Results show good coincidence among the three methods in the coarse particle detection ($\eta < 40\%$; see AGO site in Figure 2.4) as well at high η values (see ERD site in Figure 2.4). Although in some "mixed" stations such as LAM (see LAM site in Figure 2.4), some discrepancies appear in η values, the differences are always < 20%. These discrepancies are partly due to differences between the measurement frequencies of each dataset (i.e. less frequent sky radiances inversions with respect to direct-sun measurements) (Holben et al., 1998; Dubovik and King, 2000). As expected, the comparison shows a better agreement of the Gobbi's graphical method with the O'Neill η values (see rigth panels in Figure 2.4) since the outputs of the Gobbi's graphical method are a subset of the products retrieved from the O'Neill algorithm (O'Neill et al., 2009). Somewhat larger discrepancies observed with respect to the sky-radiance Dubovik inversion products (see left panels in Figure 2.4) are likely due to the current Dubovik inversion output which is equivalent to what the community refers to as sub-micron fraction as opposed to the SDA retrival (O'Neill et al., 2005).

2.4 Results and discussion

The classification scheme is applied to the 39 AERONET stations considered in this study. Seasonal average behaviour is represented in Figure 2.5 and Figure 2.6 as well as Table 2.2. Results for eighteen representative locations are reported in Figure 2.7 (BAN, ILO, DAH, SAA, CVR and IZO), Figure 2.8 (ARE, GRA, BLI, AVI, ORI and LAM) and Figure 2.9 (ROM, THE, CRE, ZIO, MUS and HMM).

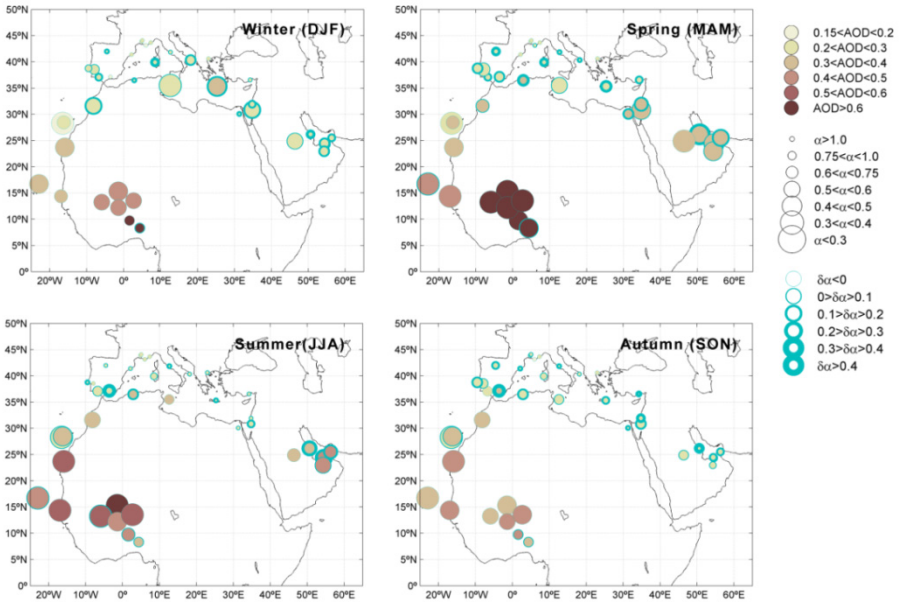

Figure 2.5 *Seasonal mean of measurements with AOD > 0.15 for each AERONET station: the colour code indicates the seasonal mean of the AOD at 675 nm, the size code is associated to the seasonal mean of the Ångström exponent calculated between 440 and 870 nm (α) and the blue contourn code is associated to the seasonal mean of the Ångström exponent difference, δα = α(440,675) - α(675,870).*

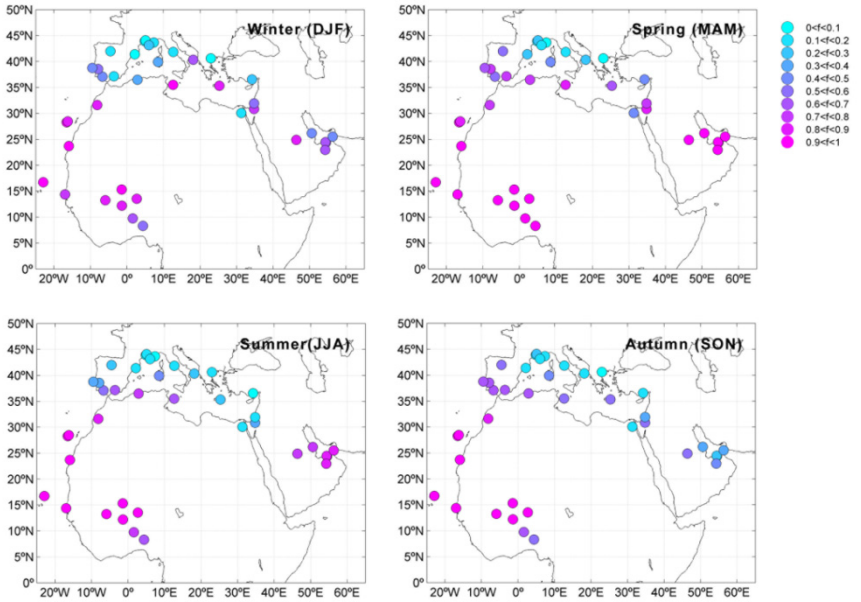

Figure 2.6 *Seasonal frequency of large aerosols (corresponding to particles with AOD > 0.15 and α < 0.75) with respect to the total number of measurements with AOD > 0.15 for each AERONET station, being 0 (blue) when no large aerosols are observed and 1 (pink) when all dataset are concentrated in this coarse fraction.*

Table 2.2 *Seasonal mean of AOD at 675 nm, Ångström exponent calculated between 440 and 870 nm (α) and the Ångström exponent difference, δα = α(440,675) - α(675,870), of large aerosols fraction (corresponding to particles with AOD > 0.15 and α < 0.75) of each AERONET site.*

	Winter			Spring			Summer			Autumn		
Station	AOD	α	δα	AOD	α	δα	AOD	α	δαa	AOD	α	δα
North-Western Africa												
AGO	0.45	0.34	-0.12	0.63	0.17	-0.13	0.65	0.14	-0.07	0.38	0.32	-0.11
BAN	0.44	0.36	-0.14	0.73	0.19	-0.11	0.52	0.22	-0.02	0.42	0.35	-0.09
CVR	0.38	0.24	-0.07	0.41	0.27	0.01	0.50	0.19	0.00	0.40	0.23	-0.08
DAH	0.39	0.29	-0.06	0.33	0.37	-0.01	0.51	0.27	-0.02	0.47	0.27	-0.05
DAK	0.39	0.40	-0.06	0.48	0.27	-0.03	0.57	0.20	-0.02	0.42	0.36	-0.03
DJO	0.77	0.47	-0.03	0.77	0.30	0.00	0.51	0.36	0.11	0.53	0.42	0.06
CIN	0.43	0.39	-0.05	0.62	0.22	-0.09	0.53	0.21	0.01	0.34	0.39	-0.03
ILO	1.01	0.49	-0.01	0.68	0.33	0.01	0.43	0.39	0.05	0.50	0.51	0.01
IZO	0.16	0.21	-0.01	0.29	0.20	-0.01	0.26	0.16	0.00	0.25	0.15	0.01
OUA	0.45	0.38	-0.10	0.64	0.25	-0.07	0.43	0.32	-0.13	0.45	0.43	-0.12
SAA	0.30	0.33	0.18	0.38	0.42	0.05	0.34	0.40	-0.02	0.33	0.33	0.00
SCO	0.21	0.43	-0.09	0.43	0.37	0.02	0.37	0.33	0.06	0.33	0.32	0.03
Iberian Peninsula and Mediterranean Basin												
AVI	0.33	0.45	0.25	0.32	0.52	0.16	0.35	0.50	0.14	0.35	0.48	0.14
BCN	0.31	0.50	0.06	0.30	0.52	0.11	0.38	0.58	0.20	0.27	0.43	0.17
BLI	0.19	0.41	0.29	0.37	0.43	0.19	0.44	0.40	0.11	0.28	0.41	0.09
ROC	0.23	0.34	0.14	0.29	0.32	0.15	0.43	0.37	0.10	0.25	0.37	0.23
CAI	0.35	0.40	0.15	0.47	0.37	0.06	0.37	0.51	0.09	0.31	0.59	0.20
CAR	0.27	0.56	0.34	0.32	0.51	0.16	0.33	0.45	0.11	0.35	0.49	0.20
ARE	0.27	0.47	0.20	0.35	0.39	0.14	0.32	0.43	0.06	0.26	0.42	0.04
EVO	0.39	0.26	0.16	0.29	0.32	0.12	0.37	0.37	0.02	0.30	0.31	0.10
CRE	0.34	0.24	0.12	0.30	0.38	0.21	0.29	0.44	0.20	0.30	0.38	0.13
GRA	0.24	0.51	0.19	0.28	0.43	0.14	0.28	0.40	0.31	0.35	0.41	0.31
ORI	0.23	0.38	0.35	0.32	0.39	0.28	0.37	0.44	0.08	0.33	0.36	0.13
ERD	0.37	0.43	0.14	0.34	0.42	0.15	0.25	0.67	0.12	0.27	0.52	0.41
LAM	0.27	0.15	0.02	0.29	0.36	0.08	0.35	0.38	0.01	0.33	0.32	0.05
LEC	0.27	0.32	0.20	0.30	0.49	0.21	0.35	0.47	0.09	0.35	0.56	0.15
ZIO	0.30	0.28	0.15	0.38	0.37	0.08	0.30	0.55	0.15	0.26	0.50	0.29
PAL	0.24	0.47	0.26	0.30	0.46	0.24	0.33	0.46	0.12	0.23	0.44	0.19
ROM	0.21	0.46	0.28	0.27	0.46	0.29	0.36	0.48	0.21	0.28	0.51	0.28
SED	0.28	0.25	0.12	0.32	0.31	0.07	0.27	0.47	0.19	0.25	0.46	0.20
THE	0.25	0.64	0.25	0.35	0.55	0.23	0.42	0.51	0.17	0.37	0.62	0.24
TUL	0.24	0.58	0.24	0.23	0.53	0.26	0.33	0.49	0.10	0.21	0.41	0.25
VIL	0.25	0.43	0.31	0.40	0.44	0.18	0.38	0.48	0.15	0.34	0.45	0.19
Middle East												
BHR	0.34	0.40	0.20	0.38	0.35	0.29	0.41	0.43	0.27	0.32	0.54	0.39
DHA	0.33	0.40	0.17	0.40	0.32	0.02	0.46	0.45	0.10	0.29	0.57	0.17
DHD	0.26	0.48	0.19	0.35	0.39	0.13	0.48	0.47	0.17	0.32	0.57	0.17
HMM	0.27	0.42	0.20	0.33	0.32	0.06	0.48	0.35	0.08	0.31	0.53	0.05
MUS	0.30	0.44	0.17	0.32	0.36	0.12	0.48	0.39	0.12	0.28	0.58	0.14
SVI	0.29	0.31	0.09	0.38	0.25	-0.08	0.34	0.42	-0.08	0.26	0.52	0.01

Figure 2.5 includes the mean seasonal AOD, α and $\delta\alpha$ for all available measurements with AOD > 0.15. Since the emphasis of the study is on coarse-mode mineral particles, the bias introduced by the AOD > 0.15 filter is not expected to be so important. In fact, AODs associated to dust conditions are usually higher (Dubovik et al., 2002). In Table 2.1, the percentage of measurements associated to AOD < 0.15 is shown. The larger percentages (> 60%) are found in stations located in the Eastern Sub-Tropical North Atlantic Iberian Peninsula and around the Mediterranean Basin where the presence of coarse-mode mineral dust is sporadic and maritime aerosols are the main aerosol constituent. Figure 2.6 and Table 2.2 refer to the coarse-particle fraction of the data which includes all data with AOD > 0.15 and α < 0.75.

As we show along the present section, pure coarse aerosols in the AdA space are always observed in the region α < 0.75 in which the fine mode contribution is always < 40%. Figure 2.6 depicts the seasonal fraction of the number of coarse mode measurements (with AOD > 0.15 and α < 0.75) with respect to total number of measurements with AOD > 0.15. Table 2.2 shows the mean seasonal contribution to AOD, and α and $\delta\alpha$ average of the coarse mode data (with AOD > 0.15 and α < 0.75). As shown in the literature (e.g. Kaufman, 1993), strong negative values of $\delta\alpha$ (between -0.5 and -0.2) indicate dominance of fine mode aerosols. We have found that under the dominance of coarse mode aerosols, such as desert dust, $\delta\alpha$ tends to be negative or slightly positive (between -0.3 and 0.1). In this respect, it is the value of α that allows to define which is the dominating fraction.

2.4.1 Sahara-Sahel

There are relatively few measurements at Sahelian sites (AGO, BAN, CIN, DAK, OUA, DJO and ILO) during summer when maximum rainfall and cloud cover occur. A larger number of measurements are observed in the winter or dry season. These stations located southward of Saharan sources show large variations of AOD and high extinctions (~ 85% of the AOD values are above 0.15 with AOD maxima > 4); α is almost inversely-proportional to AOD, and $\delta\alpha$ is negative or slightly positive (ranging between -0.3 and 0.1, e.g. BAN in Figure 2.7) which indicates that AOD increases are often related to an increase in particle size due to desert dust outbreaks or local dust resuspension. High extinction values (AOD > 1) are related to large particles with α < 0.3 and $\delta\alpha$ < 0 that corresponds to η < 40% and R_f ~ 0.3 μm which are assumed to be typical of pure desert dust conditions.

As shown in Figure 2.6, the proportion of large particles (AOD > 0.15 and α < 0.75) is high during the whole year (> 50%), especially in spring (when coarse aerosols represent more than 85% of the data) and summer. Dust transport downwind from source regions vary seasonally. This transport is driven by the latitudinal shift of the Intertropical Front which corresponds to the convergence zone between the northern winds, called the Harmattan, and the monsoon winds coming from the South. From late February to early May the Harmattan wind is maximum (Sultan et al., 2005). Notice that DJO and ILO show the highest frequency of coarse fractions in spring (Figure 2.6).

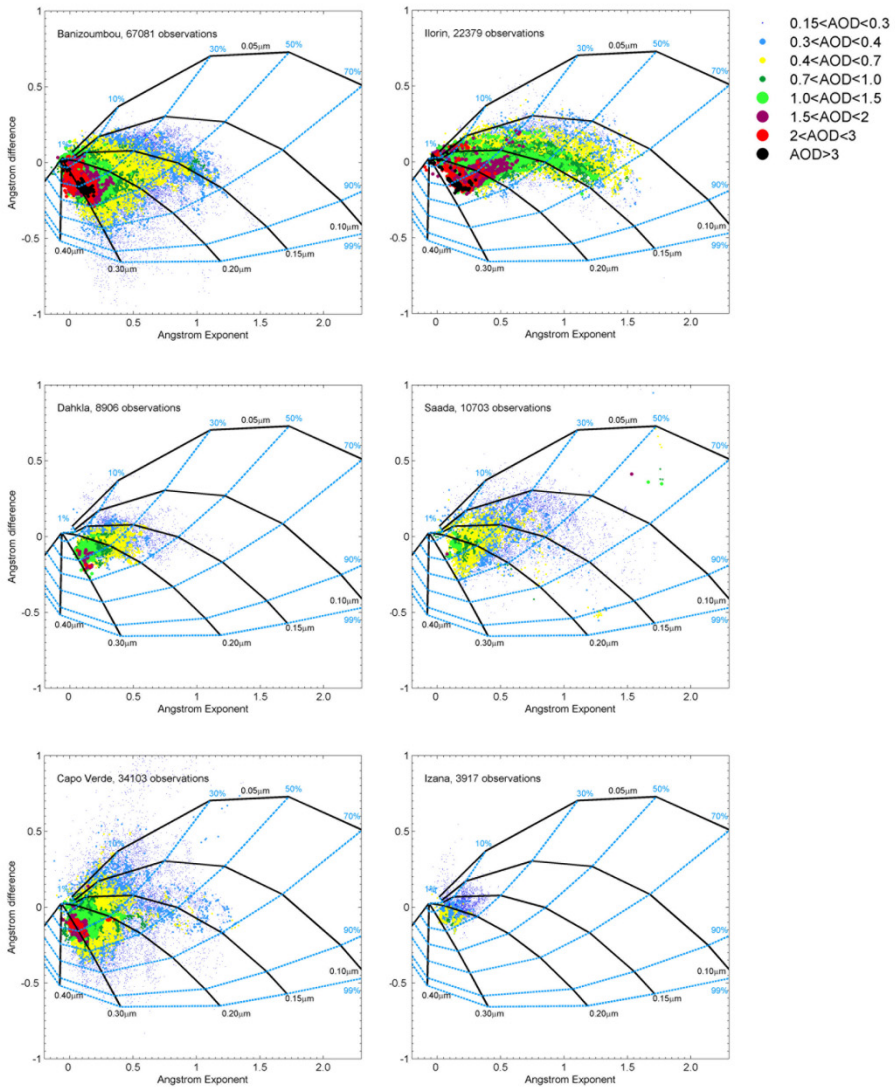

Figure 2.7 *Ångström exponent difference, $\delta\alpha = \alpha(440,675) - \alpha(675,870)$, as a function of the 440 – 870 nm Ångström exponent and AOD at 675nm (color code) for BAN, ILO, DAH, SAA, CVR and IZO AERONET sites. Acronyms are defined in* ***Table 2.1****.*

On the other hand, these stations clearly detected a second aerosol type (i.e. see ILO in Figure 2.7) contributing to the turbidity (AOD up to 1.5) with high α values (~ 1.5) and negative $\delta\alpha$ (< -0.2) that corresponds to η ~ 70% and R_f ~ 0.13 μm. As shown in Figure 2.5, ILO and DJO stations present larger contributions of fine aerosols (especially in late autumn-winter) than the rest of sites in this region. This is due to the well-known presence of fine biomass burning aerosols originating from the sub-Sahel zone (Ogunjobi et al., 2008). The Savannah vegetation is characteristic of the Sudanian zone where fire activities are important during winter. During this season, the interaction of mineral dust and biomass burning aerosols is at its maximum over the region. Thus, all sites present a similar behaviour in the AdA space, associated to R_f constant values (~ 0.15 μm) and η variying between 40 and 70% (see BAN and ILO in Figure 2.7). Furthermore, as shown in Figure 2.5, all sites present the lowest AOD values in summer and autumn (coinciding with maximum rainfall and cloud cover). Particularly in ILO and DJO, we observe a decrease in α values and an increase of $\delta\alpha$ values (~ 0.10) which indicates the interaction of two separate particle modes. This is due to the presence of fine aerosols originating from anthropogenic activities along the Nigeria coast.

At higher latitudes, DAH and SAA (both included in Figure 2.7) present relatively few measurements during winter, the period of maximum rainfall and cloud cover. They show an important coarse fraction during the whole year (Figure 2.6) which is associated to large mineral particles with α < 0.6 and $\delta\alpha$ slightly negative that corresponds to η < 50% and AOD maxima < 2 (Figure 2.7). As shown in Figure 2.6, maximum dust contributions are observed in summertime when the Intertropical Front is found in its northernmost position.

In addition to large mineral particles, SAA (Figure 2.7) presents a small fraction of fine aerosols (α ~ 1.4 and $\delta\alpha$ ~ -0.5) related to low AODs (< 0.2) which corresponds to η ~ 70% and R_f ~ 0.13 μm associated to pollution aerosols from local and regional activities. Thus, SAA shows positive $\delta\alpha$ values (especially in winter) due to the presence of different aerosol modes (e.g. maritime, desert dust and fine pollution aerosols) except in summertime (Figure 2.5) when enhanced Saharan dust activity and favourable transport conditions to this area occur (Middleton and Goudie, 2001).

2.4.2 Eastern Tropical North Atlantic

CVR is located approximately 600 km northwestern of DAK, in the outflow of Saharan dust from West Africa. In spite of its coastal location CVR (Figure 2.7) presents a similar behaviour to the continental station DAK, characterized by a large coarse fraction (Figure

2.6) associated to $\eta < 50\%$ and AOD maxima < 3. High aerosol loading from spring to autumn (Figure 2.5) associated to low α values and high extinctions indicates that mineral dust dominates the aerosol regime, due to frequent Saharan dust outbreaks. The situation is more complex in wintertime when the aerosol loading is lower. In this period, the contribution of sea salt and small particles is significant. As shown in Figure 2.7, such fine particles conditins associated to a $\eta \sim 70\%$ change to higher coarse fractions along R_f constant curves (~ 0.15 μm). Chemical analysis from samples taken at ground level, and air mass trajectory analysis (Chiapello et al., 1999) explain such fine aerosols as sulfates transported from urban and industrial regions in southern Europe and/or northwestern Africa, and biomass burning from Savannah fires, as well as, contributions of local anthropogenic sources.

2.4.3 Eastern Sub-Tropical North Atlantic

Roughly 100 km west of the Moroccan coast, in the Canary Islands, we find SCO at sea level and IZO 2370 m abose sea level (a.s.l.). Quasi-permanent subsidence conditions in the free troposphere together with frequent trade winds flow in the lowest troposphere resulting in a strong and stable temperature inversion (located at 1400 m a.s.l. on average) that separates a dry free troposphere from a relatively fresh and humid oceanic boundary layer (Torres et al., 2002). The proximity to the Sahara desert and the regional atmospheric circulation exert a decisive influence on the dust climatology of this region (Viana et al., 2002; Querol et al., 2004a; Alonso-Pérez et al., 2007). Although these sites are situated very close to each other, they present a very different behaviour (SCO is located at ~ 50 m a.s.l. within the oceanic boundary layer, whereas IZO is located at ~ 2370 m a.s.l., normally under free troposphere conditions).

Thus, the background conditions at IZO are associated to low AOD values (~ 85% of its AOD values are under 0.15, e.g. Table 2.1). As shown in Figure 2.7, AODs above 0.15 are associated to large particles with $\alpha < 0.25$ and $\delta\alpha \sim 0$ that correspond to $\eta < 30\%$ (Figure 2.7), i.e. values similar to the ones observed at sub-Sahelian sites. In winter, AOD > 0.15 represents less than 1% of the recorded data while in summer AOD > 0.15 represents about a 50%. This shows an enhancement of Saharan dust transport at this site during summer, in agreement with Prospero et al. (1995).

SCO is located in the city centre of Santa Cruz de Tenerife in the vicinity of the city harbour. This site presents a large coarse fraction associated to $\eta < 70\%$ and AOD maxima below 1.5. High aerosol loading from spring to autumn (Figure 2.5) associated to low α values and high extinctions indicates that mineral dust dominates the aerosol regime, due to

frequent Saharan dust outbreaks. The predominance of the trade winds (NE) in the oceanic boundary layer plays a key role in the atmospheric dynamics of this site. It favours the dispersion of pollutants from local urban and industrial activities over the ocean together with the occasional transport of European polluted air masses to this region (Viana et al., 2002). Consequently, the proportion of fine anthropogenic aerosols at SCO is lower than those in regions with similar urban and industrial development in continental environments (Rodríguez and Guerra, 2001; Rodríguez et al., 2008). In general, this fine fraction of pollution aerosols appears well-mixed with coarse mode aerosols like maritime particles (~ 50% of its AOD > 0.15 are associated to $\delta\alpha > 0$). Thus, as shown in Figure 2.6, the coarse fraction of this urban site remains very high during all the year.

Long-range dust transport above the trade wind inversion layer at IZO is observed from early summer to early-autumn. Low level dust intrusions are detected at SCO mainly in winter (from January to March) and in autumn, in agreement with the previous studies in this North Atlantic region (e.g. Torres et al., 2002; Viana et al., 2002; Alonso-Pérez et al., 2007).

2.4.4 Iberian Peninsula

At higher latitudes, we find the Iberian Peninsula. The air masses arriving to this region are driven by the Azores high pressure system which intensifies during the warm season inducing very weak pressure gradient conditions all over the region (Martin-Vide, 1984). This favours the development of local thermal circulations, such as coastal and mountain breezes. EVO, ROC, ARE, GRA and PAL sites in the Iberian Peninsula show a frequent background situation associated to low AOD values (~ 70% of its AOD values are lower than 0.15, see Table 2.1). High extinctions (AOD > 1) are associated to large particles with $\alpha < 0.6$ and $\delta\alpha \sim 0$ that correspond to $\eta < 30\%$ with a marked South-to-North gradient with AODs maxima < 2 in ARE (Figure 2.8) and < 1 in ROC and PAL. These large particles are linked to frequent African dust plumes affecting this area mainly in early-spring and summer (Rodríguez et al., 2001b; Alados-Arboledas et al., 2003; Silva et al., 2003; Querol et al., 2004a; Lyamani et al., 2005; Elias et al., 2006; Toledano et al., 2007b; Wagner et al., 2009).

All these sites show a second cluster (see ARE and GRA in Figure 2.8) associated to $\alpha > 1.5$ and $\delta\alpha < -0.2$. These values correspond to $\eta \sim 80\%$ and $R_f \sim 0.13$ μm related to polluted and continental air masses (Alados-Arboledas et al., 2003; Querol et al., 2004a; Toledano et al., 2007b). In fact, local pollution episodes (mainly in late autumn and winter) as well as emissions from Central and Eastern Europe (Querol et al., 2004a) and sometimes as far as the Eastern Coast of North America (Alados-Arboledas et al., 2008) are potential

sources of fine aerosol in this region. The one-mode fine aerosol ($\delta\alpha < 0.1$ and $\alpha > 1.2$) observed at ARE and GRA throughout the year are possibility due to its proximity to a large industrial area (Toledano et al., 2007b).

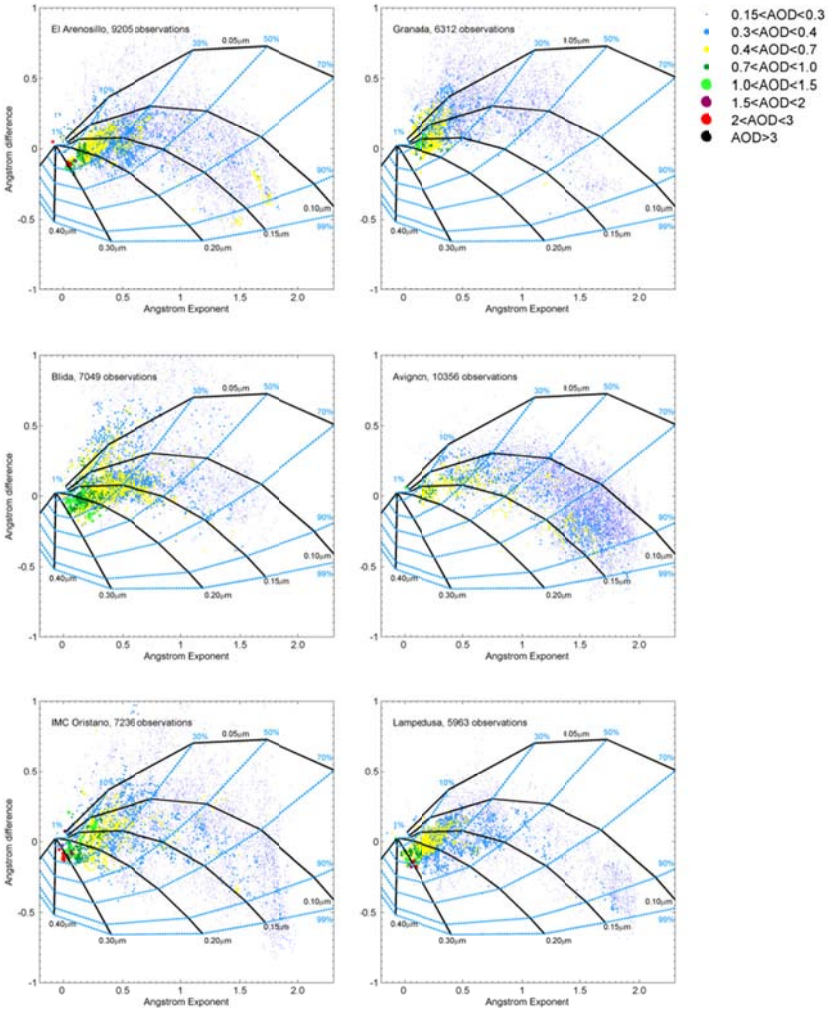

Figure 2.8 *Ångström exponent difference, $\delta\alpha = \alpha(440,675) - \alpha(675,870)$, as a function of the 440 – 870 nm Ångström exponent and AOD at 675nm (color code) for ARE, GRA, BLI, AVI, ORI and LAM AERONET sites. Acronyms are defined in* ***Table 2.1****.*

In summertime, under high isolation and low humidity conditions, fine biomass burning aerosols from fires in the Iberian Peninsula and Southern France (Belo, 2004; Elias et al., 2006) can be detected. AODs during these pollution events ($0.15 < AOD < 0.7$) are lower

than those recorded during African dust outbreaks but clearly higher than those observed during background Atlantic advection conditions. This fine particle cluster grows following the constant R_f curves (~ 0.13 μm) due to the presence of coarse particle (likely maritime aerosols). Additionally, in winter (under stagnant conditions), a growth of AOD along constant η lines (~ 85%), linked to both coagulation-aging and hydration, is observed.

Although African dust outbreaks over the Iberian Peninsula can occur throughout the year, its contribution to AOD is more important in spring (Figure 2.6). In this season, the coarse cluster usually appears well-mixed with other types of small particles as indicated by positive δα values (~ 0.20). Additionally, it is remarkable the seasonal differences (Figure 2.5) between the sites located in south-western part of the Peninsula (ARE, ROC and EVO) and south-eastern (GRA) indicating different transport patterns at both areas.

2.4.5 Mediterranean Basin

The Mediterranean basin is characterized by cold winters and hot summers. The stable anticyclonic weather conditions permits continuous measurements over long periods, especially in summer.

2.4.5.1 Western Mediterranean

The stations located in the Northwestern Mediterranean coast are close to numerous industrial and urban sources of primary pollutants. AVI (Figure 2.8), TUL, CAR, VIL, BCN, ORI (Figure 2.8) and BLI (Figure 2.8) sites present an important fine particle cluster in the AdA space ($\alpha > 1.6$ and $\delta\alpha < -0.3$) associated to $\eta \sim 80\%$ and $R_f \sim 0.12$ μm. In fact, over 70% of their datasets are associated to this fine particle cluster (Figure 2.6) which corresponds to moderate extinctions (AOD < 0.7). AOD growth is linked to both coagulation-aging and hydration increase of R_f. At the same time coarse particles, likely maritime aerosols, superimpose their signal onto this fine mode. As shown in AVI (Figure 2.8), a concurrent increase in AOD and coarse mode fraction along the R_f curves (~ 0.12 μm) is observed. Conversely, highest extinctions (AOD maxima > 1) are related to large particles ($\alpha < 0.7$) that corresponds to $\eta < 40\%$. This coarse particle cluster is associated to large dust aerosols from North African deserts. As shown in Table 2.2, coarse fraction exhibits positive δα values throughout the year which indicates the presence of small particles mixed with this coarse mode. The Northwestern Mediterranean coast is characterized by a high frequency of sea breeze conditions, which are intensified by topography. Under weak pressure gradients, coastal and nearby mountain breeze regime predominates favouring the development of polluted atmospheric layers at several heights

(Pérez et al., 2004; Jiménez et al., 2006). Thus, Saharan dust is found at high altitudes while, fine pollution aerosols are concentrated at lower altitudes (e.g. Pérez et al., 2004). By late summer-early autumn, North African highs, located at surface level, and Atlantic depressions west of Portugal, favour air mass transport at low levels from the Western Sahara, Mauritania and the Sahel to the Northwestern Mediterranean (Moulin et al., 1998; Rodríguez et al., 2001; Escudero et al., 2005). These meteorological conditions are typically associated to the presence of rain resulting in the well-known "red rains" (Ávila et al., 1998). Thus, most of the Saharan intrusions during these rainy periods have not been recorded into our dataset because AERONET instruments do not operate during rain events.

At southern latitudes, ORI, on the west coast of Sardinia, and BLI, in the Algerian coast, exhibit high extinctions (AOD > 0.7) in the coarse fraction. This is caused by frequent North African dust advections. Both sites (included in Figure 2.8) present highest extinctions (AOD > 1) in the coarse mode ($\alpha < 0.4$ and $\delta\alpha \sim 0$) that corresponds to $\eta <$ 30%. Additionally to this coarse cluster, we detect in the AdA space a small fraction of fine aerosols ($\alpha \sim 1.6$ and $\delta\alpha \sim -0.5$) possibly from local anthropogenic sources and European pollution which is most important at the ORI site. This fine cluster is related to low extinctions (AOD < 0.3) and $\eta > 70\%$. A simultaneous growth of AOD and coarse fraction (indicated by a decrease of α) along constant R_f curves is associated to cloud contamination or to the presence of coarse particles (maritime and dust aerosols). At the same time, coarse particles (likely dust) superimpose their signal onto this fine mode particles.

As shown in Figure 2.6, the coarse fraction is more important in BLI than ORI during all year due to its proximity to African sources. Maxima contributions in spring and summer and minima in winter are observed, coinciding with the maximum and minimum incidence of Saharan dust transport, respectively, in this part of the Mediterranean basin (Barnaba and Gobbi, 2004). Note the similarities in Figure 2.5 and Figure 2.6 between BLI and GRA (in the Iberian Peninsula) indicating common African dust sources and pathways at both locations.

2.4.5.2 Central Mediterranean

At about 130 km east of the Tunisian coast, LAM (Figure 2.8) shows an important cluster in the coarse mode in the AdA space ($\alpha < 0.5$ and $\delta\alpha \sim 0$) associated to frequent Saharan dust outbreaks to this site (Pace et al., 2006) that corresponds to $\eta < 50\%$. This coarse contribution is high throughout the year (Figure 2.6) and high extinctions (AOD > 1 and ranging up to 2.5) are related to almost pure desert dust ($\eta < 30\%$, $\alpha < 0.3$ and $\delta\alpha \sim 0$) as

observed in Sub-Sahelian sites. Moreover, a second aerosol type (Figure 2.8) with AOD < 0.4 and $\alpha \sim 1.8$ that corresponds to $\eta \sim 90\%$ and $R_f \sim 0.14$ μm is observed. A growth of AOD and coarse fraction is found along the constant R_f curves due to the presence of coarse particles. In summertime, when wet removal is practically absent and photochemical reactions are favoured, the contribution of small pollution particles is maximum (Figure 2.6). They are related to long-range transport of urban and industrial aerosols from Western, Central and Eastern Europe as well as from biomass burning (Pace et al., 2006). In winter, AOD > 0.15 represents < 7% of data and it is associated to dust events (Figure 2.5 and Figure 2.6). In this season, the high contribution of aerosols associated to lower AOD values (< 0.15) indicates contribution of maritime aerosols and a minimum incidence of long range transport.

Further north, in the Italian Peninsula, ROM (Figure 2.9) and LEC sites show an important fine cluster in the AdA space ($\alpha > 1.8$ and $\delta\alpha \sim -0.4$) that corresponds to $\eta \sim 80\%$ and $R_f \sim 0.12$ μm. The fine mode at ROM is mainly due to secondary particles of local origin, and long range transport is a minor component (Gobbi et al., 2004). On the contrary, LEC presents a more important contribution of fine pollution aerosols transported from Central and Eastern Europe (Lelieveld et al., 2002), and from the Atlantic Ocean (De Tomasi and Perrone, 2003). LEC is also affected by fine particles originated by frequent summertime forest fires (Perrone et al., 2005). At both sites, a simultaneous growth of AOD and coarse fraction (indicated by a decrease of α) along constant R_f curves in the AdA space is associated to the presence of coarse particles (likely dust). In addition, in ROM (Figure 2.9), the extension of fine pollution particles to higher AOD occurs perpendicularly to the black line due to the presence of these large particles. Additionally, both sites are impacted by Saharan dust with AOD > 0.4 (with AOD maxima of 1.5) and $\alpha < 0.75$ that corresponds to $\eta < 30\%$. This coarse cluster is more important at LEC than at ROM (Figure 2.6) and it usually appears well-mixed with other small particles (Table 2.2). Thus, ROM and LEC present different seasonal features (Figure 2.5). The high contribution of large size aerosols at LEC in winter (Figure 2.5 and Figure 2.6) is due to the lower contribution of long-range transported fine particles and a higher weather instability that does not favour the accumulation of fine particles. From spring to autumn, a decrease of α values (Figure 2.5) is associated to an increase of the frequency of long-range transport of Saharan dust to southern and central Italy (Barnaba and Gobbi, 2004, Gobbi et al., 2004; Mona et al., 2006).

2.4.5.3 Eastern Mediterranean

In the Eastern Mediterranean large particles are quasi inexistent at THE (Figure 2.9). This site is characterized by rather heavy pollution being strongly influenced by regional (Central

and Eastern Europe) and local urban and industrial sources as well as by biomass burning that may also contribute sporadically from areas at the northern coast of the Black Sea (Gerasopoulos et al., 2003; Kazadzis et al., 2007). As shown in Figure 2.9, high extinctions (AOD > 0.7) mainly cluster in the fine mode ($\alpha \sim 1.8$ and $\delta\alpha \sim -0.3$) that corresponds to $\eta \sim 85\%$ and $R_f \sim 0.13$ μm. This fine polluted cluster presents a growing AOD linked to both coagulation-aging (along constant $\eta \sim 85\%$) and hydration-type increase along constant R_f curves. Occasional events of long-range transport of desert dust are observed only in summer (Figure 2.6) and commonly appear mixed with fine pollution aerosols (Figure 2.9). These desert dust events are associated to AODs between 0.7 and 1 as also suggested in Balis et al. (2006).

In the Eastern Mediterranean, CRE (Figure 2.9), ERD, ZIO (Figure 2.9), SED and CAI sites present high extinctions (AOD > 1) associated to clustering in the coarse mode ($\alpha < 0.75$) in the AdA space. They are related to large mineral aerosols originated in desert dust source regions such as Anatolian plateau, Saharan and Negev deserts (Andreae et al., 2002; Kubilay et al., 2003; Derimian et al., 2006) corresponding to $\eta < 40\%$. As shown in Figure 2.6, maximum contribution of the coarse particles, associated to high extinctions, is observed in spring in this area. During this season, long-range Saharan dust transport and uplifted dust particles from surrounding deserts are very important (Kubilay et al., 2000; Kubilay et al., 2003; Barnaba and Gobbi, 2004).

The aerosol climatology of CRE site (Figure 2.9) is strongly determined by the maritime environment with high concentrations of sea-salt aerosols (> 65% of its AOD is < 0.15) which constitute the background conditions. The CRE data shows high AOD (> 0.7), mainly clustering in the coarse mode ($\alpha < 0.6$ and $\delta\alpha \sim 0$) that corresponds to $\eta < 30\%$ (Figure 2.9). These large particles are related to long-range transport from Sahara, and, to a minor degree, from source regions in the eastern part of Mediterranean basin (such as Anatolian plateau, Saharan and Negev deserts) and Middle East (Dayan et al., 1991; Kubilay et al., 2000; Barnaba and Gobbi, 2004; Fotiadi et al., 2006). As shown in Figure 2.5 and Figure 2.6, maximum contributions of this coarse mode are observed in winter and spring. In winter, AOD > 0.15 represents < 20% of data and it is associated to dust events (Figure 2.5 and Figure 2.6). In this season, high contribution of aerosols associated to lower AOD values (< 0.15) is a consequence of the background situation dominated by the presence of maritime aerosols (Fotiadi et al., 2006; Kalivitis et al., 2007; Gerasopoulos et al., 2007). In spring, a decrease of $\delta\alpha$ values (~ 0) in the coarse mode with respect to the rest of the year (Table 2.2) indicates an increase of long-range dust transport to this area. Contributions from urban-industrial aerosol intrusions into the region from the Eastern Europe, Balkan area, and Anatolia are maxima in summer (Figure 2.5 and Figure 2.6). This

fine mode (α > 1.5 and $\delta\alpha$ ~ -0.2) is associated to low AODs (< 0.4) and corresponds to η > 70%. The growth to higher AODs and coarse fractions occurs perpendicularly to the constant R_f line due to the coexistence of coarse aerosols (likely maritime) and small pollution particles. Therefore, it is a common situation that they appear well-mixed as indicated by positives values of $\delta\alpha$ throughout the year (Figure 2.5).

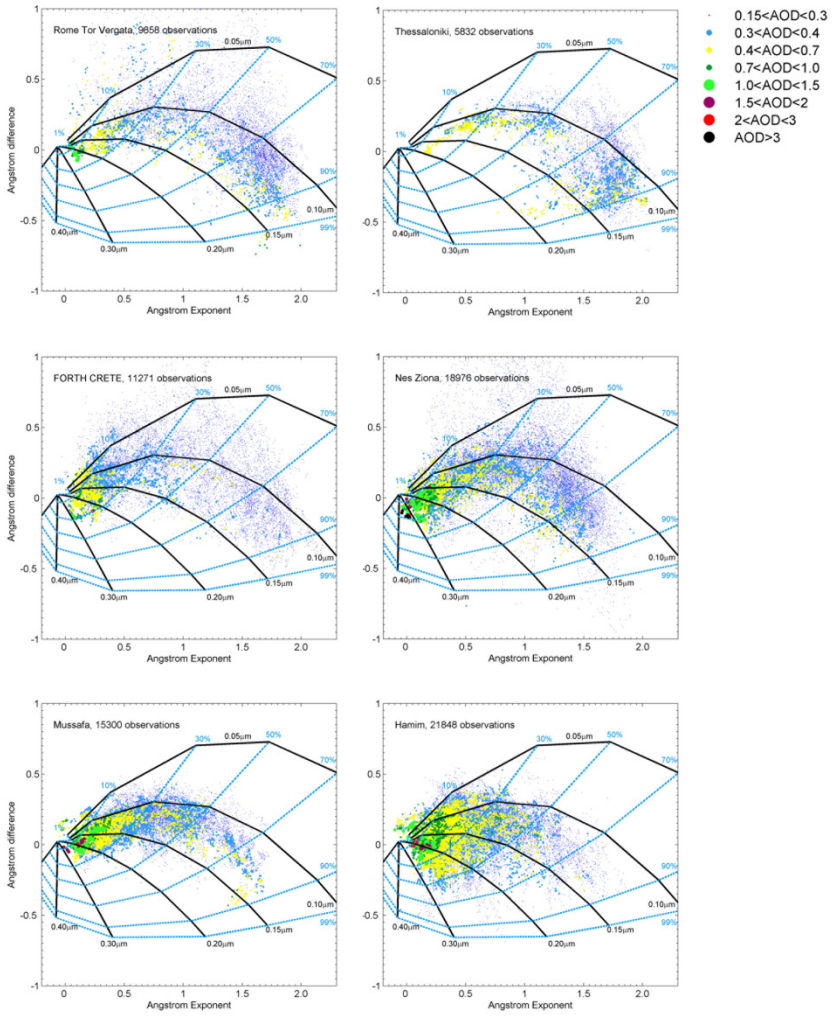

Figure 2.9 *Ångström exponent difference, $\delta\alpha = \alpha(440,675) - \alpha(675,870)$, as a function of the 440 – 870 nm Ångström exponent and AOD at 675nm (color code) for AERONET sites. Acronyms are defined in* ***Table 2.1****.*

A second cluster in the fine mode region ($\alpha \sim 1.6$ and $\delta\alpha \sim -0.3$), that corresponds to $\eta \sim 70\%$ and $R_f \sim 0.14$ μm, is observed. This fine mode is associated to pollution particles and it is especially remarkable at coastal sites Turkey and Israel such as ERD and ZIO (Figure 2.6), where the urban-industrial local emissions are significant. Most of the long-range transported aerosol in this region is attributed to Central and Eastern Europe, especially along the Israeli coast (Sciare et al., 2003; Fotiadi et al., 2006), as well as to Southern Russia (Andreae et al., 2002; Derimian et al., 2006) with additional contributions from marine biogenic activities and forest fires in the region. This fine cluster presents an increase in AOD and coarse mode fraction along the constants R_f curves (see ZIO in Figure 2.9), moreover, the growth to higher AODs also occurs perpendicularly to the constant R_f line. This is due to the coexistence of mineral dust and fine pollution aerosols. Additionally, in high-pollution locations (such as ZIO and ERD), branching of data along η lines is observed which is associated to coagulation-aging growth. The contribution of small pollution particles is maximum in summer (Figure 2.6), when wet removal is practically absent and the accumulation of pollution is favoured.

2.4.6 Middle East

The sites located in the Arabian Peninsula (MUS, DHA, DHD, BHR, HMM and SVI) provide a relatively large amount of measurements thanks to stable weather conditions in this region. The United Arab Emirates and the Persian Gulf include strong regional desert dust sources of predominately coarse mode-size particles, as well as important fine mode pollution particle sources from petroleum extraction and processing facilities which are located on islands, sea-platforms and coastal regions of the Persian Gulf. Thus, as shown in Figure 2.5, the coastal sites in the northeastern part of the United Arab Emirates such as MUS, DHA and DHD, as well as BHR in the Persian Gulf, attain positive $\delta\alpha$ values during almost all year (~ 0.2) which indicate the coexistence of two particle modes.

For the coastal sites of MUS (Figure 2.9), DHA, DHD and BHR, we observe desert dust with AOD maxima of 1.5, $\alpha < 0.75$ and $\delta\alpha \geq 0$ that corresponds to $\eta < 40\%$. As opposite, small particles from petroleum industry emissions are associated to fine mode ($\alpha \sim 1.6$ and $\delta\alpha \sim -0.2$) and AOD < 0.7 corresponding to $\eta > 70\%$ and $R_f \sim 0.13$ μm. The interaction of mineral dust and pollution is strong at these coastal sites. In the AdA space, this mixed region follows R_f constant curves and is associated to η between 40 and 70% (see MUS in Figure 2.9). Additionally, and due to the proximity of these stations to the sea, an increase in AOD is linked to both coagulation-aging and hygroscopic-type increase in R_f.

Conversely, at the inland desert sites, as HMM (Figure 2.9) and SVI, desert dust is the main aerosol constituent, being associated with high AOD (> 0.7 ranging up > 2) mainly clustering in the coarse mode ($\alpha < 0.75$ and $\delta\alpha$ variable). This cluster corresponds to $\eta <$ 50%. HMM (~ 125 km inland from the Gulf; Figure 2.9) shows a contribution of small particles from industrial emissions that corresponds to $\eta \sim 80\%$ and $R_f \sim 0.13$ μm. This transport is consequence of regional sea and land breeze circulations in this area (Eck et al., 2008) which produce occasional increases of fine mode particles from offshore petroleum operations. This fine mode presents a growth of AOD and coarse mode fraction along the constants R_f curves. Otherwise, SVI is located in the middle of the Arabian Peninsula, near to At Riyad (the capital of Saudi Arabia and its largest city) and far away from the Persian Gulf or other industrialized areas. SVI presents its highest extinctions (AOD > 1) in the coarse mode region ($\alpha < 0.75$ and $\delta\alpha < 0.1$) which presents an expanded particle size range suggesting significant variations in the particle size-distribution. It ranges from almost pure coarse-mode dust particles (associated to $\alpha < 0.3$ and $\eta < 30\%$) to a mixture of coarse particles and regional fine-mode pollution aerosols ($\eta < 70\%$) caused by anthropogenic activities in the region (Kaskaoutis et al., 2007).

As shown in Figure 2.6, the contribution of large particles is maximun in spring and summer. In spring, all sites present similar AODs and α values (Figure 2.5). It is associated to maximum desert dust local activity (Smirnov et al., 2002b; Eck et al., 2005; Kim et al., 2007; Kaskaoutis et al., 2007). On the contrary, in summer, MUS, DHA, DHD and HMM show higher AODs than BHR and SVI coinciding with a general increase of α values (Figure 2.5). In this season, the southwest monsoon introduces a northwesterly flow over the Arabian Peninsula bringing extremely dry and dust-loaded air from the Iraq and southern Iran deserts (Liu et al., 2000). In addition to long range transport, regional sea-land breeze circulations cause both, a regional transport of polluted and humid air masses from Persian Gulf to inland regions, and a dust transport from these regions towards the coast and the Gulf (Eck et al., 2008) favouring a mixing of desert dust and fine pollution aerosols.

2.5 Summary and conclusions

In this chapter, we have provided an aerosol characterization focusing on the contribution of mineral particles based on direct-sun observations of 39 AERONET stations which include at least an annual cycle within the 1994 - 2007 period. These stations are located in the region most affected by the presence of Saharan and Arabian desert dust: Northern Africa, Northeastern Atlantic, the Mediterranean Basin and Middle East. In addition to large mineral particles, fine pollution aerosols, originated in industrialized countries

surrounding the Mediterranean Sea and in the Persian Gulf, and biomass burning aerosols, produced in the Sahel and southern European countries, dominate the atmospheric aerosol load in this region.

The method used to discriminate different aerosol types, introduced in Gobbi et al. (2007), relies on the combined analysis of the Ångström exponent (α) and its spectral curvature, here represented by $\delta\alpha = \alpha(440,675) - \alpha(675,870)$. Plotting data in these coordinates was shown to allow for inference of aerosol fine mode size (R_f) and fractional contribution (η) to total AOD by means of reference points. It is also possible to separate the AOD increase due to fine-mode aerosol humidification and/or coagulation, from AOD growth due to the increase in coarse particles concentrations or cloud contamination.

In areas around the Sahara desert, mineral dust is found to be the main aerosol constituent, being associated with coarse mode particles a corresponding to $\eta < 40\%$. Highest extinctions (AOD > 4) are related to $\eta < 30\%$ and $R_f \sim 0.3$ μm that we assumed as typical of pure Saharan dust particles. Superimposed to this coarse cluster, small particles associated to fine mode ($\alpha > 1.5$ and $\delta\alpha \sim -0.3$), that corresponds to $\eta \sim 70\%$ and $R_f \sim 0.13$ μm, are also observed. In the Sahel region, this fine contribution is limited to winter and it is originated by biomass burning. At northern latitudes, the fine cluster is most important and is linked to the local or regional urban-industrial emissions. Frequently, the interaction of large mineral particles and small aerosols results in well-mixed particles with to $\delta\alpha > 0$. Eastern Tropical and sub-Tropical North Atlantic sites located in the outflow of Saharan dust from West Africa present similar behaviour to the continental stations located at the same latitudes, characterized by a large mineral dust fraction from spring to autumn.

In spite of the Iberian Peninsula sites showing frequent background conditions associated to low AOD values (< 0.15), high extinctions (AOD > 1) are associated to large particles with $\alpha < 0.6$ and $\delta\alpha \sim 0$ that correspond to $\eta < 30\%$, with a marked South-to-North gradient. This is linked to frequent African dust plumes affecting this area mainly in early-spring and summer. Additionally, a second cluster associated to $\alpha > 1.5$ and $\delta\alpha < -0.2$ that correspond to $\eta \sim 80\%$ and $R_f \sim 0.13$ μm can be related to polluted European continental air masses.

The highest polluted sites in the central-eastern Mediterranean show measurements clustering in the fine mode ($\alpha > 1.5$ and $\delta\alpha \sim -0.3$) that corresponds to $\eta > 70\%$ and $R_f \sim 0.13$ μm. In this case, the AOD increase is linked to both coagulation-aging and hydration type increase in R_f. Furthermore, a North-to-South AOD gradient, related to the coarse mode ($\alpha < 0.75$ and $\delta\alpha$ variable) with $\eta < 40\%$, is associated to seasonal dust export. In

general, the maximum dust activity appears in spring and summer over the whole Mediterranean Basin. In wintertime, the high contribution of aerosols associated to lower AOD values (< 0.15) indicates significant contributions from maritime aerosols compared to dust. However, some few dust outbreaks can also take place in this season. In general, desert dust appears well-mixed with other types of particles like fine pollution aerosols. They are associated to AOD < 1, but in some intense Saharan outbreaks (with $\delta\alpha \sim 0$) can reach AOD values of about 2.

In Middle East, all sites show high extinctions (AOD up to 3) mainly clustering in the coarse mode with $\eta < 50\%$. These extinctions are lower than those observed at the African sites. In coastal sites of the Persian Gulf, fine-mode aerosols ($\alpha > 1.6$ and $\delta\alpha \sim -0.3$) largely produced by the oil industry are observed. They are associated to $\eta > 70\%$ and $R_f \sim 0.13$ μm. The AOD increase is linked to both coagulation-aging and hydration-type increase in R_f due to very humid conditions in the Gulf. This variability of atmospheric particles type in conjunction with highly variable regional meteorology, results in a high variety of conditions in this region: some days are dominated by large particle desert dust, while others by fine pollution particles. However most of the days are characterized by a mixture of these two aerosol types.

Finally, this study confirms the robustness of the method of Gobbi et al. (2007) based on direct-sun measurements (more frequent and accurate than sky measurements) to track and characterize mixtures of pollution aerosol and mineral dust. We have also found that in the dataset we analysed $\delta\alpha < 0$ values can be related to a dominant single mode fraction, independently whether it corresponds to fine (high α) or to coarse (low α) aerosols.

The aerosol characterization presented in this chapter is used in the model quantitative evaluation and the analysis of results presented in the following chapters.

Chapter 3

3 Development and evaluation of the BSC-DREAM8b model

3.1 Introduction

Substantial impacts of dust upon climate and environment (IPCC, 2007) have increased the need to better understand and predict the atmospheric dust cycle. In this regard, a number of experimental and operational dust forecast systems have been developed in recent years, such as the global models Navy Aerosol Analysis and Prediction System (NAAPS; Westphal et al., 2009) and the aerosol model at the European Centre for Medium-range Weather Forecasts (ECMWF; Morcrette et al., 2007); and some regional models as BSC-DREAM8b (Nickovic et al., 2001; Pérez et al., 2006a,b), SKIRON (Nickovic and Dobricic, 1996; Kallos et al., 1997; Nickovic et al., 1997), CHIMERE-DUST (Menut et al., 2008; Schmechtig et al., 2011), MOCAGE (Martet and Peuch, 2009) and CUACE/Dust (Chinese Unified Atmospheric Chemistry Environment/Dust; Zhou et al., 2008).

The updated BSC-DREAM8b model is operated and further developed at BSC-CNS (www.bsc.es/projects/earthscience/DREAM/). Moreover, BSC-DREAM8b is one of the regional mineral dust models participating in the NA-ME-E Node of the SDS-WAS Programme. The history of the model starts with its predecessor, a single particle size dust model (Nickovic and Dobricic, 1996) initially developed in the World Laboratory Centre, Erice, Italy in the period 1991 - 1993. This model was implemented in the Tunisian Meteorological Service, where the first ever-successful operational regional dust forecast was performed during March-May 1995. The model was transferred to the University of Athens in 1995 where it was further improved and routine daily dust forecasts were established during 1996 - 1998 within the SKIRON project. Further model developments continued in ICoD, University of Malta, and resulted in the DREAM version of the model (Nickovic et al., 2001), which was routinely run in ICoD during the period 1998 - 2005. In May 2005, the operational DREAM dust forecasting system was transferred to the Environmental Modelling Laboratory of the Technical University of Catalonia (UPC) and in September 2006 to BSC-CNS where the model and its further developments are run on routine basis. While the forecast model domain had traditionally covered a region comprising the Mediterranean and the northernmost African sources, from 2006 the operational dust forecast at BSC-CNS was extended further covering the larger part of Europe to the north, sub-Saharan Africa to the south and the Arabian Peninsula to the east (Figure 3.1). BSC-DREAM8b provides the operational dust forecast at BSC-CNS since

May 2009. The main improved features of BSC-DREAM8b (Pérez et al., 2006a,b) with respect to the original DREAM model version are a more detailed size bin distribution and the inclusion of dust-radiation interactions.

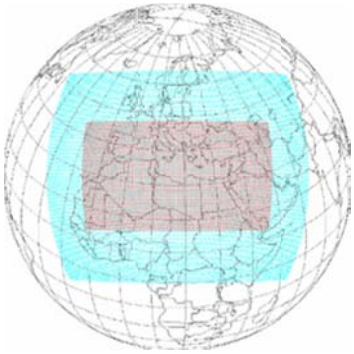

Figure 3.1 *Mediterranean (in red) and North Africa-Europe-Mediterranean (in blue) forecast domains of the operational versions of BSC-DREAM.*

In the last years, both operational versions have been used for dust forecasting and as dust research tools in North Africa and the Mediterranean (e.g. Amiridis et al., 2009; Klein et al., 2010; Alonso-Pérez et al., 2011). Several case studies have outlined the good skills of DREAM (e.g. Balis et al., 2006; Kishcha et al., 2007) and BSC-DREAM8b (e.g. Pérez et al., 2006a,b; Papanastasiou et al., 2010) concerning both the horizontal and vertical extent of the dust plume in the Mediterranean Basin. Furthermore, daily evaluation of BSC-DREAM8b with near-real time observations is conducted in BSC-CNS (www.bsc.es/plantillaH.php?cat_id=522). Currently, the daily operational model evaluation includes satellites (MODIS and MSG) and AERONET sun photometers. DREAM and BSC-DREAM8b have also been validated and tested over longer time periods in the European region (e.g. Jiménez-Guerrero et al, 2008; Pay et al., 2010; Pay et al., 2011) and against measurements at source regions for the SAMUM (Haustein et al., 2009) and BODEX campaigns (Todd et al., 2008).

The implementation of new model versions for operational applications requires extensive verification. On-going developments need to be evaluated in order to achieve better understanding and knowledge of dust source processes, size distributions and optical properties. The validation of regional mineral dust models is difficult. Measurements of aerosol properties from ground or space exist. However, all these remote sensing measurements are highly integrated: not only over the atmospheric column but also over all aerosol components. Thus investigations for the treatment of a particular aerosol type may

be limited to seasons and regions, when or where that aerosol type dominates the aerosol composition.

In this chapter, we first evaluate the performance and discuss the limitations of DREAM and BSC-DREAM8b and we test and discuss updates in the emission and deposition schemes. The domain covers Northern Africa, the Mediterranean Basin and Middle East. The evaluation is performed using hourly AOD data from the AERONET network (Holben et al., 1998) for year 2004. Satellite aerosol products are used to compare and analyse the modelled dust seasonal cycles. The chapter is organized as follows. Section 3.2 describes the main characteristics of DREAM and BSC-DREAM8b as well as the new components that will be evaluated. Section 3.3 describes the observational data and introduces the evaluation strategy. In Section 3.4 we discuss the results of the evaluation of several model versions. Finally, conclusions are included in Section 3.5.

3.2 Model description, new components and experimental set-up

The DREAM model solves the Euler-type partial differential nonlinear equation for dust mass continuity and it is fully embedded as one of the governing prognostic equations in the atmospheric NCEP/Eta atmospheric model (Janjic, 1977, 1979, 1984, 1990, 1994, 1996a, b; Mesinger et al., 1988; Zhao and Carr, 1997). In this section we describe the original and the current operational versions of the model together with other new components that will be evaluated. Table 3.1 lists the main characteristics of the different versions evaluated in this contribution.

3.2.1 Operational versions

In the operational versions of the model, the dust emission scheme parameterizes the vertical dust flux F_k for each particle bin k following Shao et al. (1993):

$$F_k = C \cdot S \cdot \beta_k \cdot \gamma_k \cdot u_*^3 \left(1 - \left(\frac{u_{*tk}}{u_*}\right)^2\right) \quad \text{for} \quad u_* \geq u_{*tk} \tag{3.1}$$

where C is a constant tuning parameter, u_* is the friction velocity, u_{*t} is the threshold friction velocity above which dust production starts, S represents the source term (which includes the desert mask), β_k is the fraction of each texture class of bin k considered in the

model and includes the influence of soil textures; and γ_k represents the ratio of the mass available for uplift and the total mass of the respective bin k.

The threshold friction velocity of the dry soil u_{*tkd} depends on the particle size which is defined following Bagnold (1941):

$$u_{*tkd} = A_k \sqrt{2gr_k \frac{\rho_k - \rho_a}{\rho_a}} \tag{3.2}$$

where g is the gravity acceleration, r_k is the particle radius size, and ρ_k and ρ_a the density of the particle and the ambient air, respectively. The parameter A_k is a function of the particle Reynolds number $(Rr)_{\rho k} = (2R_k u_{*tk})/\nu$ and $\nu = 0.000015$ m^2/s. For the considered particles sizes in the model A_k is specified by using available empirical data (White, 1979). In this formulation u_{*tkd} decreases with decreasing particle size (r_k), neglecting cohesive forces among small particles. In practice, this emission scheme directly entrains dust-sized particles into the atmosphere and includes the influence of soil structure and particle size distribution by means of S, β_k and γ_k.

Soil moisture effects on the threshold friction velocity are included following Fecan et al. (1999):

$$u_{*tk} = u_{*tk} \sqrt{1 + 1.21(w - w')^{0.68}} \tag{3.3}$$

where w is the ground wetness predicted by the model, and w' is the amount of adsorbed water which is an increasing function of the clay fraction in the soil.

Additionally, DREAM includes a viscous sublayer between the surface and the lowest atmospheric model layer (Janjic, 1994), by assuming a physical similarity between mass/heat/momentum exchanges over surfaces such as ocean with that of mobilized dust particle over desert surfaces (Chamberlain, 1983; Segal, 1990).

The model includes a simple wet scavenging scheme which uses a basic precipitation model with a constant washout ratio (see Nickovic et al., 2001). Dry deposition scheme follows Giorgi (1986) which calculates dry deposition velocity relative to the bottom transport model as a function of particle size and it is applied to any type of surface. This scheme includes processes of deposition by turbulent and Brownian diffusion, gravitational settling, interception and impaction on the surface roughness elements. Furthermore, the model considers desert dust aerosols as inert and particle growth under humid conditions is not taken account.

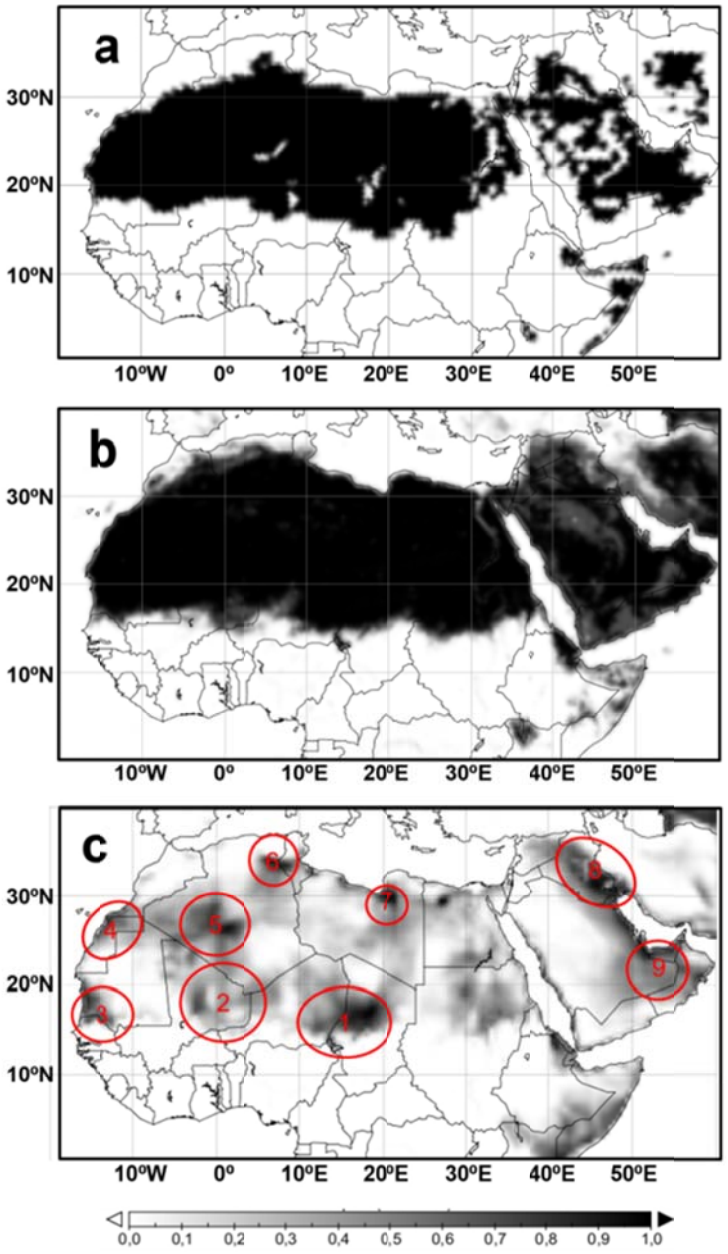

Figure 3.2 *In the top and central panels, source mask function (**S**) based on the arid and semi-arid categories of the 10-min SSiB (a) and Olson World Ecosystem and the 1-km USGS land use datasets (b). In the bottom panel (c), regional distributions of the source function (**G**) from Ginoux et al. (2001) in the grey scale. The red circles indicate dust emission source areas discussed in the text: (1) Bodélé, (2) Mali, (3) Mauritania, (4) Western Sahara-Morocco, (5) Algeria-Adrar, (6) North of Algeria-Tunisia, (7) Lybia desert, (8) An-Nafud desert and (9) Rub' Al Khali desert.*

Table 3.1 *Summary of the main features of each model version used in the present analysis: model version, status, texture type dataset, threshold friction velocity, horizontal and vertical flux, source size distribution, preferential sources, wet and dry deposition, number of bins and radiative feedbacks. The codes denote the following references. B41: Bagnold (1941); D87: D'Almeida (1987); D87N01: D'Almeida (1987) modified with the correction factors used by Nickovic et al. (2001); G01: Ginoux et al. (2001); G86: Giorgi (1986); IW82: Iversen and White (1982); MB95: Marticorena and Bergametti (1995); N01: Nickovic et al. (2001); S93: Shao et al. (1993), P06: Pérez et al. (2006a); White (1979); Z01: Zhang et al. (2001).*

Model version	Status	Texture and vegetation types dataset	Threshold friction velocity	Horizontal flux	Vertical flux	Source size distribution	Preferential sources	Wet dep.	Dry dep.	Number of bins	Radiative feedbacks
M4	Operational (DREAM)	FAO/UNESCO 4km SSiB and Olson World Ecosystem. 10-min	B41	-	S93	N01	No	N01	G86	4	No
M8	Operational (BSC-DREAM8b)	FAO/UNESCO 4-km USGS Global 1-km	B41	-	S93	D87	No	Corrected	G86	8	P06
D8	Research	FAO/UNESCO 4-km USGS Global 1-km	B41	-	S93	D87N01	No	Corrected	Z01	8	P06
DG8	Research	FAO/UNESCO 4-km USGS Global 1-km	B41	-	S93	D87N01	G01	Corrected	Z01	8	P06
N8	Research	STATSGO-FAO 5-min USGS Global 1-km	IW82	W79	MB95	D87	No	Corrected	Z01	8	P06
NG8	Research	STATSGO-FAO 5-min USGS Global 1-km	IW82	W79	MB95	D87	G01	Corrected	Z01	8	P06

In the original DREAM version (hereafter referred as M4, see Table 3.1), the source mask S is calculated from remapping the arid and semi-arid categories of the Olson World Ecosystems database (EPA, 1992) at 10-minutes resolution to the regional model domain (Fig. 3.2a). For soil textures, a combination of the Zobler near-surface global soil texture (Staub and Rosenzweig, 1987) at 1º resolution and the UNEP/GRID gridded FAO/UNESCO 4km soil units is used. For each soil texture class the fractions of clay, small silt, large silt and sand are estimated from the soil texture triangle (Hilell, 1982). In this version of the model the four different particle classes are assumed to have a typical particle radius of 0.73, 6.1, 18 and 38 μm, respectively. For long-range transport, only the first two dust classes are relevant for the analysis since their lifetime is larger than about 12 hours. To obtain the AOD we use a constant specific cross section (σ_λ^*):

$$AOD(\lambda) = \sigma_\lambda^* M \tag{3.4}$$

where M is the column mass loading in the 2 smaller size classes (0.73 and 6.1 μm). AOD_{fine} is calculated with the column mass of the first dust particle class and AOD_{coarse} is calculated with the column mass of the second dust particle class.

From 2003 onwards a research version of the model started to emerge. Following the idea of improving weather forecasts by including the dust radiative effect, an online interactive dust-radiation scheme was under development in the period 2002 - 2005, (Nickovic, 2002; Nickovic, 2005) and was successfully finalized in Pérez et al. (2006a) showing the positive impact of including dust-radiation interactions in the short-term weather forecast. The main features of BSC-DREAM8b (hereafter referred as M8, see Table 3.1), described in Pérez et al. (2006a), are a new source function S based on the arid and semi-arid categories of the 1 km USGS land use data set (Fig. 3.2b), a more detailed particle size distribution which includes 8 size bins within the 0.1 – 10 μm radius range according to Tegen and Lacis (1996) as listed in Table 3.2, a source distribution derived from D'Almeida (1987), and dust radiative feedbacks (Pérez et al., 2006a). Because important overestimations of the simulated dust concentration were observed during intense wet events in the Mediterranean Basin in M4, an updated wash-out ratio was introduced in M8.

Table 3.2 *Dust size bins introduced in the BSC-DREAM8b model. The bin intervals are taken from Tegen and Lacis (1996). Here $r_{min} - r_{max}$ are minimum and maximum radius and r_{eff} is effective radius for each size bin.*

Bin Number	$r_{min} - r_{max}$ (μm)	r_{eff} (μm)
1	0.1 - 0.18	0.15
2	0.18 – 0.3	0.25
3	0.3 – 0.6	0.45
4	0.6 – 1	0.78
5	1 – 1.8	1.3
6	1.8 – 3	2.2
7	3 – 6	3.8
8	6 - 10	7.1

For M8, AOD is calculated with the following expression:

$$AOD(\lambda) = \sum_{k=1}^{8} AOD_k(\lambda) = \sum_{k=1}^{8} \frac{3}{4\rho_k r_k} M_k Q_{ext}(\lambda)_k \qquad (3.5)$$

where for each size bin k: ρ_k is the particle mass density, r_k is the effective radius, M_k is the column mass loading and $Q_{ext}(\lambda)_k$ is the extinction efficiency factor at wavelength λ which was calculated using Mie scattering theory. AOD_{fine} and AOD_{coarse} are calculated in this version with bins 1 to 4 and 5 to 8, respectively.

3.2.2 New model components

In addition to the evaluation of the operational versions of the model we test and compare the behaviour of the model with several new components, including a new dry deposition scheme and a modified source size distribution (D8), a more physically-based dust emission scheme (N8), and the use of a topographic preferential source mask in combination with the two different emission schemes (DG8 and NG8). The main features are described below and summarized in Table 3.1.

3.2.2.1 Source size distribution and dry deposition

D8 is based on M8 with a modified mass size distribution at sources and a new dust deposition scheme based on Zhang et al. (2001). The modified source size distribution introduces a correction in the proportion between emitted coarse and fine fractions to the D'Almeida's (1987) mass size distribution. These correction factors are the same than those used in the original model version by Nickovic et al (2001). The new deposition scheme based on Zhang et al. (2001) replaces the one of Giorgi (1986) and calculates particle dry deposition velocities as a function of particle size and density as well as relevant meteorological variables and land use. As a different of earlier size-dependent particle dry deposition models (like the Giorgi's scheme), this latter dry deposition scheme produces more realistic deposition velocities for sub-micron particles in better agreement with the experimental results (Zhang et al., 2001). This deposition scheme includes simplified empirical parameterizations for the deposition processes of Brownian diffusion, impaction, interception and gravitational settling detailed in Slinn (1982).

3.2.2.2 Emission scheme

Wind tunnel studies have shown that for particles with radius < 35 μm, the threshold friction velocity increases with decreasing radius (Iversen and White, 1982), and at sources the direct emission of small dust particles by wind is negligible. Sandblasting and disaggregation of clay and silt particles by large particles in saltation dominate the vertical flux of dust, which is strongly sensitive to the size distribution of saltating particles.

N8 is based on M8 with the dust deposition scheme based on Zhang et al. (2001) and a more physically-based dust emission scheme. In this case, a horizontal saltation flux H is simulated according to White (1979) as follows:

$$H = c_s \frac{\rho_a}{g} u_*^3 \sum_{k=1}^{4} \left(1 + \frac{u_{*tk}}{u_*}\right)\left(1 - \frac{u_{*tk}^2}{u_*^2}\right) s_k \quad \text{for} \quad u_* \geq u_{*tk} \tag{3.6}$$

where c_s is a dimensionless factor taken as 2.61 (White, 1979), ρ_a is the air density, u_* is the wind friction velocity, g is the gravitational constant, u_{*tk} is the threshold wind friction velocity and s_k is the relative surface area of each soil population k (i.e., clay, silt, fine-medium sand and coarse sand). In this case the threshold friction velocity shows an optimum particle diameter range for uplifting between 60 and 80 μm and is parameterized using the semi-empirical relationship of Iversen and White (1982). For smaller and larger particles the threshold friction velocity increases due to inter-particle cohesion forces and

gravity, respectively. As in the previous model versions, soil moisture effects on the threshold friction velocity are included following Fecan et al. (1999).

The vertical flux F follows the empirical relationship of Marticorena and Bergametti (1995):

$$F = C \cdot S \cdot \delta \cdot H \tag{3.7}$$

where C is the tuning constant, S represents the source function (which includes the desert mask), and δ is the so called horizontal to vertical flux ratio reflecting the availability of dust in the soil. To specify the soil size distribution we use the soil textures of the hybrid STATSGO-FAO soil map. In this database, the FAO two-layer 5-minute global soil texture is remapped into a global 30-second regular latitude-longitude grid. We use 4 soil populations in the model distinguishing among fine-medium sand and coarse sand according to the criteria used in Tegen et al. (2002).

3.2.2.3 Preferential sources

Enclosed basins containing former lake beds or riverine sediment deposits provide an abundance of small clay-sized particles that are loosely bound, and dominate global dust emission according to the TOMS aerosol index (AI) satellite retrieval (Prospero et al., 2002). Modelling studies show that inclusion of these "preferred" source regions improves the realism of the model dust load in the vicinity of the sources (Zender et al., 2003b). To identify these regions, we test the source function G described in Ginoux et al. (2001) based upon topography which is described as follows:

$$G_i = \left(\frac{z_{max} - z_i}{z_{max} - z_{min}} \right)^5 \tag{3.8}$$

which is defined as the probability to have an accumulated alluvium sediments in the grid cell i of altitude z_i , and z_{max} and z_{min} are the maximum and the minimum elevations in the surrounding 10º x 10º topography, respectively (see Fig. 3.2c). We analyse the impact of the preferential source function of Ginoux et al. (2001) in conjunction with the two emission schemes in D8 and N8. In these model simulations G is multiplied with the source term S in D8 and N8 which will be referred as DG8 and NG8, respectively.

3.2.3 Model experimental set-up and tuning

We evaluate and discuss annual simulations over the extended operational domain, which includes Northern Africa, the Mediterranean and Middle East (Fig. 3.1, blue grid). The

simulated dust distributions consist of 366 daily runs for year 2004. The initial state of dust concentration is defined by the 24-hour forecast of the previous-day model run. Only in the "cold start" of the model, concentration is set to zero. The cold start of the model was initiated on 23 December 2003. The Final Analyses of the National Centers of Environmental Prediction (FNL/NCEP; at 1º x 1º) at 0 UTC are used as initial meteorological conditions and boundary conditions at intervals of 6 hours. The resolution is set to 1/3º in the horizontal and to 24 layers extending up to approximately 15 km in the vertical.

Because dust emission is a non-linear function of wind speed and depends on many other factors that are poorly known at the scale of the model grid, dust emission in models is constrained with observations (Cakmur et al., 2006). In this analysis, we optimize the tuning parameter C in Equations (3.1) and (3.7) for all the experiments by minimizing the weighted sum of the squared difference between the model and observed values of AOD from the measurements available during the study period presented in the next section. A posteriori model calibration is necessary to compare different model versions and understand regional differences among them.

3.3 Data and evaluation methods

3.3.1 Observational data

In the present chapter, quality-assured direct-sun data in the 440 - 870 nm wavelength range is used since these channels are highly accurate and they are available in all AERONET instruments. In order to achieve a good temporal and spatial coverage, the selection of the AERONET stations for the present model evaluation is based on two criteria: their localization in the simulation domain (box at 0 - 45º N and 26ºW - 60ºE) and the amount of the data during our study year. All operational stations in 2004 that collected data on at least 100 hours, over a minimum period of 2 months have been selected. Additionally on those sites where the SDA retrieval (see Section 2.3) is available (mainly in the Mediterranean and Middle East regions) the contribution of each aerosol fraction is analysed. Figure 3.3 shows the location of the 44 selected AERONET sites and Table 3.3 lists additional information including type of site, observation periods, percentage of cloud screened data and the availability of SDA products.

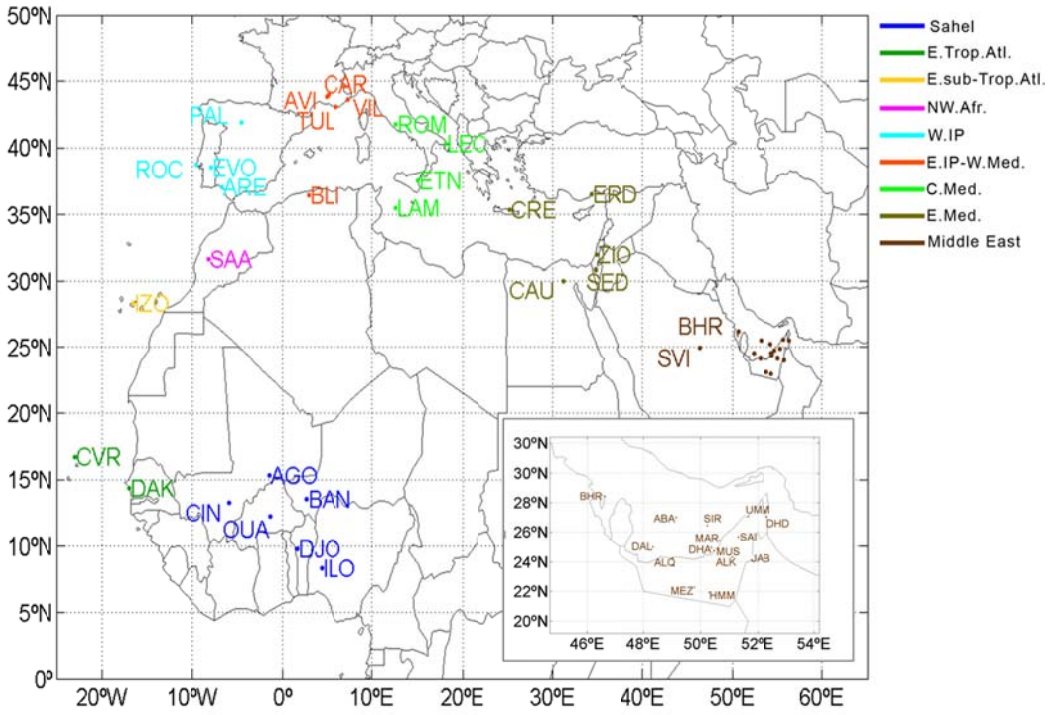

Figure 3.3 *Spatial distribution of 44 selected AERONET stations over the study domain. Acronyms are described in the Table 3. The different colours indicate the different regions which are defined as: Sahel, Eastern Tropical Atlantic (E.Trop.Atl), Eastern sub-Tropical Atlantic (E.sub-Trop.Atl), Northwestern Africa (NW.Afr), Western Iberian Peninsula (W.IP); Eastern Iberian Peninsula-Western Mediterranean (E.IP-W.Med), Central Mediterranean (C.Med), Eastern Mediterranean (E.Med) and Middle East.*

In addition to the AERONET comparison, we qualitatively compare the modelled dust AOD to seasonal satellite aerosol distributions from TOMS, MISR, MODIS/Aqua sensors (Figure 3.4, Figure 3.5, Figure 3.6 and Figure 3.7). In the visible and near IR, deserts are highly reflective and accurate retrievals of AOD are difficult because single view multispectral satellite instruments are generally unable to separate the atmospheric and surface contributions to the measured radiances. Among other causes, differences between the different aerosol satellite products are partly due to the use of different sensors that work in different spectral channels, orbits and spatial resolutions as well the algorithms used for the production of the corresponded aerosol product. In spite of these differences, there are some features in common.

TOMS AI (Torres et al., 1998; Prospero, 2002; Ginoux et el., 2003) is a semi-quantitative aerosol product that indicates the presence of absorbing aerosols like desert dust. The algorithm is based on the perturbation of the backscattered UV flux that originates below the aerosol layer and it could retrieve aerosol data in partially clouded pixels. MISR is a unique blend of directional and spectral data that allows to use aerosol retrieval algorithms

which do not depend on explicit radiometric surface properties. As such, MISR can retrieve aerosol properties like AOD over a variety of terrain, including highly reflective surfaces like deserts (Martonchik et al., 2004). The MISR observation repeat time is only 3 or 4 visits per month for those latitudes where Earth's large desert areas occur. In the present analysis, we use the collection C005 AOD data (cloud free) at 550 nm from MODIS/Aqua sensor. The MODIS aerosol algorithm is comprised of two independent algorithms, one for deriving aerosols over land and the second for aerosols over ocean (Levy et al., 2003; Remer et al., 2005). However, algorithm over land has been developed to be used only low ground reflectance (i.e. over dark vegetation). For this reason, the MODIS/Aqua Deep Blue AOD product has been included in the analysis. The MODIS/Aqua Deep Blue algorithm employs radiances from blue channels for which the surface reflectance is low enough that the presence of dust brightens the total reflectance and enhances the spectral contrast (Hsu et al., 2004). Thus, the MODIS/Aqua Deep Blue AOD product basically provides information over arid and semi-arid areas. Figure 3.4, Figure 3.5, Figure 3.6 and Figure 3.7 include a combination of the seasonal averages of MODIS/Aqua Deep Blue AOD and the collection C005 AOD data.

As shown by the satellite data in Figure 3.4, Figure 3.5, Figure 3.6 and Figure 3.7 in general MODIS features a higher AOD than MISR. This could be linked to the lower MISR observation frequency. While its temporal resolution (the repeat time is only 3 or 4 visits per month) is high enough to capture the major seasonal dust activity, it may be too low to reproduce some regional sources.

3.3.2 Evaluation strategy

In order to quantitative compare the modelled optical data in the mid-visible spectrum with measurements at 550 nm, AOD at 550 nm from AERONET observations are obtained from data between 440 and 870 nm following the Ångström's law. Because AERONET data are acquired at 15-minute intervals on average, all AERONET measurements within ±30 minutes of the model hourly outputs were extracted and used for comparison with the model.

The presence of different types of aerosols mixed with dust in the measurement points should introduce a negative bias in the comparison between dust model outputs and observations. In general, the model should underpredict the dust AOD for increasing Ångström exponents (α) because of the influence of anthropogenic pollution (Pérez et al., 2006b). In order to evaluate mineral dust models, observations have to be segmented into their different aerosol component, and the contribution of dust has to be extracted.

Table 3.3 *Location and description of the 44 selected AERONET stations in our study domain. Class of location which are defined as stations: above 1000 m (H), in arid and desert areas (D), in the ocean (O), in remote and urban areas (R/U) and in littoral areas (C); coordinates, altitude, the number of total level 2.0 direct-sun measurements (Dataset) and the number of hours (N), days (Dy.) and months (M) in the observation periods, the percentage of cloud screened data of the selected AERONET stations (F) and the availability of the quality-assured SDA retrieval products (SDA).*

Station name	Code	Zone	Class	Lon.(°/E)	Lat.(°/N)	Alt.(m)	N	Hr.	Dy.	Mo.	F(%)	SDA
Abu_Al_Bukhoosh	ABA	Middle East	R/UC	53.1	25.5	24.5	2021	580	83	4	33.22	
Agoufou	AGO	Sahel	D	-1.5	15.3	305.0	10967	2815	316	12	30.27	
Al_Khaznah	ALK	Middle East	R/U	55.1	24.2	192.0	3959	1024	100	4	19.86	X
Al_Qlaa	ALQ	Middle East	R/UC	53.0	24.1	5.0	2245	482	44	3	19.44	X
Avignon	AVI	W.Med	R/U	4.9	43.9	32.0	7131	1368	220	12	34.52	
BAHRAIN	BHR	Middle East	R/UC	50.6	26.2	25.0	2423	610	77	3	27.33	
Banizoumbou	BAN	Sahel	D	2.7	13.5	250.0	11000	2842	325	12	32.00	
Blida	BLI	W.Med	R/UC	2.9	36.5	230.0	4598	1998	264	12	33.55	X
Cabo_da_Roca	ROC	W.IP	R/UC	-9.5	38.8	140.0	4179	1259	197	10	39.17	
Cairo_University	CAI	E. Med	R/U	31.2	30.0	50.0	1061	338	52	3	58.56	
Capo_Verde	CVR	E.Trop.N.Atl	O	-22.9	16.7	60.0	1583	477	70	4	37.23	X
Carpentras	CAR	E.IP-W.Med	R/U	5.1	44.1	100.0	6905	1979	242	11	37.12	X
Dakar	DAK	E.Trop.N.Atl	R/UC	-17.0	14.4	0.0	9742	2520	301	12	28.69	
Dalma	DAL	Middle East	R/UC	52.3	24.5	0.0	4422	1435	161	6	32.38	X
Dhabi	DHA	Middle East	R/UC	54.4	24.5	15.0	7128	1813	203	8	22.05	X
Dhadnah	DHD	Middle East	R/UC	56.3	25.5	81.0	5057	1252	161	7	21.55	X
Djougou	DJO	Sahel	R/U	1.6	9.8	400.0	4517	1166	136	7	31.39	
El_Arenosillo	ARE	W.IP	R/UC	-6.7	37.1	0.0	9235	2437	302	12	23.7	
ETNA	ETN	C. Med	R/UC	15.0	37.6	736.0	871	226	40	3	39.25	X
Evora	EVO	W.IP	R/U	-7.9	38.6	293.0	7860	2205	266	12	29.75	
FORTH_CRETE	CRE	E. Med	R/UC	25.3	35.3	20.0	9634	2352	272	12	24.9	X
Hamim	HMM	Middle East	D	54.3	23.0	209.0	7899	1715	183	7	23.39	X
IER_Cinzana	CIN	Sahel	D	-5.9	13.3	285.0	6488	1659	195	7	29.6	
Ilorin	ILO	Sahel	R/U	4.3	8.3	350.0	840	390	66	3	36.06	X
IMS-METU-ERDEMLI	ERD	E. Med	R/UC	34.3	36.6	3.0	7223	1832	235	11	19.83	X
Izana	IZO	E.sub-Trop.N.Atl	HO	-16.5	28.3	2391.0	5358	1260	145	7	29.79	
Jabal_Hafeet	JAB	Middle East	R/U	55.8	24.1	1059.0	2971	719	83	5	35.20	X
Lampedusa	LAM	C. Med	R/UC	12.6	35.5	45.0	2561	848	139	8	30.63	
Lecce_University	LEC	C. Med	R/U	18.1	40.3	30.0	5489	1671	219	10	34.28	X
MAARCO	MAR	Middle East	R/UC	54.7	24.7	10.0	2298	559	56	3	25.53	X
Mezaira	MEZ	Middle East	D	53.8	23.1	204.0	6001	124	1166	5	19.14	X
Mussafa	MUS	Middle East	R/UC	54.5	24.4	10.0	2912	590	75	3	28,57	X
Nes_Ziona	ZIO	E. Med	R/U	34.8	31.9	40.0	9441	2592	299	12	33.09	X
Ouagadougou	OUA	Sahel	D	-1.4	12.2	290.0	7133	1911	271	12	34.51	
Palencia	PAL	W.IP	R/U	-4.5	42.0	750.0	7389	2010	265	12	32.69	
Rome_Tor_Vergata	ROM	C. Med	R/U	12.6	41.8	130.0	2256	601	106	8	40.05	
Saada	SAA	NW.Afr	D	-8.2	31.6	420.0	6053	1360	158	6	25.67	
Saih_Salam	SAI	Middle East	D	55.3	24.8	84.0	5537	1191	111	5	21,36	X
SEDE_BOKER	SED	E. Med	D	34.8	30.9	480.0	11904	2915	310	12	24.54	X
Sir_Bu_Nuair	SIR	Middle East	R/UC	54.2	25.2	10.0	1512	445	60	3	39,11	X
Solar_Village	SVI	Middle East	D	46.4	24.9	764.0	10086	2409	284	11	23,55	X
Toulon	TUL	W.Med	R/UC	6.0	43.1	50.0	430	128	24	2	42.09	
Umm_Al_Quwain	UMM	Middle East	R/UC	55.7	25.5	20.0	5336	1335	135	6	19,03	X
Villefranche	VIL	W.Med	R/UC	7.3	43.7	130.0	7120	1936	235	11	32.81	

Following the results obtained in the aerosol characterization shown in Chapter 2, we implemented a simple method to separate the contribution of dust over our study area, based on the combination of AOD, α and $\delta\alpha$. For the quantitative model evaluation against AERONET data, we only take into account desert dust (i.e. aerosols associated with high extinctions and coarse-particle dominated fraction). Aerosol data with $\alpha < 1$ and $\delta\alpha < 0.1$ have been considered as desert dust. All data with $\alpha > 1.5$ is associated to fine anthropogenic aerosols and have been considered no-dust situations. Therefore, we have ascribed and observed dust AOD of 0 for $\alpha > 1.5$ in the comparison. Measurements outside these ranges are associated with mixed aerosols and not included in the quantitative model evaluation.

At those sites where the SDA products are available (mainly in Middle East and Mediterranean regions as shown in Table 3.3) the AOD evaluation is complemented with AOD_{coarse}. As indicated in Chapter 2, AOD_{coarse} is fundamentally associated to maritime/oceanic aerosols and desert dust. Since sea-salt is related to low AOD (< 0.03; Dubovik et al., 2002) and mainly affects coastal stations, high AOD_{coarse} values are mostly related to mineral dust. In order to evaluate the performance of the different model configurations, we use a set of statistics. Discrete statistics such as correlation coefficient (*r*), mean bias (MB) and root mean square error (RMSE), measure the skill of the model when performing diagnostic analyses of dust AOD at specific points where AERONET sites are located.

3.4 Results and discussion

Mineral dust is the most important aerosol constituent in Northern Africa and Middle East. As shown by the satellite data in Figure 3.4, Figure 3.5, Figure 3.6 and Figure 3.7, dust activity and transport evolve during the year as changing seasons bring strong winds and low precipitation to different regions (Prospero et al., 2002; Engelstaedter et al., 2006; Klose et al., 2010). Satellite observations show two major dust sources in the Bodélé Basin and at the Mali-Mauritania border, which present maximum aerosol concentrations in spring and summer. The different satellite estimates do not show a clear seasonal pattern in Arabia, where the MODIS Deep Blue AOD product presents low extinction values in comparison with the relatively strong signal in TOMS AI or MISR AOD particularly in summer and autumn.

In Northern Africa, the winter dust activity is greatest in low latitudes; as the year progresses, dust activity shifts to higher latitudes (Prospero et al., 2002; Klose et al., 2010). From October to December, dust activity appears to be very limited over the entire area

and from April to June is observed the highest dust occurrence (Middelton and Goudie, 2001; Schepanski et al., 2007). The transport is driven by the latitudinal shift of the Intertropical Front which corresponds to the convergence zone between the northern winds, called the Harmattan, and the monsoon winds coming from the South. From late February to early May the Harmattan wind index is maximum (Sultan et al., 2005) inducing strong winds in the Sahel. During summertime, the dust activity is at maximum (Prospero et al., 2002; Engelstaedter et al., 2006) and the dust transport moves to northern latitudes. Although much of the dust is raised locally over Middle East, substantial amounts of dust come from the Sahara (Middelton and Goudie, 2001). Over much of the Arabian Peninsula, dust is active all year long, but is relatively low in winter months. Dust activity in Middle East grows strong in spring and summer, and weakens in autumn (Prospero et al., 2002).

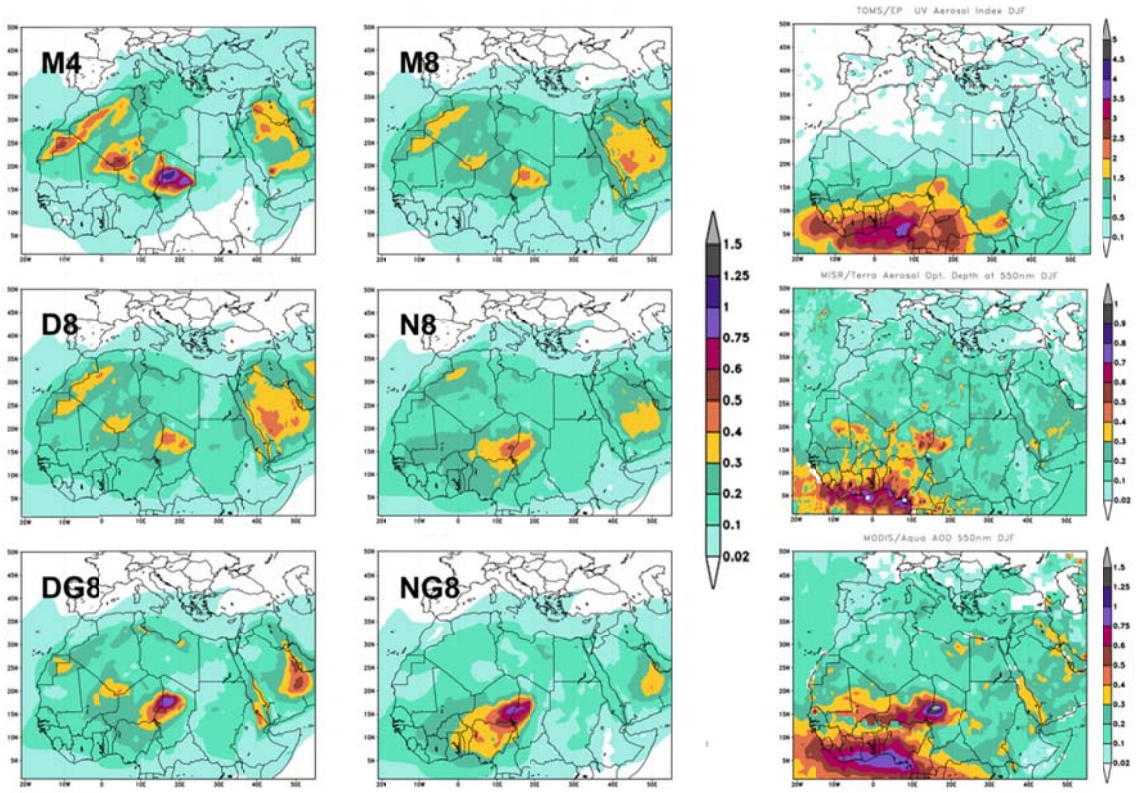

Figure 3.4 *The distribution of the dust AOD modelled in winter 2004 by M4, M8, D8, N8, DG8 and NG8 (left and central panels). The distribution of the observed aerosols in winter 2004 over the study region (right panels) using a seasonal average of TOMS UV Aerosol Index (AI), MISR AOD as well as a combination of MODIS Aqua AOD products (Collection 005 and Deep Blue).*

Simulated seasonal average AOD for the different model experiments are shown for winter (Figure 3.4), spring (Figure 3.5), summer (Figure 3.6) and autumn (Figure 3.7). Regionally averaged time series of the observed and simulated daily AOD and of the monthly mean bias are displayed for the Sahel, and the Eastern Tropical and sub-Tropical North Atlantic (Figure 3.8), north-western Africa, the western Iberian Peninsula and Western Mediterranean (Figure 3.9), as well as, Central and Eastern Mediterranean and Middle East (Figure 3.10). Regionally averaged time series of the observed and simulated daily AOD_{coarse} are displayed for the Mediterranean and Middle East in Figure 3.11. The Taylor's diagram (Taylor, 2001) by regions presented in Figure 3.12 concisely summarizes the degree of correspondence between simulated and observed fields. On this diagram the correlation coefficient, the centered root-mean-square (RMS) and the standard deviation of the simulated values are shown. Together these statistics provide a quick summary of the degree of pattern correspondence, allowing one to gauge how accurately a model simulates the observations.

3.4.1 Operational versions

In winter and spring, satellites highlight a strong aerosol signal over the Sahel and the Gulf of Guinea (Figure 3.4 and Figure 3.5). Dust is carried southwestward from the Bodélé in Western Chad and adjacent areas at low levels by the northeasterly Harmattan winds (Chiapello et al., 1995; Kim et al., 2009; Cavalieri et al., 2010). Both M4 and M8 strongly underestimate the AOD observations in the Sahelian sites (Figure 3.12) with mean bias between -0.5 and -1.0, and achieve very low correlations (0.24 for M4 and 0.18 for M8, see Figure 3.8). The interaction of desert dust and biomass burning aerosols in the region partly hampers the dust model evaluation but does not explain the significant mismatch of the model. Note that in M4 and M8, AOD values are below 0.1 south of 12ºN in winter (Figure 3.4). This result suggested a severe underestimation in the emission from south Saharan sources, a problem in the low-level dust transport over the region or a combination thereof. With respect to the latter, a detailed analysis of the simulated dust transport in M4 and M8 reveals a very efficient dry deposition along the southwestward dust transport (not shown). Also some important sources over Eastern Niger and the Mali-Mauritania border appear to be misrepresented by M4 and M8 throughout the year (particularly in summer) in comparison to satellite data. Figure 3.8 shows that the model tends to overestimate the summer AOD in the Eastern Tropical North Atlantic AERONET sites where it achieves annual correlations of 0.24 for M4 and 0.34 for M8 that may reflect deficiencies in the transport from the Mali-Mauritania border source. Under the influence of the Harmattan, dust storms in the Sahara are quite frequent, for example, on the alluvial plain of Bilma (Niger) and Faya Largeau (Chad). Dust is transported from these regions to the Gulf of Guinea (e.g. Middleton and Goudie, 2001).

In contrast to TOMS AI retrievals, MISR and MODIS AOD indicate significant aerosol content over several other dust source areas, including the zone of the Chotts in Algeria and Tunisia, in summer, as well as, the region of Libya, Egypt and Sudan, in spring.

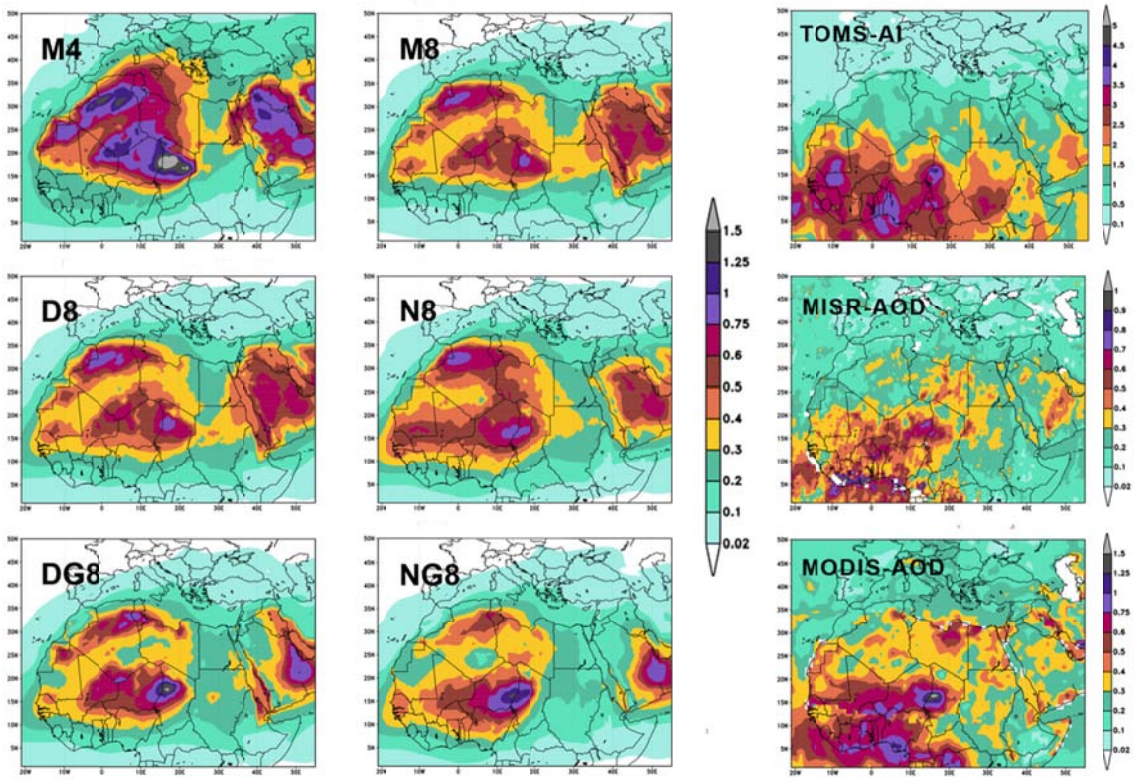

Figure 3.5 *The distribution of the dust AOD modelled in spring 2004 by M4, M8, D8, N8, DG8 and NG8 (left and central panels). The distribution of the observed aerosols in spring 2004 over the study region (right panels) using a seasonal average of TOMS UV Aerosol Index (AI), MISR AOD as well as a combination of MODIS Aqua AOD products (Collection 005 and Deep Blue).*

From winter to summer, M4 and M8 show a clear overestimation of the dust activity in Algeria when compared to satellite estimates. Maximum dust transport from the North of Algeria and Tunisia is observed in spring over the Central-Eastern Mediterranean shifting towards the Western Mediterranean in summer. While there are important differences between M4 and M8, both model versions strongly overestimate the satellite (Figure 3.4, Figure 3.5 and Figure 3.6) and AERONET AOD (Figure 3.8 and Figure 3.9), especially M4. The overestimated dust emissions in Algeria are always related to the lee of the Atlas Mountains and are a common pattern in M4 and M8. Several causes could induce the overestimation of dust emission in this area. For example, the misrepresentation of a small-

scale atmospheric convection processes in this complex region by the meteorological driver could overestimate the surface winds and consequently the dust emissions. These misrepresentations could be associated to not enough spatial horizontal resolution. Other reasons could be linked to the description of the vertical coordinate (Eta) in the model. Otherwise, threshold friction velocity is essentially a property of the soil surface, rather than that of a soil particle. The soil humidity in the model is climatologically described introducing errors in the calculation of the threshold friction velocity.

In spring, dust events in the Western-Central Mediterranean are usually driven by low-pressure systems with presence of rain (Avila et al., 1998; Moulin et al., 1998). In this season, M4 clearly tends to overestimate the AOD over the Central-Western Mediterranean AERONET sites coinciding with periods with no data available from AERONET due to clouds and/or rain (Figure 3.8 and Figure 3.9). The AOD is better represented in M8 due to a lower dust emission in Algeria and a more efficient dust wet removal in this version.

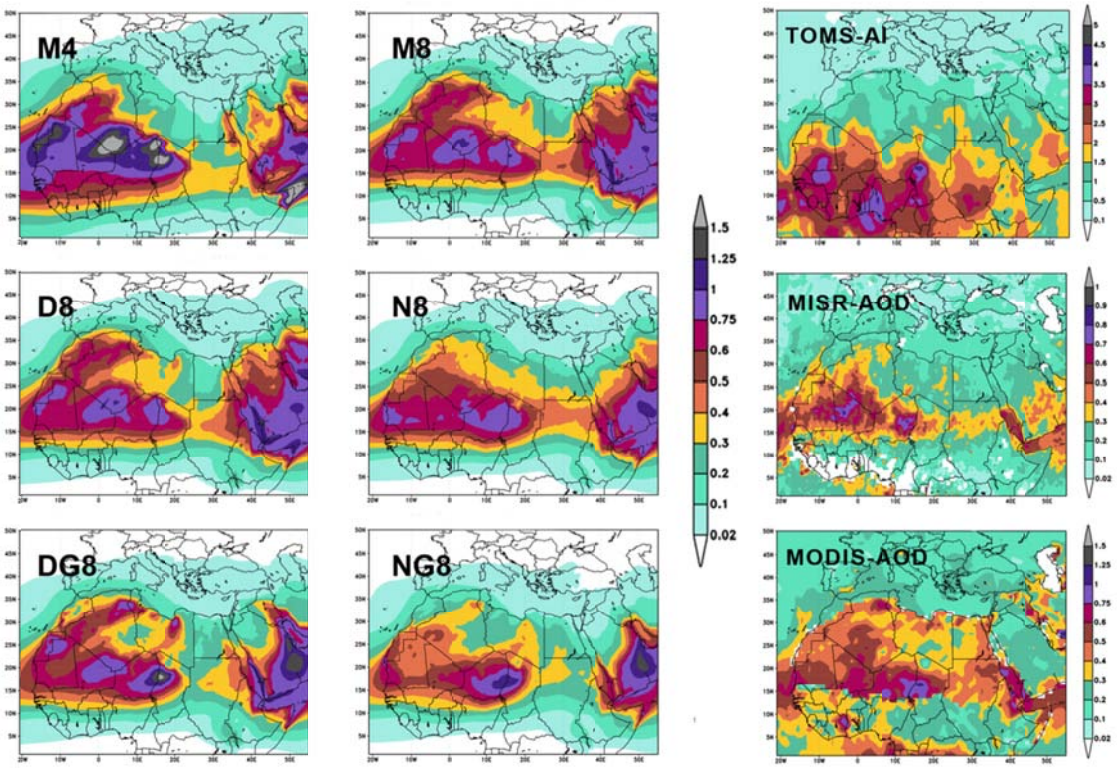

Figure 3.6 *The distribution of the dust AOD modelled in summer 2004 by M4, M8, D8, N8, DG8 and NG8 (left and central panels). The distribution of the observed aerosols in summer 2004 over the study region (right panels) using a seasonal average of TOMS UV Aerosol Index (AI), MISR AOD as well as a combination of MODIS Aqua AOD products (Collection 005 and Deep Blue).*

In summer, M8 simulates a lower AOD than M4 at sources in Chad, Niger, Mali and southern Algeria showing a better match with satellite observations (Figure 3.6). However, the strong dust emissions in Northern Mali indicated by the observations are not reproduced by both model versions. The overestimation of M4 is also observed at AERONET sites along the dust transport in the Eastern Tropical and sub-Tropical North Atlantic (Figure 3.8). Both versions indicate a strong dust source in southern Algeria, which does not appear in the satellite observations. However, the strong dust emissions in Northern Mali indicated by the observations are not reproduced by both model versions. The simulated dust AOD at sources is generally weaker in M8 than in M4 with the exception of certain areas around of the Red Sea and Middle East. This is partly explained by the increased transport bin resolution in M8 making long-range transport more efficient.

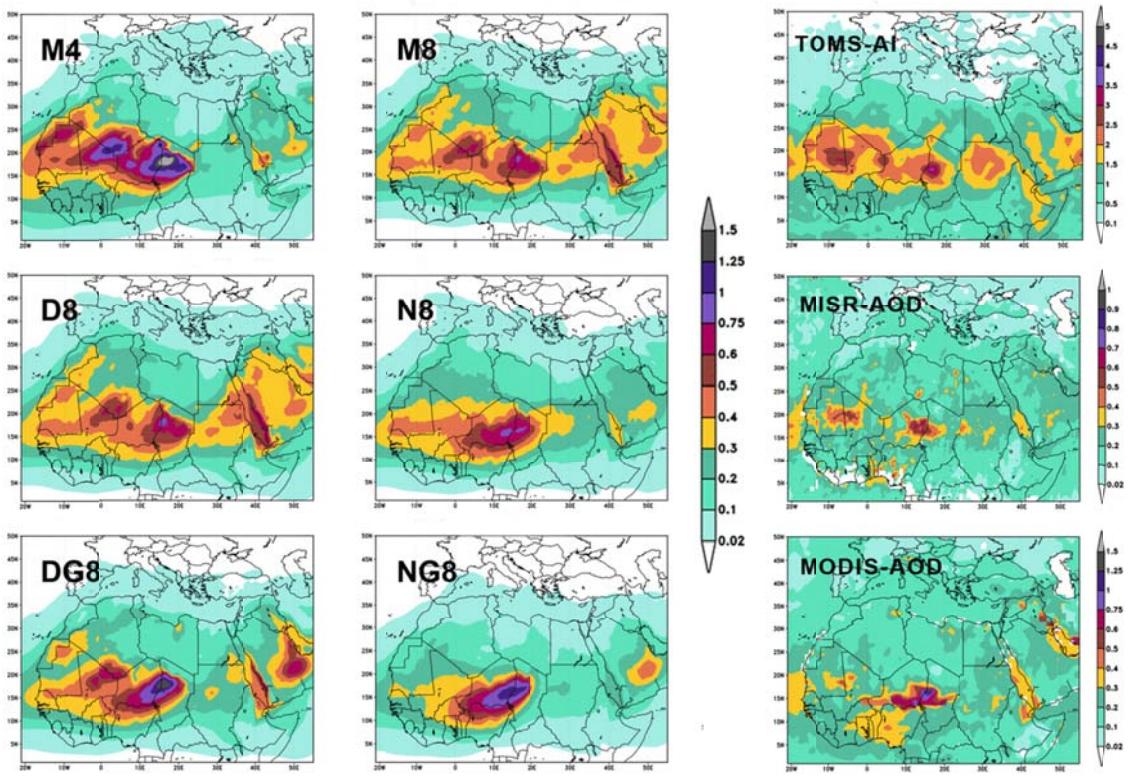

Figure 3.7 *The distribution of the dust AOD modelled in autumn 2004 by M4, M8, D8, N8, DG8 and NG8 (left and central panels). The distribution of the observed aerosols in autumn 2004 over the study region (right panels) using a seasonal average of TOMS UV Aerosol Index (AI), MISR AOD as well as a combination of MODIS Aqua* AOD *products (Collection 005 and Deep Blue).*

In Middle East, the maximum local desert dust activity is detected in spring (Smirnov et al., 2002b; Kim et al., 2007). In contrast to M8, M4 simulates a maximum AOD in winter and

spring over the An-Nafud desert in the northern part of the Arabian Peninsula (Figure 3.4 and Figure 3.5). In spring, the comparison with AERONET shows that M4 presents better seasonal correlations than M8 (0.59 for M4 and 0.53 for M8). This is partly linked to the different source mask used in each model version (see Table 3.1 and Figure 3.2a and Figure 3.2b). In both model versions maximum summer activity shifts towards southern latitudes over the Rub' Al Khali desert (in the southwestern part of the Arabian Peninsula, see Figure 3.6). M4 and M8 suffer strong overestimations (Figure 3.10 and Figure 3.12) with an annual mean bias of 0.20 and 0.33, respectively. In summer, the presence of sea-breeze circulations cause regional dust transport from inland regions to the Persian Gulf (Eck et al., 2008) favouring a mixing of desert dust and fine pollution aerosols as shown in Chapter 2. The daily variability is rather poorly captured (correlations of 0.29 and 0.14 in M8 and M4, respectively). During this season, Middle East is affected by long range transport from Iraq and southern Iraq deserts (Liu et al., 2000), and the dust transport is more efficient in M8. As shown in Figure 3.11, the AOD_{coarse} is reasonably well reproduced by M4 and M8 indicating that the observed AOD overestimations are linked to overestimations in the fine fraction of the dust AOD.

As a summary, the evaluation of the operational versions has highlighted significant limitations of the modelling system. The model strongly underestimates the AOD in the Sahel and the Eastern Tropical North Atlantic regions in winter and spring. It also overestimates the AOD in Northern Algeria and the dust transport towards the Western and Central Mediterranean mainly in spring. The Mali-Mauritania source is not represented in the model. The model places a hot spot in southern Algeria not highlighted by the satellite. Finally the AOD overestimation in Middle East is, at least partly, related to the overestimation of the fine dust fraction.

3.4.2 New model components

3.4.2.1 Source size distribution and dry deposition

One of the possible reasons for the strong mismatch in the Sahel was a too efficient dry deposition scheme in the model. With the inclusion of a new dry deposition scheme, D8 considerably improves the transport over the Sahel in winter and autumn. On average, the winter correlation in the Sahelian sites increases from 0.16 with M8 to 0.43 with D8. However, severe underestimation still persists in D8 with a mean bias of -0.43 (Figure 3.8). Besides the improvement in the Sahel, over the rest of the domain and seasons the total AOD behaviour in D8 is similar to that of M8. The modified source size distribution of the model included in D8 improves the simulation of the fine fraction in Middle East (not shown here). In D8, the overestimation of the total AOD in this region is related to the

coarse fraction (Figure 3.11) particularly in summertime. Specific sensivity tests of the mass size distribution at sources and its relation to coarse and fine AOD would be required.

3.4.2.2 Emission scheme

When we evaluate the physically-based dust emission scheme model version (N8), we observe an increase in the Atlantic dust transport, in better agreement with satellite observations (Figure 3.4, Figure 3.5, Figure 3.6 and Figure 3.7), and significant changes in dust mass distribution in the simulation domain. In contrast to D8, the simulated dust AOD by N8 decreases in the Maghreb, south of Algeria and Mauritania, and increases in the Bodélé Depression, south of Niger, Nigeria, Benin and Chad through the year in better agreement with satellite observations. In comparison with AERONET observations, the improvement is clearly visible in the Sahel, where the model achieves a winter correlation of 0.60 (Figure 3.12) and winter mean bias of -0.18. Also better results are obtained in the Eastern Tropical North Atlantic AERONET sites (CVR and DAK) with an annual correlations of 0.58 (see Figure 3.8 and Figure 3.12).

Maximum differences between D8 and N8 are detected in the Maghreb, Algeria and Mauritania in spring and summer (Figure 3.5 and Figure 3.6). In contrast to D8, the emissions in N8 in the North of Mauritania are strongly inhibited in spring (Figure 3.5) as well as in the North of Algeria and North of Libya in summer (Figure 3.6). Dust outbreaks with origin in the area of Mauritania are linked to Atlantic trajectories that are capable to reach the Iberian Peninsula as shown in the MODIS observation during spring and summer (Figure 3.5 and Figure 3.6). The comparison with AERONET shows that D8 presents better seasonal correlation than N8 (0.59 for D8 and 0.47 for N8, Figure 3.9 and Figure 3.10). If we take a closer look at the coarse component of the AOD (see Figure 3.10), in areas affected by long-range transport as the Mediterranean Basin (Figure 3.11), AOD_{coarse} is reasonably well reproduced by D8 and N8 particularly in the Western-Central Mediterranean AERONET sites (with annual correlations of 0.58 for D8 and 0.56 for N8 for Western Mediterranean sites; and 0.52 for D8 and 0.45 for N8 for Central Mediterranean sites).

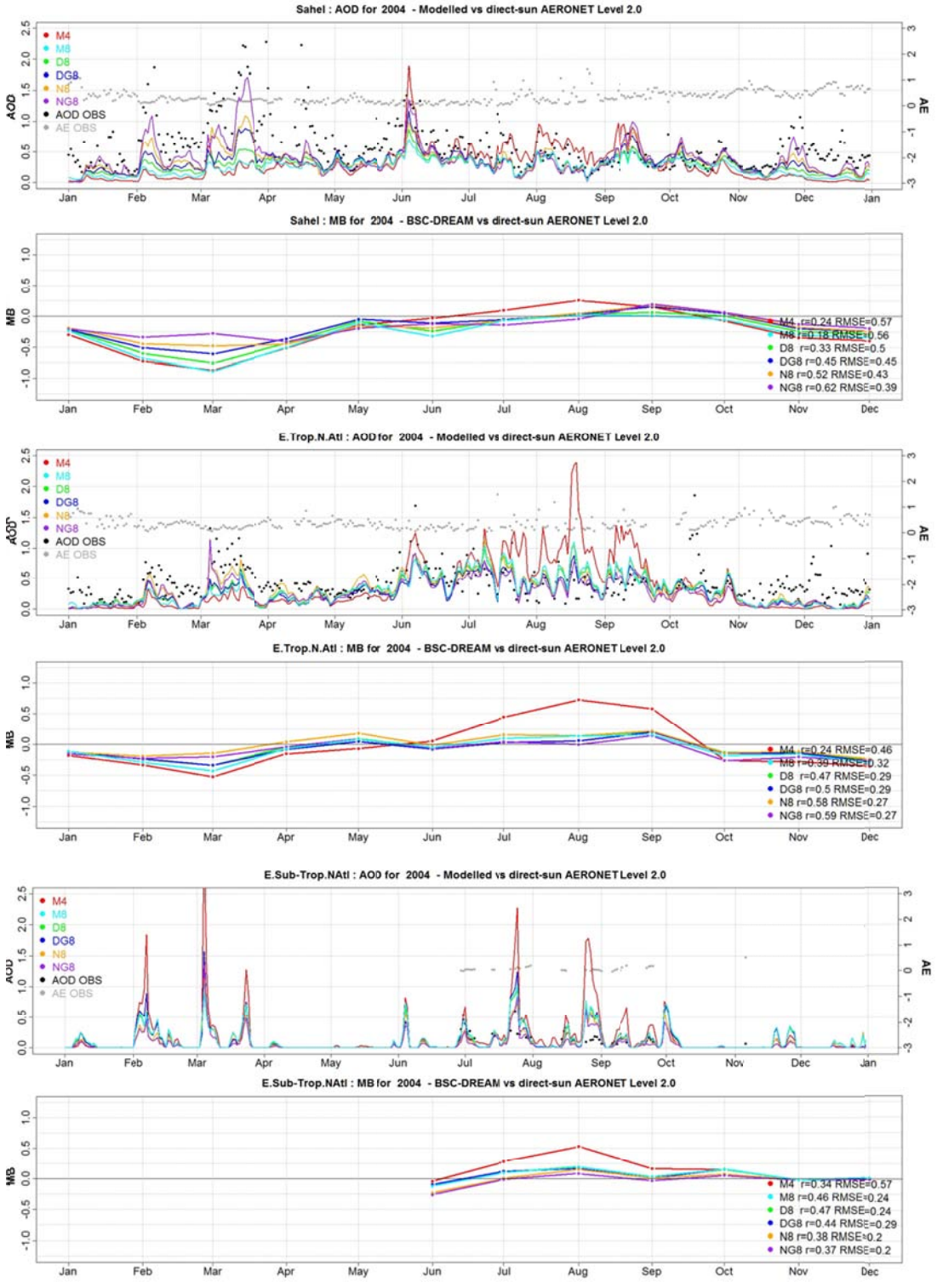

Figure 3.8 *Temporal series of the modelled (M4, M8, D8, DG8, N8 and NG8) vs. direct-sun AERONET measurements averaged by regions in daily basis as well the monthly evolution of mean bias (MB). This second panel also includes (in the legend) the annual values of the correlation coefficient (r) and root mean square error (RMSE) of each model version averaged for each region represented. From the top to the bottom: Sahel, Eastern Tropical North Atlantic and Eastern sub-Tropical North Atlantic regions.*

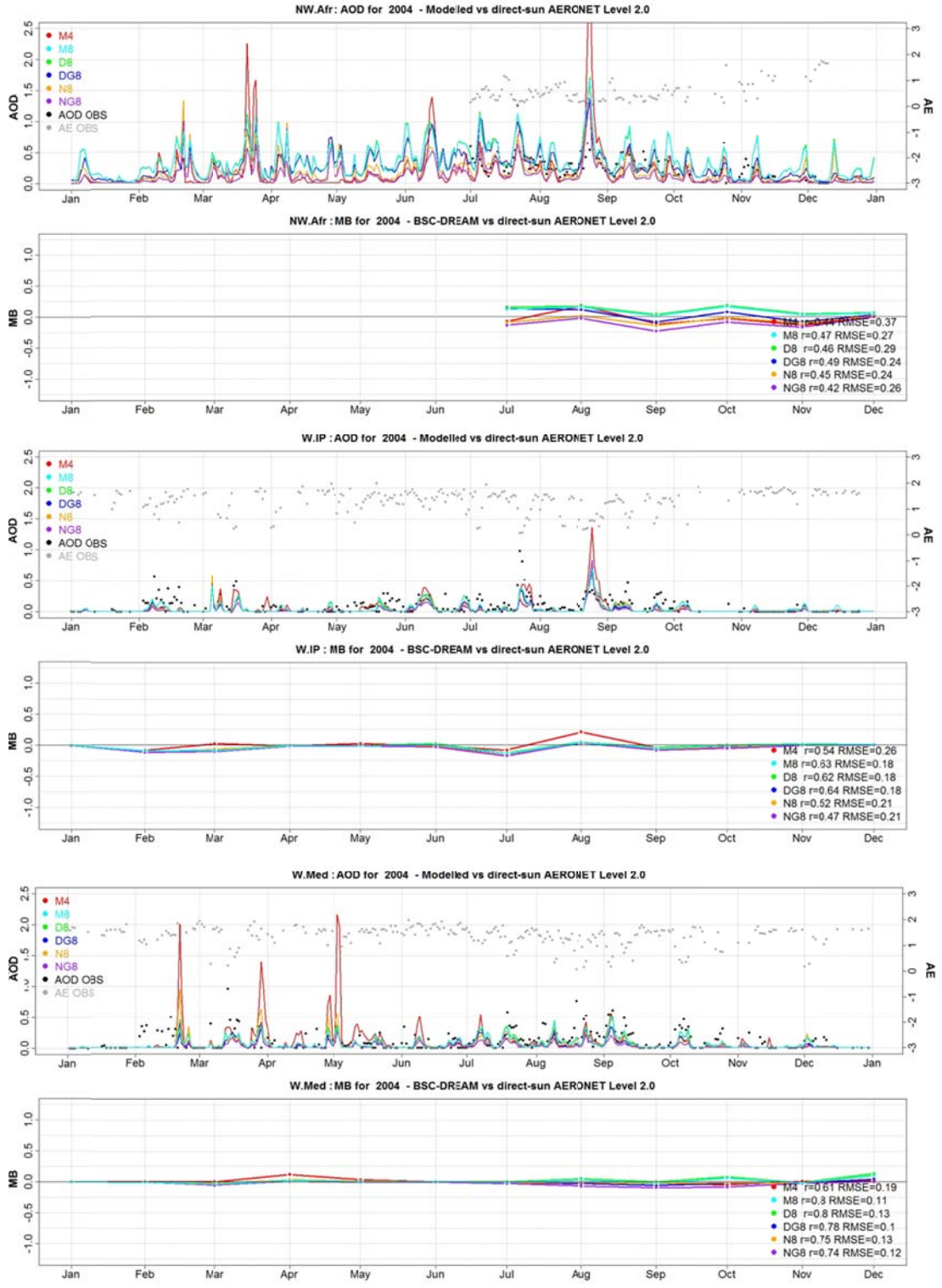

Figure 3.9 *Temporal series of the modelled (M4, M8, D8, DG8, N8 and NG8) vs. direct-sun AERONET measurements averaged by regions in daily basis as well the monthly evolution of mean bias (MB). This second panel also includes (in the legend) the annual values of the correlation coefficient (r) and root mean square error (RMSE) of each model version averaged for each region represented. From the top to the bottom: North-western Africa, Western Iberian Peninsula, Eastern Iberian Peninsula-Western Mediterranean regions.*

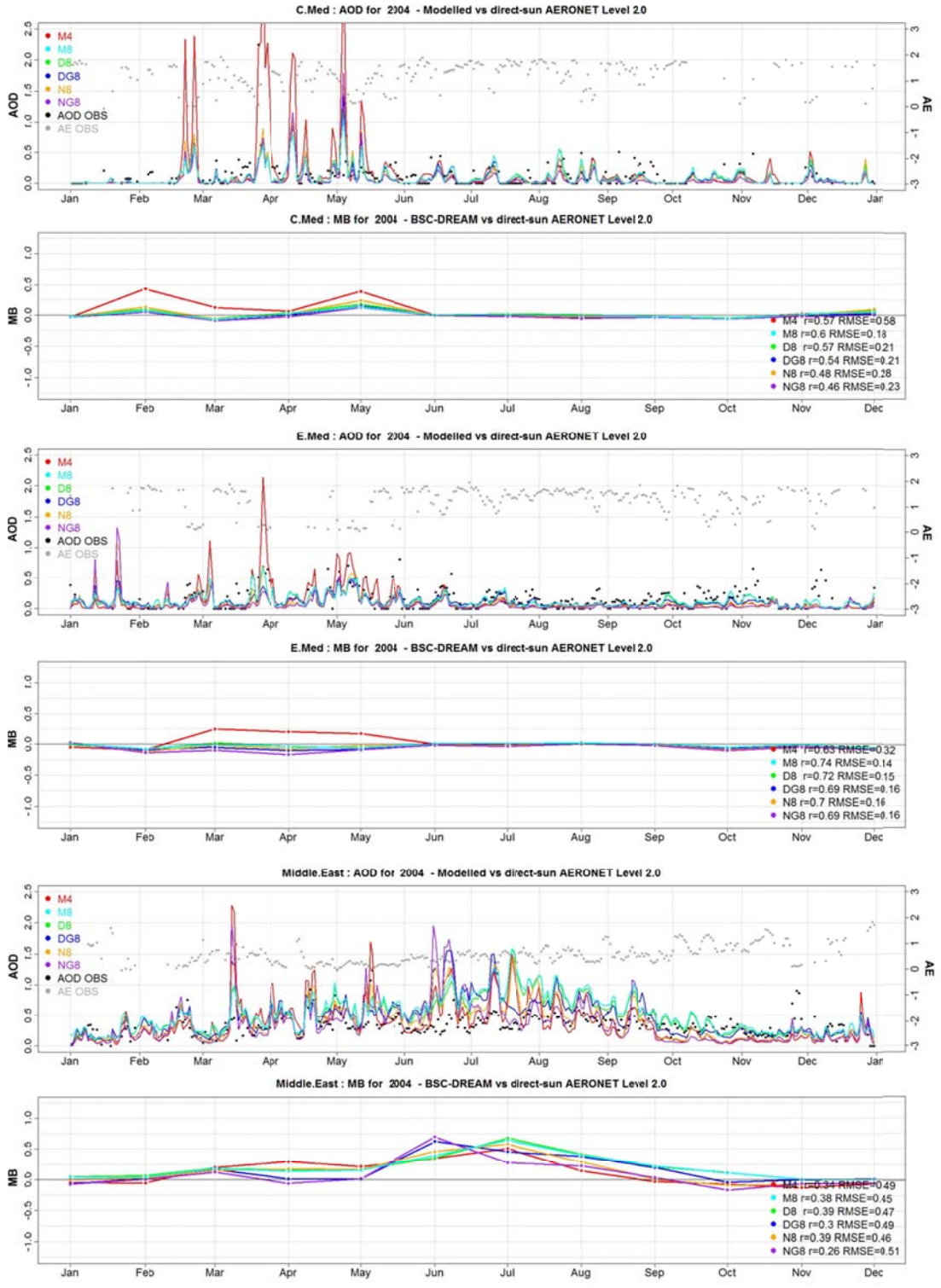

Figure 3.10 *Temporal series of the modelled (M4, M8, D8, DG8, N8 and NG8) vs. direct-sun AERONET measurements averaged by regions in daily basis as well the monthly evolution of mean bias (MB). This second panel also includes (in the legend) the annual values of the correlation coefficient (r) and root mean square error (RMSE) of each model version averaged for each region represented. From the top to the bottom: Central Mediterranean, Eastern Mediterranean and Middle East regions.*

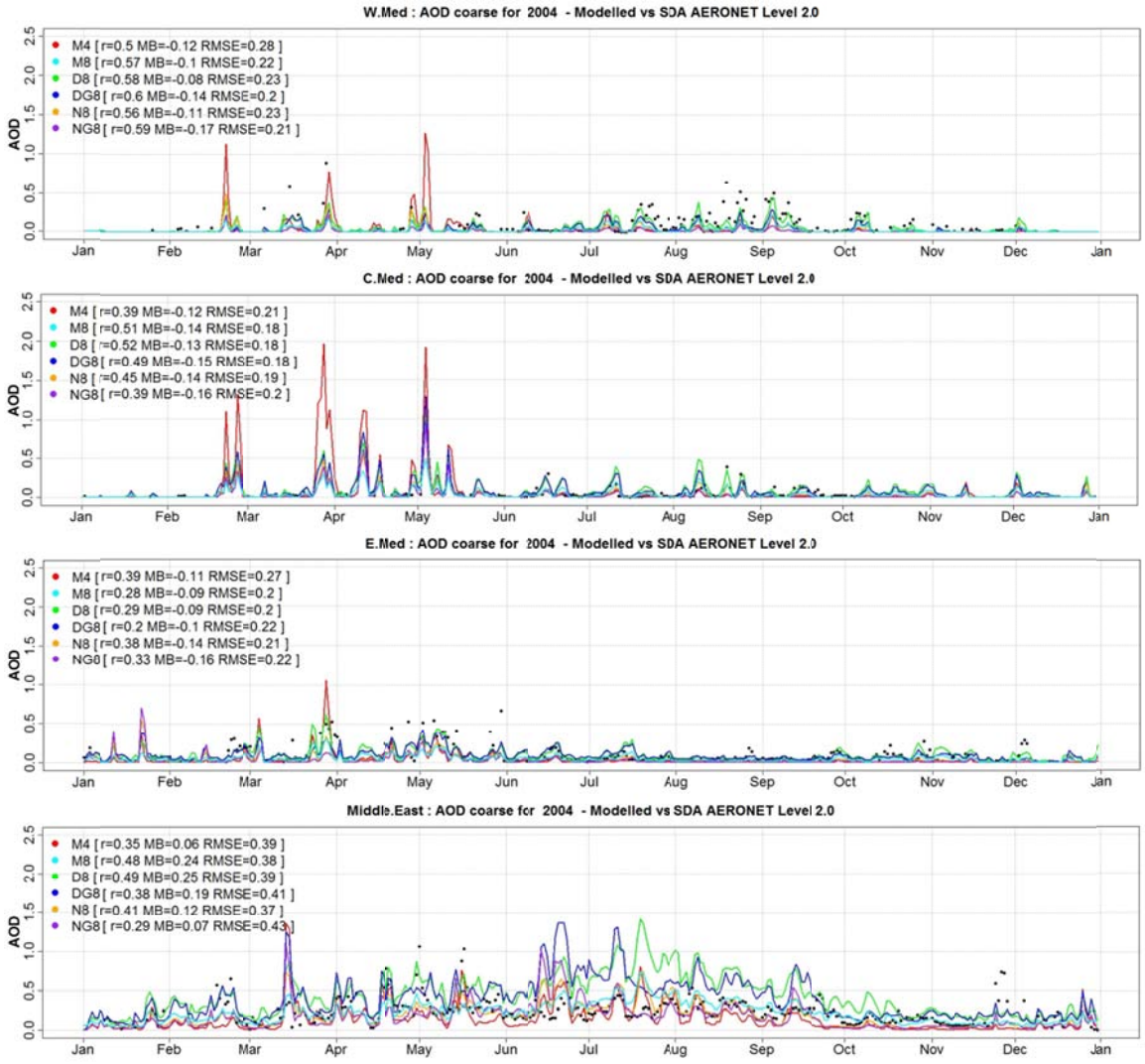

Figure 3.11 *Temporal series of the modelled AOD_{coarse} (M4, M8, D8, DG8, N8 and NG8) vs. SDA AERONET retrievals averaged by Mediterranean and Middle East regions which includes (in the legend) the annual values of the correlation coefficient (r), mean bias (MB) and root mean square error (RMSE) of each model version averaged for each region represented.*

In Middle East, as in the case of the operational versions, D8 and N8 overestimate the AERONET observations (Figure 3.12), particularly in summer (Figure 3.10). In contrast to D8, maximum seasonal AOD values in N8 are confined to the South-eastern Arabian Peninsula. High AOD values are simulated by D8 in Iraq and the An-Nafud desert, in the north part of the Arabian Peninsula. This is, at least partly, linked to the slightly better results obtained by D8 in the Eastern Mediterranean sites during summer, which are affected by long-range dust transport from Middle East (seasonal correlations are 0.30 for D8 and 0.25 for N8, see Figure 3.12). As shown in Figure 3.11, the AOD_{coarse} is reasonably

well reproduced by N8 indicating that the observed AOD overestimations are linked to overestimations in the fine fraction of the dust AOD (not shown here) as in the case of M8.

As the results shown, in some regions the physically-based emission scheme presents worse results than the model versions that include the original emission scheme of the model in the comparison against the total AOD from AERONET measurements. It is not straightforward to attribute the discrepancies to specific aspects of the model since the emission scheme depends on multiple surface, soil, and meteorological features and includes threshold processes and non-linear relationships. One of the main responsible of the regional differences between the different model versions is how dust sources are defined in each model version. This introduces differences in the mass available for uplift of the respective size class, and consequently the modelled dust concentrations. Otherwise, the physically-based emission scheme better reproduce the balance between fine and coarse fractions despite worth results observed in the total AOD with respect the original emission scheme of the model. These results highlight the complexity of the problem since model improvements in some regions (or dust parameterizations) might be accompanied by deterioration in some others. Otherwise, the increased understanding of wind-erosion physics has enabled the development of dust emission schemes on a firmer footing.

3.4.2.3 Preferential source approach

The inclusion of the topographic preferential source mask *G* from Ginoux et al. (2001) (see Figure 3.2c) in both emission schemes (DG8 and NG8) enhances the dust emission in the Bodélé during winter and autumn in better agreement with satellite observations (Figure 3.4 and Figure 3.7). An increase of Atlantic dust transport during winter and autumn is observed as well as a better correspondence with AERONET observations in the Sahelian and Eastern Tropical North Atlantic sites during wintertime (Figure 3.4). The annual correlation in DG8 and NG8 increases by ~12% and ~10% with respect to D8 and N8 on average for the Sahelian AERONET sites (Figure 3.12). In spite of these improvements, underestimations persist in this region. These underestimations are common features observed in the dust global models which affect the Atlantic transport to America (Huneeus et al., 2011) and it could be linked to missing or underestimated sources in the model, for example in Bilma (west of Bodélé Depression in Eastern Niger) and Faya Largeau (Chad) as indicated in the MODIS AOD observations (Figure 3.4, Figure 3.5, Figure 3.6 and Figure 3.7). Furthermore, during the northward migration of the monsoon trough at the end of the Harmattan season, unstable atmospheric conditions develop as warm and humid air flows over the heated land surface, generating intense thunderstorms. These thunderstorms have the potential to entrain large quantities of dust into the

atmosphere. These meteorological processes are largely underrepresented by the numerical models (e.g. Knippertz et al., 2009) and they could also be linked to underestimations of the simulated dust concentrations in this region.

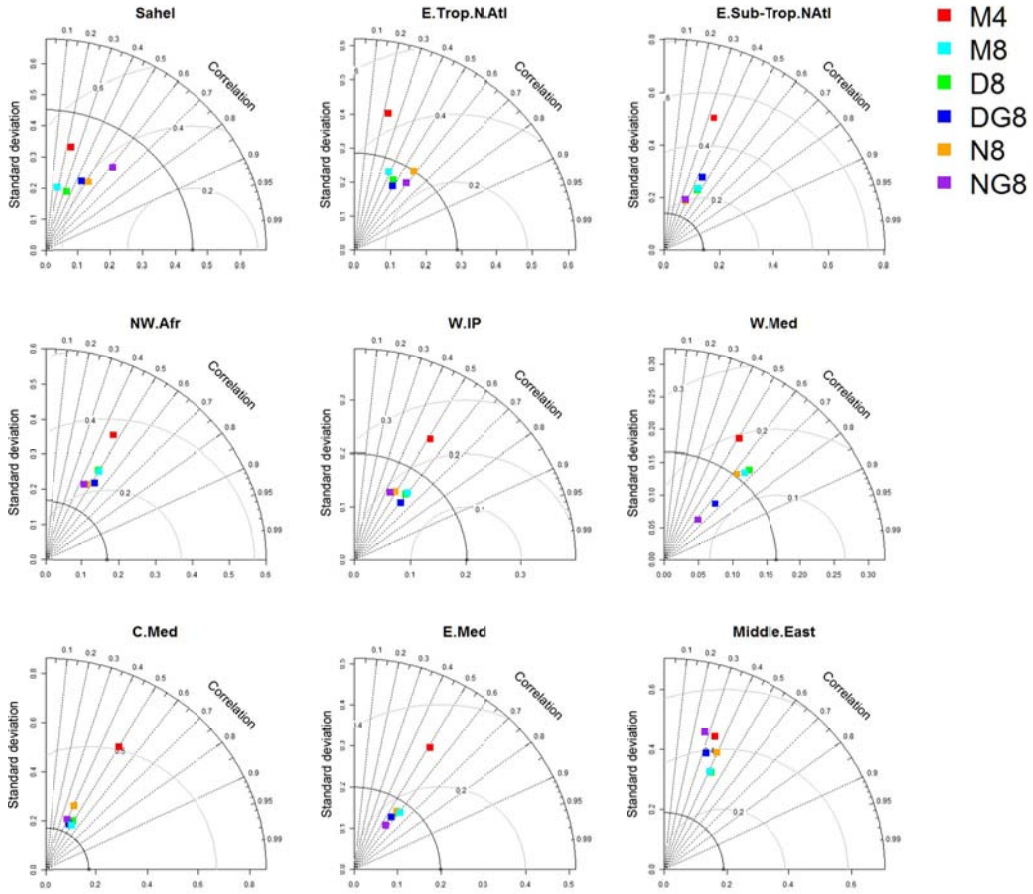

Figure 3.12 *Taylor's diagrams for M4, M8, D8, DG8, N8 and NG8 model version against the filtered AOD direct-sun AERONET observations by regions. The radial distance from the origin is proportional to the standard deviation of a pattern. The centered root-mean-square (RMS) difference between the test and reference field is proportional to their distance apart (in the same units as the standard deviation). The correlation between the two fields is given by the azimuthal position of the test field.*

In DG8 and NG8, maximum seasonal values shift towards Tunisia and Northern Libya during spring and summer and decrease the AOD seasonal concentrations in Sudan in better agreement with the MODIS and MISR aerosol products (Figure 3.5 and Figure 3.6). On average, the annual correlation increases from 0.46 with D8 to 0.49 with DG8 and decreases from 0.45 with N8 to 0.42 with NG8 in the North-western African sites (Figure 3.12). Both DG8 and NG8 show slightly worse results than D8 and N8 in the

Mediterranean AERONET sites (see Figure 3.12). Also, the northern Mauritania border source is further omitted by the topographic preferential source approach. As a result, on average, in the AOD comparison with the AERONET sites located in North-Western Africa region the annual correlation of DG8 increases ~ 6% with respect D8 and NG8 decreases ~ 7% with respect N8 (Figure 3.12).

The preferential source mask restricts the dust production in north-eastern Saudi Arabia and Iraq (see Figure 3.4, Figure 3.5, Figure 3.6 and Figure 3.7). On the contrary, in summer it shows an increase of the dust production in Ash Sharqiyah and in the south-eastern Saudi Arabia which is associated to the overestimations observed in June (Figure 3.10) in the AERONET sites located in areas of the Persian Gulf. On the other hand, DG8 and NG8 are capable of reproducing some summer episodes in the Persian Gulf associated to regional sea-breeze circulations as the dust event on mid-July (Figure 3.10). On average, the annual correlation in Middle East decreases from 0.39 with D8 to 0.30 with DG8 and from 0.39 with N8 to 0.26 with NG8 (see Figure 3.12).

3.5 Summary and conclusions

In this chapter, the original version of the DREAM model (M4) and the updated BSC-DREAM8b (M8) together with 4 research model versions have been analysed for year 2004 over a domain covering Northern Africa, the Mediterranean and Middle East. In addition to a more detailed size bin resolution and an updated wash-out ratio in the wet deposition, the analysed research model versions include a new dry deposition scheme based on Zhang et al. (2001) and a modified source size distribution (D8), a more physically-based dust emission scheme (N8), and the inclusion of a topographic preferential source mask in their respecitive emission schemes (DG8 and NG8). The preferential source mask is based upon approach from Ginoux et al. (2001) and the new dust emission module is more physically based and includes a new soil texture.

An annual comparison of the modelled AOD against data from 44 AERONET stations is conducted on hourly basis. For this quantitative model evaluation, a new methodology is used to discriminate dust contributions from direct-sun AERONET measurements based on the combination of AOD, Ångström exponent (α) and its spectral curvature ($\delta\alpha$). Additionally, in those sites where the SDA retrieval of AERONET is available, we performed a semi-quantitative evaluation of the simulated fine and coarse AOD (i.e AOD_{coarse} and AOD_{fine}). Satellite aerosol products from TOMS, MISR and MODIS sensors are also included in the analysis to check the ability of the model to qualitatively reproduce the observed seasonal spatial desert dust distributions. As a result, the weaknesses and

strengths of the model in the prediction of dust concentrations are discussed in terms of inaccuracies in the emission, transport and deposition of desert dust.

The comparison with satellite derived data highlights that the versions based on the original emission scheme misrepresent dust sources over Eastern Nigeria and at the Mali-Mauritania border and overestimate the AOD in northern Algeria. In contrast, N8 shows its ability to reproduce the dust fields in the Bodélé Depression, south of Niger, Nigeria, Benin and Chad. On the other hand, the sources located in the Maghreb region are inhibited by N8. In the Middle East, the seasonal satellite products do not show a clear pattern. In all the model versions maximum summer activity are found in southern latitudes over the Rub' Al Khali desert. As a difference to the versions based on the original emission scheme, N8 inhibits the simulated dust production in Iraq and the An-Nafud desert during winter and spring.

The results of the comparison with the AERONET measurements have shown that M4 and M8 strongly underestimate the AOD in the Sahel during the winter Harmattan season and overestimate the AOD in spring over the Mediterranean and in summer over Middle East achieving rather low annual correlations (~ 0.35).

The implementation of a new deposition scheme after Zhang et al. (2001) in D8 considerably improves the transport over the Sahel in winter and autumn. However, significant underestimations over the Sahelian AERONET sites and overestimations in Middle East still persist. In the overall domain an annual correlation of 0.42 is obtained for D8.

For N8, an increase in the Atlantic dust transport and significant changes in the spatial dust mass distribution in northern Africa are in better agreement with the observations. However, in Middle East, overestimations persist during summertime. As a result, the dust fields of N8 show reasonably good correspondence with the AOD AERONET data obtaining an annual correlation of 0.53. Inaccuracies observed in the comparison with observed AOD_{coarse} and AOD_{fine} from AERONET retrievals emphasize the necessity to conduct more detailed sensitivity tests of the mass size distribution of the model at sources and its relation to coarse and fine AOD.

For DG8, the preferential source mask constitutes a useful approach particularly in North African sources. In this case, the placement and magnitude of the main dust sources (i.e. Bodélé, Mauritania and Algeria) are in better agreement with the satellites. Therefore, dust concentrations are increased in the Sahel during wintertime and consequently, the Atlantic dust transport towards America. The annual correlation is increased about 12% in the Sahelian sites. The long-range dust transport towards Europe is better reproduced

particularly in North-western Africa and the Western Iberian Peninsula. In the south-eastern part of the Arabian Peninsula, the preferential source mask increases the dust emission causing overestimations of the model and a reduction of the annual correlation of about 9%.

For NG8, the inclusion of the preferential source mask does not introduce an improvement in the modelled AOD dust fields. In fact, the Mauritania border and the region of Libya, Egypt and Sudan sources are mostly omitted by the topographic preferential source approach. Moreover, overestimations observed during summer in Middle East in NG8 are also found in any other model version and a decrease of the annual correlation of about 13% in this region. In this latter case, only the modelled dust fields in the Sahel region present improvements with respect to the observations.

To summarize the research model versions improve the results of the operational model versions. By regions, NG8 is the version better reproducing the localization and magnitude of the main dust source in North Africa (i.e. Bodélé) and D8 shows the best match with the observations in Middle East. On average for the Mediterranean, Iberian Peninsula and North-western Africa regions, DG8 is the version which better captures the observed background AOD and the timing of the observed dust peaks. Finally, considering the entire domain of simulation, N8 is the version with most accurate results not only in source regions but also areas affected by long-range dust transport.

The results presented in this study will be used to improve the operational dust predictions of BSC-DREAM8b and for selecting the most appropriated model components in long-term reanalysis depending on the region of study. In the near future, it is planned to implement some of these updates (tested and analysed in the present analysis) in a new operational version at BSC-CNS.

As shown in Chapter 2, different classes of particles can be found in the European atmosphere: mineral dust, originated from the Sahara desert and from arid regions in the Iberian Peninsula; polluted particles, produced mainly in urban and industrial areas of Continental and Eastern Europe; marine aerosol, continuously formed over the Mediterranean itself or transported from the North Atlantic; and biomass burning particles, often produced in forest fires, mainly during the summer. Thus, it is common that mineral dust appears mixed with other aerosols. The following chapter analyses the aerosol contributions over Europe using the annual simulation of the CALIOPE system which includes a non-climatic representation of mineral dust by means added the BSC-DREAM8b outputs.

Chapter 4

4 Aerosol modelling over Europe and the contribution of desert dust

4.1 Introduction

The European Union (EU) has shown great interest in the transport and dynamics pollutants in the atmosphere. It has developed an overall strategy through the setting of long-term air quality objectives. A series of Directives has been introduced to control levels of certain pollutants and to monitor. The EU directive on ambient air quality and cleaner air which entered into force in June 2008 and have been transposed into the national legislation of each Member State by June 2010 (European Commission, 2008), introduced daily and annual PM_{10} limit values of 50 $\mu g/m^3$ and 40 $\mu g/m^3$, respectively, from year 2010. Also this directive introduces a $PM_{2.5}$ annual limit value of 25 $\mu g/m^3$ to be assumed from year 2015. In this regard, the objectives proposed by the EU are usually less well attained in southern Europe than in northern countries (Yttry and Aas, 2006). Reports from countries around the Mediterranean Basin and Eastern Europe show high levels of atmospheric PM compared to Northern and some central European regions (Querol et al., 2009). Both anthropogenic (transport sector, industrial processes, power generation and biomass burning, among others) and natural emissions (African dust, resuspension, sea spray, forest fires, primary biological particles and biogenic secondary organic compounds, windblown dust), as well as orographic and climatic factors contribute to the ocurrence of (or cause) those enhanced levels. When PM_{10} values are exceeded due to natural events (such as desert dust outbreaks or volcano eruptions), Member States shall inform the Commission, providing the necessary justification to demonstrate that such exceedances are due to natural events.

Air quality models are useful to understand the dynamics and transport of pollutants and as well as administer and regulate air quality. In recent years a number of experimental and operational air quality forecast systems have been developed around the world. Nowadays, in Europe, 23 modelling systems routinely simulate the air quality over Europe, 7 systems also operate in forecasting mode (Menut and Bessagnet, 2010): PREV'AIR, EURAD, EMEP-CWF, MATCH, MOCAGE, CHIMERE, and CALIOPE.

In the frame of the CALIOPE system (Baldasano et al., 2008a; http://www.bsc.es/caliope), BSC-CNS operates a air quality forecasting system for Spain (at 4 km x 4 km horizontal resolution) and Europe (at 12 km x 12 km horizontal resolution) with WRF-ARW/HERMES-EMEP/CMAQ and desert dust forecasts with

BSC-DREAM8b (Nickovic et al., 2001; Pérez et al., 2006a,b). In contrast to many other European modelling systems, CALIOPE includes a non-climatic representation of African dust transport in its forecast mode. The forecasts are evaluated on a daily basis against ground-based and satellite observations to establish confidence in the modelling system predictions among users, identify problems and routinely improve the system (Baldasano et al., 2010).

Pay et al. (2010) presented a full year evaluation of the CALIOPE system for the European domain for gaseous pollutants (O_3, NO_2 and SO_2) and PM levels (PM_{10} and $PM_{2.5}$) against EMEP ground-based measurements. The study shows that the skill scores of the system lie within the range of most European models and that while the dynamics of $PM_{2.5}$ and PM_{10} are rather well reproduced, concentrations remain systematically underestimated by a factor of 2 on average.

Among other issues, the present chapter provides a description of the desert dust patterns over Europe and their contribution to the European air quality levels by means an annual simulation of the CALIOPE modelling system. The objectives of this chapter are: 1) to provide a detailed quantitative assessment of the capabilities of the CALIOPE system to simulate the daily aerosol distribution over Europe for year 2004 in terms of PM levels, AOD and chemical composition; 2) to understand the underestimation of the PM mass; 3) to estimate and analysing the spatial and seasonal distribution of the different aerosol fractions over Europe based on the model results and observations; and 4) to estimate the exceedances of the EU limits due to natural desert dust.

The chapter is organized as follows. Section 4.2 describes the CALIOPE system and the observational datasets used for the model evaluation. In section 4.3 we use aerosol chemical composition from EMEP/CREATE and AOD from the AERONET network to identify the origin of the discrepancies in PM levels. The evaluation of the AOD is particularly useful for validating and analysing the capabilities of the modelling system to reproduce long-range transport of desert dust from North Africa. In Section 4.4 we estimate and analyse the spatial and seasonal distribution of the different natural and anthropogenic aerosol fractions over Europe applying a simple bias correction to the model based on the results of the evaluation. African dust transport and its contribution over Europe are analysed in detail. Finally, Section 4.5 summarizes the findings.

4.2 Methods

4.2.1 Description of the CALIOPE system

CALIOPE is a state-of-the-art air quality modelling system that integrates an emission-processing model (HERMES-EMEP), a meteorological driver (WRF-ARW), a chemical transport model (CMAQ) and a mineral dust driver (BSC-DREAM8b). The configuration used in the present work is described in Pay et al. (2010). In the next sections, the models from the aerosols are estimated (i.e. CMAQ and BSC-DREAM8b) are described in detail.

4.2.1.1 Photochemical model: CMAQ

The Models-3 Community Multiscale Air Quality Modeling system (CMAQ; Byun and Ching, 1999; Binkowski, 1999; Byun and Schere, 2006) is used to study the behaviour of air pollutants from regional to local scales. CMAQ version 4.5, used in this study, has been extensively evaluated under various conditions and locations (Jiménez et al., 2003; Roy et al., 2007; Appel et al., 2007, 2008). Following the criteria of Jiménez et al. (2003) the Carbon Bond IV chemical mechanism is applied (CBM-IV, Gery et al., 1989). The production of sea salt aerosol (SSA) is implemented as a function of wind speed and relative humidity (Gong, 2003; Zhang et al., 2005) through the AERO4 aerosol module. The AERO4 module distinguishes among different chemical aerosol components namely nitrate, sulphate, ammonium, elemental carbon and organic carbon with three subcomponents (primary, secondary anthropogenic and secondary biogenic), sodium and chlorine. Unspecified anthropogenic aerosols and aerosol water are additionally kept as separate components. Unspecified aerosols consists of the non-carbon atoms associated with organic carbon as well as PM emissions that are not explicitly speciated in HERMES-EMEP emission model, which includes traces elements, primary ammonium and other unidentified mass in the speciation profiles (Appel et al., 2007). Aerosols are represented by three size modes (Aitken, accumulation and coarse mode), each of them assumed to have a lognormal distribution (Binkowski and Roselle, 2003). Secondary inorganic aerosols (SIA) are generated by nucleation processes and include/consits of nitrate, ammonium and sulphate aerosols. Secondary organic aerosol (SOA) can be formed from aromatics (anthropogenic organic aerosols) and terpenes (biogenic organic aerosols, Schell et al., 2001). Furthermore, an assumption of the CMAQv4.5 model is that organics influence neither the water content nor the ionic strength of the aerosol particles (Binkowski and Roselle, 2003). The aerosol microphysical description is based on a modal aerosol model (Binkowski and Roselle, 2003) using the ISORROPIA thermodynamic equilibrium model (Nenes et al., 1998). For a more complete description of the processes implemented in CMAQ, the reader is referred to Byun and Schere (2006).

AOD at 550 nm from CMAQ outputs is calculated using a simple approach described by Malm et al. (1994) and Binkowski and Rosselle (2003). The method is known as the "reconstructed mass-extinction method". The extinction coefficient (β_{ext}), which is a function of wavelength (λ), is a sum of the attenuation by scattering (β_s) and absorption (β_a). The model-predicted AOD is calculated by summing the product of the extinction and layer thickness (ΔZ_i) over the number of layers (N) in the column:

$$AOD = \sum_{i=1}^{N} (\beta_s + \beta_a)_i \Delta Z_i \tag{4.1}$$

We estimate the model-predicted $\beta_{ext} = \beta_s + \beta_a$ using this semi-empirical approach for extinction calculation which depends on aerosol mass and humidity as follows:

$$\beta_s = 0.003 f(RH)\left\{\left[NH_4^+\right] + \left[SO_4^-\right] + \left[NO_3^-\right]\right\} + 0.004[OC] + 0.001\left[PM_{fine}\right] + 0.0006\left[PM_{coarse}\right]$$

$$\beta_a = 0.01[EC] \tag{4.2}$$

where the brackets in the above equations indicate mass concentration in mg/m^3 and all coefficients in the equation represent the specific extinction cross section at 550 nm (in m^2/mg). When implementing the above equation, the term in brackets is determined by adding ammonium mass (NH_4^+) plus sulphate mass (SO_4^{2-}) plus nitrate mass (NO_3^-). Organic carbon (OC) is taken as the sum of all non-light absorbing organic species. Light absorbing carbon is elemental carbon (EC). PM_{fine} mass is taken as the unspeciated portion of $PM_{2.5}$ and the fine fraction of sodium (Na^+) and chloride (Cl^-), and the PM_{coarse} mass represents all coarse mode aerosols that includes the unspeciated portion of PM_{10} and the coarse fraction of chloride (Cl^-) and sodium (Na^+). The mass concentration for each of these species is directly obtained from CMAQ. The relative humidity correction factor, *f(RH)*, takes into account that the growth and phase change of hygroscopic particles affect their light-scattering effiency (Malm et al., 1994). *f(RH)* is parameterized from data published by Tang et al. (1981) as a function of the relative humidity from the WRF-ARW meteorological model and it varies between 1 (at low RH) and 21 (at RH = 99%).

4.2.1.2 Mineral dust model: BSC-DREAM8b

For the present chapter, we have used the current BSC-DREAM8b operational version of the model described in detail in the Section 3.2.1 (i.e. M8).

4.2.2 Simulation

The CALIOPE system is run on a regional scale (12 km x 12 km in space) to model the European domain (see Figure 4.1). The simulation consists of 366 daily runs (1 h in time) to simulate the entire year of 2004.

CALIOPE system uses the inventory of the anthropogenic emissions of SO_2, NO_x, NMVOC, CO, PM_{10}, $PM_{2.5}$, and NH_3 derived from the 2004 annual EMEP emission database (EMEP, 2007). Raw emission data are processed by by High-Elective Resolution Modeling Emission System (HERMES, see Baldasano et al., 2008b) in order to provide a comprehensive description of the emissions to the air quality model. The inventory distinguishes the source categories following the Selected Nomenclature Air Pollution (SNAP). Disaggregation of EMEP (50 km resolution) data is performed in space (12 km x 12 km) and time (1 h). Natural PM emissions (such as wildfire emissions) and primary biogenic emissions (such as pollen, bacteria, fungal, and fern spores, viruses, fragments of animals and plants, virus, etc.) containing organic compounds, are not included in the emission model.

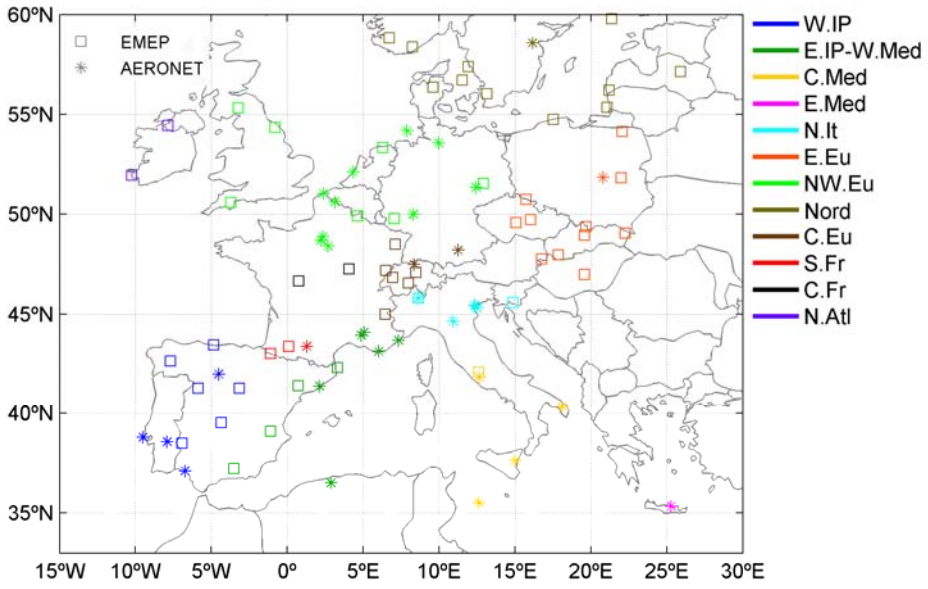

Figure 4.1 *Study domain and spatial distribution of 54 selected EMEP stations (indicated by square marks) and 35 selected AERONET stations (indicated by star marks) over the study domain. The different colours indicate the different regions which are defined as: Western Iberian Peninsula (W.IP); Eastern Iberian Peninsula-Western Mediterranean (E.IP-W.Med), Central Mediterranean (C.Med), Eastern Mediterranean (E.Med), North of Italy (N. It), Eastern Europe (E.Eu), Northwestern Europe (NW.Eu), Southern France (S.Fr), Central Europe (C.Eu), Nordic (Nord), Central France (C.Fr) and North Atlantic (N.Atl).*

The Advanced Research Weather Research and Forecasting (WRF-ARW) Model v3.0.1.1 (Michalakes et al., 2004; Skamarock and Klemp, 2008) is used to provide the meteorology to the chemical transport model. WRF-ARW (version v3.0.1.1) is configured with a grid of 479 x 399 points and 38 σ vertical levels (11 characterizing the planetary boundary layer, PBL). The model top is defined at 50 hPa to resolve properly the troposphere-stratosphere exchanges. WRF-ARW initial and boundary conditions (at intervals of 6 h) are based on the Final Analyses of the National Centers of Environmental Prediction (FNL/NCEP; at 1º × 1º) at 12 UTC.

The CMAQ horizontal grid resolution corresponds to that of WRF-ARW. Its vertical structure was obtained by a collapse from the 38 WRF-ARW layers to a total of 15 layers steadily increasing from the surface up to 50 hPa with a stronger concentration within the PBL. CMAQ boundary conditions are based on the global climate chemistry model LMDz-INCA2 (Szopa et al., 2009) developed by the Laboratoire des Sciences du Climat et l'Environnement (LSCE). Monthly mean data for the year 2004 are interpolated in the horizontal and vertical dimensions to force the major chemical concentrations (i.e. O_3, NO, NO_2, HNO_3, HCHO, H_2O_2, PAN and CO) at the boundaries of the domain (Piot et al., 2008). A detailed description of the INteractive Chemistry and Aerosol (INCA) model is presented in Hauglustaine et al. (2004) and Folberth et al. (2006). One source of the underestimation of aerosol species is related to the fact that long-range transport is not taken into account. We include chemical lateral boundary conditions from LMDz-INCA2 global model for gas-phase species, but we could not provide similar boundary conditions for aerosols species.

The initial state of dust concentration in the BSC-DREAM8b model is defined by the 24-hour forecast from the previous-day model run. The FNL/NCEP (at 1º x 1º) files at 0 hours UTC are used as initial conditions and boundary conditions at intervals of 6 hours. The resolution is set to 1/3º in the horizontal and to 24 layers extending up to approximately 15 km in the vertical. The domain of simulation covers northern Africa, the Mediterranean Sea, Europe and Middle East. An offline coupling is applied to the calculated concentrations of particulate matter over the European domain from CMAQ outputs (Jiménez-Guerrero et al., 2008b).

4.2.3 Observations

4.2.3.1 Surface PM and chemical composition from EMEP/CREATE Networks

For the evaluation of $PM_{2.5}$ and PM_{10}, we have used the same observational dataset included in the analysis of Pay et al. (2010). In this study, model simulated PM concentrations are compared with ground-based measurements from the European

Monitoring and Evaluation Programme (EMEP) monitoring network for the year 2004. EMEP stations are located at a minimum distance of approximately 10 km from large emission sources (Larssen et al., 1999). EMEP stations are assumed to be representative of regional background concentrations (Torseth and Hov, 2003). A total of 16 and 25 stations for $PM_{2.5}$ and PM_{10} respectively have been used to evaluate the model predictions. Details on the location of the EMEP stations used for this comparison can be found in Table 4.1.

Modelled aerosol concentrations of chemical species are compared with ground-based measurements provided by EMEP and the FP5/GMES project CREATE at 54 rural background stations. The uncertainty of the PM measurements strongly depends on the method and chemical composition of the collected aerosol. Usually the collected filters are weighted at 50% relative humidity (Tsyro, 2005). Error sources which lead to a bias are potential losses of semivolatile compounds (particularly ammonium nitrate and carbonaceous aerosols) from the filters at temperatures higher than 20ºC as well as gas condensation on filters which could introduce positive measurements artefacts. SIA components can be measured with an uncertainty of about ±10% for major species (Putaud et al., 2004). In this context, European legislation (2008/50/EC) establishes that measurement groups have to demonstrate that the uncertainty of $PM_{2.5}$ and PM_{10} meets the quality objective of 25%. However legislation does not establish any quality objective for uncertainty of chemical species yet. SIA components collected within CREATE are measured by ion chromatography in which the error is usually within 10% (Putaud et al., 2000).

One source of model underestimation of measured SIA components is related with the size fraction of aerosol components in both measurements and the model. The observed concentrations are available in total mass fraction, without any discrimination of size since EMEP sites typically used filter-packs to measure sulphate, nitrates and ammonium and captured particles are approximately PM_{10} fraction. In contrast, the CMAQv4.5 model considers speciated inorganic aerosol only in the $PM_{2.5}$ fraction. One exception is marine sulphate aerosol which is present also in the coarse fraction.

In this chapter, measured PM_{10}, $PM_{2.5}$ and their chemical aerosol components (i.e. sulphates, nitrates, ammonium, sea salt and carbonaceous matter) are available on a daily and annual basis. The main characteristics and location of these EMEP/CREATE stations are described in Table 4.1 and their locations are displayed in Figure 4.1. The CALIOPE system is evaluated at 54 stations: 53 for sulphate (SO_4^{2-}), 27 for nitrate (NO_3^-), 15 for ammonium (NH_4^+), 9 for sodium (Na^+), 5 for chloride (Cl^-) and 2 for carbonaceous matter (EC and OC). The measurements are well documented and available on the EMEP web page (http://www.emep.int).

Table 4.1 *List of EMEP stations. Coordinates, altitude and the chemical species measured of the 54 selected EMEP stations are included. The code is composed by 2-letter country code plus 2-digit station code. Zone of location is defined in* ***Figure 4.1****.*

Station Name	Code	Zone	Lat.(º/N)	Lon.(º/E)	Alt.(m)	Network	Na^+	Cl^-	SO_4^{-2}	NO_3^-	NH_4^+	OC	EC
Anholt	DK08	Nord	56.717	11.517	40	EMEP	x		x				
Barcarrota	ES11	W.IP	38.476	-6.923	393	EMEP			x	x			
Birkenes	NO01	Nord	58.383	8.250	190	EMEP/CREATE	x	x	x	x	x	x	x
Cabo de Creus	ES10	E.IP-W.Med	42.319	3.317	23	EMEP			x	x			
Campisábalos	ES09	W.IP	41.281	-3.143	1360	EMEP			x	x			
Chopok	SK02	E.Eu	48.933	19.583	2008	EMEP			x				
Deuselbach	DE04	NW.Eu	49.767	7.050	480	EMEP			x				
Diabla Gora	PL05	E.Eu	54.150	22.067	157	EMEP			x				
Donon	FR08	C.Eu	48.500	7.133	775	EMEP			x				
Els Torms	ES14	E.IP-W.Med	41.400	0.717	470	EMEP			x	x			
Eskdalemuir	GB02	NW.Eu	55.313	-3.204	243	EMEP			x				
High Muffles	GB14	NW.Eu	54.334	-0.808	267	EMEP			x				
Illmitz	AT02	E.Eu	47.767	16.767	117	EMEP	x		x	x	x		
Iraty	FR12	S.Fr	43.033	-1.083	1300	EMEP			x				
Iskrba	SI08	N.It	45.567	14.867	520	EMEP	x	x	x				
Ispra	IT04	N.It	45.800	8.633	209	EMEP			x	x	x		
Jarczew	PL02	E.Eu	51.817	21.983	180	EMEP			x	x	x		
Jungfraujoch	CH01	C.Eu	46.550	7.983	3573	EMEP		x	x	x	x		
Kollumerwaard	NL09	NW.Eu	53.334	6.277	1	EMEP				x	x		
Kosetice	CZ03	E.Eu	49.583	15.083	534	EMEP			x				
K-puszta	HU02	E.Eu	46.967	19.583	125	EMEP			x	x	x		
La Tardière	FR15	C.Fr	46.650	0.750	746	EMEP			x				
Le Casset	FR16	C.Eu	45.000	6.467	746	EMEP			x				
Leba	PL04	Nord	54.750	17.533	2	EMEP			x	x	x		
Liesek	SK05	E.Eu	49.367	19.683	892	EMEP			x	x			
Lough Navar	GB06	N.Atl	54.443	-7.870	126	EMEP			x				
Melpitz	DE44	NW.Eu	52.53	12.93	86	CREATE	x	x	x	x	x	x	x
Montandon	FR14	C.Eu	47.183	6.500	746	EMEP			x				
Montelibretti	IT01	C.Med	42.100	12.633	48	EMEP			x	x	x		
Morvan	FR10	C.Fr	47.267	4.083	620	EMEP			x				
Niembro	ES08	W.IP	43.442	-4.850	134	EMEP			x	x			
O Savñao	ES16	W.IP	42.653	-7.705	506	EMEP			x	x			
Payerne	CH02	C.Eu	46.817	6.950	510	EMEP			x				
Penausende	ES13	W.IP	41.283	-5.867	985	EMEP			x	x			
Peyrusse Vieille	FR13	S.Fr	43.375	0.104	236	EMEP			x				
Preila	LT15	Nord	55.350	21.067	5	EMEP			x				
Råö	SE14	Nord	57.400	11.917	5	EMEP			x				
Revin	FR09	NW.Eu	49.900	4.633	390	EMEP			x				
Rigi	CH05	C.Eu	47.069	8.466	1030	EMEP			x				
Risco Llamo	ES15	W.IP	39.517	-4.350	1241	EMEP			x	x			
Rucava	LV10	Nord	56.217	21.217	5	EMEP			x	x	x		
Skreâdalen	NO08	Nord	58.817	6.717	475	EMEP	x	x	x	x	x		
Sniezka	PL03	E.Eu	50.733	15.733	1603	EMEP			x	x	x		
Starina	SK06	E.Eu	49.050	22.267	345	EMEP			x	x			
Svratouch	CZ01	E.Eu	49.733	16.033	737	EMEP			x				
Tange	DK03	Nord	56.350	9.600	13	EMEP	x		x				
Topolniky	SK07	E.Eu	47.960	17.861	113	EMEP			x	x			
Utö	FI09	Nord	59.779	21.377	7	EMEP	x		x		x		
Valentina Observatory	IE01	N.Atl	51.940	-10.244	11	EMEP	x		x				
Vavihill	SE11	Nord	56.017	13.150	175	EMEP			x				
Víznar	ES07	E.IP-W.Med	37.233	-3.533	1265	EMEP			x	x			
Yarner Wood	GB13	NW.Eu	50.596	-3.713	119	EMEP			x				
Zarra	ES12	E.IP-W.Med	39.086	-1.102	885	EMEP			x	x			
Zoseni	LV16	Nord	57.133	25.917	183	EMEP			x	x	x		

4.2.3.2 Aerosol optical depth from AERONET network

As shown in Chapter 2, AERONET stations provide columnar aerosol optical parameter information (like AOD, AOD_{fine} and AOD_{coarse}) through direct measurements and inversion techniques. These data constitute a high-quality, ground-based aerosol climatology and, as such, have been widely used for aerosol process studies, as well as for evaluation aerosol models. For the present analysis, all operational stations within our study domain (i.e. the European continent) that collected data on at least 30 hours in 2004 have been selected for the model evaluation.

Table 4.2 and Figure 4.1 describe and show the location and the main characteristics of the 35 selected AERONET sites within our study region. Table 4.2 lists additional information including type of site, observation periods, percentage of cloud screened data and the availability of SDA retrieval products. Quality-assured direct-sun data in the 440 - 870 nm wavelength range is used to calculate the AOD at 550 nm obtained by the Ångström's equation adjustment. The contribution of each aerosol fraction is analysed using the SDA retrieval products (AOD_{fine} and AOD_{coarse}).

4.3 Model evaluation

There is a number of metrics that can be used to examine performances of air quality models (U.S. EPA, 1984, 1991; Cox and Tikvart, 1990; Weil et al., 1992; Chang and Hanna, 2004; Boylan and Russell, 2006; Dennis et al., 2010). Correlation coefficient (r), root mean squared errors (RMSE), mean bias (MB) and normalized bias error (MNBE) are commonly used by the modelling community. For the evaluation of PM concentrations, Boylan and Russell (2006) suggested the mean fractional bias (MFB) and the mean fractional error (MFE). Additionally, they propose model performance goals (the level of accuracy that is considered to be close to the best a model can be expected to achieve) and criteria (the level of accuracy that is considered to be acceptable for modelling applications) that vary as a function of concentration and extinction. A model performance goal is met when both the MFE and MFB are less than or equal to 50% and ±30%, respectively, and a model performance criterion is met when both MFE and MFB are less than or equal to 75% and 60%, respectively. The model-to-data statistics MB, MNBE, RMSE, MFE and MFB are selected for this study, together with the measured and modelled mean and the correlation coefficient. Comparisons are made for annual and monthly basis as well as 4 seasonal periods: winter (DJF) corresponding to December, January and February, spring (MAM) corresponding to March, April and May, summer (JJA) corresponding to June, July, August and autumn (SON) corresponding to September, October and November. Measured PM_{10}, $PM_{2.5}$ and their chemical aerosol components (i.e. sulphates, nitrates, ammonium, sea salt

and carbonaceous matter) from EMEP/CREATE networks are available on a daily basis except for carbonaceous matter which are available on a annual basis. Moreover, since AERONET data are acquired at 15-minute intervals on average, all AERONET measurements within ±30 minutes of the model outputs have been extracted and used for the model comparison at an hourly and daily basis.

Given that comparisons between simulations and observations are small among sites located in the same area, statistical indicators have been averaged over the regions indicated in Figure 4.1 by colours and defined in Table 4.1 and Table 4.2.

Table 4.2 *List of AERONET stations. Zone of location of the 35 AERONET stations which is defined in* ***Figure 4.1****. Class of location which is defined as stations: in remote (R), urban (U) or sub-rural (S) areas and in littoral localizations (C); coordinates, altitude, the number of measurements (Dataset), the number of hours (Hr.), the number of days (Dy.) and months (Mo.), the percentage of cloud screened data (F) in the observation periods of the 35 selected AERONET stations and the availability of the quality-assured SDA retrieval products (SDA).*

Station name	Code	Zone	Class	Lon.(°/E)	Lat.(°/N)	Alt.(m)	N	Hr.	Dy.	Mo.	F(%)	SDA
Avignon	AVI	E.IP-W.Med	U	4.88	43.93	32	7131	1998	264	12	34.52	
Barcelona	BCN	E.IP-W.Med	U/C	2.12	41.39	125	201	59	11	1	39.12	
Belsk	BEL	E.Eu	R	20.79	51.84	190	3173	1039	150	10	41.49	x
Blida	BLI	E.IP-W.Med	S/C	2.88	36.51	230	4598	1368	220	12	33.55	x
Cabo da Roca	ROC	W.IP	R/C	-9.50	38.78	140	4179	1259	193	10	39.17	
Carpentras	CAR	E.IP-W.Med	R	5.06	44.08	100	6905	1979	242	11	37.12	x
Dunkerque	DUN	NW.EU	U/C	2.37	51.04	0	871	331	65	6	56.17	
El Arenosillo	ARE	W.IP	R/C	-6.73	37.11	0	9235	2437	302	12	23.70	
ETNA	ETN	C.Med	U/C	15.02	37.61	736	871	226	40	3	39.25	x
Evora	EVO	W.IP	U	-7.91	38.57	293	7860	2205	266	12	29.75	
Fontainebleau	FON	NW.EU	R	2.68	48.41	85	1411	568	106	9	53.65	x
Forth Crete	CRE	E.Med	S/C	25,28	35,33	20	9634	2352	272	12	24.90	x
Hamburg	HAM	NW.EU	U	9.97	53.57	105	2094	691	115	11	46.59	x
Helgoland	HEL	NW.EU	R/C	7.89	54.18	33	470	202	40	7	40.42	x
IFT-Leipzig	LEI	C.Eu	U	12.44	51.35	125	1567	642	129	12	49.15	x
ISDGM CNR	CNR	N.It	R/C	12.33	45.44	20	5029	1566	209	11	48.26	x
Ispra	ISP	N.It	S	8.63	45.80	235	3942	1301	200	12	44.50	x
Laegeren	LAE	C.Eu	R	8.35	47.48	735	2694	848	125	10	41.24	x
Lampedusa	LAM	C.Med	R/C	12.63	35.52	45	2561	848	139	8	30.63	
Le Fauga	FAU	S.Fr	R	1.28	43.38	193	3736	1131	176	11	40.73	
Lecce University	LEC	C.Med	R	18.11	40.34	30	5489	1671	219	10	34.28	x
Lille	LIL	NW.EU	U	3.14	50.61	60	943	346	71	8	51.99	
Mainz	MAI	C.Eu	S	8.30	50.00	150	3191	1058	172	11	48.94	x
Modena	MOD	N.It	U	10.95	44.63	56	1899	554	70	4	41.35	
Munich Maisach	MUN	C.Eu	R	11.26	48.21	520	153	74	18	4	48.35	x
Nicelli Airport	NIC	N.It	S/C	12.38	45.43	13	389	94	10	2	27.45	
Palaiseau	PLS	NW.EU	S	2.21	48.70	156	2725	889	139	10	45.08	
Palencia	PAL	W.IP	U	-4.52	41.99	750	7389	2010	265	12	32.69	
Paris	PAR	NW.EU	U	2.33	48.87	50	106	34	7	2	38.59	
Rome Tor Vergata	ROM	C.Med	R	12.65	41.84	130	2256	601	106	8	40.05	
SMHI	SMH	Nord	U	16.15	58.58	0	493	182	25	2	34.73	x
The Hague	HAG	NW.EU	S/C	4.33	52.11	18	1376	476	73	7	49.67	
Toulon	TUL	E.IP-W.Med	U/C	6.01	43.14	50	430	128	24	2	42.09	
Venise	VEN	N.It	R/C	12.51	45.31	10	10257	1872	230	12	36.34	
Villefranche	VIL	E.IP-W.Med	S/C	7.33	43.68	130	7120	1936	235	11	32.81	

4.3.1 Ground level $PM_{2.5}$ and PM_{10} concentrations

Before evaluating PM composition, it is important to ensure that reactive gases are well reproduced, since a major fraction of ambient PM arises from atmospheric gas-to-particle conversion (Meng et al., 1997). In Pay et al. (2010) the CALIOPE model output for gas and particulate phase concentrations are compared with ground-based measurements from the EMEP monitoring network for year 2004 over Europe. This model evaluation showed that the modelling system is able to reproduce daily variations of gas phase pollutants (SO_2, NO_2 and O_3) as well as their spatial distribution and seasonal evolution.

In Table 4.3 and Figure 4.2a,b and Figure 4.2f,g depict the annual and seasonal statistical results of the evaluation of PM and the daily of the all-European average time series from model and observation. The model presents a clear systematic negative bias of $PM_{2.5}$ (annual MB = -6.30 $\mu g/m^3$), although it is able to reproduce the daily evolution through the year with an annual correlation between $PM_{2.5}$ model calculated and observed of 0.47 (Figure 4.2a). Higher correlations are observed during wintertime and lower underestimations are detected in autumn (MB = -5.0 $\mu g/m^3$).

PM_{10} is more underestimated (annual MB = -10.30 $\mu g/m^3$) than $PM_{2.5}$ although the evolution over year 2004 is well reproduced (Figure 4.2b) with higher correlations (r = 0.57) than for $PM_{2.5}$. The modelled coarse fraction includes the contribution of unspeciated anthropogenic mass, sea salt and desert dust. One source of uncertainty in the PM_{10} comparison comes from the fact that the aerosol module of CMAQv4.5 (AERO4) considers coarse mode aerosols as dry and inert. Several studies in Spain and the Mediterranean regions (e.g. Rodríguez et al., 2002; Querol et al., 2004b, 2009) suggest that from mid-spring to mid-autumn most of nitrate is present as Ca and/or Na salts in the 2.5 – 10 μm fraction. Other potential forms of nitrate and sulphate, such as salts linked to the reaction of acid pollutants with dust (Rodríguez et al., 2002; Querol et al., 2004b, 2009) are not considered in the simulated PM_{10}. Higher PM_{10} correlations are observed in summertime and in the southern European stations affected by Saharan dust outbreaks (see Figure 4.3). The modelled desert dust contributions to $PM_{2.5}$ and PM_{10} are on average 20% and 25%, respectively, increasing to 33% and 35% for Mediterranean stations. Although the model calculates considerable contribution of dust to both $PM_{2.5}$ and PM_{10}, higher annual correlation is observed in PM_{10} than in $PM_{2.5}$. This is associated to overestimations of $PM_{2.5}$ (see Figure 4.2f) during desert dust outbreaks in southern Europe sites (Pay et al., 2011). Therefore, despite the total dust mass (i.e. PM_{10}) is well captured by the BSC-DREAM8b model, its size distribution tends to overestimate the finer fractions (i.e. $PM_{2.5}$) in agreement with the results presented in Chapter 3.

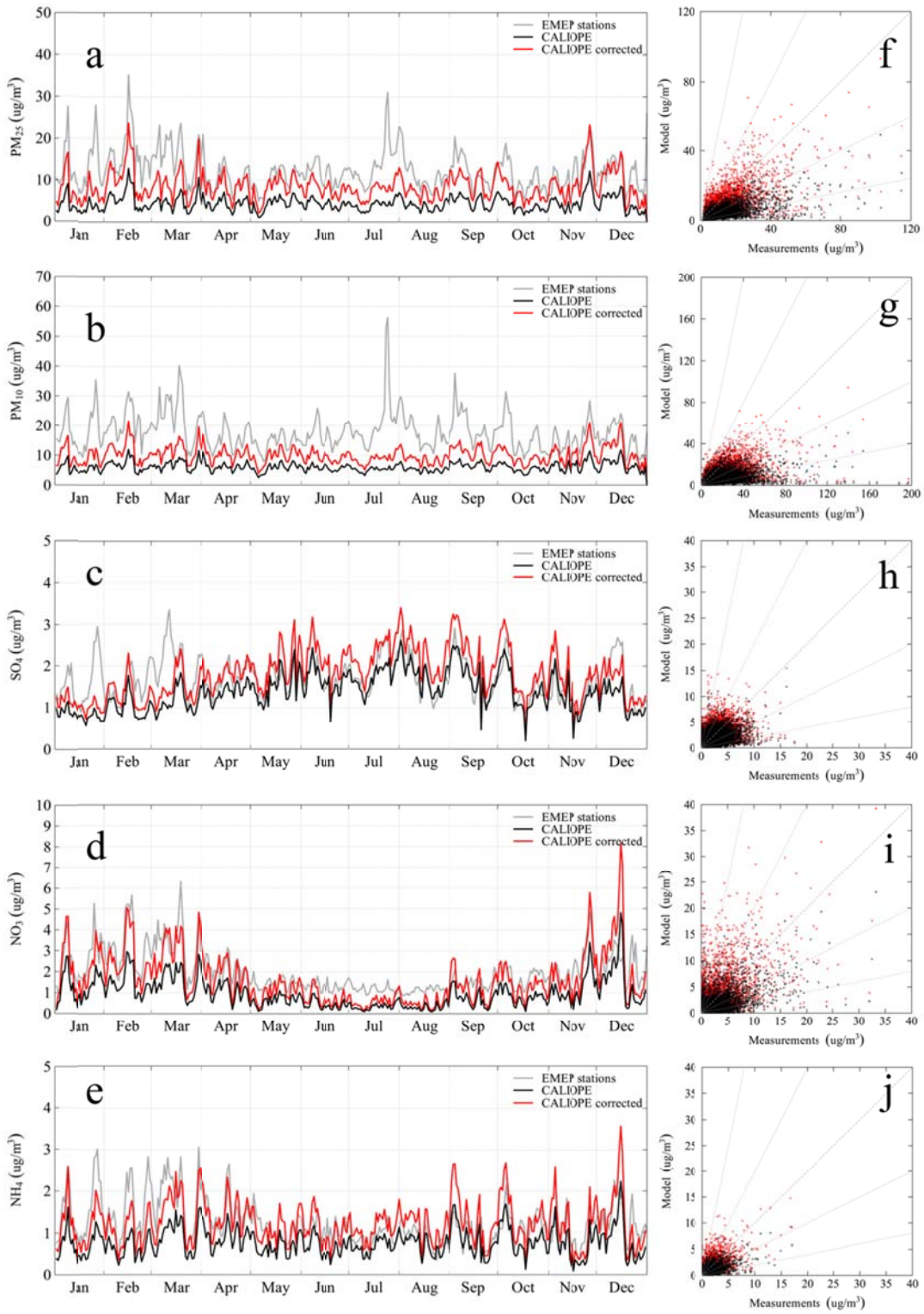

Figure 4.2 *Modelled (black lines), corrected-modelled (red lines) and measured (grey lines) time series (right) and scatter plots (left) of daily mean concentrations for $PM_{2.5}$, PM_{10}, sulphates, nitrates and ammonium at the EMEP/CREATE stations, respectively. The scatter plots include the 1:1, 1:2, 2:1, 1:5 and 5:1 reference lines. Correction factors of the* ***Table 4.5*** *are applied to nitrates, sulphates, ammonium and EC + OC in the corrected-modelled series.*

Table 4.3 *Seasonal and annual statistics obtained with CALIOPE over Europe for 2004 at the EMEP/CREATE stations for SIA (i.e. sulphate, nitrate, and ammonium) and SSA (i.e. chloride and sodium). Winter: January, February and December; Spring: March, April, May; Summer: June, July, August; Autumn: September, October, November. The number of data points indicates the number of pair measurement-model used to compute the statistics. The calculated statistics are: measured mean for available data, modelled mean for the whole year, correlation (r), Mean Bias (MB), Mean Normalized Bias Error (MNBE), Root Mean Square Error (RMSE), Mean Fractional Bias (MFB) and Mean Fractional Error (MFE).*

		Data Points	Obs. Mean (μg/m³)	Mod. mean (μg/m³)	*r*	MB	MNBE(%)	RMSE (μg/m³)	MFB(%)	MFE(%)
PM2.5 daily (16 stations)	Annual	5118	12.3	5.7	0.47	-6,30	-45.0	11.2	-72	80
	Winter	1171	12.2	4.8	0.62	-8,40	-47.0	15.3	-78	86
	Spring	1264	12.2	5.2	0.50	-6,70	-50.0	10.6	-79	84
	Summer	1396	11.5	6.8	0.49	-5,40	-45.0	9.1	-71	78
	Autumn	1287	12.3	6.2	0.52	-5,00	-39.0	9.3	-62	72
PM10 daily (25 stations)	Annual	8389	17.8	7.5	0.57	-10,30	-50.0	15.8	-79	84
	Winter	1994	18.0	6.6	0.54	-11,20	-47.0	18.2	-78	86
	Spring	2087	17.7	7.1	0.54	-10,50	-54.0	15.0	-84	87
	Summer	2204	18.5	8.2	0.60	-10,50	-54.0	16.1	-83	86
	Autumn	2104	17.0	8.1	0.62	-9,00	-44.0	13.5	-70	77
Sulfate daily (53 stations)	Annual	18227	1.7	1.4	0.49	-0,30	33.6	1.3	-8	55
	Winter	4524	1.5	1.0	0.30	-0,50	11.6	1.6	-24	65
	Spring	4675	1.8	1.4	0.50	-0,50	15.2	1.4	-19	54
	Summer	4598	1.8	1.7	0.59	-0,10	52.7	1.2	7	47
	Autumn	4430	1.6	1.5	0.58	-0,10	55.5	1.2	4	55
Nitrate daily (31 stations)	Annual	8968	2.0	1.0	0.58	-1,00	-9.7	2.3	-87	113
	Winter	2208	2.7	1.4	0.60	-1,10	21.6	3.1	-68	99
	Spring	2264	2.3	1.1	0.56	-1,10	-6.5	2.6	-76	104
	Summer	2252	1.2	0.4	0.29	-0,80	-55.6	1.3	-121	133
	Autumn	2244	1.8	0.9	0.53	-0,80	2.4	2.0	-84	115
Ammonium daily (19 stations)	Annual	4944	1.2	0.8	0.62	-0,50	32.8	1.2	-32	72
	Winter	1239	1.4	0.7	0.70	-0,80	28.2	1.5	-42	80
	Spring	1300	1.5	0.8	0.62	-0,60	23.1	1.3	-37	73
	Summer	1205	1.0	0.7	0.48	-0,20	38.9	0.8	-22	63
	Autumn	1200	1.1	0.8	0.64	-0,30	42.1	0.9	-24	70
Chloride daily (5 stations)	Annual	1434	0.3	0.3	0.46	0,00	413.9	0.5	49	106
	Winter	355	0.4	0.3	0.44	-0,10	297.5	0.6	14	97
	Spring	368	0.3	0.3	0.38	0,00	308.7	0.7	39	104
	Summer	362	0.1	0.3	0.53	0,10	598.2	0.3	78	115
	Autumn	349	0.3	0.4	0.64	0,10	451.9	0.5	65	109
Sodium daily (9 stations)	Annual	3204	0.7	1.2	0.67	0,50	176.1	1.6	16	77
	Winter	794	0.9	1.5	0.70	0,60	176.3	1.9	18	81
	Spring	806	0.7	1.1	0.64	0,50	176.6	1.6	10	79
	Summer	805	0.6	0.9	0.67	0,30	128.3	1.1	11	72
	Autumn	799	0.8	1.4	0.65	0,70	223.7	1.8	26	77

The results obtained by the CALIOPE system for $PM_{2.5}$ and PM_{10} are in the range of those shown in other European modelling studies (see Section 4 of the work of Pay et al., 2010). However, the MFE and MFB for $PM_{2.5}$ and PM_{10} do not meet the performance criteria proposed by Boylan and Russell (2006). Many studies have recognized the difficulty of models to simulate the mass of PM over Europe (Matthias, 2008; Pay et al., 2010). The underestimation of PM_{10} is, among others, the result from the lack of fugitive dust emissions, resuspended matter, a possible underestimation of primary carbonaceous particles, the inaccuracy of SOA formation, the difficulty of representing primary PM emission from wood burning and other sources not considered in the emission inventory as pollutant sources over North Africa (Rodríguez et al., 2011) and a more general lack of process knowledge on aerosol removal and dispersion and transport processes.

4.3.2 PM chemical composition

Chemical composition measurements can help to identify model limitations in simulating the physical and chemical processes leading to the formation of SIA (namely, sulphates, nitrates and ammonium), SOA and SSA. For the sake of comparison with EMEP stations different size modes are lumped to obtain the total sulphate (Aitken, accumulation and coarse modes), nitrate (Aitken, accumulation and coarse modes), ammonium (Aitken and accumulation modes), chloride and sodium (accumulation and coarse modes) and carbonaceous matter concentration (i.e. organic and elemental carbon). Table 4.3, Figure 4.2c-e, Figure 4.2h-j, Figure 4.3 and Figure 4.4 show the annual and seasonal statistics as well as the all-European temporal evolution of the model and ground-level EMEP/CREATE measurement concentrations for SIA components calculated on a daily basis.

The overall annual variability of the modelled sulphate concentrations (Figure 4.3) reproduces the measurements with $r = 0.49$. Better results during summer ($r = 0.59$) when sulphate concentrations reach maximum levels due to enhanced photochemistry, low air mass renovation at regional scale and the increase of the summer mixing layer depth favouring the local mixing of polluted air masses (Querol et al., 2009). On average, annual sulphate levels are underestimated by 18%, thus smaller than $PM_{2.5}$, with winter having the largest bias. Significant winter underestimations are located at stations in Eastern Europe (E.Eu region), where the mean bias per station ranges from -0.5 $\mu g/m^3$ to -2.5 $\mu g/m^3$ (Figure 4.3). On the contrary, at stations in the region of France (S.Fr and C.Fr) and near the Northern Atlantic (N.Atl) the simulated sulphate exceeds the measurements by 0.3 $\mu g/m^3$ and 0.4 $\mu g/m^3$, respectively (Figure 4.4). With respect to the temporal evolution the model presents the highest correlations in the Iberian Peninsula and Western Mediterranean Basin, ranging between 0.48 and 0.81 (see Figure 4.3). Model evaluation of

gas precursors SO_2 in the framework of the CALIOPE system over Europe (Pay et al., 2010) shows a positive mean bias for SO_2 which suggests that SO_4^{2-} formation in the system is often limited by oxidant availability and not always by SO_2 availability. Winter underestimation of sulpahte is a common issue in most models integrated in Europe which represent a direct couplet of sulfur chemistry with photochemistry, even detected with CMAQv4.5 over Europe (Matthias, 2008). This feature can be probably explained by a lack of model calculated oxidants or missing reactions (Kasibhatla et al., 1997).

On average, modelled nitrate concentrations reproduce well the daily variability of the observations through the year (r = 0.58), presenting higher concentrations in winter and lower levels in summer due to its thermal instability (Querol et al., 2009). The modelling system simulates lower aerosol nitrate concentrations than those measured (underestimations ~ 50%), particularly in winter and spring (MB = -1.1 $\mu g/m^3$). On average, nitrate formation is limited by the availability of nitric acid over land, which may be related with the underestimation of the modelled NO_2 concentrations outlined and discussed in Pay et al. (2010). The largest underestimations are located over Eastern Iberian Peninsula–Western Mediterranean (E.IP-W.Med) and Central Mediterranean (C.Med) area with MB of -1.8 $\mu g/m^3$ and Eastern Europe area (E.Eu region, except at Illmitz and Sniezka stations) with MB of -1.5 $\mu g/m^3$ (Figure 4.4). As in the case of sulphate, the model presents the best correlative skills over the Western Iberian Peninsula with relatively high correlations ranging from 0.40 to 0.65 by stations (Figure 4.3), and annual MB and RMSE less than 1 $\mu g/m^3$. One source of underestimation is related to the fact that CMAQv4.5 (AERO4) does not consider the formation of $Ca(NO_3)_2$ and $NaNO_3$ salts in the coarse fraction which are account to be significant in Spain from mid-spring to mid-autumn (Rodríguez et al., 2002; Querol et al., 2004b, 2009). Ammonium-nitrate is usually dominant in winter whereas calcium- and/or sodium-nitrate dominate in summer (Rodríguez et al., 2002; Querol et al., 2004b, 2009). Ammonium-nitrate mostly occurs in $PM_{2.5}$, whereas calcium- and/or sodium-nitrate nitrate mostly occur in the coarse $PM_{2.5-10}$ mode (Rodríguez et al., 2002; Querol et al., 2004b, 2009). This could be related with the underestimations observed in Eastern Spain, particularly in summer (Figure 4.4). Moreover, correlations between the simulated and the observed values are rather low in summer in Spain (Figure 4.3).

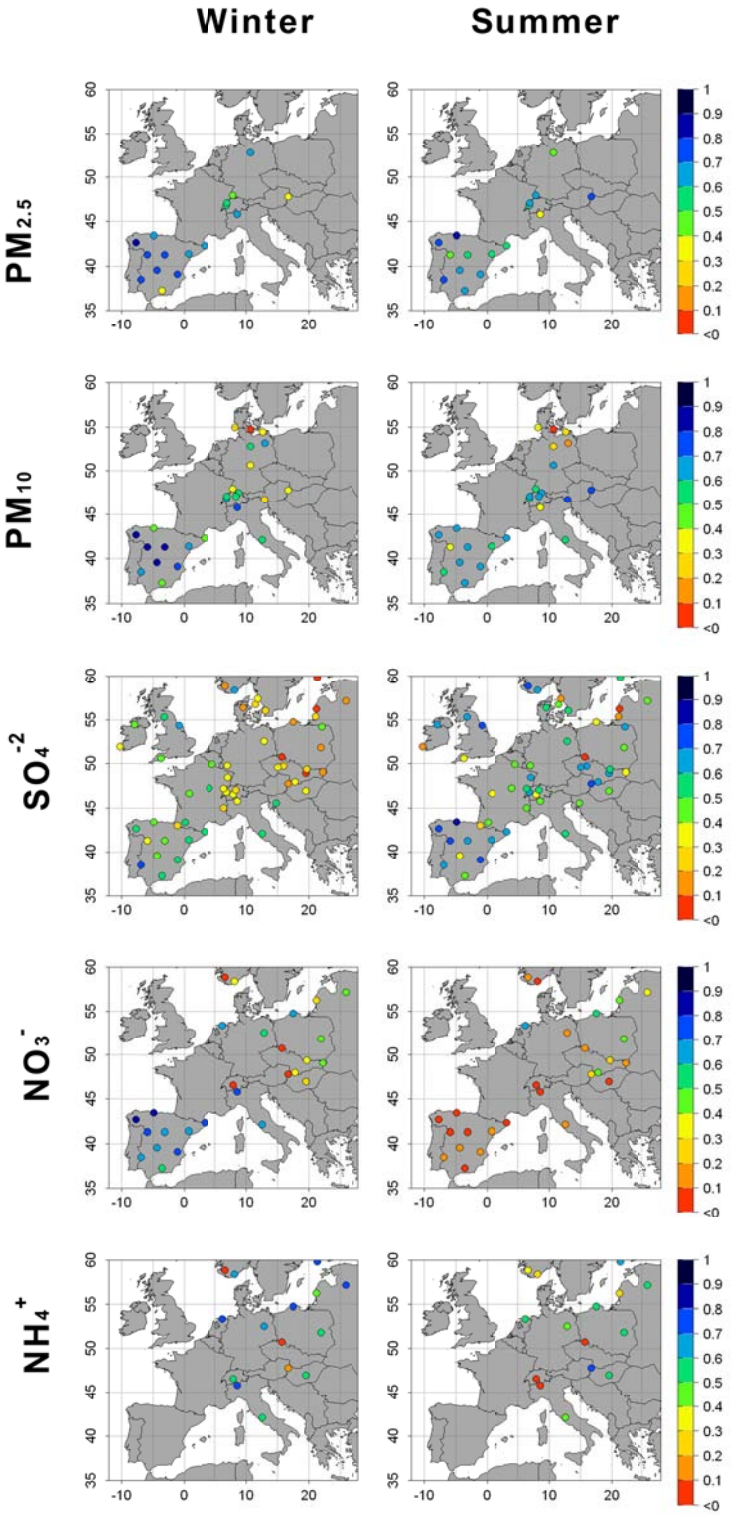

Figure 4.3 *Spatial distribution of the correlation coefficient at all stations for $PM_{2.5}$, PM_{10}, SO_4^{-2}, NO_3^- and NH_4^+. The two columns represent the winter (left panels) and summer (right panels) seasons for 2004, respectively for each parameter.*

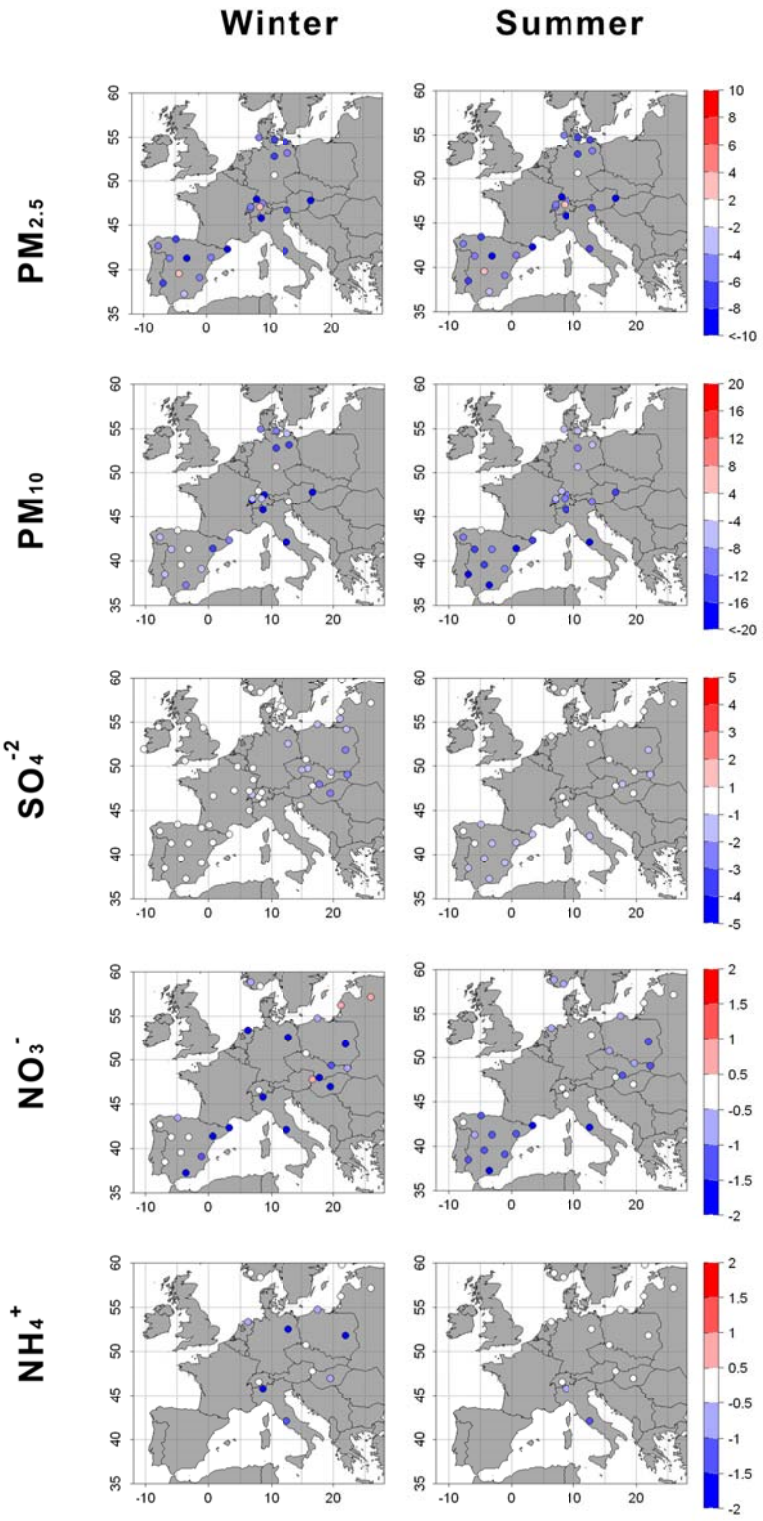

Figure 4.4 *Spatial distribution of mean bias at all stations for $PM_{2.5}$, PM_{10}, SO_4^{-2}, NO_3^- and NH_4^+. The two columns represent the winter (left panels) and summer (right panels) seasons for 2004, respectively for each parameter.*

In air masses with a continental signature, aerosol nitrate and sulphate are associated with ammonium (Schaap et al. 2004; Querol et al., 2009). Atmospheric ammonia is first neutralized by sulphuric acid to form ammonium sulphate. Remaining ammonia may then combine with nitric acid to form ammonium nitrate (Seinfeld and Pandis, 1998). 94% of NH_3 total emissions are attributed to agriculture and livestock (EMEP, 2007). Livestock sources vary during the year since volatilization of NH_3 from the animal waste is a function of temperature (Gilliland et al, 2003). Seasonality in NH_3 emission is expected since field application of fertilizers occurs during specific seasons (Asman, 2001). In the CALIOPE system over Europe, annual emissions of NH_3 are derived from the 2004 annual EMEP emission database (EMEP, 2007). However, detailed agricultural registers are not generally available in many countries (e.g. Menut and Bessagnet, 2010).

The evaluation of modelled ammonium concentrations with measurements shows the annual trend is correctly reproduce (Figure 4.2e) with high correlation coefficient (r = 0.62, see Table 4.3 and Figure 4.3). Although, the modelled ammonium annual mean underestimates observed mean by a 36%, with the highest bias in winter (MB = -0.8 $\mu g/m^3$). However, the temporal variability is correctly captured during this season (r = 0.70).

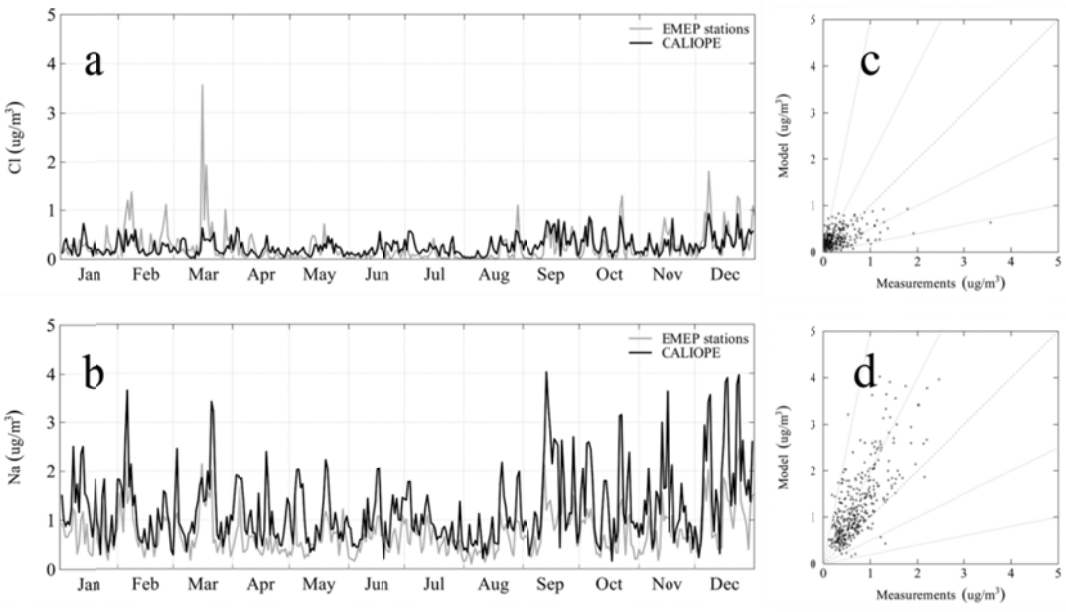

Figure 4.5 *Modelled (black lines) and measured (grey lines) time series (left) and scatter plots (right) of daily mean concentrations for sea salt chemical species (i.e. chlorine and sodium), at the EMEP/CREATE stations, respectively. The scatter plots include the 1:1, 1:2, 2:1, 1:5 and 5:1 reference lines.*

For sea salt component (i.e., sodium and chloride), the modelling system reproduces the daily variability with annual correlations for sodium and chloride of 0.67 and 0.46 respectively (Table 4.3 and Figure 4.5). It should be noted that the results are strongly biased towards measurements obtained in northern Europe, since 9 out of 10 stations are located there (see Table 4.1). There are four coastal stations where the model simulates slightly higher chloride and sodium concentrations than those measured while at continental areas sea salt tends to be underestimated. Correlation for sodium is higher than for chloride since sodium is considered as inert in the atmosphere. One source of uncertainty is related to the fact that AERO4 considers coarse mode aerosols as dry and inert. This approach does not allow important aerosol processes, such as the replacement of chloride by nitrate in mixed marine/urban air masses (Kelly et al., 2010) especially intense in summer when nitric acid is released by the thermal instability of ammonium nitrate (Querol et al., 2004b). Moreover, degassing of Cl^- is not implemented in the model, and heterogeneous reactions are not taken into account. The coarse mode in the AERO4 module in CMAQv4.5 (Binkowski and Roselle, 2003) is implemented in a non-interactive way. That is, fine particles do not coagulate with coarse particles, nor do coarse particles coagulate with each other.

Both OC and EC can contribute significantly to $PM_{2.5}$ and PM_{10} in urban and kerbside sites, and their mass fraction might be higher than the sum of the inorganic components (Putaud et al., 2004). Unfortunately, a detailed investigation of the organic aerosol cannot be done for the present study since there are only very few measurements available that cover a longer time, therefore OC and EC could only be evaluated at two CREATE stations: Birkenes (NO01) and Melpitz (DE44) in 2004 on an annual basis. So the results of the carbonaceous aerosol are far from being representative and currently subject to re-evaluation by the European Supersites for Atmospheric Aerosol Research project (EUSAAR; http://www.eusaar.net/) which searchs the integration of measurements of atmospheric aerosol properties performed in high quality European ground-based stations. The observed values are approximately a factor of 4 higher than the modelled values. This factor is higher than that obtained by Matthias (2008) at Birkenes in 2001 (factor of 3) partly because carbonaceous particles from biomass burning emissions were taken into account in the aforementioned study. There are other studies that demonstrate that SOA are underestimated by current models by a factor of 6 (Volkamer et al., 2006). The large uncertainties are associated with (1) probable underestimation of primary carbonaceous emission (Cooke and Wilson, 1996; Bond et al., 2004; Tsyro et al., 2007; Monsk et al., 2009) and (2) the state-of-the-science concerning to SOA formation pathways (Eder and Yu, 2006; Edney et al., 2007; Appel et al., 2008).

In the anthropogenic emissions used in the CALIOPE system the primary traffic emissions have the highest contribution of OC and EC (80% of $PM_{2.5}$), followed by combustion in energy and transformation industries (60% of $PM_{2.5}$). Additionally, the absence of some natural PM sources (such as wildfire emissions) and primary biogenic emissions (such as pollen, bacteria, fungal and fern spores, viruses, fragments of animals and plants, virus, etc) contributes to OC underestimation in PM. Wildfire emissions during 2004 were significantly important in southern Europe during summer (European Commission, 2005). Additionally, the traditional 2-product SOA model adopted from CMAQv4.5 (Binkowski and Roselle, 2003) does not include SOA formation from isoprene and sesquiterpenes. The absence of the isoprene-SOA route on SOA may impact significantly in southern Europe during summer where the predominant vegetation types favour isoprene as the main biogenic VOC (Keenan et al., 2009).

As a summary, the modelling system fairly well reproduces the daily variability of the main aerosol components in Europe. However their concentrations are in most cases strongly underestimated. The most important underestimations are observed for total carbonaceous material (i.e. OC and EC). The total amount of SIA is on average underestimated by 18-50%. SSA is underestimated over inland and overestimated at coastal sites of northern Europe.

4.3.3 Aerosol optical depth

The evaluation of the AOD is particularly useful for validating the capabilities of the modelling system to reproduce European regional transport as well the long-range transport of desert dust from North Africa at high altitudes.

The modelling system is quantitatively compared against direct-sun AOD measurements (AOD) and the AOD mode products from the SDA retrieval (AOD_{fine} and AOD_{coarse}). Modelled AOD_{fine} includes ammonium, sulphate, nitrate, SSA, OC and EC as well unspeciated mass fine portion from CMAQ as well sub-micron desert dust from BSC-DREAM8b. Modelled AOD_{coarse} is the sum of the super-micron fraction of desert dust from BSC-DREAM8b and SSA and unspeciated mass coarse portion from CMAQ. Table 4.4 and Figure 4.6 show the annual and seasonal statistics as well as the temporal evolution of the model and ground-based AERONET measurements for AOD, AOD_{fine} and AOD_{coarse} calculated on an hourly and daily basis.

Table 4.4 *Seasonal and annual statistics obtained with CALIOPE over Europe for 2004 at the AERONET stations for AOD, AOD_{fine} and AOD_{coarse}. Winter: January, February and December; Spring: March, April, May; Summer: June, July, August; Autumn: September, October, November. The number of data points indicates the number of pair measurement-model used to compute the statistics. The calculated statistics are: measured mean for available data, modelled mean for the whole year, correlation (r), Mean Bias (MB), Mean Normalized Bias Error (MNBE), Root Mean Square Error (RMSE), Mean Fractional Bias (MFB) and Mean Fractional Error (MFE).*

		Data Points	Obs. Mean	Mod. mean	r	MB	MNBE(%)	RMSE	MFB(%)	MFE(%)
AOD hourly (35 stations)	Annual	34925	0.18	0.10	0.51	-0,07	-31.0	0.15	-53	66
	Winter	4175	0.12	0.07	0.36	-0,05	-23.1	0.13	-49	69
	Spring	9099	0.19	0.11	0.49	-0,07	-32.3	0.16	-57	70
	Summer	14249	0.19	0.11	0.49	-0,08	-34.8	0.16	-56	66
	Autumn	7402	0.16	0.10	0.62	-0,06	-26.6	0.13	-45	58
AOD_{fine} hourly (16 stations)	Annual	15914	0.22	0.10	0.52	-0,13	-48.7	0.19	-75	80
	Winter	1459	0.14	0.06	0.42	-0,09	-45.9	0.16	-78	87
	Spring	3828	0.24	0.11	0.55	-0,13	-49.5	0.19	-77	82
	Summer	7250	0.24	0.10	0.45	-0,14	-50.7	0.20	-77	80
	Autumn	3377	0.21	0.10	0.62	-0,12	-44.9	0.19	-69	74
AOD_{coarse} hourly (16 stations)	Annual	15914	0.06	0.02	0.63	-0,04	-72.9	0.07	-134	139
	Winter	1459	0.05	0.02	0.25	-0,04	-69.4	0.07	-133	141
	Spring	3828	0.07	0.02	0.58	-0,04	-73.3	0.09	-137	142
	Summer	7250	0.05	0.02	0.70	-0,03	-73.1	0.06	-135	139
	Autumn	3377	0.06	0.02	0.71	-0,04	-73.6	0.07	-130	133
AOD daily (35 stations)	Annual	4920	0.18	0.11	0.56	-0.07	-28.2	0.14	-47	60
	Winter	792	0.12	0.07	0.41	-0.05	-23.6	0.12	-46	63
	Spring	1267	0.19	0.12	0.52	-0.07	-28.8	0.15	-51	64
	Summer	1689	0.20	0.12	0.55	-0.08	-33.3	0.15	-51	60
	Autumn	1172	0.16	0.11	0.67	-0.06	-24.5	0.12	-39	52
AOD_{fine} daily (16 stations)	Annual	2318	0.22	0.10	0.59	-0.12	-45.1	0.18	-69	74
	Winter	304	0.14	0.06	0.45	-0.08	-43.8	0.14	-71	80
	Spring	556	0.25	0.12	0.58	-0.13	-45.9	0.18	-70	75
	Summer	919	0.24	0.10	0.53	-0.14	-47.5	0.19	-70	73
	Autumn	539	0.21	0.10	0.68	-0.11	-41.0	0.19	-62	69
AOD_{coarse} daily (16 stations)	Annual	2318	0.06	0.02	0.70	-0.04	-74.6	0.07	-134	-138
	Winter	304	0.05	0.01	0.24	-0.04	-71.0	0.07	-132	138
	Spring	556	0.07	0.02	0.65	-0.05	-72.7	0.08	-134	138
	Summer	919	0.05	0.02	0.77	-0.03	-76.9	0.06	-139	141
	Autumn	539	0.06	0.02	0.80	-0.04	-74.6	0.06	-130	131

The model reproduces the AOD hourly and daily variability with an annual correlation of 0.51 and 0.56 respectively on average (Table 4.4, Figure 4.6a and Figure 4.7) and underestimates the hourly and daily AOD by 41 and 38% respectively (Table 4.4, Figure 4.6a and Figure 4.8).

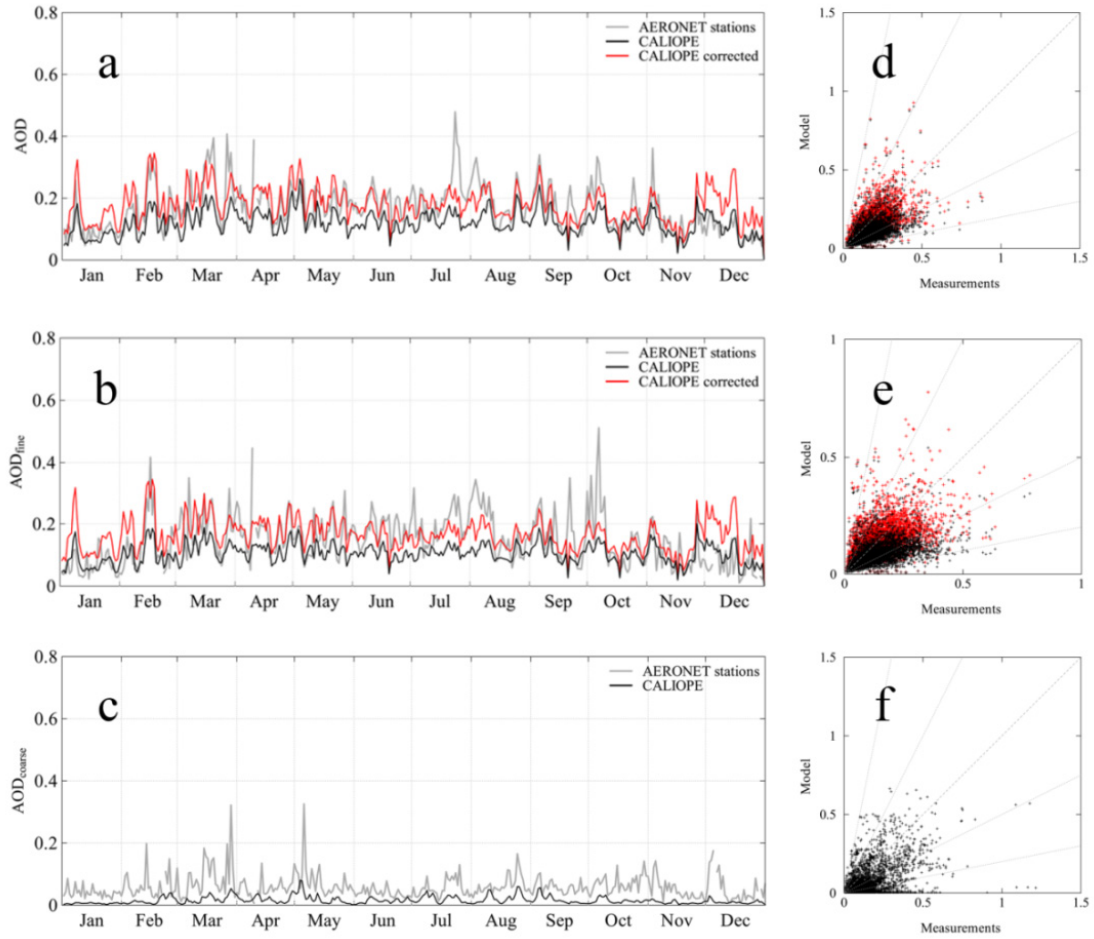

Figure 4.6 *Modelled (black lines), corrected-modelled (red lines) and measured (grey lines) time series (right) in daily mean concentrations and scatter plots (left) in hourly mean concentration values for AOD, AOD_{fine} and AOD_{coarse} at the AERONET stations, respectively. The scatter plots include the 1:1, 1:2, 2:1, 1:5 and 5:1 reference lines. Correction factors of the* ***Table 4.5*** *are applied to nitrates, sulphates, ammonium and EC + OC in the corrected-modelled series.*

If we take a closer look to the desert dust component and its role on the model data agreement, its influence is remarkable. When considering only CMAQ outputs the annual simulated AOD underestimation rises up to 61% for hourly values and 58% for daily values and the annual correlation decreases to 0.39 for the hourly values and to 0.40 for daily values. Due to the proximity to the African continent, the differences between

CMAQ-alone and CMAQ+BSC-DREAM8b are larger in the Iberian Peninsula and Mediterranean sites. Correlations remarkably improve from 0.16 to 0.59, 0.39 to 0.58, 0.31 to 0.49 and 0.05 to 0.50, for the Western Iberian Peninsula, Eastern Iberian Peninsula-Western Mediterranean, Central Mediterranean and Eastern Mediterranean, respectively for hourly values. Averaging for the entire study region, desert dust contributions represent ~ 35% of the AOD and over the Iberian Peninsula and Mediterranean ~ 51% on average. These results are consistent with the aerosol characterization presented in Chapter 2.

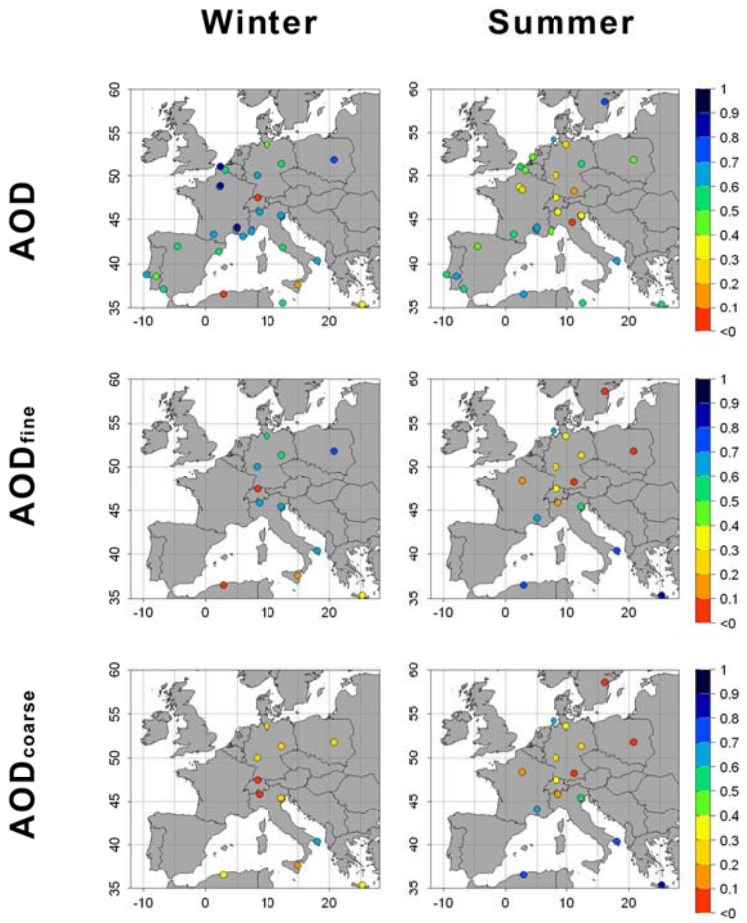

Figure 4.7 *Spatial distribution of the correlation coefficient at all stations for AOD, AOD_{fine} and AOD_{coarse} in hourly basis. The four columns represent the winter (left panels) and summer (right panels) seasons for 2004, respectively for each parameter.*

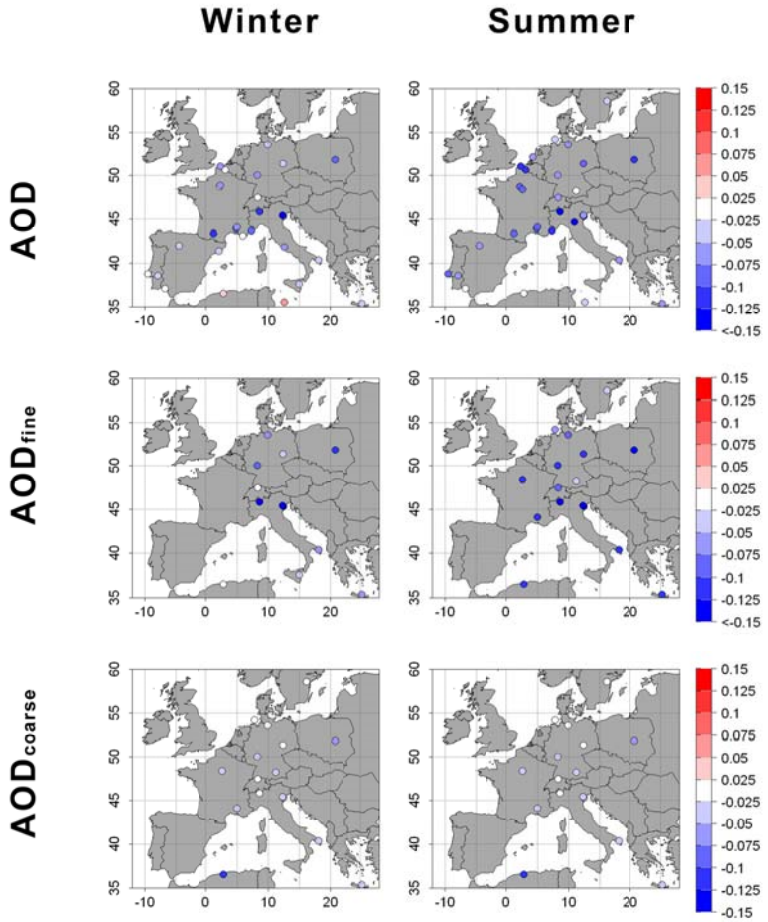

Figure 4.8 *Spatial distribution of mean bias at all stations for AOD, AOD_{fim} and AOD_{coarse} in hourly basis. The four columns represent the winter (left panels) and summer (right panels) seasons for 2004, respectively for each parameter.*

Because the evaluation of the aerosol model performance is hampered by the lack of routine data above the surface, satellite observations offer new opportunities for model evaluation. In Figure 4.9, the seasonal averages for 2004 of the collection C005 AOD data (cloud free) at 550 nm from MODIS/Aqua sensor (Levy et al., 2003; Remer et al., 2005) are qualitatively compared with the modelled aerosol fields. Additionally, superimposed to MODIS values, the AERONET seasonal mean values are included showing moderate differences between both observational datasets. Among other causes, this is partly because the satellite products are obtained from 2 images per day as a difference of AERONET measurements.

In general, the CALIOPE system reproduces the main seasonal AOD patterns observed in MODIS AOD product despite of the important underestimations at hot spots located in Northern Italy, Eastern and North-western Europe as shown in the comparison with AERONET data. The dust transport from North Africa is well captured with maximum AOD values in the Eastern Mediterranean region in spring shifting to Central and Western Mediterranean regions in summer.

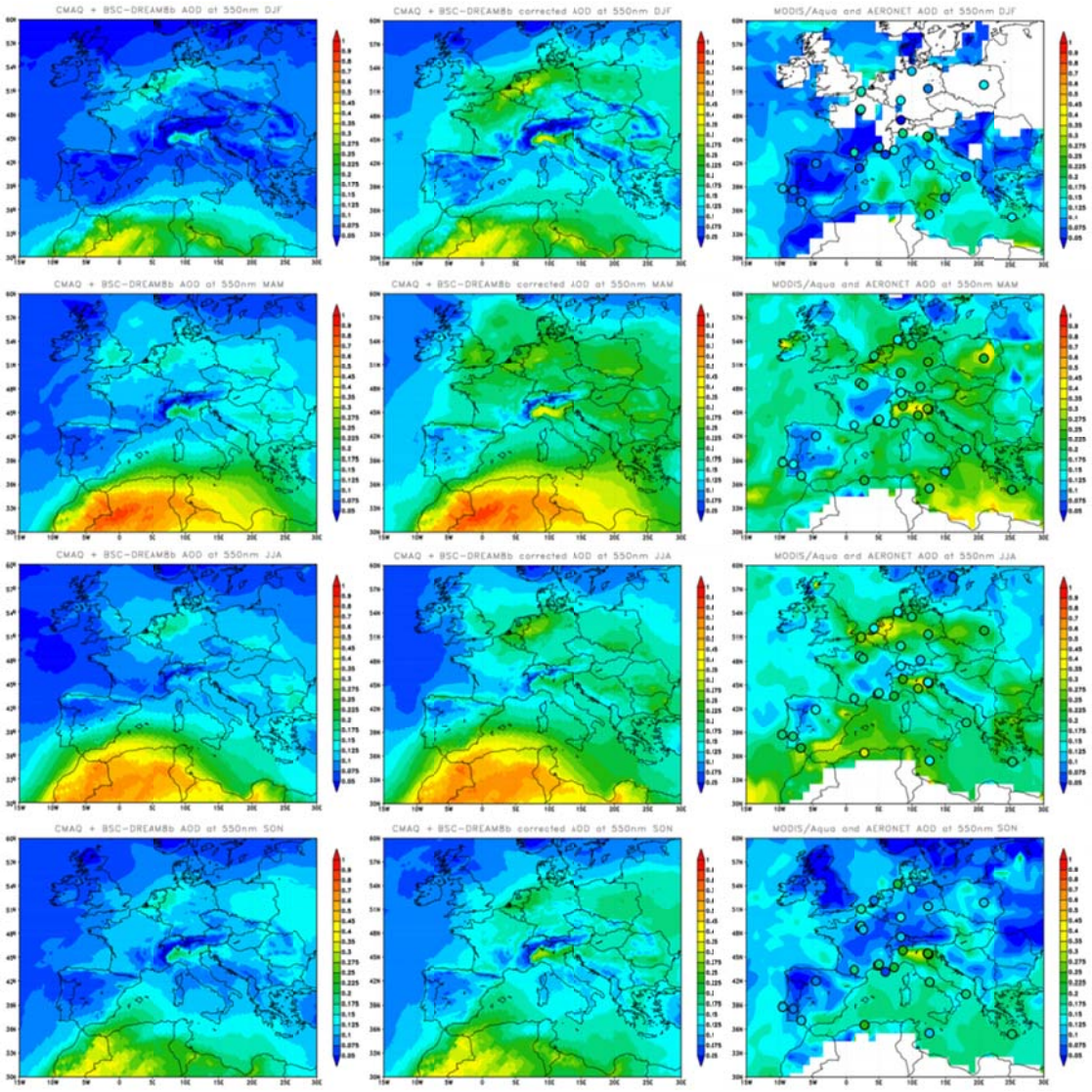

Figure 4.9 *Seasonal AOD average (from the top to bottom panels) of CMAQ + BSC-DREAM8b without correction factor (left panels), CMAQ + BSC-DREAM8b with correction factors for sulphates, nitrates, ammonium and EC + OC (central panels) and MODIS/Aqua AOD product as well AERONET seasonal mean values (colour points). Correction factors of the* ***Table 4.5*** *are applied to nitrates, sulphates, ammonium and EC + OC in the corrected-modelled series.*

The aerosol fields obtained with CALIOPE are similar to those shown in other European modelling studies (e.g., POLYPHEMUS; Tombette et al., 2008; CHIMERE, Péré et al., 2010). In another study with CMAQ (Matthias, 2008), the modelled AOD was 20 - 70% lower than AERONET observations. In contrast to our results, the best scores in this study were achieved in northern sites where desert dust contributions are smaller, which again highlights the importance of desert dust in southern latitudes. The evaluation of the POLYPHEMUS system (Tombette et al., 2008), which also did not consider desert dust, against 19 AERONET stations underestimated the hourly AOD average from 0.02 to 0.07 and correlations ranged from 0.40 to 0.87 obtaining the best results in the northern European sites. In the evaluation of the CHIMERE model against 13 AERONET stations presented in Péré et al. (2010), correlations lied within the range of 0.50 – 0.74 .The values obtained in the present work lie within the range of these studies with correlations of 0.40 – 0.72 depending on the region.

We take a closer look now at the fine and coarse components of the AOD. The annual and seasonal statistical results obtained for AOD_{fine} and AOD_{coarse} are presented in Table 4.4, Figure 4.7 and Figure 4.8 and the temporal series are shown in Figure 4.6b and Figure 4.6c, respectively. The modelled desert dust contributions to AOD_{fine} and AOD_{coarse} are on average 22% and 88%, respectively. The largest discrepancies between model and data are associated to AOD_{fine} (MB = -0.13 and RMSE = 0.19, Table 4.4), but the hourly variability is reasonably well captured (r = 0.52, see Figure 4.6b and 6). The best scores are found in SMHI site in the Nordic region (r = 0.70, RMSE = 0.04 and MB = -0.03) where no desert dust is present in the fine mode AOD and where the frequent background situation is associated with low values. The largest error in AOD_{fine} is found for Northern Italy (RMSE = 0.29 and MB = -0.20). The correlation remains moderately high though (~ 0.52), indicating that the modelling system is able to reproduce reasonably well the background AOD and reproduce the occurrence of peaks dust outbreaks. Northern Italy includes one of the most polluted regions in Europe, the Po Valley (Mélin and Zibordi, 2005) and the model indicates almost no contribution from dust (desert dust contributions to AOD less than 4%) in agreement with the results of the aerosol characterization from Gobbi et al. (2007). In this area, the air stagnation in a mountain-surrounded valley favours the photochemical reactions that produce SIA and the fine mode growth (Gobbi et al., 2007) together with frequent humid conditions in winter which favours the nucleation and growth of aerosols.

The overall annual variability of the modelled AOD_{coarse} agrees fairly well with measurements (r = 0.63, see Figure 4.6c). The best scores are found in the Mediterranean Basin ($0.6 < r < 0.8$, RMSE < 0.09 and MB ~ -0.04, on average in hourly mean values for the entire Basin) particularly in summertime coinciding with the maximum AOD_{coarse} values

and maximum activity in the desert dust sources (Middelton and Goudie, 2001). The largest discrepancies are found in Nordic countries (r = 0.06, RMSE = 0.03 and MB = -0.02) and Eastern Europe (*r* = 0.18, RMSE = 0.10 and MB = -0.06). In general, highest AOD_{coarse} values are linked to the presence of desert dust. However, some coarse events in North-western and Eastern Europe are not captured by the modelling system (not show here). They could link to the occurrence of the coarse sodium and calcium nitrate because high levels of sulphate neutralize ammonium (Querol et al., 2009).

The ESCOMPTE experiment (Mallet et al., 2003; Cross et al., 2004), which investigated the microphysical and optical properties of the aerosol around Marseille in the summer 2001, showed that 90% of the light extinction is due to anthropogenic aerosol and only 10% is due to natural aerosol (SSA and desert dust). 44% of the anthropogenic extinction was due to ammonium sulphates, followed by 20% from EC and 21% by OM. Nitrate aerosol had a weak contribution (~ 5%). In the present study, at the Western Mediterranean sites (i.e. AVI, CAR, TUL and VIL) during the summer months of the year 2004, 28% of the light extinction is due to natural aerosol (SSA and desert dust) and 72% is due to anthropogenic aerosol. In our model, 54% of the anthropogenic extinction is due to ammonium sulphates, followed by nitrate (~ 13%) and EC and OC with ~ 6% and ~ 9%, in that order. These results reveal important underestimates of total carbonaceous material (EC + OC) species. The important underestimations of EC and OC can be partly explained by the influence of local emissions and natural sources as indicated in Section 4.3.2. The uncertainties associated to the emission inventory for black carbon may be an important cause for the discrepancy (Baldasano et al., 2008b).

One of the sources of uncertainties in the AOD model evaluation arises from the fact that the optical properties and lifetime of dust and anthropogenic substances (particulates and gases species) can be drastically altered through mixing and chemical reactions. For example, dust and black carbon form aggregates and this process makes the former more absorbing to visible and infrared radiation. In some parts of the world, dust particles are often found to be coated with nitrates and sulphates. The Mediterranean and northern Africa region is for example a hot spot where Saharan dust and pollutants from Europe interact (e.g. Rodríguez et al., 2011).

4.4 Aerosol distribution over Europe

4.4.1 Model bias correction

Several studies have demonstrated the benefit of adjusting site-specific air quality model predictions using observational data to reduce systematic model error (e.g. Hogrefe et al.,

2006; Djalalova et al., 2010). Bias-adjustment strategies range from the relatively simple mean bias and multiplicative ratio adjustments used by McKeen et al. (2005) to the more complex Kalman Filter techniques (Manders et al., 2009; Kang et al., 2010; Sicardi et al., 2011). In the present section, we intend to provide an estimation of the spatial and seasonal distribution of the different aerosol components over Europe with our model results including an a posteriori correction. The evaluation (see Sect. 4.3) consistently reveals a similar degree of fine fraction underestimation on both surface levels and column-integrated values (AOD). In this regard, the correction applied use the results of the evaluation against measured chemical aerosol surface concentrations on total mass fraction on a daily basis described in the Sect. 4.2.3.1.

We calculate spatially homogeneous, for all Europe, multiplicative correction factors per aerosol species and apply it to the mass concentrations in the model. The main limitation of this method is the application of a spatially homogeneous correction factor for a large region such as Europe. However, as shown in the model evaluation results, the seasonal variability has stronger impact than the geographical differences in the formation of the secondary atmospheric aerosols. As described below the modelled bulk parameters: PM levels and AOD significantly improve after correcting the bias of each aerosol species individually.

Table 4.5 *Seasonal and annual multiplicative correction factors to SIA (sulphates, nitrates and ammonium) and EC + OC obtained minimizing a weighted sum of the squared difference between the modelled and measured chemical aerosol surface concentrations on total fraction mass on a daily basis over Europe for 2004. Winter: January, February and December; Spring: March, April, May; Summer: June, July, August; Autumn: September, October, November.*

	Sulphates	Nitrates	Ammonium	OC+EC
Winter	1.7	1.7	2.0	4
Spring	1.4	1.8	1.7	4
Summer	1.2	1.9	1.4	4
Autumn	1.1	1.5	1.2	4
Annual	1.3	1.7	1.6	4

For carboneous compounds (i.e. EC and OC), a spatially homogeneous mean annual multiplicative correction factor of 4 is estimated (see Sect. 4.3.2). For the SIA (i.e. sulphates, nitrates and ammonium) components the correction factor is calculated from the modelled and observed mean daily values. We employ a weighted sum of the squared difference between the modelled and observed values. We minimize this sum to identify

the magnitude of the aerosol concentration that is in optimal agreement with the observations. Table 4.5 shows the spatially homogeneous multiplicative correction factors obtained for each chemical species. The bias corrected simulation is then evaluated against the bulk PM and AOD observations from EMEP and AERONET respectively (Table 4.6).

Table 4.6 *Seasonal and annual statistics obtained with CALIOPE and the seasonal correction factors of* ***Table 4.5*** *applied to sulphates, nitrates, ammonium and EC + OC over Europe for 2004 at the EMEP stations for $PM_{2.5}$ and PM_{10} and at the AERONET stations for AOD_{fine} and AOD. Winter: January, February and December; Spring: March, April, May; Summer: June, July, August; Autumn: September, October, November. The number of data points indicates the number of pair measurement-model used to compute the statistics. The calculated statistics are: measured mean for available data, modelled mean for the whole year, correlation (r), Mean Bias (MB), Mean Normalize Bias Error (MNBE), Root Mean Square Error (RMSE), Mean Fractional Bias (MFB) and Mean Fractional Error (MFE).*

		Data Points	Obs. Mean	Mod. mean	r	MB	MNBE(%)	RMSE	MFB(%)	MFE(%)
PM2.5 daily (16 stations)	Annual	5118	12.30	10.02	0.61	-2,31	-6.2	8.89	-22	47
	Winter	1171	12.20	10.38	0.67	-3,26	-3.2	11.72	-18	55
	Spring	1264	12.20	9.83	0.59	-2,34	-12.3	8.36	-33	45
	Summer	1396	11.50	9.95	0.55	-2,21	-13.2	7.54	-28	45
	Autumn	1287	12.30	9.94	0.62	-1,51	4.8	7.71	-19	45
PM10 daily (25 stations)	Annual	8389	17.80	11.65	0.62	-6,16	-20.7	12.91	-38	54
	Winter	1994	18.00	11.85	0.65	-6,15	-15.3	14.15	-32	57
	Spring	2087	17.70	11.97	0.59	-5,70	-24.6	15.15	-38	51
	Summer	2204	18.50	11.19	0.60	-7,35	-30.6	16.15	-48	56
	Autumn	2104	17.00	11.62	0.66	-5,38	-11.5	17.15	-35	52
AOD_{fine} hourly (16 stations)	Annual	15914	0.22	0.15	0.55	-0,07	6.3	0.16	-36	6
	Winter	1459	0.14	0.10	0.56	-0,05	15.5	0.13	-26	55
	Spring	3828	0.24	0.18	0.57	-0,06	2.3	0.16	-32	50
	Summer	7250	0.24	0.15	0.48	-0,08	1.6	0.16	-35	50
	Autumn	3377	0.21	0.14	0.66	-0,08	15.2	0.16	-36	52
AOD hourly (35 stations)	Annual	34925	0.18	0.15	0.56	-0,02	-16.5	0.13	-12	46
	Winter	4175	0.12	0.11	0.48	-0,00	-13.4	0.01	1	49
	Spring	9099	0.19	0.18	0.55	-0,01	-19.7	0.14	-12	45
	Summer	14249	0.19	0.16	0.53	-0,04	-18.5	0.14	-16	45
	Autumn	7402	0.16	0.14	0.66	-0,03	-10.0	0.12	-13	46
AOD_{fine} daily (16 stations)	Annual	2318	0.22	0.16	0.61	-0.07	-13.3	0.15	-28	46
	Winter	304	0.14	0.11	0.54	-0.03	0.0	0.12	-19	48
	Spring	556	0.25	0.19	0.60	-0.06	-11.9	0.15	-25	44
	Summer	919	0.24	0.16	0.56	-0.08	17.1	0.16	-30	46
	Autumn	539	0.21	0.14	0.71	-0.07	-16.1	0.16	-31	48
AOD daily (35 stations)	Annual	4920	0.18	0.14	0.60	-0.04	-1.9	0.12	-15	42
	Winter	792	0.12	0.11	0.57	-0.01	-14.4	0.10	-3	43
	Spring	1267	0.19	0.17	0.55	-0.02	-3.1	0.12	-16	40
	Summer	1689	0.20	0.15	0.59	-0.05	-7.4	0.12	-20	43
	Autumn	1172	0.16	0.13	0.70	-0.03	-3.8	0.11	-18	44

The corrected $PM_{2.5}$ and PM_{10} results present a much better agreement with the observations if correction factors are applied (Figure 4.2 and Table 4.6). The annual underestimations are reduced from 53% to 18% for $PM_{2.5}$ and from 58% to 35% for PM_{10}. Correlations increase from 0.47 to 0.59 for $PM_{2.5}$ and from 0.57 to 0.61 for PM_{10}. In fact, the MFE and MFB for the corrected $PM_{2.5}$ fall within the performance goal meanwhile the corrected PM_{10} fall within the performance criterion proposed by Boylan and Russell (2006). Correlation, RMSE, MFB and MFE of $PM_{2.5}$ and PM_{10} with correction factors are significantly better than those obtained in Pay et al. (2010) by applying a factor of 2 to total $PM_{2.5}$ and PM_{10}.

The annual underestimations are reduced from 57% to 32% for hourly AOD_{fine} and from 41% to 13% for hourly AOD while correlations increase from 0.52 to 0.56 for hourly AOD_{fine} and from 0.51 to 0.56 for hourly AOD (Table 4.4, Table 4.6 and Figure 4.6). Similar results are obtained for daily AOD and AOD_{fine} (see Table 4.4, Table 4.6 and Figure 4.6). Finally, Figure 4.9 highlights the closer agreement of the model corrected seasonal AOD distribution with the MODIS/Aqua satellite product in comparison with the uncorrected model estimates. The corrected simulation provides more realistic information for the analysis of the aerosol spatial and temporal patterns over Europe.

4.4.2 Spatial and seasonal distribution of aerosol fractions

Figure 4.10 shows the modelled annual mean of $PM_{2.5}$, PM_{10}, AOD and AOD_{fine}. The highest annual mean aerosol concentrations (AOD > 0.3 and PM_{10} > 30 $\mu g/m^3$) are found over the Po Valley and the Benelux region (Belgium, The Netherlands, Luxembourg) where values are dominated by fine anthropogenic aerosols. A second maximum is found over South-eastern Europe, namely in Greece, Macedonia, Bulgaria and Rumania, and over the Moldavia, Ukraine, and Poland (AOD ~ 0.2) and southern Europe (AOD > 0.2 and PM_{10} > 20 $\mu g/m^3$). Aerosol concentrations decrease towards the North and North-western Europe reaching the lowest values in the northern region (AOD < 0.15) in agreement with the modelling study of Schaap et al. (2004). Low values are also found over the major European mountain chains (e.g. the Alps, Massif Central, the Pyrenees and the Carpathians) with AOD < 0.1 and PM_{10} < 10 $\mu g/m^3$.

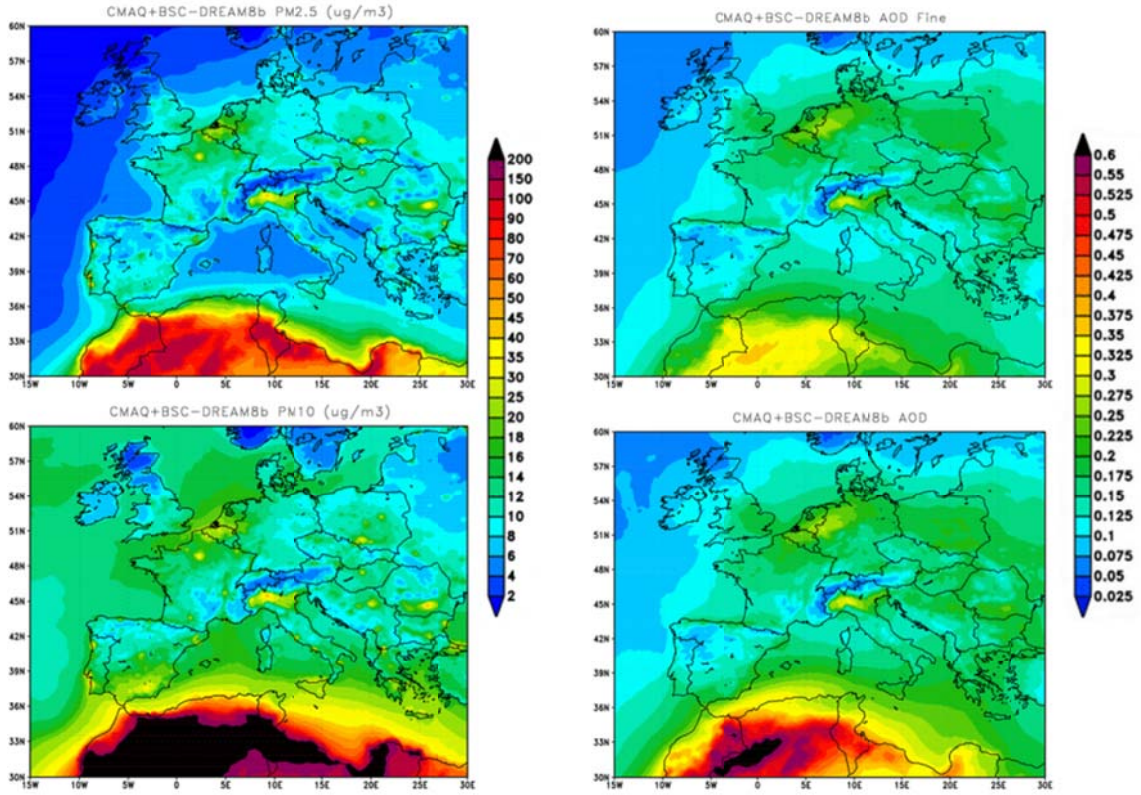

Figure 4.10 *Annual average of $PM_{2.5}$ (in $\mu g/m^3$), PM_{10} (in $\mu g/m^3$), AODfine and AOD obtained with the corrected CMAQ + BSC-DREAM8b simulations. Correction factors of the* ***Table 4.5*** *are applied to nitrates, sulphates, ammonium and EC + OC.*

We distinguish some common features in the column-integrated and surface distributions such as the high values over the North of Italy and the Netherlands. There are also significant contrasts as for instance the maritime areas in the North Atlantic region and Eastern Europe. Differences over the North Atlantic region are associated to the relatively low SSA extinction (Dubovik et al, 2002) in comparison to its impact on PM_{10} values. Over the continent, differences between PM surface concentrations and AOD are partly due to the dilution conditions related to the PBL height due to changes in the vertical mixing and to the moisture content affecting the optical properties of aerosols (Gupta and Christopher, 2009). On the other hand, aerosols in the free troposphere are transported from other regions, significantly contributing to the total AOD (e.g. Amiridis et al., 2005). Figure 4.11 and Figure 4.12 present the mean seasonal PM_{10} and AOD together with the fractions of anthropogenic (nitrate, sulphate, ammonium and OC + EC) and natural aerosols (SSA and desert dust).

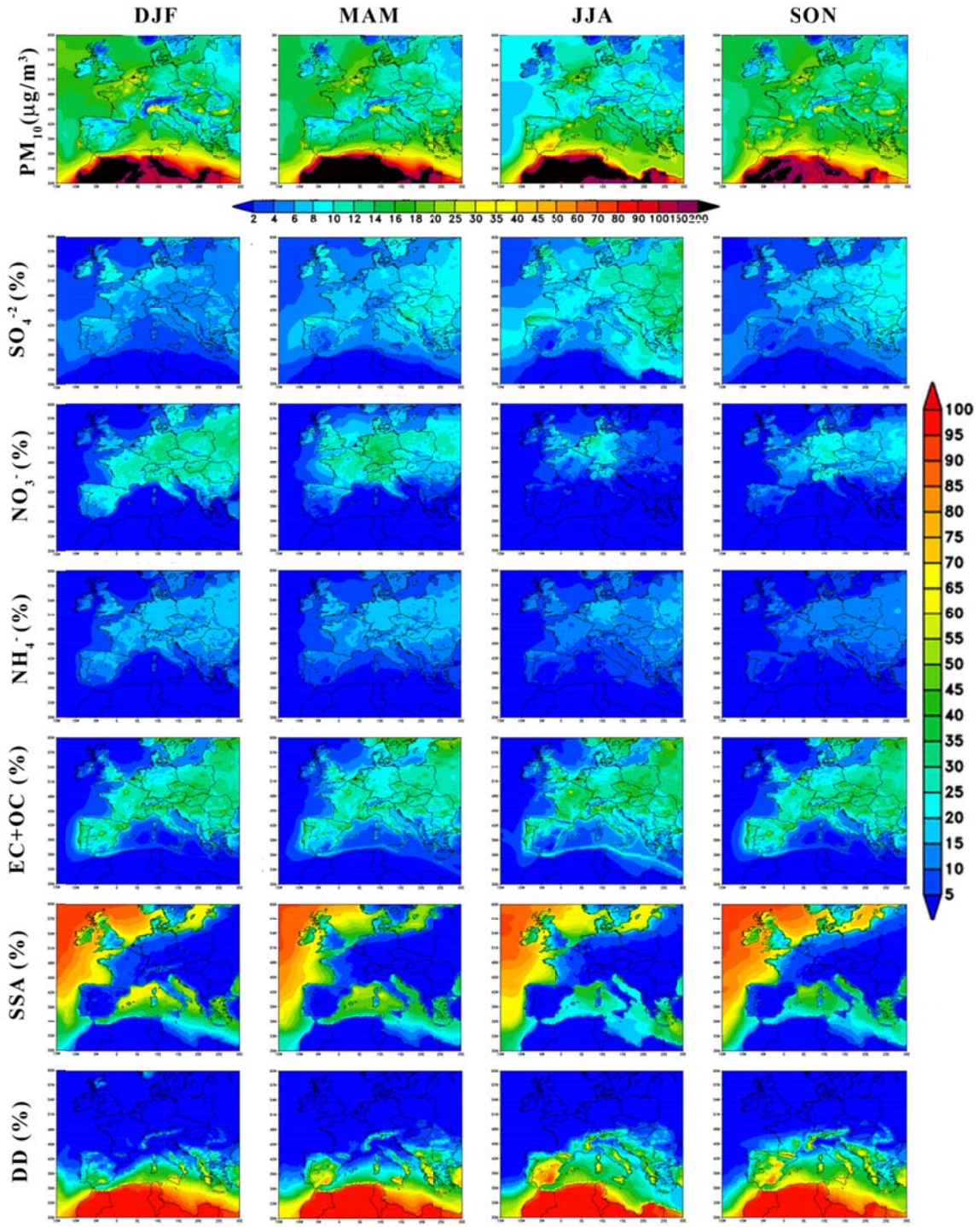

Figure 4.11 *Seasonal average (from winter to autumn, from left to right panels) of PM_{10} (in $\mu g/m^3$) and the seasonal contributions (in %) of sulphates (SO_4^{-2}), nitrates (NO_3^-), ammonium (NH_4^-), carboneous matter (EC + OC), sea salt aerosols (SSA) and desert dust (DD) to PM_{10} with correction factors of the* ***Table 4.5*** *applied to nitrates, sulphates, ammonium and EC + OC.*

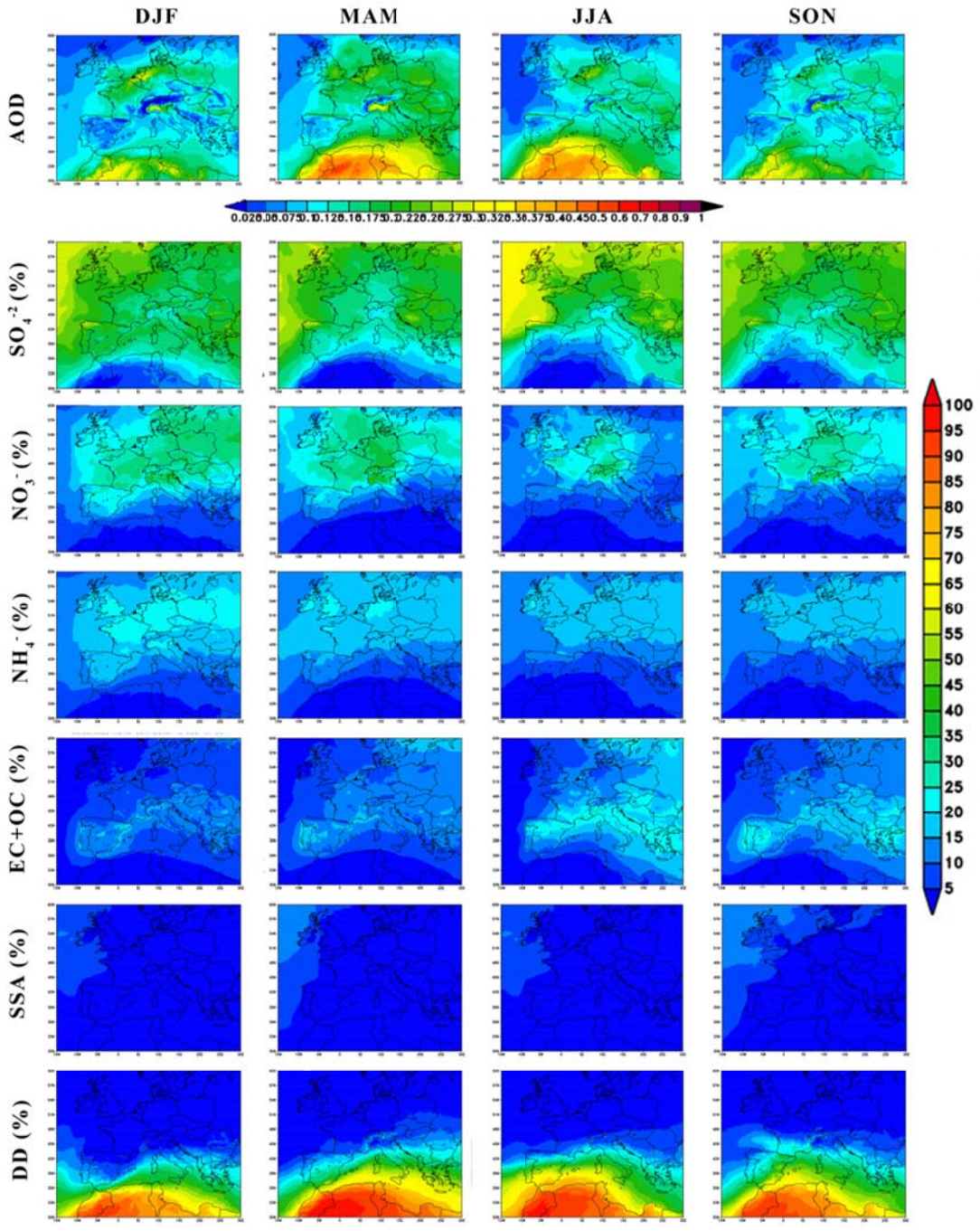

Figure 4.12 *Seasonal average (from winter to autumn, from left to right panels) of AOD and the seasonal contributions (in %) of sulphates (SO_4^{-2}), nitrates (NO_3^-), ammonium (NH_4^-), carboneous matter (EC + OC), sea salt aerosols (SSA) and desert dust (DD) to AOD with correction factors of the* ***Table 4.5*** *applied to nitrates, sulphates, ammonium and EC + OC.*

Despite SO_x emissions are rather constant throughout the year, a clear seasonal trend is observed in the modelled sulphate PM_{10} and AOD during the warm season due to high temperature and low relative humidity that favour the oxidation of SO_2 and the formation of sulphate under the presence of hydroxyl radical (e.g. Querol et al., 2009). In summer, sulphate AOD reaches average values above 0.12 in Eastern Europe, with a maximum of 0.28 over Romania. High surface concentrations of sulphate are calculated in summer over the Aegean Sea (~ 5 $\mu g/m^3$) due to the shipping traffic emissions and over the Balkans regions (above 5 $\mu g/m^3$) due to emissions from power plants.

Nitrate levels present a strong seasonal variability with the highest values during the cold months (Figure 4.11 and Figure 4.12). In winter nitrate contributions to PM_{10} levels and AOD up to 40% are observed over the entire European continent. In summer the highest contributions are localised in the Central Europe. Ammonium concentration shows slight variations throughout the year (Figure 4.11 and Figure 4.12). The highest contributions to PM_{10} and AOD (~ 15% and ~ 20%, respectively) are observed in winter and the lowest contributions (< 10%) in summer. Maximum surface concentrations of nitrate (~ 4.6 $\mu g/m^3$) and ammonium (~ 3 $\mu g/m^3$) are simulated over most European countries in winter, with the highest levels over the Po Valley (> 8 $\mu g/m^3$ and > 5 $\mu g/m^3$ for nitrates and ammonium, respectively). Their maximum contribution to AOD is found in the Po Valley (~ 0.10) and to a lesser extent in the Benelux area (~ 0.08).

EC is a primary pollutant so its spatial variability is relatively high. Major sources of EC include diesel engines, particulate heavy-duty trucks, and combustion process (including biomass and fossil fuel), thus high levels are associated with urban areas and maritime routes. In contrast, OC is emitted directly or, in a large proportion, formed from the condensation of low-volatility organic compounds. Thus, the spatial variability of OC is between that of purely primary and secondary pollutants. Major primary sources of OC include diesel and gasoline-burning engines, biomass burning and some industrial processes, so OC will be found in urban and rural background environments.

OC + EC are concentrated at hot spot locations where they are found in the fine fraction with maximum $PM_{2.5}$ values of ~ 6 $\mu g/m^3$ and AOD_{fine} values up to 0.01. Maximum OC+EC contributions are observed in summer (Figure 4.11 and Figure 4.12). OC + EC estimations should be taken with precaution due to few measurements available over Europe for the model evaluation results as well as the considerable uncertainties associated to the calculations of EC and OC. Also, SSA contributes weakly to the AOD with an average mean annual value of less than 0.01. At surface levels, the mean contribution of SSA to PM_{10} in the Mediterranean Sea reaches up to 40% (~ 10 $\mu g/m^3$) and up to 80% (15 $\mu g/m^3$) in the North Atlantic.

Sulphates and nitrates contribute up to 80% of the PM_{10} and AOD in latitudes beyond 41ºN (Figure 4.11 and Figure 4.12). Maxima SIA and carbonaceous matter are mainly concentrated at hot spot localizations in Europe where they are found in the fine fraction.

In contrast to anthropogenic sources, which are mainly located in the European continent, mineral dust sources affecting Europe's PM levels are mostly found in North African deserts. One distinct feature of the CALIOPE modelling system with respect to other European systems is the inclusion of the influence of African dust on a non-climatological basis by means of the offline coupling with the BSC-DREAM8b model. Desert dust exhibits a strong seasonal variability throughout the year. Maximum desert dust transport to Europe occurs from spring to early autumn according to the model results (Figure 4.11 and Figure 4.12), while minimum desert dust contributions are found in winter over the entire region. In spring, an increase of dust outbreaks and high desert dust contributions (> 40%) are observed in the Central and Eastern Mediterranean regions. In summer, the maximum desert dust contribution is shifted towards the Western Mediterranean and the Southern Iberian Peninsula. In the South-eastern Iberian Peninsula, desert dust contributes about 60 - 70 % of the PM_{10} and AOD levels which reach 40 $\mu g/m^3$ and 0.2, respectively (Figure 4.11 and Figure 4.12).

The simulated seasonal patterns are in agreement with observational studies using ground-based (see Chapter 2) and satellites observations (e.g. Barnaba and Gobbi, 2004; Antoine and Nobileau, 2006). Long-range transport of Saharan dust across the United Kingdom appears to be much less frequent than for Southern and Central Europe (Ryall et al., 2002) as a consequence of typical atmospheric circulation patterns. Dust particles penetrate to Northern Europe reaching the United Kingdom and the North Sea in winter (contributions to PM_{10} ~ 15% in northern United Kingdom in winter see Figure 4.11). African dust outbreaks have been long recognized to cause exceedances of the European air quality thresholds (Rodríguez et al., 2001; Barnaba and Gobbi, 2004; Querol et al., 2004b; Papanastasiou et al., 2010).

Table 4.7 shows the number of exceedances of the daily PM_{10} air quality limit value established by the European Commission (i.e. 50 $\mu g/m^3$) for each EMEP station included in the present analysis for 2004 as well as the number of exceedances obtained from the simulated values. As a result, the number of exceedances of the daily PM_{10} threshold obtained from the 25 EMEP stations for 2004 is underestimated by the CALIOPE modelling system (241 observed days versus 72 simulated days that exceed the daily PM_{10} threshold). In those stations mostly affected by desert dust outbreaks like the Spanish EMEP sites, these differences are reduced (with 80 observed versus 37 simulated days that

exceed the daily PM_{10} threshold) indicating the improvement that represents the inclusion of desert dust contribution in model simulations.

Table 4.7 *Number of exceedances of the PM_{10} daily European limit value (50 $\mu g/m^3$) from EMEP observations, CALIOPE modelled values and BSC-DREAM8b modelled values. Correction factors of the* ***Table 4.5*** *are applied to nitrates, sulphates, ammonium and EC + OC.*

Station name	Country	Number of exceedances of the PM_{10} daily limit value		
		EMEP	CMAQ + BSC-DREAM8b	BSC-DREAM8b
Illmitz	Austria	28	1	0
Vorhegg	Austria	1	0	0
Payerne	Switzerland	9	0	0
Tanikon	Switzerland	7	0	0
Chaumont	Switzerland	0	0	0
Rigi	Switzerland	0	0	0
Westerland	Germany	6	0	0
Langenbrugge	Germany	5	0	0
Schauinsland	Germany	1	0	0
Neuglobsow	Germany	2	0	0
Schmucke	Germany	0	0	0
Zingst	Germany	5	0	0
Keldsnor	Denmark	3	0	0
Viznar	Spain	25	18	12
Niembro	Spain	0	0	0
Campisabalos	Spain	9	4	2
Cabo de Creus	Spain	0	0	0
Barcarrola	Spain	8	2	2
Zarra	Spain	9	9	4
Penausende	Spain	4	1	1
Els Torms	Spain	15	1	0
Risco Llamo	Spain	10	2	1
O Savinao	Spain	2	0	0
Montelibretti	Italy	21	4	0
Ispra	Italy	71	30	0

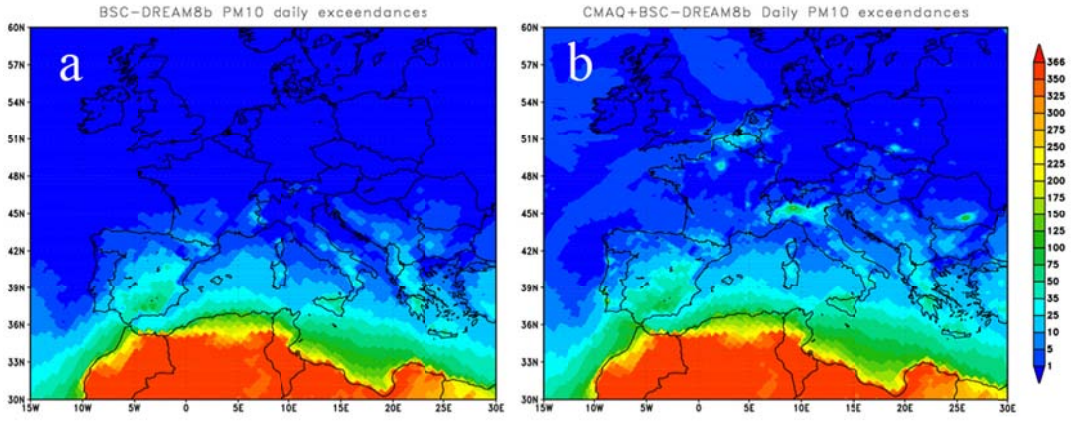

Figure 4.13 *Number of the days exceeding the EU PM_{10} daily threshold (> 50 μg/m³) for (a) BSC-DREAM8b and (b) BSC-DREAM8b + CMAQ derived aerosol. Correction factors of the* ***Table 4.5*** *are applied to nitrates, sulphates, ammonium and EC + OC.*

In Figure 4.13 we provide a spatial estimate of the number of days in which the daily PM_{10} European air quality threshold (50 μg/m³) is exceeded due to natural dust events. Figure 4.13a provides an estimate based only on desert dust levels. Large regions from Iberian Peninsula to Greece (in the North Mediterranean arc, < 45ºN) exceed the threshold while the number of daily exceedances increases southwards reaching up to about 75 days per year in the southernmost areas. When we include the other aerosol components (Figure 4.13b), a significant number of exceedances appear in well-known European hot spots. In particular, the threshold is exceeded more than 75 days in the Po Valley, Eastern Europe and in the Benelux regions. Additionally in those regions most affected by the presence of desert dust (in the North Mediterranean arc, < 45ºN), the number of exceedances notably increases with respect to the desert dust only case achieving up to 100 days in mountainous areas in the southeastern Iberian Peninsula. We note that Figure 4.13b only represents a lower end estimate of the total number of exceedances given that the PM_{10} mass is significantly underestimated in the modelling system (about 6 μg/m³ on average).

4.5 Summary and conclusions

We have presented a detailed aerosol evaluation and characterization over Europe for year 2004 using the CALIOPE modelling system. We performed a detailed model evaluation of PM levels, AOD and chemical composition to quantify the model skills and identify the causes of discrepancy.

The aerosol evaluation against EMEP/CREATE and AERONET networks shows that the modelling system can reproduce reasonably well the daily variability of the main aerosol components in Europe. However aerosol levels are in most cases underestimated. On the one hand, the larger underestimation in PM_{10} compared with $PM_{2.5}$ suggests missing sources of coarse PM in the modelling system, which affect mainly these larger fractions. On the other hand, the evaluation of the chemical composition highlights important underestimations of the modelled fine fractions particularly for carbonaceous matter (EC and OC; underestimations ~ 200%) and SIA (i.e. nitrates, sulphates and ammonium; the total amount of SIA is on average underestimated by 18 - 50%).

We calculated spatially homogenous multiplicative correction factors for carboneous matter (EC and OC) and SIA components that minimize the differences between the modelled and observed values. The results of the corrected simulation highlight the fact that besides increasing the total mass budget (the annual underestimations are reduced by ~ 35% and 23% for $PM_{2.5}$ and PM_{10}, respectively), the correction by species and seasons improves the simulation of the variability of the bulk parameters with respect to the observed values (the annual correlation increases from 0.47 to 0.59 for $PM_{2.5}$, and 0.57 to 0.61 and PM_{10}, respectively). Also the corrected model AOD is significantly improved when compared to MODIS satellite AOD fields.

Aerosols over Europe are dominated by 1) local anthropogenic emissions, 2) the proximity to the African desert and 3) atmospheric dynamics at synoptic scale. The mean annual PM concentration decreases towards the North and North-Western Europe reaching the lowest values in the northernmost regions. The highest aerosol concentrations are found over the industrialized and populated areas of the Po Valley and the Benelux regions. A second maximum is detected over Eastern and Southern Europe. High values in southern Europe are linked to the transport of large particles from Sahara desert. Maximum values are found in spring in the Eastern Mediterranean and in summer over the Iberian Peninsula and the Central-western Mediterranean. SIA are concentrated in the fine fractions and they are the main contributors to the PM_{10} and AOD values in the European continent reaching up to 80% for latitudes beyond 40ºN.

Desert dust exhibits a strong seasonal variability throughout the year. Minimum desert dust concentrations are observed over the entire study region in winter and they are confined to North Africa. From spring to early autumn, maximum desert dust contributions (reaching up to 60%) are observed in the Mediterranean and in southern regions of the Iberian Peninsula. This indicates the importance of the desert dust transported from North Africa in the aerosol budget in southern European countries. As a result, we estimate that the presence of mineral dust from African deserts cause exceedances of the daily PM_{10} EU air

quality threshold (50 μg/m^3) in latitudes south of 45ºN reaching up to more than 75 days per year in the southernmost regions.

Despite the rather satisfactory performance of the modelling system, several aspects are now under further implementation in the framework of the CALIOPE project. Wind-blown dust should be taken into account especially in dry and arid regions as well resuspension from paved roads in urban areas (see Pay et al., 2011). Biomass burning and natural NO_x are currently not treated in the CALIOPE modelling system and could contribute to the NO_2 underestimation. The uncertainties associated to the emission inventory for black carbon may be an important cause for the discrepancy between observed and modelled values; however, the uncertainties in the state-of-the-science of SOA formation and in the equilibrium sulphate/nitrate/ammonium should be further investigated. We also expect further improvements with the new version of CMAQ (CMAQv5.0) that features a new aerosol module, AERO5, containing substantial scientific improvements over the AERO4 released in CMAQv4.5. CMAQv5.0 allows semi-volatile aerosol components to condense and evaporate from the coarse mode and non-volatile sulphate to condense on the coarse mode. Dynamic mass transfer is simulated for the coarse mode, whereas the fine modes are equilibrated instantaneously with the gas phase.

Finally, these results highlight the fact that the air quality models are useful tool to complement the understanding of the observed values and the process that involve the aerosol cycle. This is very useful for implementing strategies that will have an impact on health concerns but also policy issues such as identification and discrimination between anthropogenic and natural contributions. In this sense, mineral aerosols transported from African deserts are an important contributor in the aerosol budged in southern European countries.

Chapter 5

5 Conclusions: Summary and recommendations

The work presented in this thesis has contributed to characterizate the desert dust content in a large area which comprises Northern Africa, Middle East and Europe. The present research has also provided the assessment of a regional dust model not only over source areas but also in regions affected by dust long-range transport. Furthermore, the present dissertation has demonstrated that the use of dust regional models in combination with ground-based measurements and satellite observations represents a very powerful tool to study a variety of air pollution issues at regional scales.

A detailed discussion of the results and their conclusions were included for each chapter. The most relevant aspects of those conclusions and recommendations for future work are included below. The last section includes the emerging areas and future challenges related to dust modelling activities.

5.1 Aerosol characterization from direct-sun AERONET observations

A reliable quantitative dust model evaluation requires an extensive analysis of the different aerosol types present in the region of study and the discrimination of the desert dust contributions in the observational dataset. The region of study includes two desert regions, the Sahara and the Arabian Peninsula, known for being the most active sources of dust in the world. Despite advances in desert dust research over the last decades, there are still significant limitations in the coverage of both ground-based networks, mainly in desert regions as Northern Africa and Middle East. Surface aerosol measurements are mostly limited to Europe (e.g. EMEP, CREATE, GAW and EUSAAR networks) and few of them include chemical speciation analysis quantifying the dust contribution.

Sun photometry has been developed in recent years to atmospheric aerosol optical and microphysical properties. AERONET (Holben et al., 1998) provides columnar aerosol optical parameter information (e.g. AOD, size distribution, single scattering albedo) through direct measurements and inversion techniques. The network consists of more than 200 identical globally distributed sun and sky-scanning ground-based automated radiometers. This dataset constitute a high-quality, ground-based aerosol climatology and, as such, has been widely used for aerosol studies, as well as for evaluation and validation aerosol satellite retrievals and model outputs.

An aerosol characterization for Northern Africa, Northeastern Atlantic ocean, Mediterranean and Middle East was presented in **Chapter 2**. The results obtained were based on the study of long-term series of quality-assured direct-sun observations of 39 stations of AERONET. The analysis of this data was conducted applying the graphical method of Gobbi et al. (2007) which allows to discriminate and to monitor different aerosol types. The method relies on the combined analysis of the Ångstrøm exponent (α) and its spectral curvature ($\delta\alpha$). Plotting data in these coordinates permits to infer aerosol fine mode size (R_f) and fractional contribution (η) to total AOD. It also allows us to separate AOD growth due to fine-mode aerosol humidification and/or coagulation from AOD growth due to the increase in coarse particles or cloud contamination.

The results confirm the robustness of Gobbi's graphical method and provide a quantification of the contribution of mineral dust the most important constituent in source regions. "Pure" desert dust conditions are observed for AOD > 0.7 (ranging up to 5), α < 0.3 and $\delta\alpha < 0$ corresponding to $\eta < 40\%$ and $R_f \sim 0.3$ μm. Small pollution particles are abundant in sites close to urban and industrial areas of Continental and Eastern Europe and Middle East, as well as, important contributions of biomass burning are observed in the sub-Sahel region in winter. These aerosols are associated to AOD < 1, $\alpha > 1.5$ and $\delta\alpha < -0.2$ corresponding to $\eta > 70\%$ and $R_f \sim 0.13$ μm. Under specific meteorological conditions, desert dust transport to Southern Europe is observed from spring to autumn and decreasing with latitude with contributions above 40% to the aerosol column content. The long-range dust transport to Southern Europe was observed mainly for $\alpha < 0.75$ for which fine mode contributions were always less than 40%. Otherwise, dust mixed with fine pollution aerosols shifts the observations to high α values (achieving values up to 1) and positive values of $\delta\alpha$. In this latest case the proportion between fine and coarse was variable.

Investigations for the treatment of a particular aerosol type may be limited to seasons and regions, when or where that aerosol type dominates the aerosol composition. In order to perform a quantitative desert dust model evaluation, it is necessary to discriminate desert dust contributions from the rest of the observational dataset. As shown in Chapter 2, it is possible to implement a simple method to separate the contribution of desert dust based on the combination of AOD, α and $\delta\alpha$. Due to its simplicity, this methodology can be used in the near-real time evaluation of the mineral dust models.

5.2 Development and evaluation of the BSC-DREAM8b model

In regions downwind of major dust sources, where frequent dust events significantly affect air quality and visibility, precise dust forecasts are useful for decision makers and the general public. The SDS-WAS Programme (Section 1.2.3) has as a main goal to enhance the ability of countries to deliver timely and quality sand and dust storm forecasts, observations, information and knowledge to users through an international partnership of research and operational communities. The current operational BSC-DREAM8b model is one of the models participating in the NA-ME-E node of the SDS-WAS Programme.

The usefulness of dust forecast models not only depends on the quality of the underlying meteorological model, but also on their skill to correctly predict dust emission and deposition. In particular, the ability of the models to simulate the precise location and intensity of dust emission events are suspected to be of major importance for the dust forecasting skill. The comparisons of different models between each other and against observations reveal eventual weaknesses of a given model and may provide an assessment of uncertainties in simulating the dust cycle.

In **Chapter 3**, DREAM and BSC-DREAM8b as well as 4 different research model versions have been annually evaluated for 2004 over Northern Africa, Mediterranean and Middle East domain in order to improve the model performances for operational dust forecasts purposes. The results of the comparison of the modelled dust AOD against AERONET data (including direct-sun and the SDA retrievals) and its ability to reproduce the observed seasonal cycle by means of aerosol distributions from TOMS, MISR, MODIS/Aqua sensors were presented.

The model evaluation results highlighted the fact that dust long-range transport is more efficient in the 8 bins model versions due to improved transport bin resolution, but it presents some deficiencies close to sources. Also, the model evaluation highlighted that the operational versions strongly underestimated the AOD in the Sahel during the winter Harmattan season and overestimate the AOD during spring rainy events in the Mediterranean. The introduction of new dry deposition scheme and an updated wash-out ratio in the wet deposition scheme, improved the long-range transport, in particular over the Mediterranean, although significant underestimation remained in the Sahel in winter. The inclusion of a topographic preferential source mask improved the localization of the main North African sources and consequently the long-range dust transport to Europe and Atlantic regions. Finally, the inclusion of a more physically-based dust emission scheme with a new soil texture database led to reasonably good results at source areas and in regions affected by dust after long-range transport. However, in the latter case, the use of a

preferential source mask did not introduce significant improvements in the comparison with the AERONET observations.

The dust cycle consists of two major physical mechanisms: first, a wind stress lifting mechanism able to raise up dust particles from some type of bare soil surfaces; second, a long range transport mechanism with a high degree of spatial coherence. The recent achievements in wind-erosion research are significant with the introduction of new land-use datasets and more complex physically-based emission schemes, but our capability for quantitative wind-erosion modelling and prediction remains to be limited for the following reasons.

- Some fundamental aspects of wind-erosion physics are not well understood. For instance, dust emission is essentially generated by abrasion (saltation bombardment) and self-abrasion (aggregates disintegration) and the rate of dust emission critically depends on the cohesive forces acting on dust particles. The threshold friction velocity, u_{*t}, is a function of several parameters. Thus, it is difficult to accurately determine the key parameters which affect wind erosion. New field experiments need to be carried so that data can be obtained and wind-erosion schemes can be rigorously verified.
- Dust mobilization normally begins when the surface wind velocity exceeds a threshold wind speed (i.e. u_{*t}). Model studies already pointed out the importance of prescribing surface properties like the surface wind fields realistically to correctly compute dust emissions. Therefore, it is important to ensure the model capability to reproduce the meteorological parameters that cause dust mobilisation. In this sense, the lack of measurements on ground levels in source regions difficult their evaluation.
- Wind-erosion events are mostly associated with sub-synoptic severe-weather events. Such weather events are also the most difficult to predict using atmospheric models. For example, dust storms in Africa are often related to the convective systems in the monsoon trough. Such systems are difficult to model as their modelling requires high spatial resolution of the atmospheric model.

5.3 Aerosol modelling over Europe and the contribution of desert dust

As shown in **Chapter 2**, the European atmosphere is composed by a variety of different aerosol types. For this reason, in order to evaluate a mineral dust regional model over Europe is necessary to take into account other different aerosol sources at the same time (i.e. natural and anthropogenic). In **Chapter 4** the long-range desert dust transport over Europe is evaluated and analysed with an annual simulation for 2004 of the CALIOPE

high-resolution air quality modelling system (12 km x 12 km). This modelling system estimates the aerosols from two models, CMAQv4.5 and BSC-DREAM8b. CMAQv4.5 calculates biogenic, anthropogenic and sea salt aerosol and BSC-DREAM8b provides the natural desert dust contribution from North Africa deserts.

The model evaluation by means of PM levels, AOD and chemical composition, highlighted important underestimations of the simulated PM. Additionally to missing aerosol sources in the modelling system, the modelled fine fractions are particularly underestimated for carbonaceous matter and secondary inorganic aerosols (namely, nitrates, sulphates and ammonium). Regarding the coarse particle fraction, we have shown that simulated PM_{10} data with the air quality modelling system, shows better correlations with observed PM_{10} when the BSC-DREAM8b dust model is implemented because it incorporates dust transport from Northern Africa indicating the importance of the mineral dust contributions over Europe.

In spite of the differences between observed and modelled values, the modelling system evaluation of **Chapter 4** presented a rather satisfactory performance in the range of other European modelling systems. The analysis of the simulated values for 2004 by CALIOPE system showed that the highest aerosol concentrations were found over the industrialized and populated areas of the Po Valley and the Benelux regions. A second maximum is detected over Eastern and Southern Europe. High values in southern Europe are linked to the transport of coarse particles from the Sahara desert which contributes up to 40% of the total aerosol mass. Close to the surface, maxima dust seasonal concentrations (> 30 $\mu g/m^3$) were found between spring and early autumn. The estimation of the number of daily exceedances of the PM_{10} EU air quality threshold (50 $\mu g/m^3$) with respect the EMEP observations was underestimated by the CALIOPE system. These differences were reduced in southern sites of Iberian Peninsula. This region is affected by desert dust outbreaks indicating the improvement that represents the inclusion of desert dust in the model simulation. We estimated that desert dust causes daily exceedances of the PM_{10} EU air quality threshold (50 $\mu g/m^3$) in large areas south of 45ºN reaching up to more than 75 days per year in the southernmost regions. This indicates the good performance of the BSC-DREAM8b model in regions affected by long-range dust transport as the Iberian Peninsula. To conclude, in order to improve the prediction of the PM mass over southern Europe and to achieve the standards set in European Directives for modelling applications, it is essential to include in the modelling system the desert dust contributions in hourly and daily basis.

5.4 Emerging areas and future challenges

In recents years the interest in the study of atmospheric dust at global and regional scales has increased significantly as indicated by some initiatives such as the SDS-WAS Programme. In this section we describe future challenges on the development of regional dust modelling and forecasting systems including their validation and application.

5.4.1 Model verification and evaluation

In spite of the latest efforts to install new AERONET sites in desert dust sources regions (e.g. Tamanrasset or Cairo); there is a gap of stations over the main dust source region, the Sahara. It will be partially filled in with three new AERONET instruments to be installed in Tunisia and Morocco. However, more AERONET sites in the main dust source regions (the Sahara and the Arabian Peninsula) are necessary. In order to complement the gap in the dust sources, new ground-based observational datasets are required to evaluate the model in these regions. The horizontal visibility (VIS) at surface level is reported by human visual estimation using some physical references in METAR and Synop reports. VIS data are available at thousands of stations in airports with aeronautic meteorological offices every 30 minutes, and in synoptic weather stations every 3 hours from 1900 to the present. Some previous studies for estimating long term trends in aerosols using VIS have been conducted in dust source regions (e.g. Mahowald et al., 2007). Moreover, PM concentrations estimated by VIS data at airports have been used in several epidemiologic (e.g., Schwartz, 1991; Abbey et al., 1995) or air quality studies (Vajanapoom et al., 2001; Ozer et al., 2007). The experience shows that useful METAR VIS information for model verification is constrained to days with severe reductions of VIS (below 10 km). Some synoptic weather stations report more accurate VIS conditions using far off references. For both dust monitoring and model verification, only VIS data over Northern Africa and Middle East is useful. However, an accurate analysis of this new observational dataset is necessary before to perform a model evaluation.

Concerning the spatial validation of simulated AOD, it can be only performed using satellite borne sensors. Sensors on board of satellite detect the radiances of various surfaces of the Earth through different spectral channels. Various satellite-sensed signals are combined (1) to identify and monitor dust storm in real time; (2) to derive land-surface and atmospheric parameters for dust modelling; (3) to retrieve dust quantities, such as dust load, optical depth, vertical dust profiles or radiative forcing, and (4) to derive long-term dust climatologies. In spite of the different satellite aerosol products are capable to reproduce the general seasonal features; important discrepancies between them are observed during the model evaluation. This is linked to the different observation

frequency, the available spectral channels of the satellite sensor, or differences in the assumptions considered in the aerosol retrieval algorithm. For example, the temporal resolution of MISR (the repeat time is only 3 or 4 visits per month over the Sahara desert) is enough to capture the major seasonal dust activity but it is sparse to reproduce some regional sources. Otherwise, TOMS was less sensitive to aerosols in the boundary layer, where aerosol residence times were short. In fact, aerosols below ~ 500 – 1500 m are unlikely to be detected by TOMS (Torres et al., 1998; Ginoux and Torres, 2003). Therefore, it is necessary to take into account these features entail satellite data interpretation and model evaluation results.

The launch of the Meteosat Second Generation (MSG) is a great opportunity for model evaluation (or data assimilation) because it combines the specific advantages of the geostationary orbit and geometric, radiometric and spectroscopic capabilities of the high resolution Radiometers. MSG is a joint project between the European Space Agency (ESA) and the European Organisation for the Exploration of Meteorological Satellites (EUMETSAT) and follows up the success of the first generation METEOSAT weather geostationary satellite series with a larger design boasting higher performance. The first in a planned series of MSG satellites was launched in 2002, entering into service with EUMETSAT in early 2004. MSG system has brought major improvements in these services through the 12 spectral bands of its radiometer, SEVIRI. The full disc view allows frequent sampling, every 15 minutes, enabling monitoring of rapidly evolving events. Recently, different quantitative and qualitative MSG/SEVIRI dust products have been develop as the RGB (red, green, blue) dust product (Schmetz et al., 2002), the IR dust index based on Brightness Temperature Differences (BTD) (Schepanski et al., 2007) or the Land Daily Aerosol (LDA) product (Govaerts et al., 2010; Wagner et al., 2010). However, it is necessary to perform an extensive checking, calibration, and improvement of these algorithms used for the retrieval of the aerosol properties before proceeding to do a reliable dust regional model evaluation.

Otherwise, the large uncertainty in simulating mineral dust (and its radiative forcing) mainly resides in the estimation of the size-resolved dust emissions in the source regions, the treatment of aerosols in models (e.g., representation of aerosol size distributions), and the determination of optical properties of mineral dust (e.g., Ginoux et al., 2001; Zender et al., 2003b; Kalashnikova et al., 2004; Balkanski et al., 2007; Darmenova et al., 2009).

Currently, bulk optical properties of dust are used in models. Some studies (e.g. Sokolik and Toon, 1999; Balkanski et al, 2007) demonstrated that mineralogical composition of dust (clays, quartz, carbonates, feldspars, sulphates, iron oxides) should be introduced into the radiative models to accurately estimates the dust optical and radiative properties.

Ongoing modelling efforts including explicit mineralogy may improve the modelled optical properties of dust (e.g. Nickovic and Pérez; 2008a,b; Nickovic et al., 2011).

An exhaustive comparison of different models with each other and against observations can reveal weaknesses of individual models and provide an assessment of uncertainties in simulating the dust cycle. Uno et al. (2006) compared multiple regional dust models over Asia in connection to specific dust events. They concluded that even though all models were able to predict the onset and ending of a dust event and were able to reproduce surface measurements, large differences existed among them in processes such as emissions, transport and deposition. Todd et al. (2008) conducted an intercomparison with five regional models for a 3-day dust event over the Bodélé depression. The analyzed model quantities presented a similar degree of uncertainty as reported by Uno et al. (2006). Kinne et al. (2003) compared aerosol properties from seven global models to satellite and ground data. In this sense, the SDS-WAS Programme seeks to document differences of dust component modules and to assemble useful data-sets for model evaluations. Satellite (MODIS, MISR, POLDER and OMI) and ground-based (EMEP, EARLINET, MPLNET and AERONET) observations will be used in this model evaluation.

5.4.2 Air quality application

Within an air quality framework, it would be desirable to specifically evaluate the simulated surface dust concentrations. The most common approach to quantifying dust contribution on ground-level is the development of chemical speciation studies, many of which have been carried out in different regions of Spain (e.g. Rodríguez, 2002). The main disadvantages of chemical speciation are the high cost and the length of the process given that these studies entail long sampling periods, chemical analyses and data interpretation. Thus, these analyses are limited to specific campaigns. Escudero et al. (2007) introduced a quantitative and simple methodology to estimate the net dust load in PM_{10} during African dust outbreaks in the Iberian Peninsula. The daily net dust load in PM_{10} attributable to an African episode in a given region can be obtained by subtracting the daily regional background level from the PM_{10} concentration value for the day with African dust outbreak at the rural station. The rural background is obtained from the monthly moving 40^{th} percentile from the PM_{10} time series after a prior extraction of the data of the days with African dust transport. Recently, this observational dataset has been used by Pay et al. (2011) in the evaluation of aerosol surface levels of the CALIOPE system across Spain to which the work performed in this thesis has contributed. This new methodology to estimate desert dust contributions in PM_{10} could be applied to European datasets for ground-level dust concentration model evaluation activities.

5.4.3 Vertical distribution of desert dust

The knowledge of the aerosol vertical distribution of desert dust can help to improve the dust model over Europe through the estimation of the uncertainties with respect to to production, particle properties, transport paths, and evolution during the particle's life time. The altitude is not easily measurable except for lidars (Papayannis et al., 2008; Tesche et al., 2009) and more recently from passive remote sensors (Pierangelo et al., 2004; Peyridieu et al., 2010).

In recent years, Raman Lidars and micro-pulse Lidars (MPL) have been increasingly used to automatically and routinely retrieve profiles of aerosol backscattering and extinction (WMO, 2007).

The NASA Micro-Pulse Lidar Network (MPLNET, http://mplnet.gsfc.nasa.gov/) was founded in 2000. At present, there are seventeen permanent sites worldwide, and several more to be completed soon. Numerous temporary sites have also been deployed in support of various field campaigns. Most MPLNET sites are co-located with sites of AERONET to provide both column and vertically resolved aerosol and cloud data. MPLNET has been providing quality near-real time lidar data through a public website since 2000.

EARLINET (www.earlinerteos.org) was established in 2000 to characterize the horizontal, vertical, and temporal distribution of aerosols on a European scale. EARLINET observations are performed on a regular schedule of one daytime measurement per week around noon, when the boundary layer is usually well developed, and two night-time measurements per week, with low background light, in order to perform Raman extinction measurements. Since May 2000, the EARLINET network has provided systematic lidar observations of vertical profiles of Saharan dust aerosols over the European continent on a coherent network basis. These observations have allowed the establishment of a significant database of vertical profiles of Saharan dust optical properties over Europe (Bösenberg et al., 2003).

Nevertheless, ground-based lidars are situated at specific locations, all of them outside the source areas, and cannot offer a complete estimation of the spatial evolution of dust altitude, while dedicated campaigns using lidars and in-situ measurements are restricted in time. Recently, ceilometers (i.e. relatively low-cost and robust mini lidars for continuous operation), have been upgraded such that one may retrieve significant aerosol information though being not as quantitative as the sophisticated lidar systems (Flentje et al., 2009). Ceilometers have the advantage to work automatically under all weather conditions in remote areas. Hernández et al. (2011) have shown a very good agreement between a ceilometer and a MPL in the detection of the Saharan Air Layer (SAL) over Canary Islands.

Future verifications of dust vertical profiles, simulated with BSC-DREAM8b, may be performed on a routine basis using high temporal resolution backscatter profiles from the MPLNet lidars operating in Barcelona (UPC) and Santa Cruz de Tenerife (INTA-CIAI/AEMET). Accurate EARLINET data may be used to analyze case studies of Saharan intrusions over Europe.

On the other hand, the remote passive sensing instruments AIRS and IASI offer a very good spatial coverage, but their new established results still need futher validation. With the launch of CALIPSO satellite provides new insight into the role that clouds and atmospheric aerosols (airborne particles) play in regulating Earth's weather, climate, air quality and model evaluation. CALIPSO combines an active lidar instrument with passive infrared and visible imagers to probe the vertical structure and properties of thin clouds and aerosols over the globe. Further investigations might face the characterization of the top of the SAL over northern Africa, from simulations with regional dust models, and the corresponding comparison and validation with a SAL climatology derived from CALIPSO observations.

5.4.4 Dust forecasting with data assimilation

Even if the approximations to a set of complex processes of the wind-erosion models were accurately represented in the models, model simulations may still diverge from reality due to inaccuracies in the initial conditions and errors in the model parameters and forcing data. This occurs often because the models are non-linear and sensitive to minute changes in initial conditions and parameters. It is a considerably advantage to use observations to constrain the model simulations close to the reality. For this purpose, methods must be derived to optimally combine observations and model simulations especially for forecasting applications. The procedure of combining observed data with the model simulations to produce an optimal prediction of an evolving system is known as *data assimilation*, optimal in a sense that the prediction error is minimized. The examples of general methods include nudging method, optimal interpolation, 3-dimensional variation (3D-Var). More advanced methods include 4-dimensional variation (4D-Var), extended Kalman Filter and ensemble Kalman Filter. Data assimilation has been widely used in numerical weather, ocean and climate predictions (e.g. Kalnay, 2003). Assimilation of dust aerosols is just in its early stage due to the lack of enough observational data sets. However, dust-related data are becoming increasingly available. Dust concentration can be derived using empirical relationship from the visibility data at a large number of weather stations as indicated previously. While the so-derived data set is relatively low in accuracy, it does have the advantages of broad spatial coverage and regular temporal coverage. Dust concentration measurements are now available from high- and low-volume samplers at air quality monitoring stations. These

measuraments are more accurate, but poor in spatial and temporal resolution. Satellite remote sensing offers an important source of data. Methods for converting satellite signals to practically useful physical quantities, such as dust load are now being developed.

Using the TOMS AI data as the initial dust loading input for a dust prediction system, Alpert et al. (2002) has found a positive improvement for the model performance. On the other hand, Niu et al. (2008) used extensively the measurements of surface visibility (phenomena) and dust loading retrieval from the Chinese geostationary satellite FY-2C to improve the performance of the Chinese Unified Atmospheric Chemistry Environment/Dust (CUACE/Dust) forecast system. This demonstrates the importance of an accurate initial dust concentration even though no data assimilation was used. In a 4D-Var approach, a factor in the dust emission parameterization scheme was assimilated by using the lidar vertical profiles of dust aerosols (Yumimoto et al., 2007). However, applications of 4D-Var remain limited as it is quite expensive for computation and not easy for system upgrade due to a close link on an adjoint model which is the inverse of the forecast model.

Currently, some models use target fields of MODIS aerosol products. For example, in the case of the global ECMWF Integrated Forecasting System (Benedetti et al., 2009), the total mixing ratio is used as control variable for the aerosol assimilation. Increments in this variable are redistributed into the different species (sea salt, desert dust, organic matter, black carbon and sulphate) according to their fractional contributions. In the case of the DREAM dust model (Pejanovic et al., 2010), an assimilation method based on the Newtonian relaxation is applied using background dust concentration of the DREAM dust model and target fields of ECMWF dust analysis in dust initial field that that includes the MODIS aerosol objective analysis.

Therefore, some progress has been made in the area of the dust prediction systems (e.g. Niu et al., 2008; Pejanovic et al., 2010) although there is insufficient homogenized dust data for this purpose particularly in dust source regions. It will be necessary to assimilate other observations, for example AODs from SEVIRI on board of MSG. Use of other sensors will also be investigated. MODIS retrievals also provide general information on the breakdown between fine and coarse particle AOD.

5.4.5 Long-term regional dust model databases

Otherwise, because dust feedbacks, research on dust has been elevated to be among the core subjects on Earth System studies. In addition to the study of long-term trends of mineral dust transport, the analysis of regional dust climate simulations is of great importance for the improvement of mid-range and long-range dust events forecasting. The

model intercomparison comparing and evaluating the temporal (on annual, seasonal and daily) and spatial variability of desert dust deposition simulated by models, could help to determine the degree of uncertainty in estimates of dust emission and transport from a range of model simulations in order to highlight the sources of uncertainty in these estimates, and point to the key foci for future research to constrain these uncertainties (e.g. Tegen et al., 2003; Kinne et al., 2006, Textor et al., 2006; Huneeus et al., 2011).

Moreover, dust regional climate simulations are being used to analyse the link between large dust plumes from the southern Sahara and the Bodélé Depression and meningitis epidemics in the Sahel region (e.g. Thomson et al., 2006; Pérez, 2010; Pérez et al., 2011a) in the dry season (winter), or the ocean fertilization by the iron that is naturally deposited from atmospheric dust intrusions into the oceans (providing nutrients for phytoplankton) (e.g. González-Ramos et al., 2009; Gallisai et al., 2010). These climatological studies may be further explored with new model simulations for long term periods.

Chapter 6

6 References

Abbey, D. E., Ostro, B. E., Fraser, G., Vancuren, T. and Burchette, R. J.: Estimating fine particulates less than 2.5 microns in areodynamic diameter (PM2.5) from airport visibility data in California. Exposure Anal Environ. Epidemiol. 5: 161-180, 1995.

Alados-Arboledas, L., Lyamani, H. and Olmo, F. J.: Aerosol size properties at Armilla, Granada (Spain), Quarterly Journal of the Royal Meteorological Society, 129(590), 2003.

Alados-Arboledas, L., Alcantara, A., Olmo, F. J., Martinez-Lozano, J. A., Estelles, V., Cachorro, V., Silva, A. M., Horvath, H., Gangl, M. and Diaz, A.: Aerosol columnar properties retrieved from CIMEL radiometers during VELETA 2002, Atmos. Environ., 42(11), 2654-2667, 2008.

Alfaro, S. C., and Gomes, L.: Modeling mineral aerosol production by wind erosion: Emission intensities and aerosol size distributions in source areas, J. Geophys. Res., 106, 18075-18018, 2001.

Alonso-Pérez, S., Cuevas, E., Querol, X., Viana, M., and Guerra, J. C.: Impact of the Saharan dust outbreaks on the ambient levels of total suspended particles (TSP) in the marine boundary layer (MBL) of the Subtropical Eastern North Atlantic Ocean, Atmos. Environ., 41, 9468-9480, 2007.

Alonso-Pérez, S., Cuevas, E., Pérez, C., Querol, X., Baldasano, J. M., Draxler, R., and de Bustos, J. J.: Trend changes of African airmass intrusions in the marine boundary layer over the subtropical Eastern North Atlantic region in winter, Tellus B, 63, 255-265, doi: 10.1111/j.1600-0889.2010.00524.x, 2011.

Alpert, P., Krichak, S. O., Tsidulko, M., Shafir, H., and Joseph, J. H.: A Dust Prediction System with TOMS Initialization, Mon. Weather Rev., 130, 2335–2345, 2002.

Amiridis, V., Balis, D. S., Kazadzis, S., Bais, A., Giannakaki, E., Papayannis, A., and Zerefos, C.: Four-year aerosol observations with a Raman lidar at Thessaloniki, Greece, in the framework of European Aerosol Research Lidar Network (EARLINET), Geophys. Res, 110, 1–12, 2005.

Amiridis, V., Kafatos, M., Perez, C., Kazadzis, S., Gerasopoulos, E., Mamouri, R. E., Papayannis, A., Kokkalis, P., Giannakaki, E., and Basart, S.: The potential of the synergistic use of passive and active remote sensing measurements for the validation of a regional dust model, Ann. Geophys, 27, 3155-3164, 2009.

Andreae, T. W., Andreae, M. O., Ichoku, C., Maenhaut, W., Cafmeyer, J., Karnieli, A., and Orlovsky, L.: Light scattering by dust and anthropogenic aerosol at a remote site in the Negev desert, Israel, J. Geophys. Res., 107, 4008, doi: 10.1029/2001JD900252, 2002.

Angström, A.: On the Atmospheric Transmission of Sun Radiation and on Dust in the Air, Geografiska Annaler, 11, 156-166, doi:10.2307/519399, 1929.

Antoine, D., and Nobileau, D.: Recent increase of Saharan dust transport over the Mediterranean Sea, as revealed from ocean color satellite (SeaWiFS) observations, J. Geophys. Res., 111, 2006.

Appel, K. W., Gilliland, A. B., Sarwar, G. and Gilliam, R. C.: Evaluation of the Community Multiscale Air Quality (CMAQ) model version 4.5: Sensitivities impacting model performance: Part I--Ozone, Atmos. Environ., 41, 9603-9615, 2007.

Appel, K. W., Bhave, P. V., Gilliland, A. B., Sarwar, G. and Roselle, S. J.: Evaluation of the community multiscale air quality (CMAQ) model version 4.5: Sensitivities impacting model performance; Part II particulate matter, Atmos. Environ., 6057–6066, doi:10.1016/j.atmosenv.2008.03.036, 2008.

Asman, W.A.H.: Modelling the atmospheric transport and deposition of ammonia and ammonium: an overview with special reference to Denmark. Atmos. Environ., 35, 1969-1983, 2001.

Aumont, O., Bopp, L., and Schulz, M.: What does temporal variability in aeolian dust deposition contribute to sea-surface iron and chlorophyll distributions?, J. Geophys. Res. Letters, 35, L07607, 2008.

Ávila, A., M. Alarcón and I. Queralt: The chemical composition of dust transported in red rains- Its contribution to the biogeochemical cycle of a holm oak forest in Catalonia (Spain), Atmos. Environ., 32(2), 179-191, 1998.

Àvila, A., and Penuelas, J.: Increasing frequency of Saharan rains over northeastern Spain and its ecological consequences, Sci. Total Environ., 228, 153-156, 1999.

Bagnold, R. A.: The physics of blown sand and desert dunes. Morrow, New York, 265, 1941.

Baldasano, J. M., Valera, E., and Jimenez, P.: Air quality data from large cities Sci. Total Environ., 307, 141-165, 2003.

Baldasano, J.M., Jiménez-Guerrero, P., Jorba, O., Pérez, C., López, E., Güereca, P., Martín, F., Vivanco, M.G., Palomino, I., Querol, X., Pandolfi, M., Sanz, M.J., Diéguez, J.J: Caliope: an operational air quality forecasting system for the Iberian Peninsula, Balearic islands and Canary islands e first annual evaluation and ongoing developments, Adv. Sci. Res., 2, 89-98, 2008a.

Baldasano, J. M., Güereca, L. P., López, E., Gassó, S. and Jimenez-Guerrero, P.: Development of a high-resolution (1 km × 1 km, 1 h) emission model for Spain: The High-Elective Resolution Modelling Emission System (HERMES), Atmos. Environ., 42, 7215-7233, 2008b.

Baldasano J.M.; M. Piot; O. Jorba; M. Goncalves; M.T. Pay; S. Basart; P. Jiménez and S. Gassó. CALIOPE: an Operational Air Quality Forecasting System for Europe and Spain. Mesoscale Modelling For Air Pollution Applications: Achievements And Challenges (COST 728 Final Workshop), Organisers: COST 728, WMO/GURME and MEGAPOLI, Geneva, 25-26, February 2010.

Balis, D., Papayannis, A., Galani, E., Marenco, F., Santacesaria, V., Hamonou, E., Chazette, P., Ziomas, I., and Zerefos, C.: Tropospheric LIDAR aerosol measurements and sun photometric observations at Thessaloniki, Greece, Atmos. Environ., 34, 925-932, 2000.

Balis, D., Amiridis, V., Kazadzis, S., Papayannis, A., Tsaknakis, G., Tzortzakis, S., Kalivitis, N., Vrekoussis, M., Kanakidou, M., Mihalopoulos, N., Chourdakis, G., Nickovic, S., Perez, C., Baldasano, J. M., and Drakakis, M.: Optical characteristics of desert dust over the East Mediterranean during summer: a case study, Ann. Geophys., 24, 807–821, 2006.

Balkanski, Y., Schulz, M., Claquin, T., and Guibert, S.: Reevaluation of Mineral aerosol radiative forcings suggests a better agreement with satellite and AERONET data, Atmos. Chem. Phys., 7, 95, 2007.

Barkan, J., Kutiel, H., Alpert, P., and Kishcha, P.: Synoptics of dust intrusion days from the African continent into the Atlantic Ocean, J. Geophys. Res, 109, 1993–2007, 2004.

Barkan, J., Alpert, P., Kutiel, H., and Kishcha, P.: Synoptics of dust transportation days from Africa toward Italy and central Europe, J. Geophys. Res., 110, 2005.

Barnaba, F., and Gobbi, G. P.: Aerosol seasonal variability over the Mediterranean region and relative impact of maritime, continental and Saharan dust particles over the basin from MODIS data in the year 2001, Atmos. Chem. Phys., 4, 2367–2391, SRef-ID: 1680-7324/acp/2004-4-2367, 2004.

Belo, N.: Caracterização das propiedades ópitcas dos aerossóis à superfície na região de Évora. Departamento de Física, Universidade de Lisboa, Lisboa, 2004.

Ben-Ami, Y., Koren, I., and Altaratz, O.: Patterns of North African dust transport over the Atlantic: winter vs. summer, based on CALIPSO first year data, Atmos. Chem. Phys, 9, 7867–7875, 2009.

Ben-Ami, Y., Koren, I., Rudich, Y., Artaxo, P., Martin, S. T., and Andreae, M. O.: Transport of Saharan dust from the Bodele Depression to the Amazon Basin: a case study, Atmos. Chem. Phys., 10, 7533–7544, 2010.

Benedetti, A., Morcrette, J. J., Boucher, O., Dethof, A., Engelen, R.J., Fisher, M., Flentje, H., Huneeus, N., Jones, L., Kaiser, J.W., Kinne, S., Mangold, A., Razinger, M., Simmons, A.J., Suttie, M., and the GEMS-AER team: Aerosol analysis and forecast in the ECMWF Integrated Forecast System: Data assimilation, J. Geophys. Res., 114, D13205, doi:10.1020/2008JD011115, 2009.

Bessagnet, B., Hodzic, A., Vautard, R., Beekmann, M., Cheinet, S., Honoré, C., Liousse, C., and Rouil, L.: Aerosol modeling with CHIMERE--preliminary evaluation at the continental scale, Atmos. Environ., 38, 2803-2817, 2004.

Betzer, P. R., Carder, K. L., Duce, R. A., Merrill, J. T., Tindale, N. W., Uematsu, M., Costello, D. K., Young, R. W., Feely, R. A., and Breland, J. A.: Long–range transport of giant mineral aerosol particles, 1988.

Binkowski, F. S.: Aerosols in MODELS-3 CMAQ, in Science Algorithms of the EPA Models-3 Community Multiscale Air Quality (CMAQ) Modeling System, edited by D. W. Byun and J. K. S. Ching, pp. 10–0 – 10–23, EPA, 1999.

Binkowski, F. S. and Roselle, S. J.: Models-3 Community Multiscale Air Quality (CMAQ) model aerosol component. 1. Model description, J. Geophys. Res., 108 (D6), 4183, doi:10.1029/2001JD001 409, 2003.

Bond, T.C., Streets, D.G. Yarber, K.F., Nelson, S.M., Woo, J.H. and Klimont, Z.: A technology-based global inventory of black and organic carbon emissions from combustion. J. Geophys. Res. Atmos., 109, D14203, doi: 10.1029/2003JD003697, 2004.

Bösenberg, J., et al.: A European aerosol research lidar network to establish an aerosol climatology, MPI-Rep. 317, Max-Planck Inst. für Meteorol., Hamburg, Germany, 2003.

Boylan, J. W. and Russell, A. G.: PM and light extinction model performance metrics, goals, and criteria for three-dimensional air quality models, Atmos. Environ., 40, 4946-4959, 2006.

Brooks, N.: Dust-climate interactions in the Sahel-Sahara zone of the northern Africa, with particular reference to late twentieth century Sahelian drought, Ph.Thesis, University of East Anglia, Norwich, 1999.

Byun, D. W. and Ching, J. K. S.: Science Algorithms of the EPA Models-3 Community Multiscale Air Quality (CMAQ) Modeling System, Atmospheric modeling division, National Exposure Research Laboratory, US Environmental Protection Agency, Research Triangle Park, NC, 27711, 1999.

Byun, D. W. and Schere, K. L.: Review of the Governing Equations, Computational Algorithms, and Other Components of the Models-3 Community Multiscale Air Quality (CMAQ) Modeling System, Appl. Mech. Rev., pp. 51–77, 2006.

Cakmur, R. V., Miller, R. L., Geogdzhayev, J., Ginoux, P., Koch, D., Kohfeld, K. E., Tegen, I., and Zender, C. S.: Constraining the magnitude of the global dust cycle by minimizing the difference between a model and observations, J. Geophys. Res, 111, 2006.

Callot, Y., Marticorena, B., and Bergametti, G.: Geomorphologic approach for modelling the surface features of arid environments in a model of dust emissions: application to the Sahara desert, Geodinamica Acta, 13, 245-270, 2000.

Carlson, T. N., and Prospero, J. M.: The Large-Scale Movement of Saharan Air Outbreaks over the Northern Equatorial Atlantic, Appl. Meteorol., 11, 283-297, 1972.

Carmichael, G. R., Tang, Y., Kurata, G., Uno, I., Streets, D. G., Woo, J. H., Huang, H., Yienger, J., Lefer, B., and Shetter, R. E.: Regional-scale chemical transport modeling in support of intensive field experiments: Overview and analysis of the TRACE-P observations, J. Geophys. Res, 108, 8823, 2003.

Cavalieri, O., Cairo, F., Fierli, F., Di Donfrancesco, G., Snels, M., Viterbini, M., Cardillo, F., Chatenet, B., Formenti, P., Marticorena, B., and Rajot, J. L.: Variability of aerosol vertical distribution in the Sahel, Atmos. Chem. Phys., 10, 12005-12023, doi:10.5194/acp-10-12005-2010, 2010.

Chamberlain, A. C.: Roughness length of sea, sand, and snow. Boundary Layer Meteorology, 25(4), 405-409, doi:10.1007/BF02041157, 405-409. 1983.

Chandra, S., Satheesh, S. K. and Srinivasan, J.: Can the state of mixing of black carbon aerosols explain the mystery of 'excess' atmospheric absorption?, J. Geophys. Res. Lett., 31(L19109), 2004.

Chang, J. C. and Hanna, S. R.: Air quality model performance evaluation, Meteorology and Atmospheric Physics, 87, 167-196, 2004.

Chiapello, I., Bergametti, G., Dulac, F., Gomes, L., Chatenet, B., Dulac, F., Pimenta, J., and Santos Suares, E.: An additional low layer transport of Sahelian and Saharan dust over the North-Eastern Tropical Atlantic. J. Geophys. Res. Lett. 22, 3191–3194, 1995.

Chiapello, I., Bergametti, G., Chatenet, B., Bousquet, P., Dulac, F., and Soares, E. S.: Origins of African dust transported over the northeastern tropical Atlantic, J. Geophys. Res., 102, 13701-13713,13709, 1997.

Chiapello, I., Bergametti, G., Chatenet, B., Dulac, F., Jankowiak, I., Liousse, C. and Santos Soares, E.: Contribution of the different aerosol species to the aerosol mass load and optical depth over the northeastern tropical Atlantic, J. Geophys. Res., 104(D4), 4025-4035, 1999.

Chiapello, I., Moulin, C., and Prospero, J. M.: Understanding the long-term variability of African dust transport across the Atlantic as recorded in both Barbados surface concentrations and large-scale Total Ozone Mapping Spectrometer (TOMS) optical thickness, J. Geophys. Res, 110, 1-9, 2005.

Christopher, S. A., and Jones, T.: Satellite-based assessment of cloud-free net radiative effect of dust aerosols over the Atlantic Ocean, J. Geophys. Res. Lett., 34, L02810, 2007.

Christopher, S. A., and Jones, T. A.: Satellite and surface-based remote sensing of Saharan dust aerosols, Remote Sensing of Environment, 114, 1002-1007, 2010.

Claquin, T., Schulz, M., and Balkanski, Y. J.: Modeling the mineralogy of atmospheric dust sources, J. Geophys. Res., 104, 22243-22256, 1999.

Colarco, P. R., Toon, O. B., Torres, O., and Rasch, P. J.: Determining the UV imaginary index of refraction of Saharan dust particles from Total Ozone Mapping Spectrometer data using a three-dimensional model of dust transport, J. Geophys. Res., 107, 4289, 2002.

Colette, A., Menut, L., Haeffelin, M., and Morille, Y.: Impact of the transport of aerosols from the free troposphere towards the boundary layer on the air quality in the Paris area, Atmos. Environ., 42, 390-402, 2008.

Cooke, W.F. and Wilson, J.J.N.: A global black carbon aerosol model. J. Geophys. Res. Atmos., 101, 19395-19409, 1996.

Córdoba-Jabonero, C., Sorribas, M., Guerrero-Rascado, J. L., Adame, J. A., Hernández, Y., Lyamani, H., Cachorro, V., Gil, M., Alados-Arboledas, L., and Cuevas, E.: Synergetic monitoring of Saharan dust plumes and potential impact on surface: a case study of dust transport from Canary Islands to Iberian Peninsula, Atmos. Chem. Phys, 11, 3067-3091, 2011.

Corradini, S., Carboni, E., Guerrieri, L., Lomboroso, L., Pugnaghi, S., and Santangelo, R.: One year of AERONET sun-photometric measurements at Lampedusa site: monthly averaged AOT comparison with satellite data and Saharan dust events detection, Óptica Pura y Aplicada, 37, 2004.

Costa, M. J., Sohn, B. J., Levizzani, V., and Silva, A. M.: Radiative forcing of Asian dust determined from the synergized GOME and GMS satellite data—A case study, J. Meteorolo. Soc. Jpn., 84, 85-95, 2006.

Cox, W. M. and Tikvart, J. A.: A statistical procedure for determining the best performing air quality simulation model, Atmos. Environ. Part A. General Topics, 24, 2387-2395, 1990.

Cros, B., Durand, P., Cachier, H., Drobinski, P., Frejafon, E., Kottmeier, C., Perros, P. E., Peuch, V. H., Ponche, J. L., and Robin, D.: The ESCOMPTE program: an overview, Atmos. Environ., 69, 241-279, 2004.

Dall'Osto, M., Harrison, R. M., Highwood, E. J., O'Dowd, C., Ceburnis, D., Querol, X., and Achterberg, E. P.: Variation of the mixing state of Saharan dust particles with atmospheric transport, Atmos. Environ., 44, 3135-3146, doi:10.1016/j.atmosenv.2010.05.030 2010.

d'Almeida, G. A.: A Model for Saharan Dust Transport, Appl. Meteorol., 25 (7), 1986.

d'Almeida, G. A.: On the variability of desert aerosol radiative characteristics. J. Geophys. Res. 92, 3017-3026, 1987.

Darmenova, K., Sokolik, I. N., Shao, Y., Marticorena, B., and Bergametti, G.: Development of a physically based dust emission module within the Weather Research and Forecasting (WRF) model: Assessment of dust emission parameterizations and input parameters for source regions in Central and East Asia, Journal of Geophysical Research, 114, D14201, 2009.

Dayan, U., Heffter, J., Miller, J., and Gutman, G.: Dust Intrusion Events into the Mediterranean Basin, Appl. Meteorol., 30, 1185–1199, 1991.

de Meij, A., and Lelieveld, J.: Evaluating aerosol optical properties observed by ground-based and satellite remote sensing over the Mediterranean and the Middle East in 2006, Atmos. Res., 2010.

de Tomasi, F., and Perrone, M.R.: Lidar measurements of tropospheric water vapor and aerosol profiles over southeastern Italy, J. Geophys. Res., 108, 4286– 4297, 2003.

de Tomasi, F., and Perrone, M. R.: PBL and dust layer seasonal evolution by lidar and radiosounding measurements over a peninsular site, Atmos. Res., 80, 86– 103, 2006.

DeMott, P. J., Sassen, K., Poellot, M. R., Baumgardner, D., Rogers, D. C., Brooks, S. D., Prenni, A. J., and Kreidenweis, S. M.: African dust aerosols as atmospheric ice nuclei, J. Geophys. Res. Lett, 30, 1732, 2003.

Dennis, R., Fox, T., Fuentes, M., Gilliland, A., Hanna, S., Hogrefe, C., Irwin, J., Rao, S. T., Scheffe, R., and Schere, K.: A framework for evaluating regional-scale numerical photochemical modeling systems, Environ. Fluid Mechanics, 1-19, 2010.

Dentener, F. J., Carmichael, G. R., Zhang, Y., Lelieveld, J., and Crutzen, P. J.: Role of mineral aerosol as a reactive surface in the global troposphere, J. Geophys. Res., 101, 22869, 1996.

Derimian, Y., Karnieli, A., Kaufman, Y. J., Andreae, M. O., Andreae, T. W., Dubovik, O., Maenhaut, W., Koren, I., and Holben, B. N.: Dust and pollution aerosols over the Negev desert, Israel:Properties, transport, and radiative effect, J. Geophys. Res., 111, doi:10.1029/2005JD006549, 2006.

Deuze, J. L., Devaux, C., Herman, M., Santer, R., and Tanre, D.: Saharan Aerosols over South of France: Characterization derived from satellite data and ground based measurements, Appl. Meteorol., 27, 680-686, 1988.

di Lorio, T., Di Sarra, A., Junkermann, W., Cacciani, M., Fiocco, G., and Fua, D.: Tropospheric aerosols in the Mediterranean: 1. Microphysical and optical properties, J. Geophys. Res, 108, 4316, 2003.

Djalalova, I., Wilczak, J., McKeen, S., Grell, G., Peckham, S., Pagowski, M., Delle Monache, L., McQueen, J., Tang, Y., Lee, P., McHenry, J., Gong, W., Bouchet, V., and Mathru, R.: Ensemble and bias-correction techniques for air quality model forecasts of surface O3 and PM2.5 during the TEXAQS-II experiment of 2006, Atmos. Environ., 44, 455-467, 2010.

Domınguez-Rodrıíguez, A, J. Abreu-Afonso, S. Rodríguez, R. Juárez-Prera, E. Arroyo-Ucar, A. Jiménez-Sosa, Y. González, P. Abreu-González, and P. Avanzas: Comparative Study of Ambient Air Particles in Patients Hospitalized for Heart Failure and Acute Coronary Syndrome, Rev Esp Cardiol., 64(8):661–666 (Document downloaded from http://www.revespcardiol.org), 2011.

Dubovik, O. and King, M. D.: A flexible inversion algorithm for retrieval of aerosol optical properties from sun and sky radiance measurements, J. Geophys. Res., 105(D16), 20676, doi:10.1029/2000JD900282, 2000.

Dubovik, O., Smirnov, A., Holben, B. N., King, M. D., Kaufman, Y. J., Eck, T. F., and Slutsker, I.: Accuracy assessments of aerosol optical properties retrieved from Aerosol Robotic Network (AERONET) Sun and sky radiance measurements. J. Geophys. Res., 105, 9791-9806, 2000.

Dubovik, O., Holben, B. N., Eck, T. F., Smirnov, A., Kaufman, Y. J., King, M. D., Tanré, D., and Slutsker, I.: Variability of Absorption and Optical Properties of Key Aerosol Types Observed in Worldwide Locations, Atmos. Sci., 59, 590-608, 2002.

Duce, R. A., Liss, P. S., Merrill, J. T., Atlas, E. L., Buat-Menard, P., Hicks, B. B., Miller, J. M., Prospero, J. M., Arimoto, R., and Church, T. M.: The atmospheric input of trace species to the world ocean, Global biogeochemical cycles, 5, 193-259, 1991.

Dulac, F., Tanre, D., Bergametti, G., Buat-Menard, P., Desbois, M., and Sutton, D.: Assessment of the African airborne dust mass over the western Mediterranean Sea using Meteosat data J. Geophys. Res., 97, 2489-2506, 1992.

Dulac, F., and Chazette, P.: Airborne study of a multi-layer aerosol structure in the eastern Mediterranean observed with the airborne polarized lidar ALEX during a STAAARTE campaign (7 June 1997), Atmos. Chem. Phys., 3, 1817–1831, 2003.

Eck , T. F., Holben, B. N., Reid, J. S., Dubovik, O., Smirnov, A., O'Neill, N. T., Slutsker, I. and Kinne, S.: Wavelength dependence of optical depth of biomass burning, urban and desert dust aerosols, J. Geophys. Res., 104(D24), 31333-31350, 1999.

Eck, T. F., Holben, B. N., Dubovik, O., Smirnov, A., Goloub, P., Chen, H. B., Chatenet, B., Gomes, L., Zhang, X. Y. and Tsay, S. C.: Columnar aerosol optical properties at AERONET sites in central eastern Asia and aerosol transport to the tropical mid-Pacific, J. Geophys. Res, 110, D06202, 2005.

Eck, T. F., Holben, B. N., Reid, J. S., Sinyuk, A., Dubovik, O., Smirnov, A., Giles, D., O'Neill, N. T., Tsay, S. C. and Ji, Q.: Spatial and temporal variability of column-integrated aerosol optical properties in the southern Arabian Gulf and United Arab Emirates in summer, J. Geophys. Res, 113, 2008.

Eder, B. and Yu, S.: A performance evaluation of the 2004 release of models-3 CMAQ. Atmos. Environ. 40, 4811-4824. doi: 10.1016/j.atmosenv.2005.08.045, 2006.

Edney, E.O., Kleindienst, T.E., Lewandowski, M. and Offenberg, J.H.: Updated SOA chemical mechanism for the community multi-scale air quality model, EPA 600/X-07/025, US Environmental Protection Agency, Research Triangle park, North Carolina, 2007.

Elias, T., Silva, A. M., Belo, N., Pereira, S., Formenti, P., Helas, G. and Wagner, F.: Aerosol extinction in a remote continental region of the Iberian Peninsula during summer, J. Geophys. Res., 111(D14), D14204, 2006.

EMEP: National Emissions Reported to the Convention on Long-range Transboundary Air Pollution (LRTAP Convention). Air Emission Annual Data Reporting (EMEP/MSC-W). Technical Report, European Environmental Agency, The Norwegian Meteorological Institute, Oslo, Norway, 2007.

Engelstaedter, S., Tegen, I., and Washington, R.: North African dust emissions and transport, Earth-Science Reviews, 79, 73-100, 2006.

Engelstaedter, S., and Washington, R.: Atmospheric controls on the annual cycle of North African dust, J. Geophys. Res, 112, D03103, 2007a.

Engelstaedter, S., and Washington, R.: Temporal controls on global dust emissions: The role of surface gustiness, J. Geophys. Res. Lett, 34, L15805, 2007b.

Environmental Protection Agency (EPA): Global Ecosystem Database, Version 1.0 Documentation Manual, EPA Global Change Research Program-NOAA/NGDC Global Change Database Program, USDC, Boulder, Colorado, 1992.

Escudero, M., Castillo, S., Querol, X., Avila, A., Alarcón, M., Viana, M. M., Alastuey, A., Cuevas, E. and Rodríguez, S.: Wet and dry African dust episodes over Eastern Spain, J. Geophys. Res., 110, 4731-4746, 2005.

Escudero, M., Querol, X., Pey, J., Alastuey, A., Pérez, N., Ferreira, F., Alonso, S., Rodríguez, S., and Cuevas, E.: A methodology for the quantification of the net African dust load in air quality monitoring networks, Atmos. Environ., 41, 5516-5524, doi:10.1016/j.atmosenv.2007.04.047, 2007.

European Commission: Forest fires in Europe 2004. Report 5. Official Publication of the European Commission. S.P.I.05.147 EN. (Source: http://www.fire.uni-freiburg.de/programmes/eu-comission/EU-Forest-Fires-in-Europe-2004.pdf), 2005.

European Commission: Directive 2008/50/EC of the European Parliament and of the Council of 21 May 2008 on Ambient Air Quality and Cleaner Air for Europe, Technical Report 2008/50/EC, L152. Off. J. Eur. Comm., 2008.

Fan, S. M., Horowitz, L. W., Levy Ii, H., and Moxim, W. J.: Impact of air pollution on wet deposition of mineral dust aerosols, J. Geophys. Res. Lett, 31, L02104, 2004.

Fan, S. M., Moxim, W. J., and Levy, H.: Aeolian input of bioavailable iron to the ocean, J. Geophys. Res. Lett, 33, 2006.

Fecan, F., Marticorena, B. and Bergametti, G.: Parametrization of the increase of the aeolian erosion threshold wind friction velocity due to soil moisture for arid and semi-arid areas. Ann. Geophys. 17, 149-157, 1999.

Flentje, H., Engelbart, D., and Thomas, W.: Aerosol Profiling within the Ceilometer Network of the German Meteorological Service; European Aerosol Conference 2009, Karlsruh, 2009.

Fiol, L. A., Fornos, J. J., Gelabert, B., and Guijarro, J. A.: Dust rains in Mallorca (Western Mediterranean): Their occurrence and role in some recent geological processes, Catena, 63, 64-84, 2005.

Folberth, G., Hauglustaine, D.A., Lathière, J., Brocheton, J.: Interactive chemistry in the Laboratoire de Météorologie Dynamique general circulation model: model description and impact analysis of biogenic hydrocarbons on tropospheric chemistry, Atmos. Chem. Phys., 6, 2273-2319, 2006.

Formenti, P., Andreae, M. O., Andreae, T. W., Galani, E., Vasaras, A., Zerefos, C., Amiridis, V., Orlovsky, L., Karnieli, A., Wendisch, M., Wex, H., Holben, B. N., Maenhaut, W., and Lelieveld, J.: Aerosol optical properties and large-scale transport of air masses: observations at a coastal and a semiarid site in the eastern Mediterranean during summer 1998, J. Geophys. Res., 106, 9807–9826, doi: 10.1029/2000JD900609, 2001.

Fotiadi, A., Hatzianastassiou, N., Drakakis, E., Matsoukas, C., Pavlakis, K. G., Hatzidimitriou, D., Gerasopoulos, E., Mihalopoulos, N., and Vardavas, I.: Aerosol physical and optical properties in the Eastern Mediterranean Basin, Crete, from Aerosol Robotic Network data, Atmos. Chem. Phys., 6, 5399-5413, 2006.

Franzen, L. G., Hjelmroos, M., Kallberg, P., Brorstrom-Lunden, E., Juntto, S., and Savolainen, A. L.: The "yellow snow" episode of northern Fennoscandia, March 1991- a case study of long-distance transport soil, pollen and stable organic compounds, Atmos. Environ., 28, 3587-3604, 1994.

Gallisai, R.: Potencial effect of dust deposition on production in the Mediterranean Sea, Universitat de Barcelona, Master Thesis, 2010.

Ganor, E., Foner, H. A., Brenner, S., Neeman, E., and Lavi, N.: the chemical composition of aerosol settling in Israel following dust storms, Atmos. Environ., 25, 1743-1755, 1991.

Ganor, E., Osetinsky, I., Stupp, A., and Alpert, P.: Increasing trend of African dust, over 49 years, in the eastern Mediterranean, J. Geophys. Res, 115, 2010.

Generoso, S., Bey, I., Labonne, M., and Bréon, F. M.: Aerosol vertical distribution in dust outflow over the Atlantic: comparisons between GEOS-Chem and Cloud-Aerosol Lidar and Infrared Pathfinder Satellite Observation (CALIPSO), J. Geophys. Res., 113, D24209, 2008.

Gerasopoulos, E., Andreae, M. O., Zerefos, C. S., Andreae, T. W., Balis, D., Formenti, P., Merlet, P., Amiridis, V., and Papastefanou, C.: Climatological aspects of aerosol optical properties in Northern Greece, Atmos. Chem. Phys. , 3, 2059-2099, 2003.

Gerasopoulos, E., Koulouri, E., Kalivitis, N., Kouvarakis, G., Saarikoski, S., Mäkelä, T., Hillamo, R. and Mihalopoulos, N.: Size-segregated mass distributions of aerosols over Eastern Mediterranean: seasonal variability and comparison with AERONET columnar size-distributions, Atmos. Chem. Phys. Discussions, 7(1), 469-497, 2007.

Gery, M. W., Whitten, G. Z., Killus, J. P. and Dodge, M. C.: A photochemical kinetics mechanism for urban and regional scale computer modeling, J. Geophys. Res., 94 (D10), 12 925–12 956, 1989.

Gillette, D. A., and Passi, R.: Modeling dust emission caused by wind erosion, J..Geophys. Res., 93, 14233-14214, 1988.

Gilliland, A. B., Dennis, R. L., Roselle, S. J., and Pierce, T. E.: Seasonal NH3 emission estimates for the eastern United States based on ammonium wet concentrations and an inverse modeling method, J. Geophys. Res., 108(D15), 4477, doi:10.1029/2002JD003063, 2003.

Ginoux, P., and Torres, O.: Empirical TOMS index for dust aerosol: Applications to model validation and source characterization, J. Geophys. Res., 108(D17), 4534, doi:10.1029/2003JD003470, 2003.

Ginoux, P., Chin, M., Tegen, I., Prospero, J. M., Holben, B., Dubovik, O., and Lin, S.-J.: Sources and distributions of dust aerosols simulated with the GOCART model, J. Geophys. Res., 106, 20255-20274 10.1029/2000JD000053 2001.

Ginoux, P., Prospero, J. M., Torres, O., and Chin, M.: Long-term simulation of global dust distribution with the GOCART model: correlation with North Atlantic Oscillation, Environmental Modelling & Software, 19, 113–128, 2004.

Giorgi, F.: A Particle Dry-Deposition Parameterization for Use in Tracer Transport Models, J. Geophys. Res., 91, 9794-9806, 1986.

Gobbi, G. P., Barnaba, F., Giorgi, R., and Santacasa, A.: Altitude-resolved properties of a Saharan dust event over the Mediterranean, Atmos. Environ., 34, 5119-5127, 2000.

Gobbi, G. P., Barnaba, F., and Ammannato, L.: The vertical distribution of aerosols, Saharan dust and cirrus clouds in Rome (Italy) in the year 2001, Atmos. Chem. Phys, 4, 351–359, 2004.

Gobbi, G. P., Kaufman, Y. J., Koren, I., and Eck, T. F.: Classification of aerosol properties derived from AERONET direct sun data, Atmos. Chem. Phys., 7, 453-458, 2007.

Gong, S. L.: A parameterization of sea-salt aerosol source function for sub- and super-micron particles, J. Geophys. Res., 17, 1097, doi:10.1029/2003GB002 079, 2003.

Gong, S. L., and Zhang, X. Y.: CUACE/Dust-An integrated system of observation and modeling systems for operational dust forecasting in Asia, Atmos. Chem. Phys., 8, 2333-2340, 2008.

González-Ramos, A., Cuevas, E., Pérez, C., Baldasano, J. M., Coca, J., Redondo, A., Alonso-Pérez, S., Bustos, J. J., and Nickovic, S.: Short-term changes in the northwest African Upwelling System induced by Saharan dust deposition events, 7, 012019, 2009.

Goudie, A. S., and Middelton, N. J.: The changing frequency of dust stroms through time, Climate Change, 20, 197-225, 1992.

Goudie, A. S., and Middleton, N. J.: Saharan dust storms: nature and consequences, Earth-Science Reviews, 56, 179-204, PII: S0012-8252 01 00067-8, 2001.

Goudie, A. S., and Middleton, N. J.: Desert Dust in the Global System, Springer Berlin Heidelberg, 2006.

Govaerts, Y. M., Wagner, S., Lattanzio, A. and Watts, P.: Joint retrieval of surface reflectance and aerosol optical depth from MSG/SEVIRI observations with an optimal estimation approach: 1. Theory, J. Geophys. Res., 115, D02203, doi:10.1029/2009JD011779, 2010.

Grini, A., and Zender, C. S.: Roles of saltation, sandblasting, and wind speed variability on mineral dust aerosol size distribution during the Puerto Rican Dust Experiment (PRIDE), J. Geophys. Res, 109, D07202, 2004.

Grini, A., Tulet, P., and Gomes, L.: Dusty weather forecasts using the MesoNH mesoscale atmospheric model, J. Geophys. Res., 111, D19205, 2006.

Grousset, F., Ginoux, P., Bory, A., and Biscaye, P.: Case study of a chinese dust plume reaching the french alps, EGS-AGU-EUG Joint Assembly, Abstracts from the meeting held in Nice, France, 6-11 April , 2003.

Gupta, P., and Christopher, S. A.: Particulate matter air quality assessment using integrated surface, satellite, and meteorological products: Multiple regression approach, J. Geophys. Res., 114, D14205, doi:10.1029/2008JD011496, 2009.

Gyan, K., Henry, W., Lacaille, S., Laloo, A., Lamsee-Ebanks, C., McKay, S., Antoine, R. M., and Monteil, M. A.: African dust clouds are associated with increased paediatric asthma accident and emergency admissions on the Caribbean island of Trinidad, International Journal of Biometeorology, 49, 371-376, 2005.

Hand, J. L., Mahowald, N. M., Chen, Y., Siefert, R. L., Luo, C., Subramaniam, A. and Fung, I.: Estimates of atmospheric-processed soluble iron from observations and a global mineral aerosol model: Biogeochemical implications, J. Geophys. Res., 109, D17205, doi:10.1029/2004JD004574, 2004.

Hansen, J., Sato, M., and Ruedy, R.: Radiative forcing and climate response, J. Geophys. Res, 102, 6831–6864, 1997.

Harrison, R.M., van Grieken, R.E.: Atmospheric particles.IUPAC series on analytical and physical chemistry of environmental system. J. Buffle and H.P. van Leeuwen. John Wiley & Sons, 610 pp., 1998.

Hauglustaine, D.A., Hourdin, F., Jourdain, L., Filiberti, M.A.,Walters, S., Lamarque, J.F., Holland, E.A.: Interactive chemistry in the Laboratoire de Meteorologie Dynamique general circulation model: description and background tropospheric chemistry evaluation. J. Geophys. Res., D04314, doi:10.1029/2003JD003957, 2004.

Haustein, K., Pérez, C., Baldasano, J. M., Müller, D., Tesche, M., Schladitz, A., Esselborn, M., Weinzierl, B., Kandler, K. and Hoyningen-Huene, W. v.: Regional dust model performance during SAMUM 2006, Geophys. Res. Lett., 36, L03812, doi:10.1029/2008GL036463, 2009.

Haustein, K., Pérez, C., Baldasano, J.M., Jorba, O., Basart, S., Miller, R.L., Janjic, Z., Black, T., Nickovic, S., Todd, M. and Washington, R.: Atmospheric dust modeling from meso to global scales with the online NMMB/BSC-Dust model: 2. Regional experiments in North Africa, Atmos. Chem. Phys. Discus., 11, 30273–30331, doi:10.5194/acpd-11-30273-2011, 2011.

Heinold, B., Helmert, J., Hellmuth, O., Wolke, R., Ansmann, A., Marticorena, B., Laurent, B., and Tegen, I.: Regional modeling of Saharan dust events using LM-MUSCAT: Model description and case studies, J. Geophys. Res., 112, D11204, 2007.

Heintzenberg, J.: The SAMUM 1 experiment over Southern Morocco: overview and introduction, Tellus B, 61, 2-11, 2009.

Hernández, Y., Alonso-Pérez, S., Cuevas, E., Camino, C., Ramos, R., Bustos, J.J., Marrero, C., Córdoba-Jabonero, C., and Gil, M.: MicroPulse Lidar and Ceilometer inter-comparison during Saharan dust intrusions over the Canary Islands, V Reunión Española de Ciencia y Tecnología de Aerosoles – RECTA 2011, CIEMAT, Madrid, Spain, 27-29 June, 2011.

Hillel, D.: Introduction to soil physics, Academic press London, 1982.

Hogrefe, C., Hao, W., Civerolo, K., Ku, J.Y., and Sistla, G: Exploring approaches to integrate observations and CMAQ simulations for improved air quality forecasts, Presented at the 5th nnual CMAQ User's Conference, Chapel Hill, NC. Available on the Internet at http://www.cmascenter.org/conference/2006/abstracts/hogrefe_session3.pdf, 2006.

Holben, B. N., Eck, T. F., Slutsker, I., Tanré, D., Buis, J. P., Setzer, A., Vermote, E., Reagan, J., Kaufman, Y., Nakajima, T., Lavenu, F., Jankowiak, I., and Smirnov, A.: AERONET: A Federated Instrument Network and Data Archive for Aerosol Characterization, Rem. Sens. Environ., 66, 1-16, 1998.

Holben, B. N., Tanre, D., Smirnov, A., Eck, T. F., Slutsker, I., Abuhassan, N., Newcomb, W. W., Schafer, J., Chatenet, B., Lavenue, F., Kaufman, Y. J., Castle, J. V., Setzer, A., Markham, B., Clark, D., Frouin, R., Halthore, R., Karnieli, A., O'Neill, N. T., Pietras, C., Pinker, R. T., Voss, K. and Zibordi, G.: An emerging ground-based aerosol climatology: Aerosol Optical Depth from AERONET, Geophys. Res., 106(12), 12067-12097, 2001.

Horvath, H., Arboledas, L. A., Olmo, F. J., Jovanovi, O., Gangl, M., Kaller, W., Sanchez, C., Sauerzopf, H., and Seidl, S.: Optical characteristics of the aerosol in Spain and Austria and its effect on radiative forcing, J. Geophys. Res, 107, 4386, 2002.

Hsu, N. C., Tsay, S. C., King, M. and Herman, J. R.: Aerosol properties over bright-reflecting source regions. IEEE Trans. Geosci. Remote Sens., 42, 557 – 569, 2004.

Huneeus, N., Schulz, M., Balkanski, Y., Griesfeller, J., Kinne, S., Prospero, J., Bauer, S., Boucher, O., Chin, M., and Dentener, F.: Global dust model intercomparison in AeroCom phase I, Atmos. Chem. Phys., 11, 7781-7816, 2011.

IPCC, Intergovernmental Panel on Climate Change: Climate change 2001: The Scientific basis, Cambridge Univ. Press, New York, 2001.

IPCC, Intergovernmental Panel on Climate Change: Climate change 2007: The physical Science Basis, Cambridge University Press, U.K., 2007.

Israelevich, P. L., Levin, Z., Joseph, J. H., and Ganor, E.: Desert aerosol transport in the Mediterranean region as inferred from the TOMS aerosol index, J. Geophys. Res., 107, 10.1029/2001JD002011, 2002.

Iversen, J. D. and White: B. R. Saltation threshold on earth, mars and venus. Wiley Online Library, 111-119, 1982.

Janjic, Z. I.: Pressure gradient force and advection scheme used for forecasting with steep and small scale topography, Contr. Atmos. Phys., 50, 186– 199, 1977.

Janjic, Z. I.: Forward-backward scheme modified to prevent twogrid-interval noise and its application in sigma coordinate models, Contr. Atmos. Phys., 52, 69– 84, 1979.

Janjic, Z. I.: Non-linear advection schemes and energy cascade on semi-staggered grids, Mon. Weather Rev., 112, 1234– 1245, 1984.

Janjic, Z. I.: The step-mountain coordinate: Physical package, Mon. Weather Rev., 118, 1429– 1443, 1990.

Janjic, Z. I.: The Step-mountain Eta Coordinate Model: Further developments of the convection, viscous sublayer and turbulence closure schemes, Mon. Weather Rev., 122, 927– 945, 1994.

Janjic, Z. I.: The Mellor-Yamada Level 2.5 turbulence closure scheme in the NCEP Eta Model", in Research Activities in Atmospheric and Oceanic Modelling, CAS/WGNE, 4.14– 4.15, World Meteorol. Org., Geneva, 1996a.

Janjic, Z. I.: The surface layer parameterization in the NCEP Eta Model, in Research Activities in Atmospheric and Oceanic Modelling, CAS/C WGNE, 4.16–4.17, World Meteorol. Org., Geneva, 1996b.

Janjic, Z. I.: A unified model approach from meso to global scales. Geophys. Res. Abstracts, 7, SRef{ID: 1607{7962/gra/EGU05{A{05 582, 2005.

Janjic, Z. I. and Black, T: A unified model approach from meso to global scales. Geophys. Res. Abstracts, 7, SRef{ID: 1607{7962/gra/EGU2007{A{05 025, 2007.

Jickells, T. D., An, Z. S., Andersen, K. K., Baker, A. R., Bergametti, G., Brooks, N., Cao, J. J., Boyd, P. W., Duce, R. A., and Hunter, K. A.: Global iron connections between desert dust, ocean biogeochemistry, and climate, 308, 67, 2005.

Jiménez, P., Baldasano, J. M. and Dabdub, D.: Comparison of photochemical mechanisms for air quality modelling, Atmos. Environ., pp. 4179–4194, doi:10.1016/S1352–2310(03)00 567–3, 2003.

Jiménez, P., Jorba, O., Parra, R. and Baldasano, J. M.: Evaluation of MM5-EMICAT2000-CMAQ performance and sensitivity in complex terrain: High-resolution application to the northeastern Iberian Peninsula, Atmos. Environ., 40(26), 5056-5072, 2006.

Jiménez-Guerrero, P., Pérez, C., Jorba, O., and Baldasano, J. M.: Contribution of Saharan dust in an integrated air quality system and its on-line assessment, Geophys. Res. Lett., 35, 2008a.

Jiménez-Guerrero, P., Jorba, O., Baldasano, J. M. and Gassó, S.: The use of a modelling system as a tool for air quality management: Annual high-resolution simulations and evaluation, Science of the Total Environment, 390(2-3), 323-340, 2008b.

Jorba, O., Perez, C., Haustein, K., Janjic, Z., Dabdub, D., Baldasano, J. M., Badia, A., and Spada, M.: Status of Development and Firsts Results at Global Scale of NMMB/BSC-CHEM: an online multiscale air quality model. Geophys. Res. Abstracts, Vol. 12, EGU2010-5228, Austria, Viena, 2-7 May, 2010.

Jung, E. and Shao, Y.: An intercomparison of four wet deposition schemes used in 3 the dust transport model, J. Global and Planetary Change, 52, 248-260, 2006.

Kalashnikova, O. V. and Sokolik, I. N.: Modeling the radiative properties of nonspherical soil-derived mineral aerosols, J. Quant. Spectrosc. Ra., 87, 137–166, 2004

Kalivitis, N., Gerasopoulos, E., Vrekoussis, M., Kouvarakis, G., Kubilay, N., Hatzianastassiou, N., Vardavas, I. and Mihalopoulos, N.: Dust transport over the eastern Mediterranean derived from Total Ozone Mapping Spectrometer, Aerosol Robotic Network, and surface measurements, J. Geophys. Res, 112, D03202, 2007.

Kallos, G., Nickovic, S., Papadopoulos, A., Jovic, D., Kakaliagou, O. and co-authors: The regional weather forecasting system SKIRON: an overview. In: Proceedings of the Proceedings of the Symposium on Regional Weather Prediction on Parallel Computer Environment, University of Athens, Greece, 1997.

Kalnay, E.: Atmospheric modeling, data assimilation, and predictability, Cambridge Univ. Press, 2003.

Kalu, A. E.: The Microphysics of the Saharan Dust and its Implications on Climate Second Workshop on Cloud Physics and Climate, International Centre for Theoretical Physics, Trieste, 1987., 1987.

Kang, D., Mathur, R., and Rao, S. T.: Assessment of bias-adjusted PM2.5 air quality forecasts over the continental United States during 2007, Geosci. Model Dev., 3, 309–320, 2010.

Kasibhatla, P., Chameides, W. L., Jonn, J.S.: A three dimensional global model investigation of seasonal variations in the atmospheric burden of anthropogenic sulphate aerosols. J. Geophys. Res., 102, 3737-3759, 1997.

Kaskaoutis, D. G., Kambezidis, H. D., Hatzianastassiou, N., Kosmopoulos, P. G. and Badarinath, K. V. S.: Aerosol climatology: on the discrimination of aerosol types over four AERONET sites, Atmos. Chem. Phys. Discuss, 7, 6357-6411, 2007.

Kaufman, Y. J.: Aerosol optical thickness and atmospheric path radiance, J. Geophys. Res, 98(D2), 2677–2692, 1993.

Kaufman, Y. J., Tanré, D., Dubovik, O., Karnieli, A., and Remer, L. A.: Absorption of sunlight by dust as inferred from satellite and ground-based remote sensing, Geophys. Res. Lett., 28, 1479-1482 doi: 10.1029/2000GL012647, 2001.

Kaufman, Y. J., Koren, I., Remer, L. A., Tanre, D., Ginoux, P., and Fan, S.: Dust transport and deposition observed from the Terra-Moderate Resolution Imaging Spectroradiometer (MODIS) spacecraft over the Atlantic Ocean, J. Geophys. Res., 110, doi:10.1029/2003JD004436, 2005.

Kazadzis, S., Bais, A., Amiridis, V., Balis, D., Meleti, C., Kouremeti, N., Zerefos, C. S., Rapsomanikis, S., Petrakakis, M. and Kelesis, A.: Nine years of UV aerosol optical depth measurements at Thessaloniki, Greece, Atmos. Chem. Phys., 7(8), 2091-2101, 2007.

Keenan, T., Niinemets, U., Sabate, S., Gracia, C., Peñuelas, P.: Process based inventory of isoprenoid emissions from European forests: model comparisons, current knowledge and uncertainties. Atmos. Chem. Phys., 9, 4053-4076, 2009.

Kelly, J.T., Bhave, P.V., Nolte, C.G., Shankar, U. and Foley, K.M. Simulating emission and chemical evolution of coarse sea-salt particles in the Community Multiscale Air Quality (CMAQ) model. Geosci. Model Dev. 3, 257-273, 2010.

Kim, S. W., Yoon, S. C., Kim, J. and Kim, S. Y.: Seasonal and monthly variations of columnar aerosol optical properties over east Asia determined from multi-year MODIS, LIDAR, and AERONET Sun/sky radiometer measurements, Atmos. Environ., 41(8), 1634-1651, 2007.

Kim, S. W., Chazette, P., Dulac, F., Sanak, J., Johnson, B., and Yoon, S. C.: Vertical structure of aerosols and water vapor over West Africa during the African monsoon dry season, Atmos. Chem. Phys., 9, 8017-8038, 2009.

Kinne, S., Lohmann, U., Feichter, J., Schulz, M., Timmreck, C., Ghan, S., Easter, R., Chin, M., Ginoux, P., Takemura, T., Tegen, I., Koch, D., Herzog, M., Penner, J., Pitari, G., Holben, B. N., Eck, T. F., Smirnov, A., Dubovik, O., Slutsker, I., Tanre, D., Torres, O., Mishchenko, M., Geogdzhayev, I., Chu,

D. A., and Kaufman, Y.: Monthly averages of aerosol properties: A global comparison among models, satellite data, and AERONET ground data, J. Geophys. Res., 108, 4634, doi:10.1029/2001JD001253, 2003.

Kinne, S., Schulz, M., Textor, C., Guibert, S., Balkanski, Y., Bauer, S. E., Berntsen, T., Berglen, T. F., Boucher, O., Chin, M., Collins, W., Dentener, F., Diehl, T., Easter, R., Feichter, J., Fillmore, D., Ghan, S., Ginoux, P., Gong, S., Grini, A., Hendricks, J., Herzog, M., Horowitz, L., Isaksen, I., Iversen, T., Kirkevag, A., Kloster, S., Koch, D., Kristjansson, J. E., Krol, M., Lauer, A., Lamarque, J. F., Lesins, G., Liu, X., Lohmann, U., Montanaro, V., Myhre, G., Penner, J., Pitari, G., Reddy, S., Seland, O., Stier, P., Takemura, T., and Tie, X.: An AeroCom initial assessment optical properties in aerosol component modules of global models, Atmos. Chem. Phys., 6, 1815–1834, doi:10.5194/acp-6-1815-2006, 2006.

Kinne, S.: Climatologies of cloud related aerosols- part 1 particle number and size, /Clouds in the perturbed climate system, edited by J.Heintzenberg and J.Charlson, ISBN: 978-0-262-01287-4, 2009.

Kishcha, P., Alpert, P., Shtivelman, A., Krichak, S. O., Joseph, J. H., Kallos, G., Katsafados, P., Spyrou, C., Gobbi, G. P., Barnaba, F., Nickovic, S., Pérez, C., and Baldasano J. M.: Forecast errors in dust vertical distributions over Rome (Italy): Multiple particle size representation and cloud contributions. J. Geophys. Res. 112, D15205, doi:10.1029/2006JD007427, 2007.

Klein, H., Nickovic, S., Haunold, W., Bundke, U., Nillius, B., Ebert, M., Weinbruch, S., Schuetz, L., Levin, Z., and Barrie, L. A.: Saharan dust and ice nuclei over Central Europe, Atmos. Chem. Phys, 10, 10211-10221, 2010.

Klose, M., Shao, Y., Karremann, M. K., and Fink, A. H.: Sahel dust zone and synoptic background, J. Geophys. Res. Lett., 37, L09802, 2010.

Knippertz, P., Trentmann, J., and Seifert, A.: High resolution simulations of convective cold pools over the northwestern Sahara, J. Geophys. Res, 114, D08110, 2009.

Koven, C. D., and Fung, I.: Identifying global dust source areas using high-resolution land surface form, J. Geophys. Res., 113, D22204, 2008.

Kubilay, N., Nickovic, S., Moulin, C. and Dulac, F.: An illustration of the transport and deposition of mineral dust onto the eastern Mediterranean, Atmos. Environ., 34, 1293-1303, 2000.

Kubilay, N., Cokacar, T. and Oguz, T.: Optical properties of mineral dust outbreaks over the northeastern Mediterranean, J. Geophys. Res., 108(D21), 4666, 2003.

Larssen, S., Sluyter, R. and Helmis, C.: Criteria for EUROAIRNET, the EEA Air Quality Monitoring and Information Network. Technical Report No. 12. European Environment Agency. http://reports.eea.eu.int/TEC12/en, 1999.

Legrand, M., Vergé-Dépré, G., and Pancrati, O.: Remote Sensing of Dust in Africa Using MSG/SEVIRI: Towards a Multichannel Dust Index, Proceedings of the Second MSG RAO Workshop (ESA SP-582). , Salzburg, Austria 9-10 September 2004., 2004.

Lelieveld, J., Berresheim, H., Borrmann, S., Crutzen, P. J., Dentener, F. J., Fischer, H., Feichter, J., Flatau, P. J., Heland, J., Holzinger, R., Korrmann, R., Lawrence, M. G., Levin, Z., Markowicz, K. M., Mihalopoulos, N., Minikin, A., Ramanathan, V., Reus, M. d., Roelofs, G. J., Scheeren, H. A., Sciare, J., Schlager, H., Schultz, M., Siegmund, P., Steil, B., Stephanou, E. G., Stier, P., Traub, M., Warneke, C., Williams, J. and Ziereis, H.: Global Air Pollution Crossroads over the Mediterranean, Science, 298(5594), 794-799, 2002.

Levin, Z., Ganor, E., and Gladstein, V.: The effects of desert particles coated with sulfate on rain formation in the eastern Mediterranean, Appl. Meteorol., 35, 1511-1523, 1996.

Levin, Z., and Cotton, W.: Aerosol Pollution Impact on Precipitation: A Scientific Review, Report of the International Aerosol Science Assessment Group to the WMO and the IUGG, Springer-Science Press, 386 pp, 2008.

Levy, R. C., Remer, L. A., Tanré, D., Kaufman, Y. J., Ichoku, C., Holben, B. N., Livingston, J. M., Russell, P. B. and Maring, H.: Evaluation of the Moderate-Resolution Imaging Spectroradiometer (MODIS) retrievals of dust aerosol over the ocean during PRIDE, J. Geophys. Res., 108(D19), 8594, doi:10.1029/2002JD002460, 2003.

Li, W. J., and Shao, L. Y.: Observation of nitrate coatings on atmospheric mineral dust particles, Atmos. Chem. Phys, 9, 1863–1871, 2009.

Li, X., Maring, H., Savoie, D., Voss, K., and Prospero, J. M.: Dominance of mineral dust in aerosol light-scattering in the North Atlantic trade winds, Nature, 380, 1996.

Liao, H., Seinfeld, J. H., Adams, P. J., and Mickley, L. J.: Global radiative forcing of coupled tropospheric ozone and aerosols in a unified general circulation model, J. Geophys. Res., 109, 2004.

Liu, M., Westphal, D. L., Holt, T. R. and Xu, Q.: Numerical Simulation of a Low-Level Jet over Complex Terrain in Southern Iran, Mon. Weather Rev., 128(5), 1309-1327, 2000.

Liu, M., and Westphal, D. L.: A study of the sensitivity of simulated mineral dust production to model resolution, J. Geophys. Res., 106, 18099-18018, 2001.

Löye-Pilot, M. D., Martin, J. M., and Morelli, J.: Influence of Saharan dust on the rainfall acidity and atmospheric input to the Mediterranean, Nature, 321, 427-428, 1986.

Luo, C., Mahowald, N. M., and Del Corral, J.: Sensitivity study of meteorological parameters on mineral aerosol mobilization, transport, and distribution, J. Geophys. Res. Lett., 108, doi:10.1029/2003JD003483, 2003.

Lyamani, H., Olmo, F. J. and Alados-Arboledas, L.: Saharan dust outbreak over southeastern Spain as detected by sun photometer, Atmos. Environ., 39(38), 7276-7284, 2005.

Mahowald, N. M., and Kiehl, L. M.: Mineral aerosol and cloud interactions, J. Geophys. Res. Lett, 30, 1475, 2003.

Mahowald, N. M., Baker, A. R., Bergametti, G., Brooks, N., Duce, R. A., Jickells, T. D., Kubilay, N., Prospero, J. M., and Tegen, I.: The atmospheric global dust cycle and iron inputs to the ocean, Global Biogeochemical Cycles, 19, doi: 10.1029/2004GB002402, 2005.

Mahowald, N. M., Ballantine, J. A., Feddema, J., and Ramankutty, N.: Global trends in visibility: implications for dust sources, Atmos. Chem. Phys. Discuss., 7, 3013-3071, 2007.

Mahowald, N. M., Kloster, S., Engelstaedter, S., Moore, J. K., Mukhopadhyay, S., McConnell, J. R., Albani, S., Doney, S. C., Bhattacharya, A., Curran, M. A. J., Flanner, M. G., Hoffman, F. M., Lawrence, D. M., Lindsay, K., Mayewski, P. A., Neff, J., Rothenberg, D., Thomas, E., Thornton, P. E., and Zender, C. S.: Observed 20th century desert dust variability: impact on climate and biogeochemistry, Atmos. Chem. Phys., 10, 10875-10893, doi:10.5194/acp-10-10875-2010, 2010.

Mallet, M., Roger, J. C., Despiau, S., Dubovik, O. and Putaud, J. P.: Microphysical and optical properties of aerosol particles in urban zone during ESCOMPTE, Atmos. Res., 69, 73-97, 2003.

Malm, W. C., J. F. Sisler, D. Huffman, R. A. Eldred and T. A. Cahill.: Spatial and seasonal trends in particle concentration and optical extinction in the United States, J. Geophys. Res., 99, 1347–1370, 1994.

Manders, A. M. M., Schaap, M. and Hoogerbrugge, R.: Testing the capability of the chemistry transport model LOTOS-EUROS to forecast PM10 levels in the Netherlands, Atmos. Environ., 43(26), 4050-4059, 2009.

Maring, H., Savoie, D. L., Izaguirre, M. A., Custals, L., and Reid, J. S.: Mineral dust aerosol size distribution change during atmospheric transport, Journal of Geophysical Research, 108, 8592, 2003.

Martet, M., and Peuch, V.H.: Aerosol modelling in MOCAGE and operational dust forecasting at Météo-France, IOP Conf. Series: Earth Environ. Sci. 7, 012008, 2009.

Marticorena, B., and Bergametti, G.: Modeling the atmospheric dust cycle: 1. Design of a soil-derived dust emission scheme, J. Geophys. Res., 100, 6415-16430, 1995.

Marticorena, B., Bergametti, G., Aumont, B., Callot, Y., N'Doume, C., and Legrand, M.: Modeling the atmospheric dust cycle: 2. Simulation of Saharan dust sources, J. Geophys. Res, 102, 4387-4404, 1997.

Martín Vide, J.: Interpretación de los mapas del tiempo, Ketres Editora SA, Barcelona, 1984.

Martin, R. V., Jacob, D. J., Yantosca, R. M., Chin, M., and Ginoux, P.: Global and regional decreases in tropospheric oxidants from photochemical effects of aerosols, J. Geophys. Res., 108, 2003.

Martonchik, J. V., Diner, D. J., Kahn, R., Gaitley, B., and Holben, B. N.: Comparison of MISR and AERONET aerosol optical depths over desert sites, J. Geophys. Res. Lett, 31, 2004.

Matthias, V.: The aerosol distribution in Europe derived with the community mustiscale air quality (CMAQ) model: comparison to near surface in situ and sunphotometer measurements, Atmos. Chem. Phys., 8, 5077-5097, 2008.

McKeen, S., Wilczak, J., Grell, G., Djalalova, I., Peckham, S., Hsie, E. Y., Gong, W., Bouchet, V., Menard, S., and Moffet, R.: Assessment of an ensemble of seven real-time ozone forecasts over eastern North America during the summer of 2004, J. Geophys. Res., 110, D21307, 2005.

Mélin F. and Zibordi, G.: Aerosol variability in the Po Valley analyzed from automated optical measurements, Geophys. Res. Lett., 32, L03810, doi:10.1029/2004GL021787, 2005.

Meloni, D., Sarra, A. d., Iorio, T. D., and Fiocco, G.: Direct radiative forcing of Saharan dust in the Mediterranean from measurements at Lampedusa Island and MISR space-borne observations, J. Geophys. Res., 109, doi:10.1029/2003JD003960, 2004.

Meloni, D., di Sarra, A., Biavati, G., DeLuisi, J. J., Monteleone, F., Pace, G., Piacentino, S., and Sferlazzo, D. M.: Seasonal behavior of Saharan dust events at the Mediterranean island of Lampedusa in the period 1999-2005, Atmos. Environ., 41, 3041-3056, 2007.

Meng, Z., Dabdub, D. and Seinfeld, J. H.: Chemical coupling between atmospheric ozone and particulate matter, Science, 277, 116, 1997.

Menut, L., Forêt, G., and Bergametti, G.: Sensitivity of mineral dust concentrations to the model size distribution accuracy, J. Geophys. Res, 112, D10210, 2007.

Menut, L.: Sensitivity of hourly Saharan dust emissions to NCEP and ECMWF modeled wind speed. J. Geophys. Res. 113, D16201, 2008.

Menut, L. and Bessagnet, B.: Atmospheric composition forecasting in Europe, Ann. Geophys., 28, 61-74, 2010.

Mesinger, F., Janjic, Z. I., Nickovic, S., Gavrilov, D. and Deaven, D. G.: The step-mountain coordinate: model description and performance for cases of Alpine lee cyclogenesis and for a case of an Appalachian redevelopment, Mon. Weather Rev., 116, 1493-1518, 1988.

Michalakes, J., Dudhia, J., Gill, D., Henderson, T., Klemp, J., Skamarock,W. and Wang,W.: The weather research and forecast model: software architecture and performance. In: Mozdzynski, E.G. (Ed.), To Appear in Proceeding of the Eleventh ECMWF Workshop on the Use of High Performance Computing in Meteorology, 25-29 October 2004, Reading, U.K, 117-124, 2004.

Middleton, N.J.: The geography of dust storms Unpublished D.Ph. thesis University de Oxford, UK, 1986.

Middleton, N. J. and Goudie, A. S.: Saharan dust: sources and trajectories, Trans. Inst. Br. Geogr., 26, 165, doi:10.1111/1475-5661.00013, 2001.

Miller, R. L., and Tegen, I.: Climate response to soil dust aerosols, Climate, 11, 3247-3267, 1998.

Mona, L., Amodeo, A., Pandolfi, M., and Pappalardo, G.: Saharan dust intrusions in the Mediterranean area: Three years of Raman lidar measurements, J. Geophys. Res., 111, D16203, doi:10.1029/2005JD006569, 2006.

Monks, P.S., Granier, C., Fuzzi, S., Stohl, A., et al.: Atmospheric composition change – global and regional air quality. Atmos. Environ., 43, 5268-5350, 2009.

Morcrette, J. J., Boucher, O., Jones, L., Salmond, D., Bechtold, P., A. Beljaars, Benedetti, A., Bonet, A. Kaiser, J. W., Razinger, M., Schulz, M., Serrar, S., Simmons, A. J., Sofiev, M., Suttie, M., Tompkins, A. M., and Untch, A.: Aerosol analysis and forecast in the European Centre for Medium-Range Weather Forecasts Integrated Forecast System: Forward modeling. J. Geophys. Res. 114, D06206, doi:10.1029/2008JD011235, 2009.

Moulin, C., Lambert, C. E., Dulac, F., and Dayan, U.: Control of atmospheric export of dust from North Africa by the North Atlantic Oscillation Nature, 387, 691-694, doi:10.1038/42679 1997.

Moulin, C., Lambert, C. E., Dayan, U., Masson, V., Ramonet, M., Bousquet, P., Legrand, M., Balkanski, Y. J., Guelle, W., Marticorena, B., Bergametti, G., and Dulac, F.: Satellite climatology of African dust transport in the Mediterranean atmosphere, J. Geophys. Res., 103, 13137-13144, 1998.

Moulin, C., and Chiapello, I.: Evidence of the control of summer atmospheric transport of African dust over the Atlantic by Sahel sources from TOMS satellites (1979–2000), J. Geophys. Res. Lett., 31, doi: 10.1029/2003GL018931, 2004.

Müller, D., Mattis, I., Wandinger, U., Ansmann, A., Althausen, D., Dubovik, O., Eckhardt, S., and Stohl, A.: Saharan dust over a central European EARLINET-AERONET site: Combined observations with Raman lidar and Sun photometer, J. Geophys. Res., 108, 4345, doi:10.1029/2002JD002918, 2003.

N'Tchayi, M., Bertrand, J., and Nicholson, S. E.: The Diurnal and Seasonal Cycles of Wind-Borne Dust over Africa North of the Equator, Appl. Meteorol., 36, 868–882, 1997.

Nenes, A., Pilinis, C. and Pandis, S. N.: ISORROPIA: A New Thermodynamic Equilibrium Model for Multiphase Multicomponent Inorganic Aerosols, Aquatic Geochemistry, 4 (1), 123–152, doi:10.1023/A:1009604003 981, 1998.

Nickovic, S., and Dobricic, S.: A model for long-range transport of desert dust, Monthly weather review, 124, 2537-2544, 1996.

Nickovic, S., Jovic, D., Kakaliagou, O. and Kallos, G.: Production and long-range transport of desert dust in the Mediterranean region: Eta model simulation. In: Proceedings of the Proceedings of the 22nd NATO/CCMS International Technical Meeting on Air Pollution Modelling and its Applications, Clermont-Ferrand, France, 2-6 June 1997.

Nickovic, S., Kallos, G., Papadopoulos, A., and Kakaliagou, O.: A model for prediction of desert dust cycle in the atmosphere, J. Geophys. Res., 106, 18113-18130, doi: 10.1029/2000JD900794, 2001.

Nickovic, S.: Dust Aerosol Modeling: Step Toward Integrated Environmental Forecasting (Invited paper), Eos. Trans. AGU, 83(47), Fall Meet. Suppl., Abstract A71E-04, 2002.

Nickovic, S.: Distribution of dust mass over particle sizes: Impacts on atmospheric optics. Paper presented at Fourth ADEC Workshop: Aeolian Dust Experiment on Climate Impact, Ministry of the Environment, Nagasaki, Japan, 2005.

Nickovic, S., and Pérez, C.: Regional Model of Atmospheric Iron Dust Transport and Deposition to the West African Atlantic Ocean. 3rd International Workshop on Mineral Dust, 15-17 September, Leipzig, Germany, 2008.

Nickovic, S., and Pérez, C.: Simulation of iron/dust in the atmosphere by a regional model. AGU Fall Meeting, 15-19 December, San Francisco, 2008.

Nickovic, S., Vukovic, A., Vujadinovic, M., Djurdjevic, V., and Pejanovic, G.: Technical note: Minerals in dust productive soils – impacts and global distribution. Atmos. Chem. Phys. Discuss., 11, 26009-26034, doi:10.5194/acpd-11-26009-2011, 2011.

Niu, T., Gong, S. L., Zhu, G. F., Liu, H. L., Hu, X. Q., Zhou, C. H., and Wang, Y. Q.: Data assimilation of dust aerosol observations for the CUACE/dust forecasting system. Atmos. Chem. Phys., 8, 3473–3482, 2008.

O'Neill, N. T., Dubovik, O. and Eck, T. F.: A modified Angstrom coefficient for the characterization of sub-micron aerosols, App. Opt., 40(14), 2368–2375, 2001.

O'Neill, N. T., Eck, T. F., Smirnov, A., Holben, B. N. and Thulasiraman, S.: Spectral discrimination of coarse and fine mode optical depth, J. Geophys. Res., 108, 4559, 2003.

O'Neill, N. T., Smirnov, A., Holben, B. and Thulasiraman, S.: Recent changes to the coarse/fine mode optical depth deconvolution algorithm, AERONET Technical memo, http://aeronet.gsfc.nasa.gov/new_web/PDF/tauf_tauc_technical_memo1.pdf, 2005.

O'Neill, N. T.: Comment on "Classification of aerosol properties derived from AERONET direct sun data" by G. P. Gobbi et al. (2007)", Atmos. Chem. Phys. Discuss., 9, 175–182, 2009.

Ogren, J.A.: A systematic approach to In situ observations of aerosols properties, in Aerosol Forcing of Climate, edited by R.J. Charlson and J. Heintzenberg, 215-226, John Wiley & Sons, Inc., New York, 1995.

Ogunjobi, K., Ajayi, V., Balogun, I., Omotosho, J. and He, Z.: The synoptic and optical characteristics of the harmattan dust spells over Nigeria, Theoretical and Applied Climatology, 93(1), 91-105, 2008.

Okin, G. S., Mahowald, N., Chadwick, O. A., and Artaxo, P.: Impact of desert dust on the biogeochemistry of phosphorus in terrestrial ecosystems, Global Biogeochem. Cycles, 18, 2004.

Ozer, P., Laghdaf, M. B. O. M., Lemine, S. O. M., and Gassani, J.: Estimation of air quality degradation due to Saharan dust at Nouakchott, Mauritania, from horizontal visibility data, Water Air Soil Pollut, 178, 79-87, 2007.

Pace, G., Sarra, A. d., Meloni, D., Piacentino, S., and Chamard, P.: Aerosol optical properties at Lampedusa (Central Mediterranean). 1. Influence of transport and identification of different aerosol types, Atmos. Chem. Phys., 6, 697–713, 2006.

Papanastasiou, D. K., Poupkou, A., Katragkou, E., Amiridis, V., Melas, D., Mihalopoulos, N., Basart, S., Pérez, C., and Baldasano, J. M.: An Assessment of the Efficiency of Dust Regional Modelling to Predict Saharan Dust Transport Episodes, Advances in Meteorology, 2010, doi:10.1155/2010/154368, 2010.

Papayannis, A., Amiridis, V., Mona, L., Tsaknakis, G., Balis, D., Bösenberg, J., Chaikovski, A., De Tomasi, F., Grigorov, I., and Mattis, I.: Systematic lidar observations of Saharan dust over Europe in the frame of EARLINET (2000–2002), J. Geophys. Res., 113, 2008.

Pappalardo, G., Amodeo, A., Amoruso, S., Mona, L., Pandolfi, M., and Cuomo, V.: One year of tropospheric lidar measurements of aerosol extinction and backscatter, Ann. Geophys., 46, 401-413, 2003.

Pay, M. T., Piot, M., Jorba, O., Gassó, S., Gonçalves, M., Basart, S., Dabdub, D., Jiménez-Guerrero, P., and Baldasano, J. M.: A Full Year Evaluation of the CALIOPE-EU Air Quality Modeling System over Europe for 2004, Atmos. Environ., 44, 3322-3342, doi:10.1016/j.atmosenv.2010.05.040, 2010.

Pay, M.T., Jiménez-Guerrero, P., Jorba, O., Basart, S., Querol, X., Pandolfi, M. and Baldasano, J.M.: Spatio-temporal variability of concetrations and speciation of particulate matter across Spain in the CALIOPE modeling system, Atmos. Environ., A*ccepted*, 2011.

Pejanovic, G., Vukovic, A., Vujadinovic, M., and Dacic, M.: Assimilation of satellite information on mineral dust using dynamic relaxation approach, Geophys. Res. Abstracts, Vol. 12, EGU2010-7353, 2010.

Péré, J. C., Mallet, M., Pont, V. and Bessagnet, B.: Evaluation of an aerosol optical scheme in the chemistry-transport model CHIMERE, Atmos. Environ., 44, 3688-3699, doi:10.1016/j.atmosenv.2010.06.034, 2010.

Pérez, C., Sicard, M., Jorba, O., Comerón, A. and Baldasano, J. M.: Summertime re-circulations of air pollutants over the north-eastern Iberian coast observed from systematic EARLINET lidar measurements in Barcelona, Atmos. Environ., 38, 3983–4000, 2004.

Pérez, C., Nickovic, S., Pejanovic, G., Baldasano, J. M., and Ozsoy, E.: Interactive dust-radiation modeling: A step to improve weather forecasts, J. Geophys. Res., 11, doi:10.1029/2005JD006717, 2006a.

Pérez, C., Nickovic, S., Baldasano, J. M., Sicard, M., Rocadenbosch, F., and Cachorro, V. E.: A long Saharan dust event over the western Mediterranean: Lidar, Sun photometer observations, and regional dust modeling, J. Geophys. Res., 111, doi:10.1029/2005JD006579, 2006b.

Pérez, C., P. Jiménez, O. Jorba, J. M. Baldasano, E. Cuevas, S. Nickovic, X. Querol: Long-term simulations (1958-2006) of Saharan dust over the Mediterranean and the Eastern North Atlantic with the DREAM regional dust model. Proceedings of IUGG 2007 Perugia-XXIV IUGG General Assembly, Italy, Perugia, 2-13, July, 2007.

Pérez, C.: How does climate influence infectious diseases? Unraveling the effects of dust and climate on meningitis epidemics in the Sahel. The Earth Institute Fellows Symposium. Columbia University, New York, May 10th, 2010.

Pérez, C., Stanton, M., Trzaska, S., Thomson, M., Ceccato, P., Diggle, P., Miller, R. L., Perlwitz, J., Adamo, S., Yetman, G., Baldasano, J. M., Cuevas, E., and Camino, C.: Forecasting Meningitis Seasonal Incidence at National and District Levels in Niger using Climate Data. 5th Merit Meeting. 10th November. Geneva, Switzerland, 2011a.

Pérez, C., Haustein, K., Janjic, Z., Jorba, O., Huneeus, N., Baldasano, J.M., Black, T., Basart, S., Nickovic, S., Miller, R.L., Perlwitz, J., Schulz, M. and Thomson, M.: An online mineral dust aerosol model for meso to global scales: Model description, annual simulations and evaluation, Atmos. Chem. Phys., 11, 13001-13027, doi: 10.5194/acp-11-13001-2011, 2011b.

Perlwitz, J., Tegen, I., and Miller, R. L.: Interactive soil dust aerosol model in the GISS GCM 1. Sensitivity of the soil dust cycle to radiative properties of soil dust aerosols, J. Geophys. Res., 106, 18167-18118, 18192, 2001.

Perrone, M. R., Santese, M., Tafuro, A. M., Holben, B. and Smirnov, A.: Aerosol load characterization over South-East Italy for one year of AERONET sun-photometer measurements, Atmos. Res., 75(1-2), 111-133, 2005.

Perry, K. D., Cahill, T. A., Eldred, R. A., Dutcher, D. D., and Gill, T. E.: Long-range transport of North African dust to the eastern United States, J. Geophys. Res., 102, 11225-11238 1997.

Peyridieu, S., Chédin, A., Tanré, D., Capelle, V., Pierangelo, C., Lamquin, N., and Armante, R.: Saharan dust infrared optical depth and altitude retrieved from AIRS: a focus over North Atlantic – comparison to MODIS and CALIPSO, Atmos. Chem. Phys., 10, 1953–1967, 2010.

Pierangelo, C., Chédin, A., Heilliette, S., Jacquinet-Husson, N., and Armante R.: Dust altitude and infrared optical depth from AIRS, Atmos. Chem. Phys., 4, 1813–1822, 2004.

Pinker, R. T., Pandithurai, G., Holben, B. N., Dubovik, O., and Aro, T. O.: A dust outbreak episode in sub-Sahel West Africa, J. Geophys. Res., 106, 22923-22930, Paper number 2001JD900118., 2001.

Piot, M., Jorba, O., Jimenez, P. and Baldasano, J.M.: The Role of Lateral Boundary Conditions and Boundary Layer in Air Quality Modelling System, Eos Trans. AGU, 8, H212+, Abstract A41H-0212, 2008.

Pope, C. A. I., Ezzati, M. and Dockery, D. W.: Fine-Particulate Air Pollution and Life Expectancy in the United States, The New England Journal Med., 360, 376–386, 2009.

Prospero, J. M., Glaccum, R. A., and Nees, R. T.: Atmospheric transport of soil dust from Africa to South America, Nature, 289, 570-572, doi:10.1038/289570a0, 1981.

Prospero, J. M., and Nees, R. T.: Impact of the North African drought and El Niño on mineral dust in the Barbados trade winds, Nature, 320, 735-738, doi:10.1038/320735a0, 1986.

Prospero, J.M., Schmitt, R., Cuevas, E., Savoie, D., Graustein, W., Turekian, K., Volz-Thomas, A., Diaz, A., Oltmans, S., Levy-II, H.: Temporal Variability of Summer-time Ozone and Aerosols in the Free Troposphere over the Eastern North Atlantic, J. Geophys. Res. Lett., 22, 21, 2925-2928, 1995.

Prospero, J. M.: Long-range transport of mineral dust in the global atmosphere: Impact of African dust on the environment of the southeastern United States, Nature, 96, 3396-3403, 1999.

Prospero, J. M., Ginoux, P., Torres, O., Nicholson, S. E., and Gill, T. E.: Environmental characterization of global sources of atmospheric soil dust identified with the nimbus 7 total ozone mapping spectrometer (TOMS) absorbing aerosol product, Rev. Geophys., 40(1), doi:10.1029/2000RG000095, 2002.

Prospero, J. M., and Lamb, P. J.: African Droughts and Dust Transport to the Caribbean: Climate Change Implications Science, 301, 1024-1027, 2003.

Putaud, J.-P., Van Dingenen, R., Mangoni, M., Virkkula, A., Raes, F., Maring, H., Prospero, J. M., Swietlicki, E., Berg, O. H., Hillamo, R. and Mäkelä, T.: Chemical mass closure and assessment of the origin of the submicron aerosol in the marine boundary layer and the free troposphere at Tenerife during ACE- 2, Tellus, 52B, 147–168, 2000.

Putaud, J.-P., Raes, F., Van Dingenen, R., Bruggemann, E., Facchini, M. C., Decesari, S., Fuzzi, S., Gehrig, R., Huglin, C., Laj, P., Lorbeer, G., Maenhaut, W., Mihalopoulos, N., Müller, K., Querol, X., Rodríguez, S., Schneider, J., Spindler, G., ten Brink, H., Torseth, K. and Wiedensohler, A.: European aerosol phenomenology 2: chemical characteristics of particulate matter at kerbside, urban, rural and background sites in Europe, Atmos. Environ., 38, 2579–2595, 2004.

Pye, K.: Aeolian Dust and Dust Deposits, Academic Press, London, 334 pp., 1987.

Querol, X., Rodríguez, S., Cuevas, E., Viana, M., and Alastuey, A.: Intrusiones de masas de aire africano sobre la Península Ibérica y Canarias: Mecanismos de transporte y variación estacional, 3ª Asemblea Hispano Portuguesa de Geodesia y Geofisica, Valencia 2002, 2002.

Querol, X., Alastuey, A., Rodríguez, S., Viana, M., Artiano, B., Salvador, P., Mantilla, E., Santos, S. G. d., Patier, R. F., Rosa, J. d. L., Campa, A. S. d. l., Menendez, M. and Gil, J. J.: Levels of particulate matter in rural, urban and industrial sites in Spain, Sci. Total Environ., 334– 335 359–376, 2004a.

Querol, X., Alastuey, A., Viana, M., Rodríguez, S., Artiano, B., Salvador, P., Santos, S. G. d., Patier, R. F., Ruiz, C. R., Rosae, J. d. l., Campa, A. S. d. l., Menendez, M., and Gilf, J. I.: Speciation and origin of PM10 and PM2.5 in Spain, Aerosol Sci., 35, 1151–1172, doi:10.1016/j.jaerosci.2004.04.002, 2004b.

Querol, X., Alastuey, A. Pey, J., Cusack, M., Pérez, N., Mihalopoulos, N., Theodosi, C., Gerasopoulos, E., Kubilay, N. and Koçak, M.: Variability in regional background aerosols within the Mediterranean, Atmos. Chem. Phys., 9, 4575-4591, doi:10.5194/acp-9-4575-2009, 2009.

Raes, F., Dingenen, R. V., Vignati, E., Wilson, J., Putaud, J.-P., Seinfeld, J. H., and Adams, P.: Formation and cycling of aerosols in the global troposphere, Atmos. Environ., 34, 4215–4240, 2000.

Rasch, P. J., Collins, W. D., and Eaton, B. E.: Understanding the Indian Ocean Experiment (INDOEX) aerosol distributions with an aerosol assimilation, J. Geophys. Res., 106, 7337-7355, 2001.

Reid, J. S., Eck, T. F., Christopher, S. A., Hobbs, P. V. and Holben, B.: Use of the Ångstrom exponent to estimate the variability of optical and physical properties of aging smoke particles in Brazil, Geophys. Res., 104(D22), 27473-27490, 1999.

Reid, J. S., Jonsson, H. H., Maring, H. B., Smirnov, A., Savoie, D. L., Cliff, S. S., Reid, E. A., Livingston, J. M., Meier, M. M., and Dubovik, O.: Comparison of size and morphological measurements of coarse mode dust particles from Africa, J. Geophys. Res, 108, 1-9, 2003.

Remer, L. and Kaufman, Y. J.: Dynamic aerosol model- Urban/industrial aerosol, J. Geophys. Res., 103(D12), 13859-13871, 1998.

Remer, L. A., Kaufman, Y. J., Tanré, D., Mattoo, S., Chu, D. A., Martins, J. V., Li, R. R., Ichoku, C., Levy, R. C., Kleidman, R. G., Eck, T. F., Vermote, E., and Holben, B. N.: The MODIS Aerosol Algorithm, Products, and Validation, J. Atmos. Sci., 62, 947-973, 2005.

Rodríguez, S. and Guerra, J. C.: Monitoring of ozone in a marine environment in Tenerife (Canary Islands), Atmos. Environ., 135, 1829-1841, 2001.

Rodríguez, S., Querol, X., Alastuey, A., Kallos, G., and Kakaliagou, O.: Saharan dust contributions to PM10 and TSP levels in Southern and Eastern Spain, Atmos. Environ., 35, 2433-2447, 2001.

Rodríguez, S., Querol, X., Alastuey, A. and Plana, F.: Sources and processes affecting levels and composition of atmospheric aerosol in the Western Mediterranean, J. Geophys. Res., 107 (D24), 2002.

Rodríguez, S., Cuevas, E., Toledo, I., Basart, S. and Goloub, P.: An Assessment of the AERONET aerosol size distributions by comparisons with in-situ measurements at Izaña Global Atmospheric Watch Station". In Proceedings of IUGG 2007 Perugia-XXIV IUGG General Assembly, Italy, Perugia, 2-13, July, 2007.

Rodríguez, S., Cuevas, E., González, Y., Ramos, R., Romero, P.M., Pérez, N., Querol, X., Alastuey, A.: Influence of sea breeze circulation and road traffic emissions on the relationship between particle number, black carbon, PM1, PM2.5 and PM2.5-10 concentrations in a coastal city, Atmos. Environ., 42 (2008) 6523–6534, 2008.

Rodríguez, S., Alastuey, A., Alonso-Pérez, S., Querol, X., Cuevas, E., Abreu-Afonso, J., de la Rosa, J.: Transport of desert dust mixed with North African industrial pollutants in the subtropical Saharan Air Layer, Atmos. Chem. Phys. Discuss., 11, 8841-8892, doi:10.5194/acpd-11-8841-2011, 2011.

Rosenfeld, D., Rudich, Y., and Lahav, R.: Desert dust suppressing precipitation: A possible desertification feedback loop, Proceedings of the National Academy of Sciences of the United States of America, 98, 5975, 2001.

Roy, B., Mathur, R., Gilliland, A. B. and Howard, S. C.: A comparison of CMAQ-based aerosol properties with IMPROVE, MODIS, and AERONET data, Geophys. Res, 112, 2007.

Ryall, D. B., Derwent, R. G., Manning, A. J., Redington, A. L., Corden, J., Millington, W., Simmonds, P. G., O'Doherty, S., Carslaw, N., and Fuller, G. W.: The origin of high particulate concentrations over the United Kingdom, March 2000, Atmos. Environ., 36, 1363-1378, 2002.

Saliba, N. A., El Jam, F., El Tayar, G., Obeid, W., and Roumie, M.: Origin and variability of particulate matter (PM10 and PM2.5) mass concentrations over an Eastern Mediterranean city, Atmos. Res., 97, 106-114, 2010.

Santese, M., Perrone, M. R., Zakey, A. S., De Tomasi, F., and Giorgi, F.: Modeling of Saharan dust outbreaks over the Mediterranean by RegCM3: case studies, Atmos. Chem. Phys., 10, 133-156, doi:10.5194/acp-10-133-2010, 2010.

Schaap, M. van Loon, M., ten Brink H.M., Dentener, and F.J. Builtjes, P.J.H.: Secondary inorganic aerosol simulations for Europe with special attention to nitrate, Atmos. Chem. Phys., 4, 857-874, doi: 1680-7324/acp/2004-4-857, 2004.

Schell, B., Ackermann, I. J., Hass, H., Binkowski, F. S. and Ebel, A.: Modeling the formation of secondary organic aerosol within a comprehensive air quality model system, J. Geophys. Res., 106 (D22), 28 275–28 293, doi:2001JD000 384, 2001.

Schepanski, K., Tegen, I., Laurent, B., Heinold, B., and Macke, A.: A new Saharan dust source activation frequency map derived from MSG-SEVIRI IR-channels, J. Geophys. Res. Letters, 34, L18803, 2007.

Schmechtig, C., Marticorena, B., Chatenet, B., Bergametti, G., Rajot, J. L., and Coman, A.: Simulation of the mineral dust content over Western Africa from the event to the annual scale with the CHIMERE-DUST model. Atmos. Chem. Phys. 11, 7185-7207, 2011.

Schmetz, J., Pili, P., Tjemkes, S., Just, D., Kerkmann, J., Rota, S. and Ratier, A.: An introduction to Meteosat Second Generation (MSG), Bulletin of American Meteorological Society, 83, 977–992, 2002.

Schuster, G. L., Dubovik, O. and Holben, B. N.: Angstrom exponent and bimodal aerosol size distributions, J. Geophys. Res, 111, D07207, 2006.

Schwartz, J.: Particulate air pollution and daily mortality in Detroit, Environ. Res., 56(204-213), 1991.

Sciare, J., Bardouki, H., Moulin, C., and Mihalopoulos, N.: Aerosol sources and their contribution to the chemical composition of aerosols in the Eastern Mediterranean Sea during summertime, Atmos. Chem. Phys., 3, 291–302, 2003.

Segal, M.:. On the impact of thermal stability on some rough flow effects over mobile surfaces. Springer, 193-198, 1990.

Seinfeld, J. H. and Pandis, S. N.: Atmospheric Chemistry and Physics: From Air Pollution to Climate Change, 1326 pp, John Wiley, New York, 1998.

Shao, Y., Raupach, M. R. and Findlater, P. A.: Effect of saltation bombardment on the entrainment of dust by wind. J. Geophys. Res. 98, 12719-12726, 1993.

Shao, Y. P., Raupach, M. R., and Leys, J. F.: A model for predicting aeolian sand drift and dust entrainment on scales from paddock to region, Australian Journal of Soil Research, 34, 309-342, 1996.

Shao, Y., Raupach, M. R., and Findlater, P. A.: Effect of Saltation Bombardment on the Entrainment of Dust by Wind, J. Geophys. Res. , 98, 12, 719-712, 726, 2003.

Shao, Y.: Simplification of a dust emission scheme and comparison with data, J. Geophys. Res., 109, D10202, 2004.

Shao, Y.: Physics and modelling of wind erosion, Springer Verlag, 2008.

Shaw, W., Allwine, K. J., Fritz, B. G., Rutz, F. C., Rishel, J. P., and Chapman, E. G.: An evaluation of the wind erosion module in DUSTRAN, Atmos. Environ., 42, 1907–1921, 2008.

Sicard, M., Rocadenbosch, F., Reba, M. N. M., Comerón, A., Tomás, S., García-Vizcaino, D., Batet, O., Barrios, R., Kumar, D., and Baldasano, J. M.: Seasonal variability of aerosol optical properties observed by means of a Raman lidar at an EARLINET site over Northeastern Spain, Atmos. Chem. Phys, 11, 175-190, 2011.

Sicardi, V., Ortiz, J., Rincón, A., Jorba, O., Pay, M. T., Gassó, S. and Baldasano, J. M.: Ground-level ozone concentration over Spain: an application of Kalman Filter post-processing to reduce model uncertainties, Geoscientific Model Development Discussions, 4, 343-384, doi:10.5194/gmdd-4-343-2011, 2011.

Silva, A., Costa, M., Elias, T., Formenti, P., Belo, N., and Pereira, S.: Ground-based aerosol monitoring at Évora, Portugal, Global Change News Letter, December, 2003.

Skamarock, W.C. and Klemp, J.B.: A time-split nonhydrostatic atmospheric model for weather research and forecasting applications. J. Comput. Phys., 227 (7), 3465-3485. doi:10.1016/j.jcp.2007.01.037, 2008.

Slinn, S. A., and Slinn, W. G. N.: Predictions for particle deposition on natural waters, Atmos. Environ., 14, 1013-1016, 1980.

Slinn, W. G. N.: Predictions for particle deposition to vegetative canopies, Atmos. Environ., 16, 1785-1794, 1982.

Smirnov, A., Holben, B. N., Eck, T. F., Dubovik, O. and Slutsker, I.: Cloud screening and quality control algorithms for the AERONET database, Rem. Sens. Environ., 73, 337-349, 2000.

Smirnov, A., Holben, B. N., Eck, T. F., Slutsker, I., Chatenet, B. and Pinker, R. T.: Diurnal variability of aerosol optical depth observed at AERONET (Aerosol Robotic Network) sites, J. Geophys. Res. Lett., 29(23), 2115, 2002a.

Smirnov, A., Holben, B. N., Dubovik, O., O'Neill, N. T., Eck, T. F., Westphal, D. L., Goroch, A. K., Pietras, C. and Slutsker, I.: Atmospheric Aerosol Optical Properties in the Persian Gulf, Atmos. Sci., 59, 620–634, 2002b.

Sokolik, I. N., and Toon, O. B.: Incorporation of mineralogical composition into models of the radiative properties of mineral aerosol from UV to IR wavelengths, J. Geophys. Res., 104, 9423-9444, 1999.

Spyrou, C., Mitsakou, C., Kallos, G., Louka, P., and Vlastou, G.: An improved limited area model for describing the dust cycle in the atmosphere, J. Geophys. Res, 115, 2010.

Squires V.R.:Chapter 1: Part I: Physics, Mechanics and Processes of Dust and Sandstorms, in the book "Global Alarm: Dust and Sandstorms from the World's Drylands", Edited by Y.Youlin, V. Squires and L. Qi, United Nations; http://www.unccd.int/publicinfo/duststorms/part0-eng.pdf, 2001.

Staub, B. and Rosenzweig, C.: Global digital data sets of soil type, soil texture, surface slope, and other properties: documentation of archived data tape, United States. National Aeronautics and Space, and Goddard Institute for Space, 1987.

Sultan, B., Labadi, K., Guegan, J. F. and Janicot, S.: Climate drives the meningitis epidemics onset in West Africa, PLoS Medicine, 2(1), doi: 10.1371/journal.pmed.0020006, 2005.

Swap, R., Garstang, M., Greco, S., Talbot, R., and Kallberg, P.: Saharan dust in the Amazon Basin, Tellus, Series B-Chem Phys. Meteorol. , 44B, 133-149, 1992.

Szopa, S., Foret, G., Menut, L. and Cozic, A.: Impact of large scale circulation on European summer surface ozone and consequences for modelling forecast, Atmos. Environ., 43, 1189-1195, 2009.

Tanaka, T. Y., Orito, K., Sekiyama, T. T., Shibata, K., Chiba, M., and Tanaka, H.: MASINGAR, a global tropospheric aerosol chemical transport model coupled with MRI/JMA 98 GCM- Model description, Papers in Meteorology and Geophysics, 53, 119-138, 2003.

Tang, I. N., Wong, W. T. and Munkelwitz, H. R.: The relative importance of atmospheric sulfates and nitrates in visibility reduction, Atmos. Environ. (1967), 15, 2463-2471, 1981.

Tanré, D., Kaufman, Y. J., Holben, B. N., Chatenet, B., Karnieli, A., Lavenu, F., Blarel, L., Dubovik, O., Remer, L. A., and Smirnov, A.: Climatology of dust aerosol size distribution and optical properties derived from remotely sensed data in the solar spectrum, J. Geophys. Res., 106, 18205–18217, Paper number 2000JD900663., 2001.

Tanré, D., Haywood, J., Pelon, J., Leon, J. F., Chatenet, B., Formenti, P., Francis, P., Goloub, P., Highwood, E. J., and Myhre, G.: Measurement and modeling of the Saharan dust radiative impact: Overview of the Saharan Dust Experiment (SHADE), J. Geophys. Res., 108, 8574, doi:10.1029/2002JD003273, 2003.

Taylor, K. E.: Summarizing multiple aspects of model performance in a single diagram. J. Geophys. Res. 106, 7183-7192, 2001.

Tegen, I., and Fung, I.: Modeling of mineral dust in the atmosphere: Sources, transport, and optical thickness, J. Geophys. Res., 99, 22,897-822,914, 1994.

Tegen, I., and Fung, I.: Contribution to the atmospheric mineral aerosol load from land surface modification, J. Geophys. Res., 100, 18707-18726, doi:10.1029/95JD02051, 1995.

Tegen, I., and Lacis, A. A.: Modeling of particle size distribution and its influence on the radiative properties of mineral dust aerosol, 101, 19237-19244, 1996.

Tegen, I., Lacis, A. A., and Fung, I.: The influence on climate forcing of mineral aerosols from disturbed soils, Nature, 380, 419-422, doi:10.1038/380419a0, 1996.

Tegen, I., Hollrig, P., Chin, M., Fung, I., Jacob, D., and Penner, J.: Contribution of different aerosol species to the global aerosol extinction optical thickness: Estimates from model results. J. Geophys. Res. 102(D20), 23.895-23.915, doi:10.1029/97JD01864, 23895-23915, 1997.

Tegen, I., Harrison, S. P., Kohfeld, K., Prentice, I. C., Coe, M., and Heimann, M.: Impact of vegetation and preferential source areas on global dust aerosol: Results from a model study, J. Geophys. Res., 107, 2002.

Tegen, I.: Modeling the mineral dust aerosol cycle in the climate system, Quaternary Science Reviews 22, 1821–1834, 2003.

Tegen, I., Werner, M., Harrison, S. P., and Kohfeld, K. E.: Relative importance of climate and land use in determining present and future global soil dust emission, J. Geophys. Res. Lett., 31, doi:10.1029/2003GL019216, 2004.

Tegen, I., Bierwirth, E., Heinold, B., Helmert, J., and Wendisch, M.: Effect of measured surface albedo on modeled Saharan dust solar radiative forcing, J. Geophys. Res., 115, D24312, doi:10.1029/2009JD013764, 2010.

Teller, A., and Levin, Z.: The effects of aerosols on precipitation and dimensions of subtropical clouds: a sensitivity study using a numerical cloud model, Atmos. Chem. Phys., 6, 67-80, SRef-ID: 1680-7324/acp/2006-6-67, 2006.

Tesche, M., Ansmann, A., Müller, D., Althausen, D., Mattis, I., Heese, B., Freudenthaler, V., Wiegner, M., Esselborn, M., and Pisani, G.: Vertical profiling of Saharan dust with Raman lidars and airborne HSRL in southern Morocco during SAMUM, Tellus, 61B, 144–164, doi: 10.1111/j.1600-0889.2008.00390.x, 2009.

Textor, C., Schulz, M., Guibert, S., Kinne, S., Balkanski, Y., Bauer, S., Berntsen, T., Berglen, T., Boucher, O., Chin, M., Dentener, F., Diehl, T., Easter, R., Feichter, H., Fillmore, D., Ghan, S., Ginoux, P., Gong, S., Grini, A., Hendricks, J., Horowitz, L., Huang, P., Isaksen, I., Iversen, I., Kloster, S., Koch, D., Kirkevag, A., Kristjansson, J. E., Krol, M., Lauer, A., Lamarque, J. F., Liu, X., Montanaro, V., Myhre, G., Penner,

J., Pitari, G., Reddy, S., Seland, Ø., Stier, P., Takemura, T., and Tie, X.: Analysis and quantification of the diversities of aerosol life cycles within AeroCom, Atmos. Chem. Phys., 6, 1777–1813, doi:10.5194/acp-6-1777-2006, 2006.

Thieuleux, F., Moulin, C., Bréon, F. M., Maignan, F., Poitou, J., and Tanré, D.: Remote sensing of aerosols over the oceans using MSG/SEVIRI imagery, Ann. Geophys., 23, 3561-3568, SRef-ID: 1432-0576/ag/2005-23-3561, 2005.

Thomson, M. C., Molesworth, A. M., Djingarey, M. H., Yameogo, K. R., Belanger, F., and Cuevas, L. E.: Potential of environmental models to predict meningitis epidemics in Africa, Tropical Medicine and International Health, 11, 781-788, 2006.

Todd, M. C.: Quantifying uncertainty in estimates of mineral dust flux: An intercomparison of model performance over the Bodélé Depression, northern Chad, J. Geophys. Res., 113, 2008.

Toledano, C., Cachorro, V. E., De Frutos, A. M., Sorribas, M., Prats, N., and De la Morena, B. A.: Inventory of African desert dust events over the southwestern Iberian Peninsula in 2000–2005 with an AERONET Cimel Sun photometer, J. Geophys. Res., 112, D21201, 2007a.

Toledano, C., Cachorro, V. E., Berjon, A., de Frutos, A. M., Sorribas, M., de la Morena, B. A. and Goloub, P.: Aerosol optical depth and Angstrom exponent climatology at El Arenosillo AERONET site (Huelva, Spain), Quarterly Journal of Meteorol. Soc., 133, 795–807, doi:10.1002/qj54,2007b.

Tombette, M., Chazette, P. and Sportisse, B.: Simulation of aerosol optical properties over Europe with a 3-D size-resolved aerosol model: comparisons with AERONET data, Atmos. Chem. Phys., 8, 7115–7132, 2008.

Torres, O., Bhartia, P. K., Herman, J. R., Ahmad, Z., and Gleason, J.: Derivation of aerosol properties from satellite measurements of backscattered ultraviolet radiation: Theoretical basis, J. Geophys. Res., 103(D14), 17099-17110, doi:10.1029/98JD00900, 1998.

Torres, C., Cuevas, E. and Guerra, J. C.: Caracterización de la capa de mezcla marítima y de la atmósfera libre en la región subtropical sobre Canarias., Asemblea Hispano Portuguesa de Geodesia y Geofisica, Valencia, 2002.

Torseth, K. and Hov, O.: The EMEP Monitoring Strategy 2004-2009. Technical report 9/2003, EMEP/CCC, 2003.

Tsyro, S. G.: To what extent can aerosol water explain the discrepancy between model calculated and gravimetric PM10 and PM2.5, Atmos. Chem. Phys., 5, 515-532, 2005.

Tsyro, S., Simpson, D., Tarrasón, L., Klimont, Z., Kupiainen, K., Pio, C. and Yttri, K.E.: Modeling of elemental carbon over Europe, J. Geophys. Res. 112 (D23S19), 2007.

U.S. EPA.: Interim Procedures for Evaluating Air Quality Models (Revised), Technical Report, EPA-450/4-91-013, U.S. Environmental Protection Agency, Office of Air Quality Planning and Standards, Research Triangle Park, NC, 1984

U.S. EPA.: Guideline for Regulatory Application of the Urban Airshed Model, Technical Report. EPA-450/4-91-013, U.S. Environmental Protection Agency, Office of Air Quality Planning and Standards, Research Triangle Park, NC, 1991.

Uno, I., Amano, H., Emori, S., Kinoshita, K., Matsui, I., and Sugimoto, N.: Trans-Pacific yellow sand transport observed in April 1998: A numerical simulation, J. Geophys. Res., 106, 18331-18318, 2001.

Uno, I., Carmichael, G. R., Streets, D. G., Tang, Y., Yienger, J. J., Satake, S., Wang, Z., Woo, J. H., Guttikunda, S., and Uematsu, M.: Regional chemical weather forecasting system CFORS: Model descriptions and analysis of surface observations at Japanese island stations during the ACE-Asia experiment, J. Geophys. Res, 108, 8668, 2003.

Uno, I., Wang, Z., Chiba, M., Chun, Y. S., Gong, S. L., Hara, Y., Jung, E., Lee, S. S., Liu, M., Mikami, M., Music, S., Nickovic, S., Satake, S., Shao, Y., Song, Z., Sugimoto, N., Tanaka, T., and Westphal, D. L.: Dust model intercomparison (DMIP) study over Asia: Overview, J. Geophys. Res., 111(D12), D12213, doi:10.1029/2005JD006575, 2006.

Vajanapoom, N., Shy, C. M., Neas, L. M., and Loomis, D.: Estimation of particulate matter from visibility in Bangkok, Thailand, Exposure Analysis and Environmental Epidemiology, 11, 97-102, 2001.

VanCuren, R. A.: Asian aerosols in North America: Extracting the chemical composition and mass concentration of the Asian continental aerosol plume from long-term aerosol records in the western United States, Geophys. Res., 108, 10.1029/2003JD003459, 2003.

Vautard, R., Bessagnet, B., Chin, M., and Menut, L.: On the contribution of natural Aeolian sources to particulate matter concentrations in Europe: Testing hypotheses with a modelling approach, Atmos. Environ., doi:10.1016/j.atmosenv.2005.01.051, 2005.

Viana, M., Querol, X., Alastuey, A., Cuevas, E. and Rodríguez, S.: Influence of African dust on the levels of atmospheric particulates in the Canary Islands air quality network, Atmos. Environ., 36, 5861–5875, 2002.

Viana, M., Pérez, C., Querol, X., Alastuey, A., Nickovic, S., and Baldasano, J. M.: Spatial and temporal variability of PM levels and composition in a complex summer atmospheric scenario in Barcelona (NE Spain), Atmos. Environ., 39, 5343–5361, doi:10.1016/j.atmosenv.2005.05.039, 2005.

Volkamer, R., Jiménez, J.L., San Martini, F. et al.: Secondary organic aerosol formation from anthropogenic air pollution: Rapid and higher than expected, Geophys. Res. Lett., 33, L17811, doi: 10.1029/2006GL026899, 2006.

Vrekoussis, M., Liakakou, E., Koc-ak, M., Kubilay, N., Oikonomoua, K., Sciare, J., and Mihalopoulos, N.: Seasonal variability of optical properties of aerosols in the Eastern Mediterranean, Atmos. Environ., 39, 7083–7094, 2005.

Wagner, F., Bortoli, D., Pereira, S., Costa, M. J., Silva, A. N. A., Weinzierl, B., Esselborn, M., Petzold, A., Rasp, K., and Heinold, B.: Properties of dust aerosol particles transported to Portugal from the Sahara desert, Tellus B, 61, 297-306, 2009.

Wagner, S. C., Govaerts, Y. M. and Lattanzio, A.: Joint retrieval of surface reflectance and aerosol optical depth from MSG/SEVIRI observations with an optimal estimation approach: 2. Implementation and evaluation, J. Geophys. Res., 115, D02204, doi:10.1029/2009JD011780, 2010.

Warneck, P.: Chemistry of the natural atmosphere. International Geophysics Series. Wiley & Sons, 41. Academy Press, 757 pp., 1988.

Washington, R., Todd, M., Middleton, N. J., and Goudie, A. S.: Dust-storm source areas determined by the total ozone monitoring spectrometer and surface observations, Annals of the Association of American Geographers, 93, 297-313, 2003.

Weil, J. C., Sykes, R. I. and Venkatram, A.: Evaluating air-quality models: review and outlook, Appl. Meteo., 31, 1121-1145, 1992.

Westphal, D. L., Curtis, C. A., Liu, M. and Walker, A. L.: Operational aerosol and dust storm forecasting. IOP Conf. Ser.: Earth Environ. Sci. 7, 012007, 2009.

White, B. R.: Soil transport by winds on Mars. J. Geophys. Res. 84, 4643-4651, 1979.

WHO: WHO air quality guidelines global update 2005, Bonn, Germany, World Health Organization, 2005.

WMO: GAW Report No. 178. Plan for the implementation of the. GAW Aerosol Lidar Observation Network. GALION. Hamburg, Germany, 27 to 29 March, 2007.

Yoshioka, M., Mahowald, N. M., Conley, A. J., Collins, W. D., Fillmore, D. W., Zender, C. S., and Coleman, D. B.: Impact of desert dust radiative forcing on Sahel precipitation: Relative importance of dust compared to sea surface temperature variations, vegetation changes, and greenhouse gas warming, Journal of climate, 20, 1445-1467, 2007.

Yumimoto, K., Uno, I., Sugimoto, N., Shimizu, A., and Satake, S.: Adjoint inverse modeling of dust emission and transport over East Asia, Geophys. Res. Lett, 34, L08806, doi:10.1029/2006GL028551, 2007.

Yttri, K. E., and Aas, W.: Transboundary Particulate Matter in Europe: Status Report 2006, EMEP Report, 2006.

Zakey, A. S., Solmon, F., and Giorgi, F.: Implementation and testing of a desert dust module in a regional climate model, Atmos. Chem. Phys., 6, 4687-4704, 2006.

Zender, C. S., Newman, D., and Torres, O.: Spatial heterogeneity in aeolian erodibility: Uniform, topographic, geomorphic, and hydrologic hypotheses, J. Geophys. Res, 108, 1980–2006, 2003a.

Zender, C., Bian, H., and Newman, D.: Mineral Dust Entrainment and Deposition (DEAD) model: Description and 1990s dust climatology, J. Geophys. Res., 108, 2003b.

Zender, C. S., Miller, R. L., and Tegen, I.: Quantifying Mineral Dust Mass Budgets: Terminology, Constraints, and Current Estimates, EOS Transactions American Geophysical Union, 85, 509-512, 10.1029/2004EO480002, 2004.

Zeng, X., Tao, W., Zhang, M., Hou, A. Y., Xie, S., Lang, S., Li, X., Starr, D. O'C., Li, X., and Simpson, J.: An indirect effect of ice nuclei on atmospheric radiation, J. Atmos. Sci., 66, 41–61, 2009.

Zhang, D. F., Zakey, A. S., Gao, X. J., Giorgi, F., and Solmon, F.: Simulation of dust aerosol and its regional feedbacks over East Asia using a regional climate model, Atmos. Chem. Phys., 9, 1095-1110, 2009.

Zhang, K., Knipping, E., Wexler, A., Bhave, P. and Tonnesen, G.: Size distribution of sea-salt emissions as a function of relative humidity, Atmos. Environ., 39, 3373–3379, 2005.

Zhang, L., Gong, S., Padro, J., and Barrie, L.: A size-segregated particle dry deposition scheme for an atmospheric aerosol module, Atmos. Environ., 35, 549-560, 2001.

Zhang, Y., and Carmichael, G. R.: The role of mineral aerosol in tropospheric chemistry in East Asia-A model study, Journal of applied meteorology, 38, 353-366, 1999.

Zhao, Q. and Carr, F. H.: A prognostic cloud scheme for operational NWP models, Mon. Weather Rev., 125, 1931- 1953, 1997.

Zhou, C. H., Gong, S. L., Zhang, X. Y., Wang, Y. Q., Niu, T., Liu, H.L., Zhao, T.L., Yang, Y.Q., and Hou, Q.: Development and evaluation of an operational SDS forecasting system for East Asia: CUACE/Dust. Atmos. Chem. Phys. 8, 787–798, 2008.

Zhu, A., Ramanathan, V., Li, F., and Kim, D.: Dust plumes over the Pacific, Indian, and Atlantic oceans: Climatology and radiative impact, J. Geophys. Res., 112, D16208, 2007.

List of Figures

List of Tables

List of Acronyms

AEMET	Spanish Weather Agency
AEROCOM	Aerosol Comparison between Observations and Models Project
AERONET	Aerosol Robotic Network
AI	Aerosol Index
AIRS	Atmospheric InfraRed Sounder
AOD	Aerosol Optical Depth
AOD_{coarse}	Coarse mode AOD ($r > 1\mu m$)
AOD_{fine}	Fine mode AOD ($r < 1\mu m$)
AOT	Aerosol Optical Thickness
BoDEX	Bodélé Dust Experiment
BSC-CNS	Barcelona Supercomputing Center-Centro Nacional de Supercomputación
BSC-DREAM8b	Dust Regional Atmospheric Model version 8 bins developed at the BSC-CNS
BTD	Brigthness Temperature Differences Product
CAAQS	Air Resources Board of California establishes California Ambient Air Quality Standards
CALIOPE	WRF-ARW/EMEP-HERMES/CMAQ/BSC-DREAM8b Modelling System
CALIPSO	Cloud Aerosol Lidar and Infrared Pathfinder Satellite Observation
CIAI	Centro de Investigación Atmosférica de Izaña
CMAQ	Model-3 Community Multiscale Air Quality Modelling System
CNN	Cloud Condensation Nuclei
CNRS	Centre National de la Recherche Scientifique (National French Center for Scientific Research)
CREATE	Construction, use and delivery of an European aerosol database
CSIC	Spanish National Research Council
CUACE	Chinese Unified Atmospheric Chemistry Environment
DD	Desert Dust
DRE	Dust Radiative Effect
DREAM	Dust REgional Atmospheric Model
EARLINET	European Aerosol Research Lidar Network
ECMWF	European Center for Medium-Range Weather Forecasts
EMEP	European Monitoring and Evaluation Programme
EPA	Environmental Protection Agency
ESA	European Space Agency
ESCOMPTE	Experience sur Site pour COntraindre les Modeles de Pollution atmospherique et de Transport d'Emissions

EU	European Union
EUMETSAT	European Organisation for the Explotation of Meteorological Satellites
EUSAAR	European Supersites for Atmospheric Aerosol Research
GADS	Global Aerosol Data Set
GAW	Global Atmospheric Watch
GlobAEROSOL	Global Aerosol from Earth Observation
GV	Guideline Values
HERMES	High-Elective Resolution Modelling Emission System
IASI	Infrared Atmospheric Sounding Interferometer
IN	Ice Nuclei
INCA	Integrated Nitrogen in Catchments Model
INTA	Instituto Nacional de Técnica Aeroespacial
IPCC	Intergovermental Panel for Climate Change
IR	Infrared
LDA	Land Daily Aerosol Product
LMA	Laboratory de Modelització Ambiental (Environmental Modelling Laboratory)
LOA	Laboratoire d' Optique Atmosphérique
LSCE	Laboratoire des Sciences du Climat et l'Environnement
LVAQ	Limit Values for Air Quality
MB	Mean Bias
MBE	Mean Bias Error
METAR	MÉTéorologique Aviation Régulière (Meteorological observation message for routine aviation)
MFE	Mean Fractional Error
MISR	Multi-angle Imaging SpectroRadiometer
MNBE	Mean Normalized Bias Error
MODIS	Moderate-resolution Imaging Spectroradiometer
MPL	Micro Pulse Lidar
MPLNET	NASA Micro Pulse Lidar Network
MSG	Meteosat Second Generation
NA-ME-E	Northern Africa, Middle East and Europe Node of the SDS-WAS Programme
NAAQS	National Ambient Air Quality Standards
NASA	National Aeronautics and Space Administration
NCEP	National Centers for Environmental Prediction
NMMb	Non-hydrostatic Multiscale Model of the Arakawa B grid
OMI	Ozone Monitoring Instrument
PBL	Planetary Boundary Layer
PHOTONS	Observation Service from INSU
PM	Particulate Matter

PM_1	Particulate Matter with an aerodynamic diameter less than or equal to 1 μm
PM_{10}	Particulate Matter with an aerodynamic diameter less than or equal to 10 μm
$PM_{2.5}$	Particulate Matter with an aerodynamic diameter less than or equal to 2.5 μm
POLDER	Polarization and Directionality of the Earth's Reflectances
PRIDE	Puerto Rico Dust Experiment
r	Correlation coefficient
RGB	Red Green Blue
RMS	Centered Root Mean Square difference
RMSE	Root Mean Square Error
SAL	Saharan Air Layer
SAMUM	Saharan Mineral Dust Experiment
SDA	Spectral Decovolution Algorithm
SDS-WAS	Sand and Dust Storm Warning Assessment and Advisory System
SeaWIFS	Sea-viewing Wide Field of view Sensor
SEEVCCC	South East European Virtual Climate Change Center
SEVIRI	Spinning Enhanced Visible and InfraRed Imager
SHADE	Saharan Dust Experiment
SIA	Secondary Inorganic Aerosols
SNAP	Selected Nomenglature Air Pollution
SOA	Secondary Organic Aerosols
SSA	Sea Salt Aerosols
SYNOP	Surface synoptic observations
TOA	Top-of-atmosphere
TOMS	Total Ozone Mapping Spectrometer
UPC	Universitat Politècnica de Catalunya (Technical University of Catalonia)
UV	Ultraviolet
VIS	Visibility
VOC	Volatile Organic Compounds excluding CO and NO_2
WHO	World Health Organization
WMO	World Meteorological Organization
WRF-ARW	Weather Research Forecasting-Advanced Research Weather Model
WWRP	World Weather Research Programme